

https://dspace.org/

In vitro assessment of the toxicity of gold nanoparticles

Vetten, Melissa Anne

2019

https://hdl.handle.net/10539/29720

Vetten, Melissa Anne, In vitro assessment of the toxicity of gold nanoparticles, University of the Witwatersrand, Johannesburg, <http://hdl.handle.net/10539/29720>

Downloaded from a DSpace repository. https://dspace.org/

IN VITRO ASSESSMENT OF THE TOXICITY OF GOLD NANOPARTICLES

Melissa Anne Vetten

A Thesis submitted to the Faculty of Health Sciences, University of the Witwatersrand, Johannesburg, in fulfilment of the requirements for the degree of Doctor of Philosophy

Johannesburg, 2019

Candidate's Declaration

I, Melissa Anne Vetten, declare that this Thesis is my own, unaided work. It is being submitted for the Degree of Doctor of Philosophy at the University of the Witwatersrand, Johannesburg. It has not been submitted before for any degree or examination at any other University.

_____

10th day of October 2019 in Braamfontein

This thesis is dedicated to my Nanna,
the late Margaret Loraine Jenkinson
13 February 1924 - 13 April 2018
You are loved and missed.

Presentations

The following national and international presentations, made by Ms. Vetten, have arisen from this thesis:

- Melissa Vetten and Mary Gulumian. *In vitro cytotoxicity and uptake of manufactured gold nanoparticles.* 5th International Symposium on Nanotechnology, Occupational and Environmental Health, Boston MA, USA, 9 – 12 August 2011 (oral presentation).
- Melissa Vetten and Mary Gulumian. *Effects of functional groups on uptake of gold nanoparticles and interleukin-6 release in bronchial epithelial cells*. 2nd Biennial Conference of the African Federation of Clinical Chemistry (AFCC), hosted by the Clinical Chemists Association of Kenya (CCAK) in collaboration with the Toxicology Society of South Africa (TOXSA) and the International Federation of Clinical Chemists, Nairobi, Kenya, 28nd – 30th September 2011 (oral presentation).
- Melissa Vetten and Mary Gulumian. *An investigation into the uptake, cytotoxicity and inflammatory response of bronchial epithelial cells exposed to engineered gold nanoparticles in vitro*. ISOTC229 meeting, Midrand, South Africa, 14 November 2011 (poster presentation).
- Melissa Vetten and Mary Gulumian. *Cell Impedance as a sensitive technique for the study of the cytotoxicity of gold nanoparticles in vitro*. 2012 Annual Meeting of the Society of Toxicology (SOT), San Francisco CA, USA, 11 – 15 March 2012 (poster presentation).
- Melissa Vetten, Jiya George and Mary Gulumian. *Effects of size on in vitro toxicity of colloidal citrate-stabilised gold nanoparticles.* The 4th International Conference on Nanoscience and Nanotechnology (NanoAfrica 2012), Bloemfontein, South Africa, 1 – 4 April 2012 (oral presentation).
- Melissa Vetten and Mary Gulumian. *Effects of size on in vitro toxicity and uptake of colloidal citrate-stabilised gold nanoparticles*. University of the Witwatersrand Faculty of Health Sciences Biennial Research Day & Postgraduate Expo, Johannesburg, South Africa, 19 September 2012 (poster presentation).
- Melissa Vetten and Mary Gulumian. *Cell impedance as a sensitive technique for the study of the cytotoxicity of gold nanoparticles in vitro*. The 46th Annual Congress of the

SASBCP in association with the Dept. of Family Medicine (UP) and TOXSA, Pretoria, South Africa, 29 September – 2 October 2012 (poster presentation).

- Melissa Vetten and Mary Gulumian. *Evaluation of uptake and cytotoxicity of citrate stabilised gold nanoparticles in Chinese Hamster Ovary (CHO) cells prior to the in vitro mammalian mutation test.* 2013 Annual Meeting of the Society of Toxicology (SOT), San Antonio TX, USA, 10 – 14 March 2013 (poster presentation).
- Melissa Vetten, Jiya George and Mary Gulumian. *In vitro genotoxicity of 14 nm citrate stabilised gold nanoparticles*. XIII International Congress of Toxicology, Seoul, Korea, 30 June – 4 July 2013 (poster presentation).
- Melissa Vetten and Mary Gulumian. *Evaluation of uptake of citrate stabilised gold nanoparticles in vitro using the CytoViva Hyperspectral Imaging (HSI) System.* The Wits Faculty of Health Sciences Research Day & Postgraduate Expo 2014, Johannesburg, South Africa, 17 September 2014 (poster presentation).
- Melissa Vetten and Mary Gulumian. *Investigation of the Endocytosis of Gold Nanoparticles into the Human Bronchial Epithelial cell line BEAS-2B.* 2015 SOT Annual Meeting, San Diego CA, USA, 22 – 26 March 2015 (poster presentation).
- Melissa Vetten and Mary Gulumian. *Investigation of the Endocytosis of 14 nm Gold Nanoparticles into the Human Bronchial Epithelial cell line BEAS-2B.* The 7th International Symposium on Nanotechnology, Occupational and Environmental Health, Legend Safari Lodge, Limpopo, South Africa. 19 – 22 October 2015 (oral presentation).
- Melissa Vetten and Mary Gulumian. *Interference of gold nanoparticles in the assessment of endotoxin contamination in vitro.* 2016 SOT Annual Meeting, New Orleans, USA, 13-17 March 2016 (poster presentation).
- Melissa Vetten and Mary Gulumian. *Demonstration of the uptake of gold nanoparticles using CytoViva technology and Transmission Electron Microscopy*. 10th Congress of Toxicology in Developing Countries (CTDC10), Belgrade, Serbia, 18-21 April 2018 (poster presentation)

Publications

The following first-author publications have arisen from this thesis:

- Vetten, M.A., Tlotleng, N., Rascher, D.T., Skepu, A., Keter, F.K., Boodhia, K., Koekemoer, L-A., Andraos, C., Tshikhudo, R. and Gulumian, M. (2013). Label-free *in vitro* toxicity and uptake assessment of citrate stabilised gold nanoparticles in three cell lines. *Particle and Fibre Toxicology* 10:50 doi:10.1186/1743-8977-10-50

- Vetten, M.A., Yah, C.S., Singh, T. and Gulumian, M. (2014). Challenges facing sterilization and depyrogenation of nanoparticles: Effects on structural stability and biomedical applications. *Nanomedicine: Nanotechnology, Biology, and Medicine* 10: 1391-1399 doi: 10.1016/j.nano.2014.03.017.

- Vetten, M., and Gulumian, M. (2019a) Differences in uptake of 14 nm PEG-liganded gold nanoparticles into BEAS-2B cells is dependent on their functional groups. *Toxicology and Applied Pharmacology* 363: 131-141 doi: 10.1016/j.taap.2018.11.014

- Vetten, M.A. and Gulumian,M. (2019b) Interference of Gold Nanoparticles with *In vitro* Endotoxin Detection Assays. *Current Nanoscience* 15: 1. https://doi.org/10.2174/1573413715666181212120013

Sections of this thesis have been reproduced from these publications. Copyright permissions to reproduce the content of these publications in this thesis have been obtained and can be found in the Appendices section.

Abstract

The hazard identification of gold nanoparticles forms an essential part of their risk assessment; however, the test methodologies used should be appropriate and applicable to ensure reliable results. In this study, various *in vitro* testing methodologies used for hazard identification were investigated for their applicability in the testing of gold nanoparticles. Preferable assays were identified, in particular, the use of label-free methodologies, such as the cell impedance based xCELLigence and the CytoViva HSI systems, were found to be ideal in order to avoid optical interference of the nanoparticles with the testing methodology.

The recommended tests were then implemented to investigate the effect of size, surface charge and different functional groups in the bronchial epithelial cell line BEAS-2B. Two citrate stabilized gold nanoparticles of 14 nm and 20 nm in diameter were tested. Moreover, the 14 nm polyethylene glycol-liganded AuNPs with either hydroxyl, carboxyl, biotin, nitrilotriacetic acid, or azide negatively charged functional groups, and the positively charged 14 nm polyethylene glycol-liganded AuNP with amine functional group were investigated. The characterization of the physicochemical characteristics and sterility of these nanoparticles were performed prior to the assessment of their toxicity, intracellular uptake and localization, and the mechanism of uptake.

The gold nanoparticles tested were not toxic or genotoxic to the BEAS-2B cells, regardless of cellular internalisation. These cellular effects were not influenced by their size or surface charge. On the other hand, surface functionalization influenced uptake, which was shown to be through a caveolin-mediated endocytosis pathway followed by accumulation within vesicles and in the cytosol. However, additional work needs to be conducted to establish the link between different functional groups and their role in endocytosis and subsequent localization and toxicity.

In conclusion, the possibility exists for the interference of nanoparticles with *in vitro* assays and this should be tested prior to their implementation. However, most importantly, the physicochemical characterization of nanoparticles is of utmost importance, which should precede the hazard identification of nanomaterials using these *in vitro* assays. These in turn, will allow the establishment of the relationship between these characteristics and any observed toxicity, which

will aid not only the risk assessment of nanomaterials but also in the establishment of predictive models in the toxicity of newly synthesised nanomaterials.

Acknowledgements

I am grateful for so many people who have been in my life through this journey.

To my family and all my friends, thank you for your love and support. Thank you for patiently listening when I was down, as well as celebrating my achievements with me. Thank you for keeping me sane, checking in on me, and knowing when to not even ask.

Thank you to my colleagues and friends at the NIOH over the years, in particular, thank you to Kailen Boodhia, Leigh-Anne Koekemoer, and Charlene Andraos for your help and moral support. Thank you all for your contribution to the interference studies. Charlene, who walked this with me, thank you for your patience and friendship – I am glad we both finally made it. I'd like to thank Mangethe Zwane for his assistance on the ESR analyses; the Immunology and Microbiology Department for the sterility testing of the nanoparticles; and Millicent Magogotya and Thabiso Mahlake for the mycoplasma testing of the cell cultures. To Dr Natasha Sanabria and Dr Sophia Kisting, your support and encouragement is appreciated, thank you.

I would like to acknowledge the Department of Science and Technology, and the National Health Laboratory Services, for the financial support of this research.

I would also like to thank the staff at Mintek's Advanced Materials Division for their assistance with the nanoparticle synthesis and characterization, and the staff at the Wits University Microscopy and Microanalysis Unit for training and assistance on their TEM.

A special thank you to Antoinette Lensink at the University of Pretoria for her assistance on the TEM uptake studies and for making time for me when I was under pressure.

Finally, I would like to thank my supervisor, Prof Mary Gulumian. Thank you for your guidance and all the opportunities you have given me over the years. I am grateful for everything that I have learnt from you.

Contents

Candidate's Declaration ii

Presentations iv

Publications vi

Abstract vii

Acknowledgements ix

Contents x

List of Abbreviations xvi

List of Figures xx

List of Tables xxiv

Chapter 1 - Introduction 1

1.1 Background and goals of the study 1

1.2 Specific goals 2

Chapter 2 - Literature Review 3

2.1 Nanoparticles 3

2.1.1 Types of engineered nanomaterials 4

2.1.1.1 Carbon-based nanomaterials 4

2.1.1.2 Metal-based nanomaterials 4

2.1.1.3 Dendrimers 5

2.1.1.4 Composite nanomaterials 6

2.2 Risk Assessment of Nanoparticles 6

2.2.1 Hazard Identification of Nanomaterials 11

2.2.1.1 Physicochemical Properties 12

2.2.1.2 Surface Activity 12

2.2.1.3 Sterility of nanoparticles 17

2.2.1.4 In vitro testing of nanoparticles 23
2.2.2 Hazard identification of gold nanoparticles 31
2.2.2.1 In vitro toxicity of gold nanoparticles 31
2.2.2.2 Uptake of gold nanoparticles 47
Chapter 3 - Methods 53
3.1 AuNPs used in this study 53
3.1.1 Synthesis of AuNPs 53
3.1.2 Use of different AuNPs 55
3.1.3 Different culture media 55
3.2 Physicochemical Properties 56
3.2.1 Transmission Electron Microscopy 56
3.2.2 Absorbance spectroscopy 56
3.2.3 Zeta potential 56
3.2.4 Effects of AuNPs on pH of culture medium 57
3.2.5 Sterility testing 57
3.2.6 Endotoxin assays 57
3.2.6.1 Calculation of MVD 57
3.2.6.2 LAL Chromogenic Assay 58
3.2.6.3 LAL Gel-clot Assay 59
3.2.6.4 rFC Assay 60
3.2.7 Redox Potential 61
3.3 Surface Activity 61
3.3.1 Electron Spin Resonance 61
3.3.2 8-Isoprostane 62
3.4 *In vitro* Toxicity testing 64

3.4.1 Cell culturing 64
3.4.2 Applicability of existing assay systems to AuNPs 64
3.4.2.1 XTT assay 65
3.4.2.2 LDH assay 65
3.4.2.3 ATP assay 66
3.4.2.4 Colony Forming Efficiency (CFE) Assay 66
3.4.2.5 Impedance Technology 68
3.4.3 Cytotoxicity of AuNPs to BEAS-2B cells 69
3.4.4 Genotoxicity 70
3.5 Intracellular Uptake 71
3.5.1 Applicability of the CytoViva HSI system for label-free assessment of uptake 71
3.5.1.1 Slide preparation 72
3.5.1.2 Dark-field microscopy 73
3.5.1.3 Hyperspectral Imaging (HSI) and Spectral Libraries 73
3.5.1.4 Principal Component Analysis (PCA) 73
3.5.1.5 Spectral Angle Mapper (SAM) 73
3.5.2 Uptake of AuNPs 73
3.5.2.1 Uptake after 2 hours at 37°C and 4°C 74
3.5.2.2 Uptake after 24 hours 74
3.5.3 Assessment of mechanism of uptake of AuNPs into BEAS-2B cells 74
3.5.3.1 Cytotoxicity of inhibitors 74
3.5.3.2 Effect of inhibitors on the uptake of AuNPs 75
3.5.4 Localisation of AuNPs using TEM 76
3.6 Summary of statistics used 77
3.7 Summary of methods 77

Chapter 4 – Results 79
4.1 Physicochemical properties 79
4.1.1 Transmission Electron Microscopy 79
4.1.2 Absorbance spectra 80
4.1.3 Zeta Potential 83
4.1.4 Effect of AuNPs on pH of culture medium 83
4.1.5 Endotoxin assays 85
4.1.5.1 Maximum Valid Dilution (MVD) 85
4.1.5.2 LAL Chromogenic Assay 85
4.1.5.3 LAL Gel-clot Assay 87
4.1.5.4 rFC Assay 88
4.1.6 Effect of AuNPs on Redox Potential of medium 88
4.2 Surface Activity 90
4.2.1 Measurement of Free Radicals 90
4.2.2 8-Isoprostane 92
4.3 *In vitro* toxicity assays 93
4.3.1 Applicability of assay systems to AuNPs 93
4.3.1.1 XTT assay 93
4.3.1.2 LDH assay 95
4.3.1.3 ATP assay 96
4.3.1.4 Colony Forming Efficiency (CFE) assay 98
4.3.1.5 Applicability of Impedance Technology 99
4.3.2 Cytotoxicity of AuNPs in BEAS-2B cells 104
4.3.3 Cytokinesis-block micronucleus (CBMN) assay for assessment of genotoxicity 106
4.4. Uptake of AuNPs 109

4.4.1 Applicability of the CytoViva HSI system for label-free assessment of uptake 109
4.4.1.1 Focal planes.....109
4.4.1.2 Dark-field images of two cell lines 111
4.4.1.3 Spectral profiles of singularly dispersed vs agglomerated AuNPs 113
4.4.1.4 Principal Component Analysis (PCA) 115
4.4.1.5 Representative images of SAM.....117
4.4.2 Uptake of AuNPs into BEAS-2B cells 121
4.4.2.1 Assessment of uptake of AuNPs after 2 hours at 37°C and 4°C.....121
4.4.2.2 Assessment of uptake of AuNPs after 24 hours at 37°C.....124
4.4.3 Mechanism of uptake of AuNPs in BEAS-2B cells 126
4.4.3.1 Cytotoxicity of Inhibitors.....126
4.4.4 Localisation of AuNPs using TEM.....131
Chapter 5 – Discussion.....135
5.1 Physicochemical Properties.....135
5.2 Surface Activity.....138
5.3 Applicability of conventional toxicity assays and the use of label free methodologies in the hazard identification of gold nanoparticles 139
5.4 Effect of AuNPs on cytotoxicity and genotoxicity of BEAS-2B cells.....143
5.5 The use of the CytoViva as a label-free methodology to assess uptake.....145
5.6 Uptake of AuNPs into BEAS-2B cells.....146
Chapter 6 – Conclusions and Recommendations.....151
Chapter 7 – Future Work.....154
Appendices.....156
Appendix A: Ethics Clearance 156
Appendix B: Copyright permission for *Particle and Fibre Toxicology* publication.....157

Appendix C: Copyright permission for *Nanomedicine: Nanotechnology, Biology, and Medicine* publication 162

Appendix D: Copyright permission for *Toxicology and Applied Pharmacology* publication .163

Appendix E: Copyright permission for *Current Nanoscience* publication 164

Appendix F: Permission to use the image shown in Figure 2.3 168

References 169

List of Abbreviations

14 nm AuNPs	14 nm citrate stabilised gold nanoparticles
20 nm AuNPs	20 nm citrate stabilised gold nanoparticles
8-OHdG	8-hydroxydeoxyguanosine
AChE	acetylcholinesterase
AP	activator protein
ARE	antioxidant response element
AM	alveolar macrophages
AU	absorbance units
AuNP	gold nanoparticle
B_0	maximum binding
bis-MPA	poly(2,2-bis(hydroxymethyl)propionic acid
CBMN	cytokinesis-block micronucleus
CI	cell index
CFE	colony forming efficiency
CTAB	cetyltrimethylammonium bromide
CNT	carbon nanotubes
Cyt-B	cytochalasin B
DC	dendritic cells
DCF-DA	dichlorofluorescein diacetate
DIC	differential interference contrast
DLS	dynamic light scattering
DMPO	5,5-Dimethyl-1-pyrroline N-oxide
DPBS	Dulbeccos' phosphate buffered saline
EDTA	ethylenediaminetetraacetic acid
EG	ethylene glycol
ENM	engineered nanomaterials
EO	ethylene oxide
EPA	Environmental Protection Agency

EPR	electron paramagnetic resonance
ESR	electron spin resonance
EU	endotoxin units
F_2-IsoPs	F_2-isoprostanes
FACS	fluorescence-activated cell sorting
FBS	foetal bovine serum
GSH	glutathione
GSSG	oxidised glutathione
GST	glutathione-S-transferase
HSI	hyperspectral imaging
HNE	hydroxynonenal
HO-1	haem oxygenase
IECs	inhibition/enhancement controls
IL	interleukin
ISO	International Organization for Standardization
ISSD	*in vitro* sedimentation, diffusion and dosimetry
JRC	Joint Research Centre
LAL	*Limulus* amebocyte lysate
LDH	lactate dehydrogenase
LMP	lysosomal membrane permeabilisation
LPS	lipopolysaccharides
MAPK	mitogen-activated protein kinase
MDA	malondialdehyde
MDCK	Madin Darby Canine Kidney
MMC	mitomycin C
MN	micronucleus
MTS	3-(4,5-dimethylthiazol-2-yl)-5-(3-carboxymethoxy-phenyl)-2-(4-sulfophenyl)-2H-tetrazolium
MTT	3-(4,5-dimethylthiazol-2-yl)-2,5-diphenyltetrazolium bromide
MVD	maximum valid dilution
MWCNT	multiwalled carbon nanotubes

NAC	N-Acetyl-L-cysteine
NADPH	nicotinamide adenine dinucleotide phosphate
NIOH	National Institute for Occupational Health
NP	nanoparticle
NPB	nucleoplasmic bridges
NSB	non-specific binding
OECD	Organisation for Economic Co-operation and Development
ORP	oxidation-reduction potential
Oxo-dG	7,8-dihydro-oxodeoxyguanine
PAMAM	polyamidoamine
PBMC	peripheral blood mononuclear cells
PEG	polyethylene glycol
PAM AuNPs	14 nm Amine-PEG-liganded gold nanoparticles
PAZ AuNPs	14 nm Azide-PEG-liganded gold nanoparticles
PBtn AuNPs	14 nm Biotin-PEG-liganded gold nanoparticles
PCA	principal component analysis
PCOOH	carboxyl-PEG
PCOOH AuNPs	14 nm Carboxyl-PEG-liganded gold nanoparticles
PDADMAC	poly(diallyldimethylammonium chloride)
PGLSA-OH	polyester
PLL	poly(L-lysine)
PPI	polypropylenimine
PNTA AuNPs	14 nm Nitrilotriacetic acid-PEG gold nanoparticles
pNA	p-nitroaniline
POH AuNPs	14 nm Hydroxyl-PEG gold nanoparticles
PSS	polystyrenesulfonate
PTT	photothermal therapy
PCR	polymerase chain reaction
PVP	poly-(*N*-vinyl)-2-pyrrolidone
QSAR	quantitative structure-activity realtionship
RBC	red blood cell

rFC	recombinant Factor C
RFU	relative fluorescence units
RNS	reactive nitrogen species
ROS	reactive oxygen species
RPT	rabbit pyrogen test
RTCA	Real-Time Cell Analyser
SAL	sterility assurance level
SAM	spectral angle mapper
SCGE	single cell gel electrophoresis
SDS	sodium dodecyl sulfate
SEM	scanning electron microscopy
SERS	surface-enhanced Raman spectroscopy
SOD	superoxide dismutase
SP	single plate
SPB	surface plasmon band
SPR	surface plasmon resonance
SWCNT	single-walled carbon nanotubes
TA	total activity
TEM	transmission electron microscopy
TG	testing guideline
TGF-β	transforming growth factor beta
TNF-α	tumour necrosis factor alpha
UFPs	ultrafine particles
XTT	2,3-bis-(2-methoxy-4-nitro-5-sulfophenyl)-2H-tetrazolium-5-carboxanilide
VNIR	visible and near-infrared
WPMN	Working Party of Manufactured Nanomaterials
WST-1	water soluble tetrazolium

List of Figures

Figure 2.1 Schematic diagram of a dendrimer. 5
Figure 2.2 Schematic diagram of the LAL coagulation pathway and its associated assays, and the pathway of the recombinant Factor C assay. Image is adapted from literature (Abate *et al.* 2017; Iwanaga 2007; Morita *et al.* 1981). 21
Figure 2.3 Diagrammatic representation of the xCELLigence RTCA technology before and after cells are added to the wells. 27
Figure 3.1 Photo of the xCELLigence RTCA system housed in the Toxicology Department at the NIOH. 68
Figure 3.2 Photo of the CytoViva HSI system housed in the Toxicology Department at the NIOH. 72
Figure 4.1 Representative TEM images (A, C, E) and absorbance spectra from 400 nm to 800 nm (B, D, F) of 14 nm AuNPs (top), 20 nm AuNP (bottom). AuNPs were suspended in water (A, B), RPMI culture medium (C, D), or Ham's F12 culture medium (E, F). Scale bars in the TEM images = 100 nm. 81
Figure 4.2 Representative TEM images (A, C) and absorbance spectra from 400 nm to 800 nm (B, D) of POH, PCOOH, PBtn, PNTA, PAZ, and PAM AuNPs (top to bottom). AuNPs were suspended in water (A, B) or RPMI culture medium (C, D) prior to analysis. Scale bars in the TEM images = 100 nm. 82
Figure 4.3 Relative changes in ORP measurements. RPMI culture medium alone was used to zero the electrode and values shown are those relative to the culture medium Error bars reflect the standard deviation. n = 2. 89
Figure 4.4 Representative ESR spectrum across a varying magnetic field (x-axis) of DMPO-OH, showing the expected 1:2:2:1 hyperfine splitting of the peak intensity (y-axis). Black arrows indicate the peaks that are measured to obtain the intensity used to estimate free radical concentration. 90
Figure 4.5 Average intensity readings obtained from ESR measurements. n = 2. Error bars represent standard deviation. * $p < 0.01$ 91
Figure 4.6 Calculated concentrations of known samples (40 pg/ml and 8 pg/ml), either without AuNPs or with 1 nM or 5 nM AuNP spikes. 92

Figure 4.7 Toxicity and interference studies of 14 nm AuNPs using the XTT assay. 94
Figure 4.8 Cytotoxicity of 14 nm AuNPs to BEAS-2B cells using the LDH assay. 95
Figure 4.9 Toxicity and interference studies of 14 nm AuNPs using the ATP assay. 97
Figure 4.10 Percentage relative toxicity of 14 nm AuNPs to MDCK cells, as determined by the CFE assay 98
Figure 4.11 Proliferation curves of (A) BEAS-2B cells, and (B) CHO cells, seeded at a range of concentrations. 100
Figure 4.12 Cell index of BEAS-2B cells showing toxicity of 500 µM hydrogen peroxide and effect of 5 nM 14 nm AuNPs in medium on cell index. 101
Figure 4.13 Normalised cell index of cells treated with AuNPs. 103
Figure 4.14 Cytotoxicity, as represented by normalised cell index, of BEAS-2B cells treated with AuNPs for 24 hours. Cells were allowed to proliferate for 24 hours prior to treatment and the cell index was normalised at the point of treatment. 105
Figure 4.15 Representative images obtained from the CBMN assay. 107
Figure 4.16 Frequencies of (A) micronuclei, and (B) nucleoplasmic bridges per 1000 binucleated cells. No statistically significant differences were observed. 108
Figure 4.17 Dark-field image at 100x magnification of BEAS-2B cells incubated with 14 nm AuNPs for 1 hr to demonstrate the observation of internatised AuNPs through various focal planes within the cell. Scale bars = 5 µm. 110
Figure 4.18 Dark-field images of BEAS-2B cells incubated with AuNPs. Dark-field images were captured at 60x magnification of BEAS-2B cells incubated with either (A) 14 nm or (B) 20 nm AuNPs for 1 hr, 4 hrs, or 6 hrs. 111
Figure 4.19 Dark-field images of CHO cells incubated with AuNPs. Dark-field images were captured at 60x magnification of CHO cells incubated with either (A) 14 nm or (B) 20 nm AuNPs for 1 hr, 4 hrs, or 6 hrs. 112
Figure 4.20 Spectral profiles of 14 nm and 20 nm AuNPs. 114
Figure 4.21 PCA analysis of 14 nm and 20 nm AuNP spectra. 116
Figure 4.22 Representative images of the SAM analyses. 118
Figure 4.23 Spectral profiles of 14 nm AuNPs following cellular uptake. 119
Figure 4.24 Spectral profiles of 20 nm AuNPs following cellular uptake. 120

Figure 4.25 Dark field images of BEAS-2B cells incubated with AuNPs for 2 hours at 37°C. Cells were treated at 1 nM AuNP. Dark-field images were captured at 60x magnification. Scale bars = 20 µm.....122
Figure 4.26 Dark field images of BEAS-2B cells incubated with AuNPs for 2 hours at 4°C. Cells were pre-incubated at 4°C for 30 mins prior to addition of AuNPs at 1 nM AuNP. Dark-field images were captured at 60x magnification. Scale bars = 20 µm.....123
Figure 4.27 Dark field images of BEAS-2B cells incubated with AuNPs for 24 hours at 37°C. Cells were treated at 1 nM AuNP. Dark-field images were captured at 60x magnification. Scale bars = 20 µm.....125
Figure 4.28 Cytotoxicity of genistein to BEAS-2B cells, represented by normalised cell index. BEAS-2B cells were treated with a range of concentrations from 25 µM to 300 µM. (A) CI values shown prior to treatment and for 24 hours after addition of inhibitor; (B) CI shown for approximately 2 and a half hours after treatment. Each concentration was run in triplicate; each figure is a representative image of one of two independent experiments. 127
Figure 4.29 Cytotoxicity of chlorpromazine, represented by normalised cell index. 128
Figure 4.30 Box and whisker chart showing the distribution of data from the inhibition of uptake experiments of (A) 14 nm AuNPs, (B) 20 nm AuNPs, and (C) PCOOH AuNPs. The box represents the interquartile range (IQR), whilst the whiskers represent 1.5 x IQR. For simplicity, only the maximum outlier is shown as ✳. Data obtained from 2 replicates of 2 independent experiments, minimum 180 cells analysed. 130
Figure 4.31 Representative TEM images of BEAS-2B cells treated with 14 nm AuNPs for 2 hours. Top image shows a single cell, whilst magnification of regions within the cell are shown in the remaining images (Scale bar = 0.5 µm) and arrows indicate nanoparticles either singularly dispersed or in small clusters. 132
Figure 4.32 Representative TEM images of BEAS-2B cells treated with 20 nm AuNPs for 2 hours. Top image shows a single cell, whilst magnification of regions within the cell are shown in the remaining images (Scale bar = 0.5 µm) and arrows indicate nanoparticles either singularly dispersed or in small clusters. 133
Figure 4.33 Representative TEM images of BEAS-2B cells treated with PCOOH AuNPs for 2 hours. Top image shows a single cell, whilst magnification of regions within the cell are shown in

the remaining images (Scale bar = 0.5 μm) and arrows indicate nanoparticles either singularly dispersed or in small clusters. 134

List of Tables

Table 2.1 List of the nanomaterials tested in the OECD WPMN Sponsorship Programme and their potential commercial applications. 9
Table 2.2 Summary of methodologies used for hazard identification of nanoparticles 30
Table 2.3 Summary of *in vitro* cytotoxicity of spherical gold nanoparticles. 32
Table 3.1 Abbreviations and structures of functional groups 54
Table 3.2 Volumes of reagents used in the 8-Isoprostane EIA assay 63
Table 3.3 Concentrations of 14 nm AuNPs used in the interlaboratory CFE study. 67
Table 3.4 Summary of methods used in this study 78
Table 4.1 Average particle size in milli-Q water, RPMI culture medium, and Ham's F12 cuture medium, as determined by TEM 79
Table 4.2 Physicochemical properties of the AuNPs 84
Table 4.3 Maximum valid dilution (MVD) values for each assay 85
Table 4.4 Average absorbance at 405 nm of particle controls and blank wells 86
Table 4.5 Calculated endotoxin concentration (EU/ml) 86
Table 4.6 Calculated geometric mean endpoints of endotoxin in AuNP suspension. 87
Table 4.7 Calculated endotoxin concentrations. Spiked samples at 0.5 EU/ml endotoxin standard added to the AuNP suspension 88
Table 4.8 Calculated Replication Index (RI) of the treated samples in the CBMN assay 106

Chapter 1 - Introduction

1.1 Background and goals of the study

Nanomaterials are increasingly developed for various applications due to their unique properties. With these developments comes an increase in the potential human and environmental exposures to these nanomaterials. It is therefore essential to ensure their safe production and use as well as protect the general environment. In order to establish appropriate regulations for nanomaterials, risk assessment needs to be conducted. The first step of this process is the hazard characterisation of these nanomaterials, which aims to identify the properties that may make them toxic and investigates the mechanisms involved in this toxicity.

There have been a number of international collaborative projects that have been established to investigate not only the hazard, but also all aspects of the risk assessment, of nanomaterials. One such program was initiated by the Organisation for Economic Co-operation and Development (OECD), namely, the Working Party of Manufactured Nanomaterials (WPMN). This program identified a number of commercially relevant nanomaterials, following which they were tested by various international research laboratories for their physicochemical properties, mammalian toxicity, and environmental fate and toxicity. The main goal of this program was to assess the applicability of various OECD testing guidelines to nanomaterials to ensure a high-quality, science-based, and harmonised approach to the risk assessment of nanomaterials. South Africa was involved in this collaborative program and proposed the testing of gold nanoparticles, which was unanimously accepted and which forms the foundation of the work presented in this thesis.

Although a number of toxicity studies on gold nanoparticles have been conducted, at times there was apparent contradiction in the results and therefore a clear conclusion on the toxicity of gold nanoparticles could not be established. One possible explanation for these contradictory results was that the assays implemented for the testing of chemicals could not be applicable for the testing of

nanomaterials. Reasons for this lack of applicability of these test systems to gold nanomaterials would include their potential surface activity and their optical properties, which will increase the possibility of interference with a number of assay systems.

Henceforth, the following is the overall aim of this study:

> To determine the interference of gold nanoparticles in conventionally used *in vitro* test systems with the ultimate goal of establishing their applicability to the hazard identification of gold nanoparticles and thus contributing to the OECD WPMN programme for toxicity testing of nanomaterials.

1.2 Specific goals

The following specific goals were set for this study to satisfy the specified aim:

1. To characterise the gold nanoparticles used in this study and describe their physicochemical properties.
2. To test for possible interference by gold nanoparticles in different *in vitro* test systems and their applicability in assessing their sterility, surface activity, toxicity, and intracellular uptake.
3. To propose a label-free system for testing the toxicity of gold nanoparticles including impedance technology and colony forming efficiency (CFE) assay.
4. To propose a label-free system for assessing the cellular uptake of gold nanoparticles including hyperspectral imaging.
5. To investigate of the effects of different physicochemical properties including size, surface charge and type of functional groups on the surface activity, toxicity, genotoxicity and cellular internalization as well as the mechanisms involved in the internalisation of gold nanoparticles.
6. To propose reliable test systems for the hazard identification for nanomaterials.

Chapter 2 - Literature Review

2.1 Nanoparticles

The International Organization for Standardization (ISO) defines nanotechnologies as the design, characterization, and production of objects on a nanometer scale by controlling their shape and size. Their document, ISO/TS 80004-2, provides a list of terms and definitions related to nano-objects; where nanoscale is a length range between 1 nm and 100 nm, and therefore nano-objects have at least one dimension in the nanoscale range (ISO 2015). Further classification of nano-objects describes nanoplates as only having one external dimension at nanoscale; nano-fibres as having two dimensions in the nanoscale; and nanoparticles (NPs) as having all three dimensions in the nanoscale. Nano-objects can also be classified based on whether they are incidental nano-objects which are generated as an unintentional by-product of a process; engineered nano-objects which are designed for a specific purpose or function; or manufactured nano-objects which are produced to have selected properties or composition. The term ultrafine particles (UFPs) is used for airborne particulate matter with an aerodynamic diameter smaller than 100 nm, and is frequently specified as PM0.1 (ISO 2015). The commonly used term nanomaterial refers to nano-objects as defined above, or materials having internal or surface structure at nanoscale (OECD 2018a).

The physicochemical properties of nanomaterials are dependent on their size (Mitchell and Tojeira 2016) where their unique properties are partly due to their higher surface-to-volume ratio which changes the manner in which they can interact with their environment, and partly because of quantum effects in the nano size range. The interesting properties that nanomaterials exhibit has led to research and development into vast array of potential applications, including water remediation (Baruah *et al.* 2016), screen printed sensors and biosensors (Trojanowicz 2016), solar collectors (Hussein 2016), phytonanotechnology (Wang *et al.* 2016), 3-dimensional photonic materials (Böttner *et al.* 2016), and medical applications (Aguilar *et al.* 2010).

2.1.1 Types of engineered nanomaterials

According to the US Environmental Protection Agency (EPA), most nanomaterials fall into one of four broad categories, namely (1) carbon-based, (2) metal-based, (3) dendrimers, and (4) composites (EPA 2007).

2.1.1.1 Carbon-based nanomaterials

Carbon-based nanomaterials are commonly hollow spheres and ellipsoids, known as fullerenes, or cylindrical tubes known as carbon nanotubes (CNT) (EPA 2007). CNTs comprise exclusively of carbon and can either be single-walled carbon nanotubes (SWCNT) or multiwalled carbon nanotubes (MWCNT) (Donaldson *et al.* 2006). SWCNT can be imagined as a sheet of graphite rolled to form seamless cylinder which is generally between 0.7 nm and 3 nm in diameter; whilst MWCNTs consist of a number of SWCNTs inside one another and generally range between 10 nm and 200 nm in diameter (Donaldson *et al.* 2006); and the length of CNTs can vary but are generally tens of microns long. The structure of CNTs result in a change in the electronic "density of states" which gives CNTs their unique electronic characteristics; as well as changes in mechanical properties such as strength and stability combined with low density (Ajayan and Zhou 2001). These unique properties have led to their development for various applications.

2.1.1.2 Metal-based nanomaterials

This category includes metal-based nanomaterials such as quantum dots, nanosilver and nanogold, and metal oxide nanomaterials (EPA 2007). In addition, metals are able to form oxide compounds that can have a variety of structural geometries and can have either metallic, semiconductor, or insulator properties (Fernández-García and Rodriguez 2011). Some of the commonly synthesized metal oxide nanomaterials are aluminium oxides (Al_2O_3), magnesium oxide (MgO), zirconium dioxide (ZrO_2), cerium oxide (CeO_2) and cerium-containing mixed-metal oxides, titanium dioxide (TiO_2) (Fernández-García and Rodriguez 2011). Aluminium oxide (Al_2O_3) nanomaterials are used as a catalyst component (Fernández-García and Rodriguez 2011) and in industrial processes, and has been

shown to have potential uses to increase the compressive strength of concrete (Nazari *et al.* 2010), and as bioaffinity support for drug delivery (Ansari and Husain 2011).

2.1.1.3 Dendrimers

Dendrimers are polymers consisting of branched units that have numerous chain ends, a schematic diagram of which is shown Figure 2.1 (Roveda Júnior and Franco 2013). Their characteristics can be controlled through the modification of the core, the number and type of the repetitive branched units, and the terminal end groups (Scott *et al.* 2005). Commonly used dendrimers include polyamidoamine (PAMAM), poly(L-lysine) (PLL), polyester (PGLSA-OH), polypropylenimine (PPI), and poly(2,2-bis(hydroxymethyl)propionic acid (bis-MPA); and many of these are available commercially (Mintzer and Grinstaff 2011). A key advantage of dendrimers is the ability to manipulate their surface through conjugation with molecules of interest, therefore making them useful for catalysis and medical applications (EPA 2007; Roveda Júnior and Franco 2013).

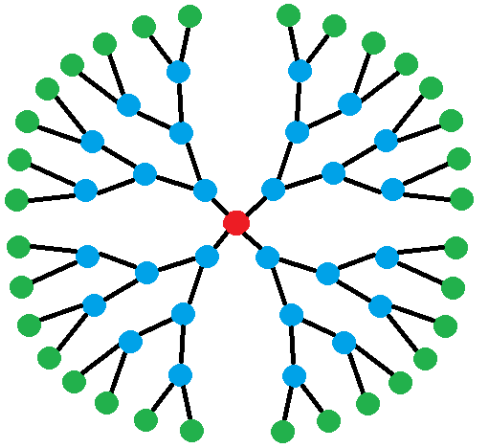

Figure 2.1 Schematic diagram of a dendrimer.
The red dot represents the core, the blue dots represent the interior branching points, and the green dots represent the surface groups (based on image from Roveda Júnior and Franco, 2013).

2.1.1.4 Composite nanomaterials

Composites combine nanoparticles with other nanoparticles or larger materials (EPA 2007). There are numerous potential applications of nanocomposites including improved or flexible batteries, production of stronger polymers, and medical applications (Boysen 2018). For example, silicon-carbon nano-composites have been developed as anodes for lithium ion batteries thereby exhibiting enhanced electrochemical properties (Wang *et al.* 2013; Wang and Fan 2013), whilst nanoporous cellulose paper can be used for flexible, ultrathin batteries (Pushparaj *et al.* 2007). In terms of developments in nanomedicine, there are numerous polymer nanocomposites that are candidates for use in tissue engineering and drug delivery (Armentano *et al.* 2010).

2.2 Risk Assessment of Nanoparticles

With these recent developments in nanotechnologies, there is an increase in the potential exposure of researchers and workers to nanomaterials during their synthesis, and exposure of the general public to consumer products containing these nanomaterials. The manufacture, marketing, and use of nanomaterials have preceded the establishment of appropriate regulations. A dilemma in the regulations of nanomaterials may exist because there is a basis for concern that nanomaterials may cause harm, however too little is known to establish an appropriate risk management regime. There has been a heavy reliance on existing regulations which were designed to manage risks of non-nanoscale materials and do not distinguish between these larger materials and their nanoscale counterparts (Lee and Stokes 2009). Currently limited occupational guidelines exist for nanomaterials and generally they are substantially lower than those for their non-nanoscale counterparts (Hussain *et al.* 2015).

In order to establish appropriate regulations for nanomaterials, risk assessment needs to be conducted. The steps for risk assessment of nanomaterials are the same as those for chemicals, namely hazard identification, hazard characterisation, exposure assessment, and risk characterisation. Hazard identification and characterisation involves the identification of nanomaterial

properties that may be hazardous to health and defines the dose-response and mechanisms of toxicity. Exposure assessment requires the detection and measurement of the nanomaterial in the workplace and in the general environment; however levels are generally higher in an occupational setting due to certain operations and handling of large quantities, than in an environmental setting (Savolainen *et al.* 2010). Risk characterisation is the final step of risk assessment which then combines these three steps to determine the likelihood of an adverse health effect at a given exposure level.

As the field of nanotechnology develops, studies investigating the toxicity of nanomaterials are critically important for hazard identification and in turn in the risk assessment mentioned above. The unique and beneficial properties of nanomaterials, such as their large surface area to mass ratio, increased surface reactivity, and altered physicochemical properties, may also alter the toxicity of these particles (Savolainen *et al.* 2010), necessitating the need for hazard identification specifically of nanomaterials. In addition, the physicochemical characteristics of nanoparticles, including any modifications to their surfaces, will also impact their biological interactions and therefore influence cellular uptake, gene expression, and toxicity (Albanese *et al.* 2012). A tiered strategy has been proposed for toxicity testing of engineered nanomaterials (Savolainen *et al.* 2010). In this approach, toxicity testing should begin with and in depth physicochemical characterization of the nanomaterials. Once characterized, the particles should undergo carefully selected *in vitro* toxicity tests of relevant endpoints. Positive and consistent results from the *in vitro* studies would lead to higher tier *in vivo* testing. Data obtained from these tiers would aid hazard identification and characterisation.

A number of international collaborative projects and platforms have been formed to assess the risk of nanomaterials. Examples of such are the NANOSOLUTIONS consortium where the aim is to develop a classification system for the safety of engineered nanomaterials (ENM) (https://nanosolutionsfp7.com/); the MARINA project which aims to develop and validate risk management models for

nanomaterials (http://www.marina-fp7.eu/); and GoodNanoGuide which provides an Internet-based platform for exchanging information on handling nanomaterials in an occupational setting (https://nanohub.org/groups/gng). One of the earlier programmes was established through the Organisation for Economic Co-operation and Development (OECD) in 2006 (http://www.oecd.org/science/nanosafety/). The OECD's Environment, Health and Safety (EHS) Programme established a Working Party of Manufactured Nanomaterials (WPMN) that addresses different aspects of the safety testing and risk assessment of manufactured nanomaterials.

The focus of the WPMN is on human health and environmental safety, and aims to ensure that the approach to the risk assessment of nanomaterials, including the hazard and exposure assessment, is of a high, science-based, and internationally harmonised standard (OECD 2011). In 2007, their "Sponsorship Programme for the Testing of Manufactured Nanomaterials" was launched where a priority list of commercially relevant nanomaterials was identified for the programme (list shown in Table 2.1), following which these were tested for their physicochemical properties, mammalian toxicity, and environmental fate and toxicity. The goal of the testing programme was to assess the applicability of existing testing guidelines to the testing of nanomaterials, and to provide information on the intrinsic properties of engineered nanomaterials (OECD 2015).

Table 2.1 List of the nanomaterials tested in the OECD WPMN Sponsorship Programme and their potential commercial applications.
(Baughman *et al.* 2002; Georgakilas *et al.* 2015; OECD 2018b).

Type of material	**Application**
Fullerenes (C60)	Cosmetics; photovoltaic cells; antioxidant
Single Wall Carbon Nanotubes (SWCNTs)	Improved properties of composite materials e.g. plastics; electrochemical devices; electronic devices
Multi Wall Carbon Nanotubes (MWCNTs)	Improved properties of composite materials e.g. plastics; electrochemical devices; electronic devices
Silver nanoparticles	Medical devices; food, hygiene and cosmetic products; household appliances; shoes and textiles; paints; electronics; photography; water filtration and purification
Titanium dioxide	Cosmetics and sunscreens; household products; paint; printing ink; plastics.
Cerium oxide	Polish for stone, ceramic and glass; self-cleaning ovens; skin and solar applications due to its UV-light absorbance.
Zinc oxide	Medicine; UV filters; paints
Silicon dioxide	Additive for rubber and plastic; strengthening in concrete; drug delivery in biomedical applications.
Dendrimers	DNA or drug delivery in medical applications.
Nanoclays	Plastic films on consumer good to reduce oxidisation; aviation and auto industries dues to their impact and strength of materials.
Gold nanoparticles	Medical and cell imaging; drug delivery and biomedical diagnostics.

South Africa was involved in the program and contributed to the testing program on the gold nanoparticles (AuNPs) (former JRC code NM 330, renamed to

JRCNM03300a) through a collaboration which included the National Institute for Occupational Health (NIOH), Mintek, and the University of Johannesburg (JRC 2016; OECD 2015). Colloidal gold, a suspension of gold nanoparticles (AuNPs) in fluid, was used to make ruby-coloured glass and ceramics as far back as the 5th or 4th century B.C., and in the Middle Ages it was used as a treatment of various diseases (Daniel and Astruc 2004). Nowadays, AuNPs have a wide range of potential applications due to the unique electronic, optical, and thermal properties. Their excellent conducting capability and high surface-to-volume ratio lends itself to AuNP-based electrochemical sensing and electro-catalytic systems (Guo and Wang 2007); whilst their optical and photothermal properties allow for applications such as cancer imaging and spectroscopic detection, and photothermal therapy (PTT) (Huang and El-Sayed 2010; Kodiha *et al.* 2015). In addition, their tunable size and easily modified surface make them appealing candidates for biomedical applications (Fratoddi *et al.* 2011) which has led to their development as therapeutic agents for use in the delivery of DNA vaccines (Noh *et al.* 2007), molecular imaging (Chanda *et al.* 2009), biological sensing and imaging applications (Murphy *et al.* 2008), and drug delivery (Acharya and Hill 2014).

The optical properties of AuNPs differ substantially from their non-nanoscale counterparts due to quantum size effects resulting in a characteristic collective oscillation frequency of the plasma resonance, known as surface plasmon resonance (SPR). The SPR induces a strong absorption band (surface plasmon band – SPB) in the visible region, which can be measured with a UV-Vis spectrophotometer. This absorption can be observed around 520 – 530 nm for AuNPs of diameter 5-20 nm, and is the origin of the deep-red colour of AuNPs in water (Daniel and Astruc 2004; Ghosh and Pal 2007; Huang *et al.* 2010; Huang and El-Sayed 2010). As the core diameter of the AuNPs increases, the SPB maximum wavelength increases, up to a wavelength of 575 nm for 99 nm AuNPs (Daniel and Astruc 2004). The SPB is dependent on both the size and the shape of the nanoparticle, allowing for optical tunability in their development for use in biological imaging (Jain *et al.* 2006).

The shape, size, and surface chemistry of the AuNPs will be determined by the conditions of synthesis. In the 20th century, a number of methods were established for the synthesis of gold nanoparticles, many of which are based on the reduction of gold salt in aqueous, organic, or in both phases (Daniel and Astruc 2004; Guo and Wang 2007). The high surface energy of AuNPs make them very reactive and prone to aggregation and therefore the AuNPs need to be stabilised during synthesis, commonly by the presence of a stabiliser, such as citrate, that binds to their surface (Guo and Wang 2007). Alternatively, the addition of surface-bound ligand molecules is frequently used to improve stability of the particles; in particular, polyethylene glycol (PEG) is used due to its simple structure and chemical stability (Sperling and Parak 2010). PEGylation of nanoparticles have also been shown to inhibit protein adsorption due to steric hindrance, resulting in less recognition by phagocytes and increasing the efficiency of nanomaterial drug delivery systems (Vonarbourg *et al.* 2006). Therefore PEG modification is used extensively in therapeutic nanoparticle design to promote prolonged blood circulation time of the nanoparticles (Cruje and Chithrani 2015). The brief of the present study is to investigate the applicability of OECD TGs and non-TGs for the assessment of AuNPs

2.2.1 Hazard Identification of Nanomaterials

The OECD WPMN Testing Programme was part of the hazard identification branch of risk assessment. The aims of the programme included the review of both OECD Test Guidelines (TGs) and non-TG *in vitro* assays, and to verify the applicability of the assays for nanomaterial testing, recognise the limitations of each assay, and to identify further issues that may need to be addressed. The recommendation from the Testing Programme was that the OECD Testing Guidelines (TG) can be applied to manufactured nanomaterials however they should be adapted where relevant to take into consideration the unique properties of the nanomaterial under study (OECD 2018c)

2.2.1.1 Physicochemical Properties

The suitable characterisation of nanomaterials forms an essential part of hazard identification prior to toxicity testing. Parameters assessed by the OECD WPMN Testing Programme included chemical composition, aggregation/agglomeration, particle size distribution, crystalline phase, dustiness, specific surface area, water solubility/dispersibility, zeta potential, photocatalytic activity, porosity, redox potential, crystallite size, and surface chemistry. Techniques such as Transmission electron microscopy (TEM), scanning electron microscopy (SEM), and dynamic light scattering (DLS) can be used to measured aggregation/agglomeration and particle size distribution. Laser-Doppler electrophoresis, electrophoretic light scattering, or photon correlation spectroscopy can measure zeta potential. Oxidation-reduction potential (ORP or redox potential) is a measure of the tendency of a substance to mediate redox reactions (Striggow 2017) and can be evaluated using potentiometry or oxygen detection. Knowledge of these physicochemical properties of the nanomaterials is essential since this will influence the toxicity of the nanomaterial as these properties will effect interactions of the nanomaterial with cellular components to which they are exposed (Shin *et al.* 2015). The evaluation performed on the results of the OECD WPMN Testing Programme found that most parameters have one or more suitable methods, however most of the methods have not been standardised (OECD 2016a).

2.2.1.2 Surface Activity

The radical formation potential of nanoparticles was included in the OECD WPMN Testing Programme and the presence of free radicals or oxidative groups on the surface of nanoparticles can be detected by electron paramagnetic resonance (EPR)/ electron spin resonance (ESR) (Knaapen *et al.* 2004). In addition, although engineered nanomaterials and the assessment of their toxicity may be emerging field, particle toxicology investigating UFPs is well established and has been shown to induce inflammation and oxidative stress (Madl *et al.* 2014). UFPs have been shown to induce oxidative stress and mitochondrial damage (Li *et al.* 2003; Xia *et al.* 2006). The generation of reactive oxygen

species (ROS) plays an important role in the ability of these particles to induce injury (Nel *et al.* 2006; Xia *et al.* 2006). Incidental particles have been shown to activate both alveolar macrophages (AM) and neutrophils in the lung, resulting in induction of ROS via both the NADPH oxidase system and phagocytic oxidative burst and inflammation (Knaapen *et al.* 2004). Incidental particles have also been shown to induce reactive nitrogen species (RNS) in the lung (Castranova *et al.* 1998; Manke *et al.* 2013). Therefore, ROS generation and oxidative stress provides a good paradigm for nanoparticle toxicity (Nel *et al.* 2006; Xia *et al.* 2006).

Under normal physiological conditions, there is a balance between levels of oxidized and reduced species within a cell resulting in an overall reduced intracellular state (Burello and Worth 2011). The presence of excessive oxidizing substances can cause an imbalance between the generation of ROS, including the superoxide anion ($O_2^{\cdot -}$), hydrogen peroxide (H_2O_2), and the hydroxyl radical ($OH^{\cdot}$) formed by the partial reduction of oxygen, and the biochemical mechanisms that neutralize and repair the damage caused by reactive intermediates. This is known as oxidative stress and results in damage to nucleic acids, proteins and lipids (Madl *et al.* 2014; Ray *et al.* 2012).

Nanoparticle-induced oxidative stress can result from the intrinsic properties of nanoparticles, or from extrinsic nanoparticle-cellular interactions (Madl *et al.* 2014). The intrinsic physicochemical properties of nanoparticles can result in ROS generation from the presence of transition metals such as copper, chromium, and vanadium, either as metal-based nanoparticles or as metal contaminants, which can produce hydroxyl radicals via Fenton-like and Haber-Weiss reactions (Madl *et al.* 2014; Manke *et al.* 2013). The Fenton reaction involves the oxidation of iron(II) by hydrogen peroxide to form iron(III), hydroxide ion, and a hydroxyl radical, as shown in the equation (Pereira *et al.* 2012):

$$Fe^{2+} + H_2O_2 \rightarrow Fe^{3+} + OH^- + OH^{\cdot}$$

Whereas Fenton-like reactions involve other transition metal ions such as Fe3+, Co2+, Mn2+ and Cu2+ in place of the iron(II), such as the following examples (Pereira *et al.* 2012; Prousek 2007):

$$Fe^{3+} + H_2O_2 \rightarrow Fe^{2+} + HO_2^{\cdot} + H^+$$
$$Cr(IV) + H_2O_2 \rightarrow Cr(V) + OH^{\cdot} + OH^-$$

Haber-Weiss reactions involve the generation of hydroxyl radicals from superoxide and hydrogen peroxide, as follows (Kehrer 2000):

$$O_2^{\cdot -} + H_2O_2 \rightarrow O_2 + OH^- + OH^{\cdot}$$

Alternatively, nanoparticle surface activity such as the presence of relatively stable free radical intermediates or redox active groups, such as semiquinone-radicals, can be responsible for intrinsic oxidant-generating properties of nanoparticles (Khalili Fard *et al.* 2015; Madl *et al.* 2014).

On the other hand, extrinsic nanoparticle-cellular interactions result in endogenous generation of ROS through mitochondrial respiration, inflammatory responses, and peroxisomes (Manke *et al.* 2013). Under normal conditions for ATP generation, the mitochondrial electron-transport chain produces small amounts of superoxide radicals; whereas under cellular stress and ATP depletion, excess superoxide radical causes the release of free iron (FeII) and the formation of the highly reactive hydroxyl radical through Haber-Weiss reactions (Milne *et al.* 2011). Inflammatory responses by phagocytic cells can result in an oxidative burst and the production of ROS as a defence mechanism against pathogens (Milne *et al.* 2011). Finally, peroxisomes are cytoplasmic organelles responsible for various metabolic functions which are known to produce hydrogen peroxide and/or superoxide anions (Milne *et al.* 2011).

A hierarchical oxidative stress model offers an explanation for the differences between minor oxidative stress that triggers antioxidant protections, and severe

oxidative stress that occurs at higher levels that results in cellular injury and death (Nel *et al.* 2006). Under normal conditions, ROS are generated at low levels and are neutralised by glutathione (GSH) and antioxidant enzymes. Excessive ROS production leads to a depletion of GSH whilst oxidised glutathione (GSSG) accumulates. At these low levels of oxidative stress, protective antioxidant and detoxification enzymes such as haem oxygenase (HO-1), glutathione-S-transferase (GST), NADPH quinine oxidoreductase, catalase, superoxide dismutase (SOD), and glutathione peroxidase, are expressed by the cells. These enzymes are under the control of the transcription factor Nrf-2 which acts via the antioxidant response element (ARE) in their promoters (Madl *et al.* 2014; Nel *et al.* 2006).

At an intermediate level of oxidative stress, pro-inflammatory responses are induced by the activation of redox-sensitive signalling pathways which initiate the expression of cytokines, chemokines, adhesion molecules, and transcription factors influencing a range of cellular responses such as proliferation, metastasis, cell growth, apoptosis, survival, and inflammation (Manke *et al.* 2013). One of these signalling pathways involves NF-κB, which induces the transcription of proinflammatory mediators such as tumour necrosis factor alpha (TNF-α), interleukin (IL)-1β, and transforming growth factor beta (TGF-β) which have been shown to be involved in the pathogenesis of fibrosis (Manke *et al.* 2013). The transcription factor Activator Protein (AP)-1 is induced in response to oxidants and is responsible for regulation of cell proliferation, differentiation and apoptosis, and thereby influences carcinogenesis (Manke *et al.* 2013). The mitogen-activated protein kinase (MAPK) cascade is also activated by oxidative stress and influences a range of cellular responses and gene expression (Manke *et al.* 2013).

At high levels of oxidative stress, ROS can potentially damage cellular macromolecules including lipids, nuclei acids, and proteins (Manke *et al.* 2013). Lipids are a major target for free radical attack. The destruction of membrane phospholipids is known as lipid peroxidation and is caused by ROS that can also

easily remove a hydrogen from a polyunsaturated fatty acid which results in a lipid radical (L˙). This, in turn, reacts with molecular oxygen to form lipid peroxyl radicals (LOO˙) which are strong oxidizing species that then convert a number of membrane phospholipids into unstable hydroperoxides that fragment into small products and resulting in a chain reaction of damage (Farber 1994). These processes result in damage to ionic channels, membrane transport proteins, increased permeability of the lipid bilayer, and possibly form biologically active isoprostanes or lipid hydroperoxides that affect apoptotic signalling pathways (Kehrer 2000). Isoprostanes are generated non-enzymatically by auto-oxidation, predominantly of arachidonic acid, and, since they contain f-type prostane rings and comprise of a number of isomers, and are termed F_2-isoprostanes (F_2-IsoPs). F_2-IsoPs are widely used as a biomarker of endogenous lipid peroxidation and oxidative stress, as they are stable and detectable in all humans tissues and biological fluids (Milne *et al.* 2011).

ROS are known to have a genotoxic effect, thereby making them possible carcinogens (Knaapen 2004). Due to the physicochemical properties of particles, it has been necessary to differentiate between primary genotoxicity, which may be caused by the intrinsic surface properties of the particles, transition metals, intracellular iron, and lipid peroxidation; and secondary genotoxicity caused by excessive and persistent formation of ROS following inflammation (Schins 2002). ROS-mediated DNA damage can occur through oxidative damage to bases, single- and double-stranded breaks, or via lipid peroxidation-mediated adducts such as malondialdehyde (MDA) and hydroxynonenal (HNE) (Schins 2002; Slupphaug *et al.* 2003). This damage can lead to structural alterations of the DNA for example base pair mutations, deletions or insertions (Knaapen *et al.* 2004). The guanine base is sensitive to oxidation and therefore the product of that oxidation, 8-hydroxydeoxyguanosine (8-OHdG), can be used as a biomarker for oxidative injury (Kehrer 2000). Although there are a number of DNA repair mechanisms are present in cells, if the oxidised bases are not effectively repaired, they can cause functional problems that can eventually result in the development of cancer (Kehrer 2000).

Although oxidation of proteins can occur, they generally tend to denature and are then removed (Kehrer 2000). However, ROS is known to affect cell signalling pathways through the formation of protein-protein disulphide linkages, protein-gluthathione mixed disulphide linkages, and through alterations of protein-protein interactions (Kehrer 2000)

Recently, more detailed upstream intracellular events have emerged to explain toxicity, or lack thereof, of nanoparticles based on their ability to cause lysosomal membrane permeabilisation (LMP) (Bunderson-Schelvan *et al.* 2016). Following phagocytosis of particles and the formation of phagolysosomes, the contents of the lysosome are degraded through hydrolytic enzymes in an acidic environment. However, if the particles are able to cause permeabilisation of the phagolysosomal membrane, then the degradative lysosomal contents are released, causing inflammation, mitochondrial ROS production and cell death. The theory suggests that particle induced toxicity is dependent on this initial LMP event.

2.2.1.3 Sterility of nanoparticles

Although not addressed in the OECD WPMN, the sterility and the presence of endotoxins can also affect the hazard identification of nanomaterials, as this contamination can elicit an immune response, and therefore sterility of the nanomaterials should be addressed prior to toxicity testing (Li and Boraschi 2016; Oostingh *et al.* 2011). In addition, endotoxin contamination may interfere with the assessment of the toxicity or benefits of the nanoparticles (Vallhov *et al.* 2006).

2.2.1.3.1 Sterilization techniques

Any medical applications of nanomaterials would require the formulation, in addition to being non-toxic, to be sterile and apyrogenic. Sterility refers to the absence of viable microorganisms such as bacteria, fungi and mould, for which the current accepted sterility assurance level (SAL) is set at 10^{-6} i.e. not more than one viable microorganism in one million parts of final product is allowed (von Woedtke and Kramer 2008). The applicability of various methodologies for sterilization of nanomaterials has been reviewed (Vetten *et al.* 2014). These

methodologies include filtration, autoclaving and irradiation, as well as formaldehyde, ethylene oxide (EO) and gas plasma treatments. The sterilization methodologies discussed have been shown, where tested, to be effective in the removal or destruction of microbial contamination. These standardized methodologies are however frequently shown to alter the physicochemical properties of NPs, the stability of the attached drug, the drug-release profiles, and the toxicity of the sterilized NPs.

Sterile filtration of nanomaterial suspensions through a 0.22 μm membrane filter has been suggested as a preferable option to remove bacterial contamination, as it does not appear to adversely affect the nanoparticles. However, this technique can only be used if the nanoparticles are small enough to pass through the filter without clogging which would result in decreased concentration of the filtrate. Other techniques such as autoclaving frequently results in the aggregation of the nanomaterials and can induce changes in their biological activities; whilst irradiation and gas plasma techniques may affect physicochemical properties of the nanomaterials. The limited information available on formaldehyde, EO and gas plasma techniques suggest that they should not be used due to either their toxicity or their ability to alter the properties of the drug-NP system. It is therefore of vital importance that the toxicity and functionality of the NPs following sterilization be assessed. From all the sterilization methodologies listed, no single process can equally be applied to all NPs and it is recommended that each NP-drug system be validated individually (Vetten *et al.* 2014).

In addition to microorganism contamination, endotoxin contamination should also be considered. Endotoxins are lipopolysaccharides (LPS) that originate from the cell membrane of Gram-negative bacteria, which are capable of stimulating a variety of pathophysiological effects such as pyrogenic reactions (fever), tissue injury and death (Magalhaes *et al.* 2007). These adverse effects are caused by the activation of the immune system by endotoxins, resulting in the release of proinflammatory mediators by monocytes and macrophages (Magalhaes *et al.* 2007). The presence of endotoxin contamination can possibly result in misleading

information about the toxicity of the nanoparticle (Li and Boraschi 2016; Oostingh *et al.* 2011).

Due to the complexity of the interactions between LPS and nanomaterials, rather than trying to remove LPS contamination from nanomaterials, it seems it would be preferable to rather keep the nanomaterial production process endotoxin-free through the use of ultrapure water, gloves, fume hoods, and effective cleaning of the work area and glassware. By implementing these modifications to the production process, (Vallhov *et al.* 2006) were able to lower the LPS concentrations in their AuNP preparation 16-24 times. However, levels of endotoxins would still need to be determined after synthesis to confirm acceptable levels.

2.2.1.3.2 Endotoxin detection assays

Testing for endotoxin contamination was originally based on their ability to induce a pyrogenic response, and was performed using an *in vivo* test called the rabbit pyrogen test (RPT). The test substance is injected into rabbits and the body temperature of the animal is monitored before injection and at every 30 minutes for 3 hours after the injection. If an increase in body temperature is observed, then the test substance is concluded to be pyrogenic (Dobrovolskaia and McNeil 2013). This test was the only official pyrogen test for 37 years, until the advent of the *in vitro* Limulus amebocyte lysate (LAL) test (Williams 2007). The test was based on observations in 1956 by Frederik Bang that Gram-negative infection of *Limulus polyphemus*, the horseshoe crab, caused intra-vascular coagulation. Then in 1964 Bang and Levin proposed that blood clotting was caused by the reaction between endotoxin and a clottable protein in the circulating amebocytes (Williams 2007). This discovery resulted in a shift from *in vivo* to the *in vitro* LAL assay to determine the presence of endotoxin. .

The biochemical pathway of the LAL assay has been well characterised and a summary of which is shown in the top half of Figure 2.2. There are three main formats of the LAL assay, namely the gel-clot, the turbidity, and the chromogenic

assay; all of which are dependent on a coagulation cascade that is triggered by endotoxin (Figure 2.2). This cascade terminates in a clotting enzyme acting on coagulogen to form coagulin that self-associates to form a clot. The formation of this clot can either be measured by an absorbance-based turbidity assay which monitors the appearance of turbidity over time, or the gel clot assay which is based on the formation of a gelatinous clot after an hour (Iwanaga 2007). Alternatively, in the chromogenic assay, the clotting enzyme acts on a colourless substrate to catalyse the release of p-nitroaniline (pNA) which can be measured spectrophotometrically. However, there is also an alternative coagulation pathway which is triggered by (1,3)-β-D-glucan (bottom half of Figure 2.2) and therefore the presence of fungal β-glucans in a test sample may also activate the cascade (Kędzierska *et al.* 2007). This may cause false-positive results for endotoxin and thus question the specificity of the LAL assay. To circumvent this possibility, a new assay has been developed which makes use of a synthetic version of the Factor C protein, namely rFC, instead of LAL (bottom half of Figure 2,2). The activated rFC (recombinant Factor C) protein then acts directly on the fluorogenic substrate, thereby utilising the endotoxin-responsive part of the LAL cascade and eliminating the potential activation by β-glucans and false positive results (Ding and Ho 2001). This assay has been implemented to measure endotoxin in an agricultural environments (Burch *et al.* 2009; Poole *et al.* 2010; Saito *et al.* 2009; Thorne *et al.* 2010) and domestic environments (Alwis and Milton 2006; Matsui *et al.* 2013; Ownby *et al.* 2010).

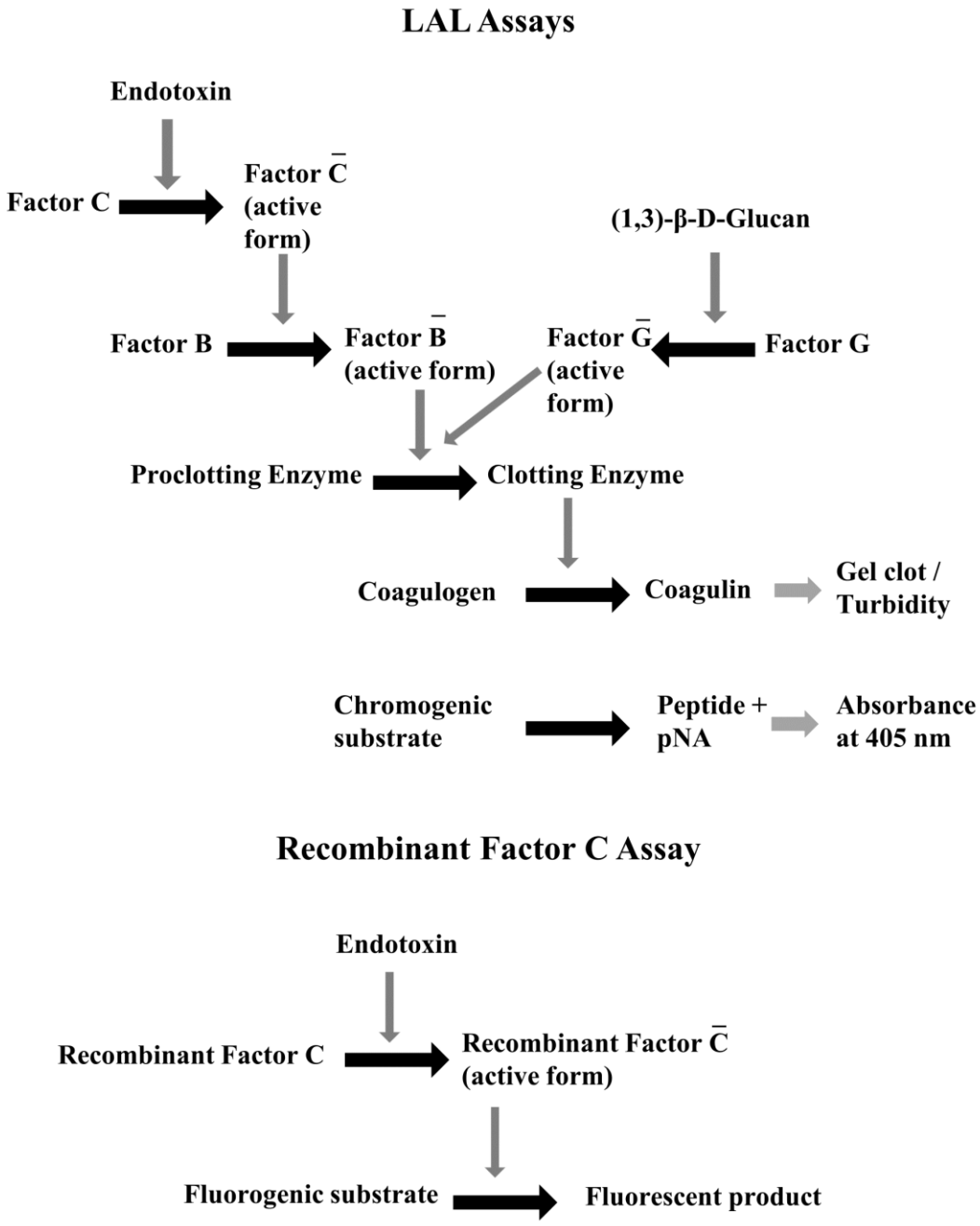

Figure 2.2 Schematic diagram of the LAL coagulation pathway and its associated assays, and the pathway of the recombinant Factor C assay. Image is adapted from literature (Abate *et al.* 2017; Iwanaga 2007; Morita *et al.* 1981)**.**

Irrespective of the assay chosen to evaluate the presence of endotoxin in nanomaterial samples, the evaluation of their interference with these test assays is critically important to avoid incorrect data interpretation. Especially considering that previously nanoparticles have been shown to interfere with *in vitro* LAL assays (Dobrovolskaia *et al.* 2009; Dobrovolskaia *et al.* 2010; Kucki *et al.* 2014; Neun and Dobrovolskaia 2011; Smulders *et al.* 2012). Interference can occur due to interactions between endotoxin and nanoparticles, or between nanoparticles and the LAL enzymes, resulting in either a decrease or increase of the sensitivity of the assay (Smulders *et al.* 2012). The large surface area and increase adsorption capacity of nanoparticles could potentially interfere with either the substrate conversion or enzymatic activity (Almutary and Sanderson 2017; Kroll *et al.* 2009; Kroll *et al.* 2012), where such interference may occur at any reaction point within the LAL cascade (Figure 2.2).

The FDA indorses the use of dilution of the sample as an approach to eliminate interference, as long as this dilution is not greater than the maximum valid dilution (MVD) for the assay in question (FDA 2012). Therefore, to evaluate interference with the assays, inhibition/enhancement controls (IECs) should be included in the experimental procedure. This involves the spiking of known amounts of endotoxin standard into the test sample at a number of dilutions, and analysing these spiked samples alongside a standard curve to observe the ability of the assay to correctly measure the spiked standard, termed "spike recovery" (Dobrovolskaia *et al.* 2010; Mccullough and Weidner-Loeven 1992). In addition, due to the optical properties of some nanoparticles, there may be additional influence by the nanoparticles on the detection of the reaction products by absorbance or fluorescence (Ong *et al.* 2014; Oostingh *et al.* 2011). Once the nanoparticles are known to be sterile, this eliminates any potential effects that these contaminants may have on the response of the cells or organism to the nanoparticles and the adverse effects of the nanoparticles alone can be investigated.

2.2.1.4 In vitro testing of nanoparticles

To test for the abovementioned adverse effects, *in vitro* testing has been developed using cells representative of potential target organs to measure various relevant endpoints and therefore aid the screening of nanomaterials as well as elicit the mechanisms of their toxicity. A number of non-TG cytotoxicity assays and OECD TG were investigated, including several genotoxicity assays.

2.2.1.4.1 In vitro toxicity testing methodologies

In vitro toxicity testing frequently involves the assessment of cell membrane integrity or metabolic activity to measure cell viability (Khalili Fard *et al.* 2015). Cell membrane integrity assays frequently rely on either the assessment of leakage of lactate dehydrogenase (LDH) from the interior of the cell to the extracellular environment, or by penetration by cell membrane-impermeable dyes such as trypan blue or neutral red that cannot enter viable cells. Metabolic activity is frequently measured by colorimetric assays that make use of tetrazolium salts, such as 3-(4,5-dimethylthiazol-2-yl)-2,5-diphenyltetrazolium bromide (MTT) that is reduced to an insoluble formazan which requires solubilisation prior to measurement spectrophotometrically. Alternative tetrazolium salts that are reduced to soluble formazans and can be measured directly are available such as 2,3-bis-(2-methoxy-4-nitro-5-sulfophenyl)-2H-tetrazolium-5-carboxanilide (XTT), 3-(4,5-dimethylthiazol-2-yl)-5-(3-carboxymethoxyphenyl)-2-(4-sulfophenyl)-2H-tetrazolium (MTS), and Water Soluble Tetrazolium (WST-1) assays (Berridge *et al.* 2005; Khalili Fard *et al.* 2015).

A number of immunohistochemical techniques have been used for the detection of apoptotic cells following exposure to nanomaterials (Hillegass *et al.* 2010), including the TUNEL assay, which detects fragmented DNA. However, this assay can potentially also label necrotic cells and therefore the Apostain technique is more specific as it labels condensed chromatin of apoptotic cells. Alternatively, flow cytometry can be implemented using double-labelling of apoptotic and necrotic cells (Hillegass *et al.* 2010).

In addition to measures of cell death, *in vitro* testing can provide preliminary information on the genotoxic potential of nanomaterials (Hillegass *et al.* 2010). In particular, *in vitro* genotoxicity testing identifies possible primary genotoxicity since the influence of secondary inflammatory events cannot alter the results (Schins 2002) The reverse mutation assay, also known as the Ames test, makes use of several strains of *Salmonella typhimurium* bacteria to determine mutagenicity of a substance in prokaryotes. Point mutations caused by ROS can be identified by assays measuring oxidised guanine bases such as 8-OHdG and 7,8-dihydro-oxodeoxyguanine (oxo-dG); whilst DNA strand breaks can be measured by the single cell gel electrophoresis assay (SCGE), also known as the Comet assay. Lastly, chromosomal damage in the form of chromosomal breakage or chromosome loss can be assessed through the chromosome aberration assay and the micronucleus assay (Hillegass *et al.* 2010; Schins 2002).

Alterations in gene expression can also provide valuable information of the potential effects of nanomaterial exposure. Northern blot analyses, ribonuclease protection assays, and real-time polymerase chain reaction (PCR) are useful for the detection and quantification of specific mRNA gene transcripts, whilst microarray analysis allows for expression profiling of thousands of genes simultaneously (Hillegass *et al.* 2010).

2.2.1.4.2 Representative in vitro cell lines

In vitro testing makes use of commercially available cell lines of representative organs, which, in this study, would be the respiratory tract since workers involved in the research and manufacture of nanoparticles have the greatest potential for inhalation exposure to airborne engineered nanoparticles. Particle deposition in the respiratory tract is greatly influenced by inertial impaction, sedimentation and diffusion, which are, in turn, related to the particle diameter, where particles less than 100 nm are primarily deposited in the alveolar and tracheobronchial regions (Carvalho *et al.* 2011). Therefore, a lung cell culture representative of the respiratory tract would be most relevant for this type of study. Availability of these include cell lines of the human airway (eg. the lung adenocarcinoma

epithelial cell lines Calu-3) and alveolar epithelium (eg. Human A549 cells), and primary cultures and cell lines of alveolar macrophages (Bakand *et al.* 2012). The immortalized human bronchial epithelial cell line BEAS-2B has been widely used as an *in vitro* model for particle toxicity. BEAS-2B cells are a frequently used cell model for bronchial epithelium in toxicity studies, as reviewed in (Steimer *et al.* 2005). This cell line has previously been used to investigate the cytotoxicity of nanoparticles such as titanium dioxide (TiO_2) NPs (Bhattacharya *et al.* 2009; Gurr *et al.* 2005), silica NPs (Eom and Choi 2009), zinc oxide (ZnO) NPs (Huang *et al.* 2010), and metal oxide NPs (Park and Park 2009).

2.2.1.4.3 Interference by nanomaterials with in vitro assays

Many of the aforementioned conventional *in vitro* testing methodologies rely on the detection of an optical reading of the assay product to determine toxicity, by either absorbance, fluorescence or luminescence. Since nanoparticles tend to be optically dense, meaning they can absorb light, they can interfere with the assay readout leading to a false estimation of viability or toxicity (Oostingh *et al.* 2011). The large surface area per unit mass of nanomaterials and their resultant high adsorption capacity increases the potential of the reaction substrate or product of the assay on to the surface of the nanomaterial thereby inhibiting the assay readout. In addition, enhanced catalytic activity of nanomaterials in converting substrate to product may cause false positive signals (Kroll *et al.* 2009). Due to these possible interferences, *in vitro* methods need to be tested for interference or employ tests that do not rely on optical detection, examples of which include the Colony Forming Efficiency (CFE) assay and the xCELLigence Real-Time Cell Analyser (RTCA).

The CFE assay is one assay that has been shown to be suitable for nanomaterial testing, as it is not susceptible to interference from nanomaterials (Ponti *et al.* 2014). It measures the survival and growth of cells over extended periods through the seeding of very low concentrations of colony-forming cells and allowing growth until colonies are formed. Analysis involves the counting of colonies under the assumption that, following treatment, each viable cell will form a

colony (Hillegass *et al.* 2010). Within the OECD WPMN framework, an interlaboratory comparison study of the CFE assay was conducted to investigate the applicability of this assay for the testing of nanomaterials by evaluating the intra and interlaboratory reproducibility of the assay. This assay was found to be a suitable, robust methodology that was reliably transferable between laboratories and showed good reproducibility; however, the technique is time-consuming and low throughput (Ponti *et al.* 2014).

Cell survival and growth can rather be measured in a more efficient way through the use of cell impedance technology which has enabled the acquisition of label-free, non-invasive measurements in real time (Atienzar *et al.* 2011). The xCELLigence RTCA is one example of such an instrument that makes use of this technology. Cells are cultured on special microtiter plates, called E-Plates, containing microelectrodes on the base of the wells. This technology is presented in Figure 2.3 where the application of an electric potential across these electrodes produces a measure of the electrode impedance that reflects the state of the ionic environment at the electrode/solution interface, known as Cell Index (CI). This impedance is influenced by the presence of cells cultured on plates on top of these electrodes, and therefore the CI values are used to monitor cell viability.

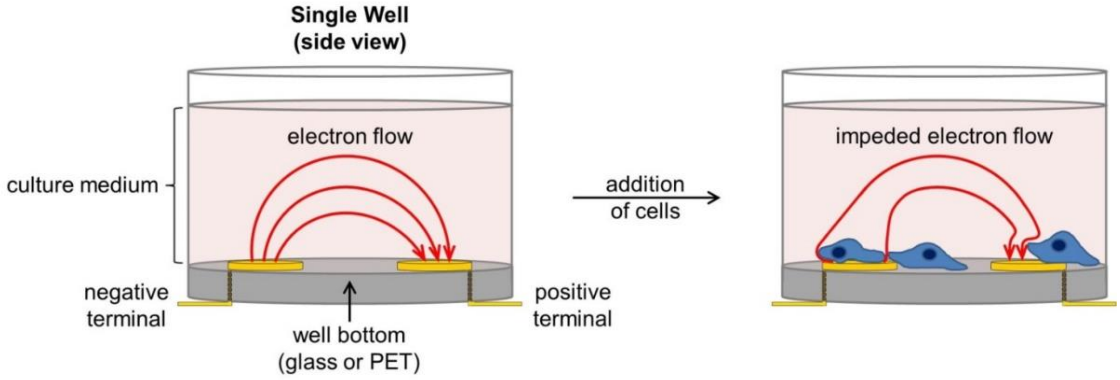

Figure 2.3 Diagrammatic representation of the xCELLigence RTCA technology before and after cells are added to the wells.
Neither the cells nor the electrodes are drawn to scale. In the absence of cells, the electric current flows freely in the culture medium between the electrodes; whereas once cells begin to adhere and grow then the current is impeded. (Image reproduced with permission from ACEA Biosciences https://www.aceabio.com/products/rtca-sp/)

In addition to an assessment of the toxicity of the nanoparticles, various *in vitro* techniques exist to assess the uptake of the nanoparticles.

2.2.1.4.4 Testing for intracellular uptake of nanomaterials

There are a number of methodologies available to detect the uptake of nanoparticles (Marquis *et al.* 2009). A frequently used technique is transmission electron microscopy (TEM) which is capable of direct imaging of the intracellular localisation of metal nanoparticles due to their high electron density (Gonciar 2014). Qualitative elemental analysis, such as electron-dispersive X-ray analysis (EDS), can be coupled to TEM to identify the chemical composition of the nanoparticles (Marquis *et al.* 2009). However, TEM is fairly time consuming due to the sample processing involved and often lacks statistical power on information such as number of particles observed. Therefore, it is frequently run in combination with inductively coupled plasma atomic emission spectroscopy (ICP-AES) to assess nanoparticle uptake through quantification of elemental

composition. ICP-AES is only able to quantify elements that are not naturally found in the body and therefore cannot be used to quantify carbon-based NPs. It is also unable to distinguish between elements within the nanoparticle and dissolved ions, provides no information of the localisation of the NPs, and cannot distinguish between NPs on the exterior of the cell and those that have been taken up by the cell (Marquis *et al.* 2009).

On the other hand, fluorescent microscopy can be used as both a quantitative and qualitative methodology for the assessment of uptake of NP (Marquis *et al.* 2009). This can be achieved through either the detection of the intrinsic fluorescence of the NPs or using fluorescent molecules attached to the NPs. However, the possibility exists that either there is inhibition or enhancement of the fluorescence by nanoparticles, or that the fluorescent molecule is removed from the NP either during or after uptake (Gonciar 2014). Additional techniques for detecting intracellular uptake of nanoparticles include Surface-enhanced Raman spectroscopy (SERS) for live cell studies which makes use of molecular vibrations to produce a vibrational fingerprint of a molecule; differential interference contrast (DIC) which makes use of two images acquired at different wavelengths to distinguish between AuNPs and cellular features; or photothermal microscopy which makes use of overlapping laser beams and the detection of small changes in temperature to image metal nanoparticles (Gonciar 2014).

Darkfield microscopy can also be implemented for the detection of NPs in cells. This technique makes use of oblique illumination and the collection of Rayleigh scattering of the light to produce a bright image on a dark background (Wang *et al.* 2010). CytoViva® has developed a patented darkfield illumination system that has enhanced the signal-to-noise ratio up to ten times as compared to standard darkfield microscopy (https://cytoviva.com/). This technology was specifically developed to image materials in the nanoscale range with minimal sample preparation. CytoViva also developed a Visible and Near-Infrared (VNIR) hyperspectral imaging (HSI) camera that enables spectral quantification of a sample. The system integrates onto the darkfield system and captures the unique

reflectance spectra of objects in the microscope field of view. In this way, a spectral signature of a known nanoparticle sample can be collected to form a library that can then be mapped onto images of cells incubated with nanoparticles, thereby allowing for the label-free confirmation of intracellular uptake of nanoparticles.

Although there are a number of possible methodologies for the assessment of toxicity and uptake of nanomaterials, a summary of those mentioned above is shown in Table 2.2, it is essential that the techniques used in any study are suitable for use with the nanomaterial in question. This was one of the issues addressed by the aforementioned OECD WPMN Testing Programme, of which the present study contributed to assessment of the applicability of various *in vitro* toxicity assays for the testing of gold nanoparticles.

Table 2.2 Summary of methodologies used for hazard identification of nanoparticles

	Parameter measured	Methodologies
Physicochemical Properties	Aggregation/agglomeration	TEM, SEM, DLS
	Particle size distribution	TEM, SEM, DLS
	Zeta potential	Laser-Doppler electrophoresis, electrophoretic light scattering, photon correlation spectroscopy
	Oxidation-reduction potential	Potentiometry, Oxygen detection
Surface Activity	Radical Formation potential	EPR / ESR
Sterility of Nanoparticles	Endotoxin contamination	*In vitro* Limulus amebocyte (LAL) test in the gel-clot, turbidity, or chromogenic assay format, Recombinant Factor C (rFC) assay
***In vitro* toxicity testing**	Cell membrane integrity	LDH, Trypan blue, Neutral red
	Metabolic activity	MTT, XTT, MTS, and WST-1 assay
	Apoptosis	TUNEL assay, Apostain, flow cytometry
	Genotoxicity	Ames test, 8-OHdG and oxo-dG assays, Comet assay, Chromosome aberration assay, micronucleus assay
	Alterations of gene expression	Norther blots, ribonuclease protection assays, real-time PCR, microarrays
	Cell viability	CFE assay, xCELLigence RTCA
Nanoparticle uptake	Qualitative analysis	TEM, EDS, fluorescent microscopy, SERS, DIC, photothermal, Darkfield microscopy, hyperspectral imaging
	Quantitative analysis	ICP-AES, fluorescent microscopy,

2.2.2 Hazard identification of gold nanoparticles

2.2.2.1 In vitro toxicity of gold nanoparticles

There is an apparent contradiction in the literature regarding the *in vitro* toxicity of gold nanoparticles. Table 2.3 provides a summary, in chronological order of publication, of the studies reviewed here that investigated the *in vitro* cytotoxicity of spherical AuNPs, and presents the effects of physicochemical properties, cell type specificity, mechanism of toxicity, and the link between uptake and toxicity. Many of these studies showed no cytotoxicity of the AuNPs under investigation (Gu *et al.* 2009; Khan *et al.* 2007; Kim *et al.* 2009; Ponti *et al.* 2009; Zhang *et al.* 2011). However, other studies have endeavoured to establish the effects of various nanoparticle characteristics and have found that size, surface chemistry, and shape may influence toxicity. Other confounding factors are the possibility of cell-type specific toxicity, and the relationship between uptake and toxicity. In addition, it has become apparent that, even though AuNPs may not be cytotoxic, they may cause adverse effects such as inflammation or genotoxicity, and therefore different toxicological endpoints and the mechanism of toxicity is of interest.

Table 2.3 Summary of *in vitro* cytotoxicity of spherical gold nanoparticles.

Cell line[a]	**Size**	**Surface chemistry**	**Incubation time; cytotoxicity assay**[b]	**Conclusion on cytotoxicity**	**Uptake (Technique used)**[c]	**Reference**
Cos-1, Red blood cells, Bacterial cultures (*E.coli*)	2 nm	Quaternary ammonium (cationic); or carboxylate (anionic)	Mammalian cells: 1 hour, 24 hour; MTT assay for Cos-1, hemolysis assay for red blood cells; Bacterial culture: overnight; adaption of bacteriophage λ assay	Cationic NPs are cytotoxic, Anionic NPs are not cytotoxic; Mammalian cells moderately more sensitive	Not studied.	(Goodman *et al.* 2004)
K562	18 nm	Citrate; biotin; CTAB	3 days; MTT assay	No cytotoxicity	Rapid uptake into endocytotic vesicles (TEM)	(Connor *et al.* 2005)
MC3T3-E1, U-2OS, SK-ES-1, MOR/P, MOR/CPR, CCD-919Sk, BLM, MV3, SMel-28, HeLa, Hek-12	1.4 nm	Triphenyl-phosphine	24 hours; MTT assay	Cytotoxicity observed; Differences in sensitivity of various cell lines	BLM cells: Distributed in both the cytoplasm and the nucleus (radioisotopes and fragmentation of cells into cytoplasmic and nuclear fraction prior to analysis of radioactivity)	(Tsoli *et al.* 2005)

Cell line[a]	**Size**	**Surface chemistry**	**Incubation time; cytotoxicity assay**[b]	**Conclusion on cytotoxicity**	**Uptake (Technique used)**[c]	**Reference**
RAW 264.7	3.5 nm	Borohydride	24 hour, 48 hour, 72 hour; MTT assay	No cytotoxicty	Uptake followed by aggregation in lysosomes (AFM, CLSM, TEM)	(Shukla *et al.* 2005)
CF-31	13 nm	Citrate	2, 4, and 6 days; proliferation measured rather than cytotoxicity	Decrease in proliferation observed	Uptake confirmed followed by accumulation in vacuoles and lysosomes (TEM,confocal microscopy)	(Pernodet *et al.* 2006)
L929, HeLa, J774A1, SK-Mel-28	0.8 nm, 1.2 nm, 1.4 nm, 1.8 nm, 15 nm	Triphenyl-phosphine	48 hours; MTT assay	0.8 nm – 1.8 nm NPs highly toxic; 15 nm NPs non-toxic; No cell-type specific differences	Yes – not studied in detail	(Pan *et al.* 2007)
A549, HepG2, BHK21	33 nm (hydro-dynamic diameter)	Citrate	A549 and HepG2: Incubation period not specified; MTT assay. A549, HepG2, BHK21: 36 hours; propidium iodide (PI) uptake	Cytotoxicity observed in A549 cells; no cytotoxicity in HepG2 and BHK21 cells;	A549 cells: Uptake confirmed but do not enter the nucleus. HepG2 and BHK21 cells: no uptake (fluorescence confocal microscopy)	(Patra *et al.* 2007)
HeLa	18 nm	Citrate	3 and 6 hours; MTT assay	No cytotoxicity	Uptake confirmed into vesicles within the cytoplasm (TEM)	(Khan *et al.* 2007)

Cell line[a]	**Size**	**Surface chemistry**	**Incubation time; cytotoxicity assay**[b]	**Conclusion on cytotoxicity**	**Uptake (Technique used)**[c]	**Reference**
HeLa	3 nm, 5 nm, 12 nm, 17 nm, 37 nm, 50 nm, 100 nm	Citrate	Not specified; MTT assay	No cytotoxicity	Not studied	(Chen *et al.* 2009)
HeLa	3.7 nm	MPA-PEG (3-mercapto-propionic acid-polyethylene glycol)	6, 12, 24, 36, 48, 72 hours; MTT	Minimal cytotoxicity	Uptake confirmed into vesicles, found through the cytoplasm, and within the nucleus; uptake plateaus at 24 hours; (ICP-MS, CLSM, TEM, fragmentation of cells into cytoplasmic and nuclear fraction prior to CLSM and ICP-MS)	(Gu *et al.* 2009)
HRMECs, CTX-TNA2, SNUOT-Rb1	20 nm, 100 nm	Not specified	48 hours; MTT assay	No cytotoxicity; No cell-type specific differences	Not studied	(Kim *et al.* 2009)

Cell line[a]	**Size**	**Surface chemistry**	**Incubation time; cytotoxicity assay**[b]	**Conclusion on cytotoxicity**	**Uptake (Technique used)**[c]	**Reference**
MDCK, HepG2	8 nm	poly(N-vinyl)-2-pyrrolidone (PVP)	72 hours; NR assay & CFE assay	No or minimal cytotoxicity; no cell-type specific differences	Uptake confirmed into vesicles (radioactivity & HPGe detectors, TEM)	(Ponti *et al.* 2009)
N9	23 nm	CTAB (cationic); PEG (anionic)	24 hours; MTT assay	CTAB highly toxic, PEG not toxic	CTAB: uptake and localization with lysosomes; PEG: No uptake (DFM)	(Hutter *et al.* 2010)
Dendritic cells (DCs) generated from bone marrow extracted from C57BL/6 mice	10 nm	Poly-(*N*-vinyl)-2-pyrrolidone (PVP)	4, 24, and 48 hours; Annexin-7AAD staining and flow cytometry	No cytotoxicity	Accumulation in cells (Bright-field microscopy)	(Villiers *et al.* 2010)
RAW 264.7	60 nm	Citrate	24 and 48 hours; MTT and LDH assays	No cytotoxicity	Uptake into intracellular vacuoles (TEM)	(Zhang *et al.* 2011)
A549, A431, NCI-H1975	17 nm	Citrate	24 hours, 72 hours; MTT and LDH assays	Cytotoxicity observed; No cell-type specific differences	A549 cells: uptake into endosomes (TEM, DFM)	(Choi *et al.* 2012)

Cell line[a]	**Size**	**Surface chemistry**	**Incubation time; cytotoxicity assay**[b]	**Conclusion on cytotoxicity**	**Uptake (Technique used)**[c]	**Reference**
Monocyte-derived DCs (dendritic cells)	10 nm, 50 nm	Carboxylic acid-based capping agent	24 and 48 hours; Annexin-PI staining and flow cytometry	Minimal cytotoxicity	Uptake confirmed into endosomes and some in the cytoplasm as small aggregates or single particles (MGG, flow cytometry, confocal microscopy)	(Tomić *et al.* 2014)
HepG2, HL-60	30 nm, 50 nm, 90 nm	Not specified	24, 48, 72 hours; MTT and LDH assays	Dose dependent cytotoxicity; 30 nm AuNPs slightly more toxic than 50 nm and 90 nm; Minor cell-type specific differences	Not studied	(Mateo *et al.* 2014)
A549, BEAS-2B, NHBE	10 nm, 7 nm	Citrate (10 nm; anionic), Chitosan (7 nm; cationic)	24 hours; LDH assay, CTB assay	Minimal cytotoxicity of most NPs; BEAS-2B: only AuNPs with highest positive charge were toxic at high concentrations; NHBE: AuNPs with highest positive charge showed dose-dependent toxicity (CTB assay)	Not studied	(Schlinkert *et al.* 2015)

Cell line[a]	**Size**	**Surface chemistry**	**Incubation time; cytotoxicity assay**[b]	**Conclusion on cytotoxicity**	**Uptake (Technique used)**[c]	**Reference**
C2C12	4.5 nm	PEG	24 hours; XTT, MTT, and calcein activity assay	No cytotoxicity	Uptake confirmed (STEM-in-SEM)	(Leite *et al.* 2015)
HepG2, HEK 293	14 nm	Citrate, Carboxyl-PEG (PCOOH)	Continuous monitoring, HepG2: 74 hours, HEK 293: 32 hours; xCELLigence RTCA	HepG2: Citrate AuNPs - Minimal cytotoxicity, PCOOH AuNPs – highly toxic dose-dependent toxicity; HEK 293: Minimal cytotoxicity	Uptake confirmed into cytoplasm and in vesicles (TEM, EDX)	(Tlotleng *et al.* 2016)
HepG2, HeLa	6.2 nm, 24.3 nm, 42.5 nm, 61.2 nm	Hydroxyl-PEG	48 hours; MTT assay	Dose dependent cytotoxicity observed; Smaller particles more toxic; HepG2 more sensitive than HeLa	Not studied	(Li *et al.* 2018)

[a] A431 human epidermoid carcinoma cells; A549 human lung carcinoma type II epithelial cells; BEAS-2B human bronchial epithelial cells; BHK21 Syrian hamster kidney fibroblast cells; BLM metastatic melanoma; C2C12 mouse myoblastoma; CCD-919Sk fibroblast cells; CF-31 human dermal fibroblast; CTX-TNA2 rat astrocytes; Hek-12 kidney cancer cells; HEK 293 human embryonic kidney cells; HeLa cervical cancer cells; HepG2 human hepatocyte cells; HL-60 human peripheral blood promyelocytic leukemia cells; HRMECs human retina microvascular

endothelial cells; J774A1 mouse macrophage; K562 leukemia; L929 mouse fibroblasts; MC3T3-E1 bone cells; MDCK Madin-Darby Canine Kidney cells; MOR/P lung cancer cells; MOR/CPR lung cancer cells; MV3 metastatic melanoma; N9 microglial cells; NCI-H1975 human lung carcinoma cells; NHBE normal human bronchial epithelial cells; RAW 264.7 murine macrophages; SK-ES-1 osteosarcoma; SK-Mel-28 human melanoma; SMel-28 melanoma; SNUOT-Rb1 human retinoblastoma cells; U-2OS osteosarcoma.

[b] CFE: Colony Forming Efficieny; CTB: CellTiter-Blue®; LDH: Lactate Dehydrogenase; MTT: 3-(4,5-dimethylthiazol-2-yl)-2,5-diphenyltetrazolium bromide; NR: Neutral Red; RTCA: real-time cell analyzer; XTT: 2,3-bis-(2-methoxy-4-nitro-5-sulfophenyl)-2H-tetrazolium-5-carboxanilide

[c]TEM: Transmission Electron Microscopy; AFM: Atomic Force Microscopy; CLSM: Confocal-Laser-Scanning-Microscopy; DFM: Dark-Field Microscopy; EDX: Energy-Dispersive X-ray; HPGe: High Performance Germanium; ICP-MS: Inductively Coupled Plasma Mass Spectrometry; MGG: May-Grunwald-Giemsa; STEM-in-SEM: Scanning Transmission Electron Microscopy mode in Scanning Electron Microscopy

2.2.2.1.1 Effect of size

One of the earliest cytotoxicity studies on AuNPs investigated the effects of 1.4 nm triphenylphosphine-liganded AuNPs on 11 cell lines, using the MTT assay (Tsoli *et al.* 2005). The particles were found to be toxic to all cell lines and the authors proposed that the toxicity of these nanoparticles was due to their small size that allowed them to enter the nucleus and interact with the major groove of DNA within the cells. In the same year, a study on the toxicity of 18 nm AuNPs in K562 leukemia cells using the MTT assay, CTAB-coated spherical AuNPs showed significant toxicity as compared to their non-toxic citrate- and biotin-coated counterparts; however, following a washing process to remove unbound CTAB, the washed CTAB AuNPs were found to be non-toxic (Connor *et al.* 2005). It was therefore proposed that smaller AuNPs were toxic whilst larger ones were non-toxic.

Concurring with this, a study of the effect of triphenylphosphine stabilised AuNPs on four cell lines, namely L929, HeLa, J774A1, and SK-Mel-28; found particles ranging in size from 1 – 2 nm were highly toxic via both apoptosis and necrosis, whilst 15 nm AuNPs were shown to be nontoxic, as determined by the MTT assay and fluorescence-activated cell sorting (FACS) (Pan *et al.* 2007). Recently, a study on hydroxyl(OH)-PEG coated AuNPs of sizes 6.2 nm, 24.3 nm, 42.5 nm, and 61.2 nm included *in vitro* studies on HepG2 and HeLa cells (Li *et al.* 2018). Dose-dependent cytotoxicity was observed using the MTT assay, and, at the highest concentration, size-dependent toxicity was observed where the smaller the nanoparticles the greater the observed cytotoxicity. In contrast though, viability studies in HeLa cells treated with citrate stabilised gold nanoparticles (size ranging 3 nm to 100 nm) showed no decrease in viability, regardless of size, also measured by the MTT assay (Chen *et al.* 2009). A study using the MTT and the LDH assay in HL-60 and HepG2 cells found dose-dependent cytotoxicity of AuNPs, where the 30 nm AuNPs in the study were only slightly more toxic than the 50 nm and 90 nm AuNPs (Mateo *et al.* 2014).

In conjunction with the possible influence of nanoparticle size, the surface characteristics will also influence the interaction of the nanoparticles with the cells.

2.2.2.1.2 Effect of surface chemistry

The importance of surface chemistry on toxicity of AuNPs was shown in 2004 where the effect of the side chains of mixed monolayer protected gold clusters (MMPCs) was investigated using the MTT assay in Cos-1 cells and human red blood cells, and using an adaptation of a bacteriophage λ assay in *Escherichia coli* cells (Goodman *et al.* 2004). In this study cationic nanoparticles, functionalised with quarternary ammonium, were shown to be moderately toxic whilst anionic particles, functionalised with carboxylate, were non-toxic. (Goodman *et al.* 2004) The authors suggested toxicity was due to electrostatic interactions of the cationic particles with the negatively charged cell membrane, resulting in lysis, and demonstrated a charge-dependent toxicity of the AuNPs. Similarly, positively charged cetyltrimethylammonium bromide (CTAB) coated spherical AuNPs were shown to be significantly more toxic than their negatively charged PEG-coated spherical equivalent in microglial N9 cells (Hutter *et al.* 2010).

Nonetheless, when AuNPs have similar surface charge, it seems that the surface functionalisation may play a role in toxicity. Negatively charged carboxyl-PEG (PCOOH) 14 nm AuNPs were shown to be highly toxic in a dose-dependent manner in HepG2 cells, as compared to their similarly charged citrate stabilised counterparts which showed only mild toxicity (Tlotleng *et al.* 2016). These studies suggest that both the charge and the functionalisation of the surface of the AuNPs influences their toxicity. However, not all AuNPs are spherical, but rather other shapes have also been synthesised and the effects of the shape on toxicity has been investigated.

2.2.2.1.3 Effect of shape

Although toxic, in order to produce gold nanorods, CTAB is necessary as a stabilizing agent during production (Takahashi *et al.* 2006). A study of the cytotoxicity of gold nanorods, using the MTS assay, in normal human gingival epithelioid cells (S-G cells) and oral cancer cells isolated form a Taiwan patient (TW 2.6 cells) showed that negatively charged polystyrenesulfonate(PSS)-capped nanorods were less toxic than positively charged CTAB stabilised nanorods (Parab *et al.* 2009).

However, Takahashi *et.al.* (2006) were able to extract CTAB through centrifugation with a phosphatidylcholine (PC)-chloroform solution, thereby replacing the CTAB with PC and decreasing the cytotoxicity of the nanorods (Takahashi *et al.* 2006). As mentioned earlier, Connor *et al.* (2005) were also able to reduce the toxicity of CTAB AuNPs through the application of a washing process to remove unbound CTAB. Another study confirmed that the observed toxicity of CTAB-coated nanorods corresponds to the toxicity of free CTAB contamination in the nanorod suspension (Alkilany *et al.* 2009). It therefore seems that initial studies reporting the toxicity of nanorods may have been caused by the presence of unbound CTAB. This is supported by the observation that CTAB-coated nanorods tested in microglial N9 cells were only slightly toxic at a high concentration, and CTAB urchin shaped AuNPs were non-toxic, whilst the PEG equivalent rods and urchin shaped AuNPs were also both non-toxic (Hutter *et al.* 2010).

Apart from the characteristics of the nanoparticles, the characteristics of the cells used in the *in vitro* studies may potentially influence the outcome of the testing.

2.2.2.1.4 Cell-type specificity

Cell-type specific differences in response to AuNPs has been observed in some studies, whilst other studies have not. These studies involved a range of commercially available cell lines, representative of numerous cell types and different target oragns including carcinomas (Choi *et al.* 2012), retinal endothelial

cells, astrocytes, and retinoblastomal cells (Kim *et al.* 2009), melanoma, carcinoma, fibroblast, and macropage cells (Pan *et al.* 2007), and epithelial, and carcinoma cells (Ponti *et al.* 2009). Where cell-type specificity can be observed, in some studies, the AuNPs are toxic to all cell lines; however, some cell lines seem to be more sensitive than others. For example, a study on the effects of 1.4 nm triphenylphosphine-liganded AuNPs on 11 cell lines, although toxic to all cell lines, the AuNPs were most toxic to the MV3 and BLM metastatic melanoma cells, followed by the U-20S osteosarcoma and the Hek-12 kidney cancer cells (Tsoli *et al.* 2005). Another study found that hydroxyl-PEG AuNPs of various sizes were more toxic to HepG2 cells as compared to the HeLa cells (Li *et al.* 2018).

Alternatively, in some cases AuNPs have been found to be highly toxic to some cell lines but not cytotoxic to others. The increased sensitivity of HepG2 cells was also shown in our laboratory, where carboxyl-PEG AuNPs were highly toxic to HepG2 cells but only minimally toxic to HEK 293 cells (Tlotleng *et al.* 2016). Another study on the effects of 33 nm citrate stabilised AuNPs on A549, HepG2, and BHK21 cells found no uptake and no cytotoxicity in both the HepG2 and the BHK21 cells; whereas the AuNPs were able to enter the A549 cells and produced cytotoxicity (Patra *et al.* 2007).

A recent study (Chueh *et al.* 2014) made use of cell impedance technology to assess the toxicity of gold nanorod with an average length of 10-40 nm in four mammalian cell lines, namely porcine kidney (PK-15), African green monkey kidney (Vero), mouse embryonic fibroblasts (NIH3T3), and human normal lung fibroblasts (MRC5). Concentration-dependent toxicity was observed, however the extent of this toxicity varied between cell lines with Vero cells showing the highest sensitivity, and PK-15 cells being the most resilient. Further differences in cell-type were observed when the toxicity of highly positive charged chitosan-coated AuNPs was shown to be the greatest in normal NHBE cells, as compared to the immortalised cell lines A549 and BEAS-2B (Schlinkert *et al.* 2015).

The cell type may also influence the mechanism and extent of uptake of the nanoparticles into the cell; and uptake has been suggested as an influencing factor in toxicity.

2.2.2.1.5 Uptake and toxicity

In two of the studies reviewed here (Hutter *et al.* 2010; Patra *et al.* 2007), uptake of AuNPs correlated with cytotoxicity, whilst lack of uptake of AuNPs correlated with non-toxicity. In addition, citrate stabilised 17 nm AuNPs were taken up and subsequently shown to be cytotoxic to human lung adenocarcinoma cells A549 and NCI-H1975, and human epidermoid carcinoma cells A431 (Choi *et al.* 2012).

However, in many other studies discussed above (Connor *et al.* 2005; Khan *et al.* 2007; Leite *et al.* 2015; Ponti *et al.* 2009; Shukla *et al.* 2005; Villiers *et al.* 2010; Zhang *et al.* 2011) uptake of the AuNPs into cells was confirmed, however this did not result in cytotoxicity. The study by Chueh et al. (2014) that found cell-type specific differences in toxicity to nanorods, also found that the level of uptake did not correspond to the toxicity. For example, NIH3T3 showed the highest accumulation of gold nanorods, however this cell line showed low toxicity compared to the other cell lines studied (Chueh *et al.* 2014).

Even in the absence of obvious cytotoxicity, subcellular pathways may be activated and adverse effects may be caused by nanoparticles.

2.2.2.1.6 Adverse effects in the absence of cytotoxicity

Following the early studies of Tsoli et al., (2005) and Connor et al., (2005), Pernodet et al (2006) subsequently chose to focus on apparently non-cytotoxic larger AuNPs, investigating potential effects on proliferation, protein expression, morphology, and changes in spreading and migration. This study involved 13 nm citrate stabilised AuNPs tested on CF-31 human dermal fibroblasts for 2, 4, and 6 days. The AuNPs caused a reduction in proliferation after incubation for 4 days, possibly linked to observed modifications to the actin structure in treated cells, or to the large accumulation of nanoparticle-containing vacuoles. These authors also

observed adverse effects on the extracellular matrix of cells, and on their ability to migrate (Pernodet *et al.* 2006).

In addition, Villiers *et al.*, 2010, investigated the effects of poly-(*N*-vinyl)-2-pyrrolidone (PVP) stabilised 10 nm AuNPs on dendritic cells generated from bone marrow extracted from C57BL/6 mice. No cytotoxicity was observed for up to 48 hours incubation and the AuNPs had no effect on the activation of the DCs. However, when treated simultaneously with LPS a strong inhibition of cytokine IL-12p70 secretion was observed, as compared to the secretion caused by LPS treatment alone, suggesting that the AuNPs may influence the immune response of cells to antigens (Villiers *et al.* 2010). In another study, 10 nm and 50 nm AuNPs, coated with a patented carboxylic acid-based capping agent, were shown to be only mildly toxic to monocyte-derived immature dendritic cells (DCs), as determined by an Annexin-PI assay (Tomić *et al.* 2014). However, at non-cytotoxic concentrations, the 10 nm AuNP were shown to impair the functioning and maturation of the immature DCs, again suggesting an adverse effect on the immune functioning of the cells.

Finally, differentiated skeletal muscle C2C12 cells showed no decrease in viability when treated with 4.5 nm PEG-AuNPs, as tested with XTT, MTT, and Calcien AM assay (Leite *et al.* 2015). However, the particles induced a dose-dependent increase in ATP production and in mitochondrial membrane potential, and altered signalling pathways that lead to increased cell sensitization and susceptibility to cell death. It is clear from the abovementioned studies that, even in the absence of obvious cytotoxicity, various responses occur and pathways are altered at sub-cellular levels; necessitating a look at the mechanisms of toxicity induced by AuNPs.

2.2.2.1.7 Mechanisms of toxicity of AuNPs

In vitro studies have also offered insights into the potential mechanism of toxicity of AuNPs. After establishing the cytotoxicity of OH-PEG AuNPs in HepG2 and HeLa cells, the authors the intracellular production of ROS using the DCFH-DA

assay and found significant production of ROS in both cell lines, where the smaller the AuNP, the greater the amount of ROS produced, which corresponded with an increased observed cytotoxicity described earlier (Li *et al.* 2018). Dose-dependent intracellular production of ROS following incubation with highly positively charged AuNPs was found in A549, BEAS-2B, and NHBE cells (Schlinkert *et al.* 2015). Interestingly, although the highest production of ROS was found in A549 cells, this did not correlate with toxicity.

Following the observation of dose-dependent cytotoxicity of AuNPs in HL-60 and HepG2 cells, Mateo et al. (2014) investigated the influence of oxidative stress. The authors found that, with the pre-incubation of the antioxidant precursor N-Acetyl-L-cysteine (NAC), a somewhat protective effect was seen in both cell lines by way of an increase in viability of the AuNP-treated cells. In both cell lines, a severe depletion of GSH, a marker of ROS detoxification, was observed; however cell-type specific changes in SOD activity were found, where a decrease of enzyme activity was seen in HepG2 cells (Mateo *et al.* 2014). In a study on HL7702 human liver cells, a severe depletion of GSH levels was observed after treatment with 8 nm AuNPs, as well as an increase in mitochondrial H_2O_2 and a loss of mitochondrial membrane potential (Gao *et al.* 2011). Together, these results suggest that, in the cell lines studied, the production of oxidative stress is one of the primary mechanisms of AuNP toxicity.

Oxidative stress-related signalling pathways have been shown to be involved in cellular responses to AuNP exposure *in vitro*. An inhibition of cell proliferation was also observed when ovarian cancer cells were treated with 20 nm citrate stabilised AuNPs and this was linked to an inhibition of the MAPK signalling cascade (Arvizo *et al.* 2013). Whilst NF-κB transcription factor activity was increased in lung epithelial cells which subsequently lead to gene expression associated with an inflammatory response (Ng *et al.* 2018). In another study, the induction of apoptosis has been shown to be the cause of cell death caused by citrate stabilised 17 nm AuNPs in A549 cells, as deduced through a bioluminescent ATP assay, cell cycle analysis using flow cytometry, and

assessment of apoptosis-related genes expression using real-time PCR (Choi *et al.* 2012).

Oxidative stress was observed in MRC-5 cells treated with fetal bovine serum (FBS) coated 20 nm AuNPs (Li *et al.* 2008; Li *et al.* 2010). In the first study, this group observed a dose-dependent induction of oxidative DNA damage, as observed by an increased quantity of 8-OHdG relative to the control, coupled with a downregulation of DNA repair genes (Li *et al.* 2008). In the latter study, an increased hydroperoxide concentration in lipid extracts was found, as well as MDA protein adducts, in treated cells. In addition, four genes related to oxidative stress pathways were significantly upregulated, namely the polynucleotide kinase 3'-phosphatase gene (*PNK*), cyclooxygenase 2 gene (*COX-2*), oxidative stress response 1 gene (*OXSR1*), and the peroxiredoxin 2 gene (*PRDX2*). PNK protein plays a role in DNA double strand break repair; whilst COX-2 is a stress inducible enzyme and a marker of inflammation that was, most likely, induce by the lipid peroxidation observed. However, both OXSR1 and PRDX2 proteins are associated with protection against oxidative stress. The authors also found induction of autophagy proteins after treatment with AuNPs and observed autophagosomes using TEM. Autophagy, or "self-eating", occurs when double-membraned vesicles, termed autophagosomes, are formed from cytoplasmic proteins and organelles which then fuse with lysosomes and are degraded (Fulda *et al.* 2010). In some cases, autophagy is a stress adaptation that prevents cell death whilst in some cases it serves as a pathway to cell death. In the Li. et al., 2010 study, the authors concluded that the induction of autophagy protected the cells from cell death caused by oxidative stress.

A few studies have shown the genotoxic potential of AuNPs. Small AuNPs of 5 nm in diameter, but not those of 20 nm or 50 nm, showed ROS production and DNA damage to HepG2 cells in the DCF-DA and comet assay respectively; and subsequent hindrance of cell cycle progression (Xia *et al.* 2017). Although no adverse effects were observed following treatment in the *in vitro* mammalian chromosome aberration test and standard *in vivo* mammalian erythrocyte

micronucleus test, a long-term *in vivo* mammalian erythrocyte micronucleus test revealed a significant increase in micronucleus formation in the cells treated with the 5 nm AuNPs. Conversely, a study in Raw264.7 cells found the genotoxic effects of 15 nm AuNPs to be greater than that of 5 nm AuNPs, as measured by the micronucleus assay (Di Bucchianico *et al.* 2014). These same authors went on to show the potential adverse genotoxic effects of contaminants in the AuNP suspension (Di Bucchianico *et al.* 2015).

Another study in HepG2 cells found DNA damage caused by 20 nm citrate stabilised AuNPs, but not 11-merceptoundecanoic acid AuNPs, even though no cytotoxicity was observed (Fraga *et al.* 2013). Cytotoxicity and genotoxicity was observed in HepG2 cells and peripheral blood mononuclear cells (PBMC) following treatment with citrate-stabilised and PAMA dendrimer-capped AuNPs (Paino *et al.* 2012). However, both of these studies made use of the comet assay to determine damage, which may be subject to interference (George *et al.* 2017). On the other hand, a study that made use of both the comet assay and the micronucleus assay found no genotoxicity for 2, 20, and 200 nm gold nano/microparticles in blood and tissue obtained from Wistar rats (Downs *et al.* 2012).

It can be seen from the literature presented here that there is conflicting toxicity data not only on the cytotoxicity of AuNPs, but also on the effects of shape, size and surface chemistry. This highlights the need for standardisation and validation of *in vitro* methodologies for the assessment of the safety of gold nanomaterials.

2.2.2.2 Uptake of gold nanoparticles

For nanoparticles to have applications in drug delivery and therapeutics, it is necessary for the nanoparticles to enter cells to exert their function, however the uptake and subsequent intracellular localisation and processing of nanoparticles will influence their toxicity. Cellular uptake of nanoparticles is known to be influenced by their size, shape, and surface chemistry, since these properties will

influence how nanoparticles interact with each other, their environment, and with cells they come into contact (Panariti *et al.* 2012).

2.2.2.2.1 Parameters determining the uptake of gold nanoparticles in vitro

The size of nanoparticles has been shown to affect their cellular uptake; however, there is no clear conclusion in the literature regarding what size is most readily taken up. In some studies, 50 nm AuNPs have been shown to have a maximum uptake. This was shown in both HeLa cells treated with citrate stabilised AuNPs of diameters 14, 30, 50, 74, and 100 nm (Chithrani *et al.* 2006), and in MCF-7 cells treated with citrate-stabilised and with bovine serum albumin (BSA) coated AuNPs with diameters of 14, 50, and 74 nm (Chithrani *et al.* 2009). A similar trend was observed in dendritic cells (DCs), where 50 nm spherical AuNPs were internalized to a greater extent than 10 nm spherical AuNPs (Tomić *et al.* 2014).

Inconsistent with the abovementioned studies, human pancreatic cancer cell lines PK-1, PK-45, and Panc-1 had the highest uptake of 20 nm AuNPs, as compared to 5, 10, 30, 40, and 50 nm spherical AuNPs (Trono *et al.* 2011). In addition, 5 nm and 20 nm citrate stabilised AuNPs were more readily taken up than 50 nm and 100 nm into human ovarian cancer cell lines OVCAR5, SKOV3, and A2780 (Arvizo *et al.* 2013). In another study, PEGylated 18 nm AuNPs were taken up to a greater extent into primary human dermal microvascular endothelial cells (HDMECs) than their 35 nm and 65 nm counterparts (Freese *et al.* 2012a). However, these authors also showed surface coating-dependant uptake of various AuNPs, and found that positively charged AuNPs were taken up to a much greater degree than neutral and negatively charged ones of the same size.

The effect of various coatings on the uptake of AuNPS *in vitro* has been investigated in the literature where most of these investigations have studied the effect of the presence of PEG on the uptake of the nanoparticles. For example, in a study comparing the uptake of either non-coated or methyl PEGylated spherical 30 nm, 50 nm and 90 nm AuNPs, where PEGylation of the AuNPs lead to dramatically decreased levels of uptake in PC-3 cells (Arnida *et al.* 2010).

Polystyrene sulfonate coated gold nanorods exhibited uptake into human mammary adenocarcinoma SKBR3 cells, whilst methoxy-PEG coated gold nanorods did not enter the cells (Rayavarapu *et al.* 2010). A study in HeLa cells of 16 nm AuNPs showed that citrate-stabilised AuNPs entered the cells whilst their PEG-modified counterparts did not (Nativo *et al.* 2008). Similarly, uptake of 14 nm, 50 nm, and 70 nm AuNPs into HeLa cells and MDA-MB-231 cells was drastically reduced when these NPs were PEGylated, as compared to their citrate-stabilised counterparts (Cruje and Chithrani 2015). However, there was an increase in uptake in HeLa cells when the PEGylated AuNPs were functionalized with synthetic peptide RGD, although these levels did not reach those of the citrate-stabilised AuNPs. Likewise, AuNPs modified with mixed PEG/peptide monolayers have been shown to enter HeLa cells in greater numbers than their PEG-only counterparts (Liu *et al.* 2007). The abovementioned literature clearly demonstrates that the presence of PEG on the surface of AuNPs results in either reduced or complete absence of uptake of these AuNPs as compared to citrate-stabilised AuNPs; however further modification of the PEG-ligands with a peptide can potentially result in an increased uptake.

A study investigating the effects of surface chemistry of gold nanorods with dimensions 18 x 40 nm, found that the negatively charged poly(4-styrenesulfonic acid) (PSS) nanorods exhibited the lowest uptake in HeLa cells, whilst those coated with PSS followed by a positively charged poly(diallyldimethylammonium chloride) (PDADMAC) exhibited the highest uptake (Hauck *et al.* 2008). The nanorods that were coated with PSS and PDADMAC and then a second layer of PSS, resulting in a negative charge closer to neutral than PSS alone, showed an intermediate uptake, highlighting the importance of charge on uptake. This study also noted the differences in uptake between two nanorods of similar positive charge but different chemistry of the attached ligands. Moreover, the shape of the nanoparticles may have an effect on the uptake, for example, PEG hydrogel nanoparticles of high-aspect-ratio (more rod-like) were internalised faster than more symmetrical nanoparticles (Gratton *et al.* 2008). This study also showed positively-charged nanoparticles to be internalised faster than negatively charged

ones. In conclusion, it would therefore seem that a combination of size, surface chemistry and shape determine the uptake of nanoparticles.

2.2.2.2.2 Localisation of AuNPs

The intracellular localisation of nanoparticles following uptake will influence how the nanoparticle is processed within the cell and will determine the possible toxicological outcomes. Two studies have shown that AuNPs are able to enter the nucleus following uptake. Since these studies involved AuNPs of 1.4 nm (Tsoli *et al.* 2005) and of 3.7 nm (Gu *et al.* 2009) in diameter, it was proposed that their entry to the nucleus was due to their small size. However, the vast majority of *in vitro* uptake studies have shown AuNPs to be distributed within vesicles (Chithrani *et al.* 2009; Connor *et al.* 2005; Hutter *et al.* 2010; Pernodet *et al.* 2006; Ponti *et al.* 2009; Shukla *et al.* 2005; Zhang *et al.* 2011); or within a combination of vesicles and cytoplasm (Choi *et al.* 2012; Khan *et al.* 2007; Tlotleng *et al.* 2016; Tomić *et al.* 2014). The localisation of nanoparticles will be influenced by the mechanism by which the nanoparticles enter the cell.

2.2.2.2.3 General mechanisms of uptake

Uptake of nanoparticles has been shown to occur through both passive and active processes (Panariti *et al.* 2012). Studies investigating passive uptake generally make use of red blood cells (RBCs) as they lack endocytic capabilities (Shang *et al.* 2014). Whereas in other cell types receptor-mediated endocytosis pathways is the primary mechanism of cellular entry for nanoparticles (Alkilany and Murphy 2010). Endocytosis mechanisms are divided into two categories, namely phagocytosis, for the internalisation of larger particles; and pinocytosis, within which falls the categories of macropinocytosis, clathrin-mediated endocytosis, caveolin-mediated endocytosis, and clathrin- and caveolae independent endocytosis (Conner and Schmid 2003). Macropinocytosis is non-selective endocytosis that involves uptake of a large volume and allows for particles >1 μm to be internalised (Murugan *et al.* 2015). To study the mechanism of endocytosis of nanoparticles, researchers have commonly used either fluorescently labelled

endocytotic markers to investigate intracellular localization, or endocytotic inhibitors to block a specific pathway to confirm whether it is involved in uptake (Kou *et al.* 2013).

The mechanism of endocytosis can be investigated through the use of known chemical inhibitors of endocytosis pathways. Genistein and chlorpromazine have both been used in studies on the endocytosis mechanisms of nanoparticles into BEAS-2B cells, where genistein has been shown to effectively inhibited the uptake of polymeric DNA nanoparticles (Kim *et al.* 2012), and chlorpromazine has been shown to inhibit the uptake of copolymer DNA nanoparticles (Boylan *et al.* 2012) and multi-walled carbon nanotubes (MWCNTs) (Haniu *et al.* 2013).

2.2.2.2.4 Mechanism of uptake of AuNPs

Previous *in vitro* studies of endocytosis mechanisms of AuNPs have often focused on the effect of nanoparticle size and uptake has been shown, for the most part, to be clathrin-mediated. Spherical transferrin-coated 14 nm and 50 nm AuNPs were both shown to enter into HeLa cells through clathrin-mediated endocytosis (Chithrani and Chan 2007). In primary human dermal fibroblast CF-31 cells, clathrin-mediated endocytosis was shown to be the mechanism of uptake for 45 nm citrate-stabilised AuNPs, however uptake of 13 nm citrate-stabilised AuNPs was not clathrin-mediated. The authors suggested phagocytosis to be the mode of entry however; they did not investigate the possibility of caveolin-mediated uptake in their study (Mironava *et al.* 2010). Clathrin-mediated endocytosis was also identified as the mechanism of uptake of spherical FBS-coated 20 nm AuNPs into MRC5 lung fibroblast cells and Chang liver cells (Ng *et al.* 2015). However, caveolin-mediated uptake was observed in a study where 4.5 nm Au-cysteine-Cy5 nanoparticles were assessed in HeLa cells (Xian *et al.* 2012). An obvious deduction regarding the effect of size of AuNPs on the mechanism of uptake cannot be made based on the abovementioned literature. However, the surface functionalisation of the AuNPs may play a role and this therefore was identified as an area of interest considering the extensive use of surface modifications of AuNPs for their intended applications.

Since these aspects of the physicochemical properties of AuNPs may influence the level and mechanism of uptake, as well as the intracellular localisation of the AuNPs; one could propose that these properties will also influence the toxicity of the AuNPs.

Chapter 3 - Methods

3.1 AuNPs used in this study

3.1.1 Synthesis of AuNPs

AuNPs were synthesized by Mintek, Randburg, South Africa. The 14 nm and the 20 nm AuNPs were prepared with sodium citrate as a reducing agent according to literature methods (Frens 1973; Turkevich *et al.* 1951). Tetrachloroaurate ($HAuCl_4.3H_2O$) and trisodium citrate ($Na_3C_6H_5O_7.2H_2O$) were purchased from Sigma Aldrich (St. Louis, USA) and used without further purification. Trisodium citrate aqueous solution was added to boiling tetrachloaurate aqueous solution, and boiled under reflux for 15 minutes. The resultant suspension was allowed to cool to room temperature and stirred overnight. The 14 nm PEG-liganded nanoparticles were prepared using ligand-exchange where citrate was replaced, resulting in the following generic formula:

$Au - S - (CH_2)_{11} - (EG)_6 -$ functional group

Where EG is ethylene glycol ($C_2H_6O_2$) with the structure:

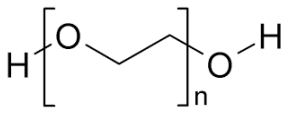

The PEG-ligand names, abbreviations, functional groups and molecular weight are shown in Table 3.1. Some of the AuNPs were 100% conjugation, meaning that the nanoparticles were saturated with the relevant PEG; whilst some were conjugated at 1% and stabilised with 99% POH. These conjugation concentrations are also shown in Table 3.1.

Table 3.1 Abbreviations and structures of functional groups

Name	Abbreviation	Molecular weight of PEG-ligands	Structure of functional group	Percentage concentration of relevant PEG
Hydroxyl-PEG	POH	468.69 g/mol	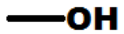	100%
Carboxyl-PEG	PCOOH	526.73 g/mol	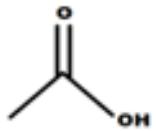	100%
Biotin-PEG	PBtn	694.00 g/mol	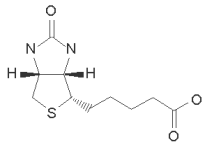	1%
Nitrilotriacetic acid-PEG	PNTA	638.82 g/mol	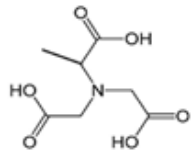	1%
Azide-PEG	PAZ	496.70 g/mol	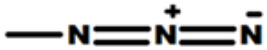	1%
Amine-PEG	PAM	504.16 g/mol		1%

The synthesis was performed under sterile conditions; however, the AuNPs were also filtered using an Acrodisc 0.2 µm Supor Membrane syringe filter (PALL, Port Washington, USA).

3.1.2 Use of different AuNPs

The 14 nm AuNPs used in this study were the chosen test substance for the South African contribution to the OECD WPMN project (JRC Nanomaterials Repository ID JRCNM03300a) and interference studies were conducted using these AuNPs. The 20 nm AuNPs were used as they were approximately double in size. The 14 nm and 20 nm AuNPs were used to demonstrate the use and benefits of label-free methodologies described in Sections 3.5.2 and 3.6.1. The 14 nm AuNP was also used in the OECD WPMN interlaboratory comparison study of the Colony Forming Efficiency (CFE) assay for assessing cytotoxicity of nanomaterials.

Toxicity and uptake studies were then performed on the 14 nm and 20 nm AuNPs to investigate the effects of size, and surface charge and type of liganded functional groups using the negatively charged 14 nm PEG-liganded AuNPs (POH AuNP, PCOOH AuNP, PBtn AuNP, PNTA AuNP, and PAZ AuNP), and the positively charged 14 nm PAM AuNP. The concentrations of the AuNPs are expressed in this study as molarity of AuNPs, given in nM, as provided by Mintek.

3.1.3 Different culture media

Three different cell culture media formulations were used in this study. RPMI culture medium consisted of RPMI-1640 medium with L-glutamine, 10% heat-inactivated foetal bovine serum (FBS) and 1% penicillin/streptomycin. Ham's F12 culture medium consisted of Ham's F12 with L-glutamine, 10% heat-inactivated FBS and 1% penicillin/streptomycin. Reagents for both the RPMI culture media and the Ham's F12 culture media were purchased from Lonza (Verviers, Belgium). DMEM culture medium contained Dulbecco's Modified Eagle's Medium with 4.5 g/l glucose, with L-glutamine, without pyruvate, supplemented

with 10% Foetal Clone II, 1% Non-Essential amino acids, and 1% Penicillin/Streptomycin, all Gibco by Life Technologies (Thermo Fisher Scientific, Waltham, USA).

3.2 Physicochemical Properties

The physicochemical properties of the 14 nm and 20 nm AuNPs, and the PEG-liganded AuNPs were characterised in milli-Q water, RMPI culture medium, and Ham's F12 culture medium. For analysis in the culture medium the AuNP stock solutions were centrifuged at 13 000 x g for 30 minutes and resuspended at a concentration of 1 nM.

3.2.1 Transmission Electron Microscopy

Transmission Electron Microscopy (TEM) was used to determine the size and shape of the AuNPs. The AuNPs in milli-Q water, RPMI culture medium, and Ham's F12 culture medium, were deposited, as droplets, on formvar-coated copper grids (Ted Pella, Redding, USA) and allowed to dry prior to analysis on a FEI Tecnai T12 TEM, operating at 120 kV. For size measurements, a minimum of 50 nanoparticles were measured using ImageJ 1.46r (National Institutes of Health, USA) to obtain an average particle diameter.

3.2.2 Absorbance spectroscopy

Absorbance spectra of the AuNPs were determined using a CE3021 spectrophotometer (Cecil Instruments, Cambridge, UK), in the range between 400 nm and 800 nm, to determine the wavelength at which the peak in absorbance is observed.

3.2.3 Zeta potential

The surface charge (zeta potential) of the AuNPs was determined using Zetasizer Nano ZS (Malvern Instruments, Malvern, UK) at 25°C.

3.2.4 Effects of AuNPs on pH of culture medium

The effect of the AuNPs on the pH of the culture medium at 37°C was measured using a Jenway 3510 pH meter (Cole-Parmer, Staffordshire, UK).

3.2.5 Sterility testing

Sterility of the AuNP suspensions received from Mintek was assessed by the Immunology and Microbiology Section at the NIOH. Sterility was confirmed by plating the samples on Tryptic soy agar (TSA) plates (Diagnostic Media Products, Sandringham, South Africa) and incubating at 37°C for 3 days to determine bacterial growth. Only AuNP samples that tested negative for bacterial contamination were used for further experiments.

3.2.6 Endotoxin assays

Three assays were assessed for their applicability for use in the detection of endotoxin in AuNPs suspensions, and this work has been published (Vetten and Gulumian 2019b). Two of these assays are regarded as traditional assays, namely the *Limulus* amebocyte lysate (LAL) chromogenic assay and the LAL gel-clot assay, and the third assay makes use of a synthetic recombinant Factor C (rFC) protein that selectively recognises endotoxin. All of these assays express endotoxin concentration in terms of endotoxin units per millilitre (EU/ml). All kits and consumables were purchased from Lonza, (Walkersville, USA), certified endotoxin-free. Where dilutions in water were required, LAL Reagent Water (Lonza, Walkersville, USA) was used.

3.2.6.1 Calculation of MVD

The maximum valid dilution (MVD) was calculated for each assay. The MVD is dependent on the desired endotoxin limit and the sensitivity of the assay. In this study, an endotoxin limit of 0.5 EU/ml was used as this is the limit for medical devices (Burkhard Dick *et al.* 2003; FDA 2012), and an acceptable level for *in vitro* cell culture products (Ryan 2004).

This calculation is given by the formula:

$$MVD = \frac{Endotoxin\ limit\ in\ EU/ml}{\lambda}$$

where λ (lambda) is the sensitivity of the assay. In this study, the chromogenic assay has a sensitivity of 0.1 EU/ml, the gel-clot assay has a sensitivity of 0.0313, and the rFC assay has a sensitivity of 0.005 EU/ml.

3.2.6.2 LAL Chromogenic Assay

The Limulus Amebocyte Lysate (LAL) QCL-1000® kit was used for the quantitative traditional Endpoint Chromogenic LAL test. For this assay, endotoxins present in sample catalyses the activation of a proenzyme in the LAL, the rate of which is determined by the concentration of endotoxin present. A colourless substrate (Ac-Ile-Glu-Ala-Arg-p-nitroaniline) is then added and the activated enzyme subsequently catalyses the release of p-nitroaniline (pNA) which is measured spectrophotometrically at 405 nm.

Lyophilised LAL reagent, *E. coli* endotoxin standard, and chromogenic substrate are reconstituted in water. All reagents are allowed to equilibrate to room temperature prior to use. For this assay, the correlation between the absorbance and the endotoxin concentration is linear in the 0.1-1.0 EU/ml range; therefore, the endotoxin stock solution is diluted in water to produce endotoxin standards of 0.1, 0.25, 0.5, and 1.0 EU/ml.

To investigate possible interference of the reaction by AuNPs, a Positive Product Control (PPC) of 0.5 EU/ml endotoxin with various AuNP dilutions was run alongside unspiked samples. A 96-well microplate was pre-equilibrated to 37°C in a digital heating block, and this temperature was maintained for the duration of the experiment. A 50 µl of sample or standard was pipetted into relevant wells and 50 µl of water was pipetted into blank wells. A 50 µl of LAL reagent was pipetted into each well and the microplate was gently tapped to mix. The microplate was incubated for 10 minutes, timed from the addition of LAL Reagent to the first

well and thereafter a 100 µl of chromogenic substrate was added to each well. The plate was tapped to mix and incubated for 6 minutes. A 50 µl of 25% acetic acid was added to each well to stop the reaction, and again the plate was tapped to mix. Absorbance was read at 405 nm on an ELx800 (BioTek, Winooski, USA) and the values of the blank was subtracted from the absorbance readings.

To serve as particle controls, a 50 µl of corresponding AuNP concentrations with 150 µl water were included on the plate. These wells did not receive LAL reagent or substrate, but received 25% acetic acid in the final step. The construction of a standard curve allowed for the quantification of endotoxin in the unknown samples. For the PPCs, the endotoxin concentrations are determined and the difference between spiked and unspiked samples calculated. The difference between these two values should be within 25% of the known spike concentration (0.5 EU/ml), i.e. be between 0.375 and 0.625 EU/ml.

3.2.6.3 LAL Gel-clot Assay

The LAL PYROGENT^{TM} Plus (0.03 EU/ml sensitivity) kit was used for the quantitative gel clot test. In this assay, reagents and test samples are mixed in tubes and incubated for an hour during which endotoxin catalyses the activation of a proenzyme to activated coagulase that then hydrolyses bonds within coagulogen which then self-associates and forms a gelatinous clot. Lyophilised LAL reagent and *E. coli* endotoxin 055:B5 standard are reconstituted with water. The endotoxin stock solution is diluted to produce endotoxin standards of 0.0156, 0.0313, 0.0625, 0.125, 0.25 EU/ml, and is used to verify the lysate sensitivity of the kit. To test for possible interference, PPCs of endotoxin concentrations ranging 0.0156 to 0.25 EU/ml were prepared using AuNP suspensions with dilution factors up to 100 as diluents, and these PPCs were analysed alongside unspiked AuNP samples.

To assess endotoxin levels in AuNP samples, 100 µl of the endotoxin standards, PPCs, unspiked AuNP dilutions, and water as a negative control, was pipetted into glass tubes. A 100 µl of LAL reagent was added to each tube, mixed and placed in

a 37°C dry bath for 1 hour. Incubation was timed from the moment each tube was placed in the dry bath. Following incubation, each tube was inverted 180°. A positive reaction i.e. the presence of endotoxin was characterised by the formation of a firm gel that remained intact momentarily when the tube was inverted. A negative reaction, signifying the absence of endotoxin, was characterised by the absence of a solid clot, even if there was an increase in turbidity or viscosity.

To verify the lysate sensitivity using the endotoxin standards, the endpoint dilution was identified as the last dilution of endotoxin that yields a positive result. The geometric mean of the endpoint was calculated by converting each value to $\log_{10}$ and obtaining the average of these values; followed by the antilog_{10} of the average log value to obtain the lysate sensitivity. Similarly, this approach was used to calculate the endotoxin concentration of the AuNP sample and the PPCs. Products are free of interference by the AuNPs if the geometric mean endpoint of endotoxin in product is within ½ to 2 times the labelled lysate sensitivity.

3.2.6.4 rFC Assay

The PyroGene™ Recombinant Factor C Endotoxin Detection Assay was used as an alternative to the traditional assays described above. *E. coli* endotoxin 055:B5, provided for use as a standard, was reconstituted in water and vigorously shaken on a vortex for 15 minutes. This standard was diluted to create a standard curve ranging from 0.005 – 5.0 EU/ml. In-between each serial dilution, tubes were vortexed for 1 minute to ensure accuracy of dilution.

For the assay, a 100 µl of water, endotoxin standards, or sample was added to relevant wells of a 96-well plate. The plate was pre-incubated at 37°C ±1°C for at least 10 minutes. A 100 µl of working reagent composed of fluorogenic substrate, assay buffer and rFC enzyme in a 5:4:1 ratio, was added to each well. Fluorescence was read at time zero at 360 nm excitation, 440 nm emission on an FLx800 plate reader (BioTek, Winooski, USA). The plate is incubated for one hour at 37°C and then fluorescence is read again. Fluorescence is measured in

Relative Fluorescence Units (RFU), and the change in signal over the hour time period, known as ΔRFU, is corrected for ΔRFU of the blank. The log ΔRFU is proportional to the log endotoxin concentration which is linear between 0.005 and 5.0 EU/ml, therefore a standard curve can be constructed and the endotoxin concentration of a sample can be calculated. The fluorescence of AuNPs alone at 360 nm excitation, 440 nm emission was measured. To test for inhibition or enhancement of the assay, the difference between the PPC and unspiked samples is calculated which should be equal the known concentration of the spike (0.5 EU/ml) within the range of 50-200%.

3.2.7 Redox Potential

The Oxidation Reduction Potential (ORP or redox potential) of 1 nM AuNPs in the RPMI culture medium was measured using a redox potential electrode (Lazar Research Laboratories, Los Angeles, USA) connected to a Jenway 3510 pH meter. The ORP, relative to RPMI culture medium, was measured, where the instrument was zeroed against RPMI medium at the beginning of the experiment, and thereafter the ORP of the RPMI medium was measured again once all measurements had been completed.

3.3 Surface Activity

3.3.1 Electron Spin Resonance

Electron Spin Resonance (ESR) on a EMX spectrometer (Bruker, Billerica, USA) was used to detect free radicals using the spin trap 5,5-dimethyl-1-pyrroline-N-oxide (DMPO, Sigma-Aldrich, St. Louis, USA). For these measurements, 100 mM DMPO, 10 mM H_2O_2 (Merck, Darmstadt, Germany) and AuNPs at 0.5 nM, 1 nM, 2 nM, and 5 nM were mixed prior to ESR measurements. For baseline correction, 100 mM DMPO was used to observe the effects of hydrogen peroxide (H_2O_2, Merck, Darmstadt, Germany) and AuNPs. Measurements were conducted using a cylindrical TM 110 Resonant cavity and a 4-bore AquaX sample cell holder. The instrument settings used were: microwave frequency: 9.5 GHz, power 15 mW, receiver gain 6.32 x 10^4, conversion time 81.92 msec, time constant 40.96 msec, modulation frequency 100 kHz, modulation amplitude 1 G, sweep

time 83.89 sec, sweep width 100 G. Instrument calibration was performed using 4-Hydroxy-2,2,6,6-tetramethylpiperidine-1-oxyl (TEMPOL, Sigma-Aldrich, St. Louis, USA). Relative free radical concentration was estimated based on the peak intensity, as measured by the peak-to-peak height of the observed spectra.

3.3.2 8-Isoprostane

8-Isoprostane is a biologically active F_2-IsoPs that is produced in abundance and therefore used as a biomarker of lipid peroxidation (Milne *et al.* 2011). The 8-Isoprostane EIA Kit (Cayman Chemical, Ann Arbor, USA) is based on the competition between 8-isoprostane and an 8-isoprostane AChE tracer (8-isoprostane-acetylcholinesterase conjugate) for binding sites of an 8-isoprostane-specific rabbit antiserum. The amount of tracer that is able to bind to the antiserum is inversely proportional to the concentration of 8-isoprostane in the sample. The 8-isoprostane standard/sample, the tracer, and the antiserum are added to a 96-well plate supplied with the kit that has rabbit IgG mouse monoclonal antibody attached to the wells, to which the antiserum-isoprostane complex binds. The plate is then washed to remove any unbound reagents. Ellman's Reagent, which contains the substrate to the tracer AChE, is added to the wells. The product of the enzymatic reaction absorbs at 412 nm. The intensity of this absorption is proportional to the amount of tracer bound to the well, which is inversely proportional to the amount of free 8-isoprostane present in the well.

UltraPure water (Cayman Chemical, Ann Arbor, USA) was used to prepare all reagents and buffers. The 8-isoprostane Standard was diluted with water to produce a stock solution that was further diluted with RPMI culture medium to produce standard solutions ranging from 5 pg/ml to 500 pg/ml for the standard curve. The 8-isoprostane tracer and the 8-isoprostane EIA antiserum were reconstituted in EIA buffer. Experiments were run in the 96-well plate supplied with the kit. Wells were allocated for the controls of blanks, total activity, non-specific binding wells (NSB), and maximum binding wells (B_0); and a six point standard curve in duplicate. To test for interference, samples were prepared containing either 8 pg/ml or 40 pg/ml of 8-isoprostane standard, analysed without

AuNPs or spiked with either 1 nM or 5 nM AuNP. Each of these were run in triplicate and the experiment was repeated twice. In addition, NSB wells were prepared containing AuNPs. Reagents were added to relevant wells as shown in Table 3.2, and in the order shown from left to right, following which the plate was covered with plastic film and incubated for 18 hours at 4°C.

Table 3.2 Volumes of reagents used in the 8-Isoprostane EIA assay

Well allocation	**EIA buffer**	**Medium**	**Standard/Sample**	**Tracer**	**Antiserum**
Blank	-	-	-	-	-
NSB	50 µl	50 µl	-	50 µl	-
B_0	-	50 µl	-	50 µl	50 µl
TA	-	-	-	5 µl (only at develop step)	-
Std/ Spike	-	-	50 µl	50 µl	50 µl
NSB AuNP spike	50 µl	-	50 µl AuNPs	50 µl	-

A vial of Ellman's Reagent was reconstituted with water. The wells of the plate were emptied and rinsed five times with Wash Buffer. A 200 µl of Ellman's Reagent was added to each well, and 5 µl of tracer was added to the total activity (TA) wells that had previously not received any reagents. The plate was covered with plastic film and placed on an orbital shaker in the dark at room temperature for 90-120 minutes.

The plastic film was removed without splashing any reagent out of the wells. The absorbance was read at 412 nm on a ELx800 plate reader. To ensure the plate was developed correctly, the values of the B_0 wells should be in the range of 0.3-1.0 Absorbance Units (AU), blank subtracted, and the values of all wells should be less than 2.0 AU. A freely available data analysis tool was used for subsequent calculations (www.caymanchem.com/analysis/eia).

3.4 *In vitro* Toxicity testing

3.4.1 Cell culturing

The bronchial epithelial cell line BEAS-2B (ATCC no. CRL-9609TM) was chosen as an appropriate *in vitro* model for inhalation toxicity. The Chinese hamster ovary CHO cell line (European Collection of Authenticated Cell Cultures, Cat. No. 85050302) was included to demonstrate the applicability of the xCELLigence RTCA system and CytoViva HSI system. The Madin Darby Canine Kidney (MDCK) cell line was used for the OECD CFE assay study.

Cell lines were routinely cultured under standard culturing conditions (37°C, 5% CO_2 in a humidified environment). BEAS-2B cells were cultured in RPMI culture medium, the CHO cells were cultured in Ham's F12 culture medium, and the MDCK cells were cultured in DMEM culture medium.

After reaching sub-confluency, the monolayer was washed with Dulbecco's phosphate buffered saline (DPBS, Lonza, Walkersville, USA) and harvested by a brief incubation with a trypsin/ethylenediaminetetraacetic acid (EDTA) solution (Sigma-Aldrich, St. Louis, USA). The cells were resuspended in culture medium and viability was determined using the trypan blue cell viability assay.

Cell lines were routinely tested for mycoplasma contamination using the MycoAlert™ Mycoplasma Detection Kit (Lonza, Walkersville, USA). Cell culture medium is mixed with MycoAlert Reagent and incubated for 5 minutes prior to reading luminescence on an FLx800 microplate reader. MycoAlert Substrate is then added and incubated for 10 minutes. Luminescence is measured again and the ratio of the second reading over the first reading is calculated. A positive result for mycoplasma contaminated is defined as a ratio >1.0; whilst a ratio of <0.9 is indicative of a negative result.

3.4.2 Applicability of existing assay systems to AuNPs

Investigations into the potential interference of AuNPs in the conventional XTT, ATP, and LDH assays, as well as the applicability of cell impedance technology

using the xCELLigence RTCA system, were conducted and published by our research group (Vetten *et al.* 2013). Results on the 14 nm AuNP from the interlaboratory comparison study on the OECD Colony Forming Efficiency (CFE) assay to assess cytotoxicity are also included.

BEAS-2B cells were seeded at 1 x 10^4 cells/well in a 96-well plate using RPMI culture medium without phenol red and were allowed to proliferate for 24 hours prior to treatment with 1 or 5 nM of 14 nm AuNPs for 1 hour, whilst untreated control cells received medium only. Cell viability was then assessed using the XTT, LDH, and ATP assays.

3.4.2.1 XTT assay

For the traditional formazan-based XTT assay, the *In Vitro* Toxicology Assay Kit (Sigma-Aldrich, St. Louis, USA) was used. Positive control cells received 500 µM hydrogen peroxide. The supplied XTT with 1% phenazine methosulfate (PMS, Sigma-Aldrich, St. Louis, USA) was reconstituted with RPMI medium without phenol red or FBS, resulting in a saturated 1 mg/ml solution. XTT solution was added to each well to a final volume of 20% per well. The plate was incubated for 2 hours and the absorbance was read at 450 nm on an ELx800. To assess possible interference with the optical readout, the absorbance of 1 and 5 nM AuNPs in RPMI culture medium without phenol red and with unreduced XTT was measured.

3.4.2.2 LDH assay

For the measurement of the release of lactate dehydrogenase (LDH), the CytoTox-ONE™ Homogeneous Membrane Integrity Assay (Promega, Madison, USA) was used. Lysis solution provided with the kit was added to designated wells to generate Maximum LDH Release values. The CytoTox- ONE™ Reagent was added to each well in a 1:1 ratio and he plate was incubated at 22°C for 10 mins. Stop solution was then added and the plate was shaken for 10 secs. LDH released into the culture medium is measured with a 10-minute coupled enzymatic assay that results in the conversion of resazurin into resorufin. Fluorescence of resorufin

was then measured at 560 nm excitation, 590 nm emission on an FLx800 plate reader.

3.4.2.3 ATP assay

The CellTiter-Glo® Luminescent Cell Viability Assay (Promega, Madison, USA) was used for determination of the presence of metabolically active cells through the quantitation of ATP. Positive control cells received 500 µM hydrogen peroxide. The CellTiter-Glo® Reagent was added directly to cells in multiwell plates. The plate was incubated at room temperature for 10 minutes to allow for the lysis of cells and the release of ATP. Luciferin is then catalysed by a stable form of luciferase in the presence of Mg^{2+}, ATP and molecular oxygen to generate the luminescent product oxyluciferin which was detected using an FLx800 plate reader. To test for interference of AuNPs with the conversion of substrate to product, the CellTiter-Glo® Reagent was incubated with 1.5 µM ATP as a co-factor and AuNPs.

3.4.2.4 Colony Forming Efficiency (CFE) Assay

This work was conducted as part of an interlaboratory comparison study on the CFE assay. A detailed SOP was provided by the Joint Research Centre (JRC) to ensure that all laboratories involved in the study followed the exact procedure. Details can be obtained in final report of this study (Ponti *et al.* 2014). NPs code C that were used in the interlaboratory study are the 14 nm AuNPs used in this thesis. It was not necessary to investigate the interference of AuNPs on this methodology as no optical measurements were needed for the assay.

In brief, MDCK cells were seeded in 60 x 15 mm dishes at 200 cells in 3 ml of DMEM culture medium, and allowed to recover in the incubator for 24 hours prior to treatment. Experimental dishes were treated with 14 nm AuNPs, untreated negative control dishes received medium only, and positive control dishes received 100 µM sodium chromate, Na_2CrO_4 (Sigma-Aldrich, St. Louis, USA).

Concentrations of the AuNPs in the interlaboratory study, as expressed in the above-mentioned report, were provided in molarity of Au; as opposed to molarity of NPs as provided by Mintek, SA, and used in this thesis. To convert number of NPs per ml to molarity of NPs, the following equation is used, as provided by Mintek:

Molarity of AuNPs (nM) = Number of nps/ml x (1.67×10^{-12})

The corresponding concentrations are provided in Table 3.3.

Table 3.3 Concentrations of 14 nm AuNPs used in the interlaboratory CFE study.

Concentrations were expressed in molarity of gold and in number of nps/ml. These values were converted to concentrations expressed in molarity of NPs, as used in the present study.

Concentrations of AuNPs in molarity of gold	Number of NPs/ml	Concentrations of AuNPs in molarity of AuNPs
1 µM	1.16×10^{10} nps/ml	0.019 nM ≈ 0.02 nM
5 µM	5.78×10^{10} nps/ml	0.097 nM ≈ 0.1 nM
10 µM	1.16×10^{11} nps/ml	0.194 nM ≈ 0.2 nM
50 µM	5.78×10^{11} nps/ml	0.965 nM ≈ 1 nM
100 µM	1.16×10^{12} nps/ml	1.937 nM ≈ 2 nM

Cells were incubated for 72 hours; thereafter medium was removed from the dishes and cells were fixed in 10% (v/v) formaldehyde solution in DPBS for 15 mins at room temperature. Cells were then stained with filtered staining solution composed of 10% (v/v) Giemsa stain (Sigma-Aldrich, St. Louis, USA) in MilliQ water for 30 mins at room temperature. Dishes were allowed to dry overnight in a fume hood prior to counting of colonies under a microscope according to the following criteria: (1) Colonies must contain at least 50 cells each; (2) the number of colonies in the negative control must not be less than 90; (3) the plating

efficiency must not be less than 45%; and (4) positive control dishes must show complete cell death.

3.4.2.5 Impedance Technology

Impedance experiments were conducted in 96-well E-Plates using the xCELLigence RTCA single plate (SP) instrument from ACEA Biosciences (San Diego, USA) with RTCA software (version 1.2), shown in Figure 3.1. BEAS-2B cells and CHO cells were utilised to investigate the applicability of label-free cell impedance technology for the assessment of cytotoxicity of AuNPs.

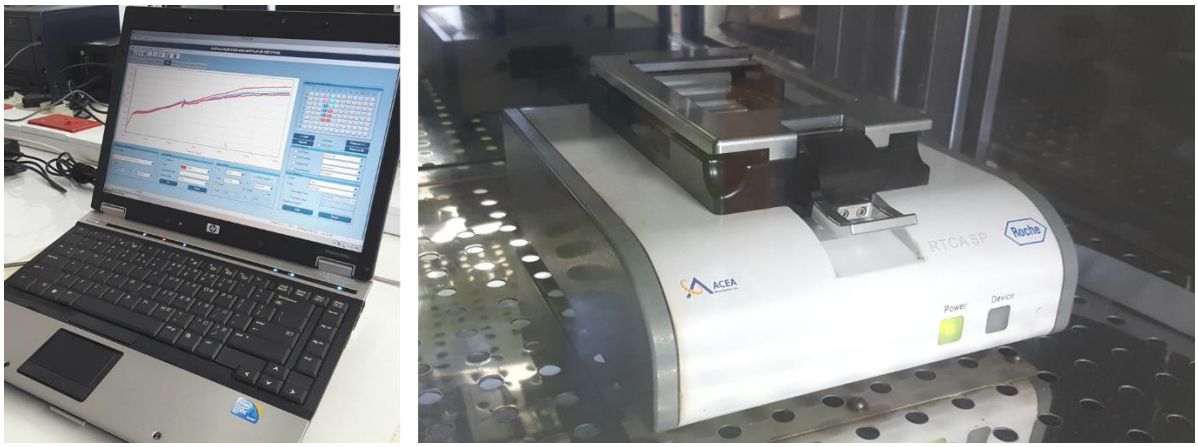

Figure 3.1 Photo of the xCELLigence RTCA system housed in the Toxicology Department at the NIOH.

Set-up of Experiments

In order to determine an ideal seeding concentration for the BEAS-2B and CHO cells, growth curves were obtained by seeding cells at a range of concentrations and acquiring a scan every 15 minutes. The BEAS-2B cells were seeded at 5 x 10^3 cells/well, 1 x 10^4 cells/well, 2.5 x 10^4 cells/well, 5 x 10^4 cells/well, and 1 x 10^5 cells/well in triplicate in a 96 well E-Plate and placed in the RTCA station. The CHO cells were seeded at 1 x 10^2 cells/well, 2 x 10^2 cells/well, 5 x 10^2 cells/well, 1 x 10^3 cells/well, 2 x 10^3 cells/well and 4 x 10^3 cells/well in a 96 well E-Plate.

To demonstrate the effect of complete cell death on observed CI, BEAS-2B cells were seeded at 1 x 10^4 cells/well in a 96-well E-Plate and allowed to proliferate for 24 hours prior to the addition of 500 µM hydrogen peroxide. Concurrently, medium-only cell-free wells had 5 nM 14 nm AuNPs added after 24 hours to determine any potential effects, if any, on CI.

Comparison of cytotoxicity in two cell lines

For cytotoxicity studies, seeded E-Plates were placed in the RTCA station and allowed to proliferate for 24 hours prior to treatment, during which time a scan was acquired every 15 minutes. Following addition of AuNPs, scans were acquired every minute for 2 hours, and then every 15 minutes for the remainder of the experiment.

Following the seeding experiments described above, a concentration of 1 x 10^4 cells/well was chosen for future experiments on the BEAS-2B cells; whilst for the CHO cells, a concentration between 2 x 10^3 cells/well and 4 x 10^3 cells/well was deemed most appropriate and therefore a seeding concentration of 3 x 10^3 cells/well was used for further experiments. The cells were treated with the 14 nm or 20 nm AuNPs at final concentrations of 1 nM, 2 nM, and 5 nM. For statistical analysis, within each experiment, CI of each curve was normalized at the point of treatment. The slope for each curve of the normalized CI for the time period between treatment point and the highest CI value, i.e. confluency, of the untreated cells was calculated. The calculated slopes were exported and a t-test was conducted using STATISTICA version 10 (StatSoft, Inc., Tulsa, USA) to investigate if the differences between treated and untreated slopes were significant. Differences were considered statistically significant if $p < 0.05$.

3.4.3 Cytotoxicity of AuNPs to BEAS-2B cells

The short-term cytotoxity of all AuNPs in BEAS-2B cells was assessed using the xCELLigence RTCA SP system. BEAS-2B cells were seeded at 1 x 10^4 cells/well and allowed to proliferate for 24 hours prior to treatment, during which time a scan was acquired every 15 minutes. Following addition of AuNPs at 1 nM, 2 nM,

and 5 nM, scans were acquired every minute for 2 hours, and then every 15 minutes for the remainder of the experiment. The acquisition of scans was stopped 24 hours after treatment.

3.4.4 Genotoxicity

Since only the 14 nm AuNP, 20 nm AuNP and PCOOH AuNPs were shown to enter the BEAS-2B cells, these three nanoparticles were investigated for their ability to induce chromosomal damage using the cytokinesis-block micronucleus (CBMN) assay. This assay had been shown in our laboratory to be suitable for the genotoxicity testing of AuNPs (George *et al.* 2017).

BEAS-2B cells were seeded at 5 x 10^5 cells in a 25 cm^2 tissue culture flask and incubated for approximately 24 hours, until the cells reached 50% confluency. Cells were treated with fresh RPMI culture medium containing either 1 nM, 2 nM, or 5 nM AuNPs, 150 ng/ml Mitomycin C (MMC, Sigma-Aldrich, St. Louis, USA) for the positive control, or medium only for the untreated control. Cells were incubated for 2 hours prior to the addition of 9 µg/ml Cytochalasin B (Cyt-B, Sigma-Aldrich, St. Louis, USA), followed by another 46 hours incubation.

At the end of the incubation period, cells were trypsinised as described in Section 3.4.1 Cell culturing. Cells were centrifuged at 200 x g for 5 minutes, and resuspended in DPBS. Cells were centrifuged again and the supernatant discarded. Cells were incubated for less than two minutes with hypotonic solution containing 50% RPMI culture medium in distilled water, followed by centrifugation and removal of the supernatant. Cells were fixed overnight in ice-cold 3:1 methanol-acetic acid solution.

The following day, cells were centrifuged and resuspended in 3:1 methanol-acetic acid solution. Microscope slides were blind coded beforehand to ensure the identity of the sample was not known during analysis. The slides were rinsed with distilled water prior to use. A few drops of cell suspension were placed on the slides which were passed through steam to aid the spreading of the cells. Slides

were air dried and stained with 5% Giemsa stain (Sigma-Aldrich, St. Louis, USA) in water for two minutes prior to rinsing with distilled water, and drying. Slides were then examined at 40x and 100x magnification using an Olympus BX41 Microscope (Olympus Corporation, Tokyo, Japan).

The number of mononucleated, binucleated, and multinucleated cells from at least 500 cells were counted and the Replication Index (RI) was calculated according to the equation (OECD 2016b):

$$RI = \frac{\left((\text{No. binucleate cells}) + (2 \times \text{No. multinucleate cells})\right) \div (\text{Total No. cells})_{\text{Treated}}}{\left((\text{No. binucleate cells}) + (2 \times \text{No. multinucleate cells})\right) \div (\text{Total No. cells})_{\text{Control}}} \times 100$$

The RI is a measure of the cytostatic activity of the treatment as compared to the untreated control. Scoring was done only in binucleated cells according to published criteria (Fenech *et al.* 2003). MN and nucleoplasmic bridges (NPB) were scored in at least 2000 binucleated cells and their frequency in at least 1000 binucleated cells was calculated. Significance was tested for using an ANOVA in Excel.

3.5 Intracellular Uptake

3.5.1 Applicability of the CytoViva HSI system for label-free assessment of uptake

BEAS-2B cells and CHO cells were utilised to demonstrate the applicability of the CytoViva Hyperspectral Imaging (HSI) System (CytoViva, Inc., Auburn, USA) to assess uptake of AuNPs, and this work has been published (Vetten *et al.* 2013). This system is shown in Figure 3.2.



Figure 3.2 Photo of the CytoViva HSI system housed in the Toxicology Department at the NIOH.

3.5.1.1 Slide preparation

BEAS-2B and CHO cells were seeded at 3 x 10^4 cells/cm^2 and 1.6 x 10^4 cells/cm^2, respectively, in 8-well Millipore Millicell EZ-slides (Merck, Darmstadt, Germany). Cells were allowed to proliferate for 24 hours prior to addition of 14 nm or 20 nm AuNPs at 1 nM, and incubation for 1, 4, or 6 hours at 37°C. Cells were washed three times with relevant culture medium, followed by three washes with DPBS, and then fixed at 4°C with 4% formalin in Tris/HCl buffer (Merck, Darmstadt, Germany) for 15 mins. Slides were washed once with DPBS and air-dried. Coverslips were immobilised onto the slides with Kaiser's glycerol gelatin (Merck, Darmstadt, Germany).

3.5.1.2 Dark-field microscopy

Dark-field images of the cells following uptake were captured at either 60x or 100x magnification using the CytoViva 150 Unit integrated onto the Olympus BX43 microscope. Images were acquired using a Dagexcel X16 camera and the associated software.

3.5.1.3 Hyperspectral Imaging (HSI) and Spectral Libraries

Hyperspectral Imaging (HSI) was performed at 60x magnification using the HSI System 1.1 and ENVI software (version 4.4). In addition to the scans of the cells treated with gold nanoparticles as described above, scans were also performed on the AuNPs alone. For this analysis, a drop of AuNP solution was placed on a microscope slide, spread out and allowed to dry. Spectral libraries were collected by selecting the spectra of particles that appear to either be singularly dispersed or had visually agglomerated to form larger particles.

3.5.1.4 Principal Component Analysis (PCA)

Principal Component Analysis (PCA) was conducted on the spectra collected for the spectral libraries, including all wavelengths acquired from 400 to 1000 nm acquired, using Statistica version 12.

3.5.1.5 Spectral Angle Mapper (SAM)

The image classification algorithm SAM (spectral angle mapper) was conducted using the ENVI software to map the spectral libraries onto the scans of the cells incubated with particles. A threshold of 0.08 maximum acceptable angles (radians) between the known and unknown spectra was applied.

3.5.2 Uptake of AuNPs

Uptake of AuNPs was assessed at both 37°C (standard culturing conditions) and at 4°C to compare energy-dependence of uptake. Making use of the label-free CytoViva HSI system and methodologies described above, the uptake of all AuNPs was assessed after in BEAS-2B cells at 1 nM. Following treatments, the slide preparation was performed as described in 3.5.1.1 Slide preparation, and

dark field microscopy was performed as described in 3.5.1.2 Dark-field microscopy.

3.5.2.1 Uptake after 2 hours at 37°C and 4°C

BEAS-2B cells were seeded at 3 x 10^4 cells/cm^2 in an 8-well Millipore Millicell EZ-slide. Cells were allowed to proliferate under standard culturing conditions for 24 hours prior to treatment. For the treatments at 4°C, cells were pre-incubated at 4°C for 30 mins prior to treatment. Cells were treated with 1 nM of AuNPs for 2 hours at either 37°C or 4°C.

3.5.2.2 Uptake after 24 hours

Due to observed lack of uptake after 2 hours of incubation at 37°C, BEAS-2B cells were also treated for 24 hours at 37°C with POH, PBtn, PNTA, PAZ, and PAM AuNPs prior to washing, fixation, and image acquisition as described above.

3.5.3 Assessment of mechanism of uptake of AuNPs into BEAS-2B cells

In order to assess the mechanism of uptake, chemical inhibitors known to block endocytosis pathways were employed. Firstly, the cytotoxity of the inhibitors was assessed to ensure that the concentrations did not kill the cells during the study. Then the cells were treated with the inhibitors prior to incubation with the AuNPs, followed by analysis using the CytoViva HSI system. This work, and that described in section 3.5.2 Uptake of AuNPs, has been published (Vetten and Gulumian 2019a)

3.5.3.1 Cytotoxicity of inhibitors

Choice and concentration of inhibitors were based on similar studies on the endocytosis mechanisms of nanoparticles into BEAS-2B cells (Boylan *et al.* 2012; Kim *et al.* 2012).

Genistein (Sigma-Aldrich, St. Louis, USA) and chlorpromazine (Sigma-Aldrich, St. Louis, USA) were selected as inhibitors of caveolin- and clathrin-mediated endocytosis respectively. In order to determine the non-cytotoxic concentrations

of these inhibitors, initial experiments were conducted to investigate their cytotoxicity at a range of concentrations, specifically, genistein from 25 µM to 300 µM and chlorpromazine from 4.4 µM to 141 µM. Cytotoxicity studies were conducted using the xCELLigence RTCA SP system. Cells were seeded at 1 x 10^4 cells/well in a 96-well E-Plate and placed in the RTCA station and allowed to proliferate for 24 hours for all cells prior to treatment, during which time a scan was acquired every 15 minutes. Old medium was removed and the cells were treated with fresh medium containing the inhibitors. Untreated control wells received an equivalent volume of fresh medium. Scans were acquired every 5 minutes for 3 hours, and then every 15 minutes for the remainder of the experiments.

3.5.3.2 Effect of inhibitors on the uptake of AuNPs

Subsequent to the identification of a non-cytotoxic concentration for each of the inhibitors, cells were seeded at 3 x 10^4 cells/cm^2 in an 8-well Millipore Millicell EZ-slide and allowed to proliferate overnight under standard culturing conditions. For treatment, either 200 µM genistein or 14 µM chlorpromazine were prepared in pre-warmed RPMI cell culture medium. Culture medium was replaced with medium containing inhibitors, or fresh medium for control. Cells were incubated for 1 hour with inhibitors, followed by addition of AuNPs to a final concentration of 1 nM, and incubation for 2 hours.

At the end of treatment, cells were washed three times with culture medium, followed by three washes with DPBS. Cells were then fixed at 4°C with 4% formalin in Tris/HCl buffer for 15 mins. Slides were washed once with DPBS and air-dried, and coverslips were immobilised onto the slides with Kaiser's gelatine.

Spectral libraries were created from scans of AuNPs alone using the particle filter feature. HSI scans of the slides were acquired using ENVI vs4.8 software the CytoViva HSI system, followed by SAM analysis. Semi-quantitative analysis was performed using ImageJ 1.46r (National Institutes of Health, USA). This approach to semi-quantitative analysis is based on previously published

nanoparticle uptake experiments (Mortimer *et al.* 2014). Pixels representing particles in cells, identified by SAM, were counted and normalised to the area of the cell, therefore resulting in a % Area for each cell that represented a measure of uptake. The % Area for each cell was then normalised to the mean % Area of the control (without inhibitors) within each experiment, to obtain a percentage uptake value relative to the control. At least 45 cells per replicate were counted; samples were prepared in duplicate on two independent days, therefore n > 190 cells. A boxplot template (Vertex42 LLC, 2011, USA) was used to analyse the distribution of data. A *t*-test was used to determine statistical significance compared to the control cells.

3.5.4 Localisation of AuNPs using TEM

Since only the 14 nm AuNP, 20 nm AuNP and PCOOH AuNPs entered the cells, only these NPs were used. BEAS-2B cells were seeded at 2 x 10^6 cells in a 75 cm^2 flask and allowed to proliferate for 24 hours. Cells were treated with 1 nM AuNPs for 2 hours at 37°C.

Medium was removed and cells were washed with DPBS and trypsinised, following which the cells were washed again with DPBS and then fixed with 2.5% gluteraldehyde (Sigma-Aldrich, St. Louis, USA) and 2% formaldehyde (Merck, Darmstadt, Germany) solution in DPBS (pH 7.4) at room temperature for 1 hour. Cells were centrifuged at 10 000 x g for 10 minutes and then placed in fresh fixative solution overnight. Cells were then washed three times in 0.075 M phosphate buffer and fixed in 0.5% aqueous osmium tetroxide (Protea Laboratory Solutions, Midrand, South Africa) for 1 – 2 hours. Cells were washed three times in double distilled water, followed by progressive dehydration in ethanol (Merck, Darmstadt, Germany) (30%, 50%, 70%, 90%, 100%, 100%, and 100%) for 10 minutes in each. Cells were then rinsed in propylene oxide (Sigma-Aldrich, St. Louis, USA) for 10 minutes prior to infiltration with Quetol (Advanced Laboratory Solutions, Randburg, South Africa):propylene oxide (ratio 1:2) for 1 hour and then Quetol:propylene oxide (ratio 2:1) for 1 hour. Cells were then

placed in pure epoxy resin Quetol for 4 hours to allow for infiltration, and then placed in fresh Quetol in moulds and allowed to polymerise at 60°C for 36 hours.

Ultrathin (90-100nm) sections were cut, picked up on grids and 4% aqueous uranyl acetate (Agar Scientific, Stansted, UK) was added for 5 mins. Samples were rinsed in double distilled water and then contrasted with Reynolds' lead citrate (Sigma-Aldrich, St. Louis, USA) for 2 mins, followed by another rinse with double distilled water. A Philips CM10, operated at 80kV, was used to acquire TEM images of the cells.

3.6 Summary of statistics used

In summary, where relevant, averages and standard deviations were calculated in Microsoft Excel 2016. Calculations for the 8-Isoprostane EIA kit was performed using Cayman Chemical's freely available tool. Standard deviations on the xCELLigence graphs were automatically calculated by the RTCA software, whilst the statistics on the slopes was conducted using STATISTICA version 10. For the CBMN assay, ANOVA testing was done in Microsoft Excel 2016. Principal Component Analysis was performed in STATISTICA version 12. Finally, analysis of the effect of inhibitors on uptake was performed using a boxplot template form Vertex42 LLC (USA).

3.7 Summary of methods

Table 3.4 provides a brief summary of the assays or instruments used in this study, and the main objective for their inclusion in this thesis.

Table 3.4 Summary of methods used in this study

Assay/technology	**Objective**
TEM	Particle size and shape, aggregation/agglomeration state
Absorbance spectroscopy	Aggregation/agglomeration state
Zeta Potential	Surface charge
pH meter	Biologically significant pH changes
Redox potential electrode	Relative redox potential
ESR	Free radicals
Endotoxin assays	Applicability of *in vitro* tests
8-Isoprostane EIA kit	
XTT assay	
LDH assay	
ATP assay	
CFE assay	
Impedance technology	
Cytoviva HSI	
Impedance technology	Cytotoxicity of AuNPs
Cytokinesis-block micronucleus assay	Genotoxicity of AuNPs
CytoViva HSI system	Uptake of AuNPs
CytoViva HSI system	Mechanism of uptake of AuNPs
TEM	Intracellular localisation of AuNPs

Chapter 4 – Results

4.1 Physicochemical properties

Physicochemical properties of nanoparticles need to be fully characterised for hazard identification in order to understand which properties of the nanoparticles influence toxicity and uptake. The physicochemical properties of all AuNPs were characterised in milli-Q water and in RPMI culture medium. In addition, the non-functionalised AuNPs, the 14 nm and 20 nm AuNPs, were also characterised in Ham's F12 culture medium.

4.1.1 Transmission Electron Microscopy

The calculated average particle diameter of at least 50 particles in water and RPMI culture medium, as well as Ham's F12 culture medium where relevant, is shown in Table 4.1. No major changes in diameter were observed when the AuNPs were suspended in either of the culture medium.

Table 4.1 Average particle size in milli-Q water, RPMI culture medium, and Ham's F12 cuture medium, as determined by TEM

	14 nm AuNP	**20 nm AuNP**	**POH AuNP**	**PCOOH AuNP**	**PBtn AuNP**	**PNTA AuNP**	**PAZ AuNP**	**PAM AuNP**
Water	14 nm (±1 nm)	24 nm (±3 nm)	14 nm (±1 nm)	15 nm (±1 nm)	15 nm (±2 nm)	16 nm (±2 nm)	14 nm (±2 nm)	15 nm (±1 nm)
RPMI culture medium	17 nm (±3 nm)	22 nm (±4 nm)	15 nm (±2 nm)	15 nm (±2 nm)	15 nm (±1 nm)	16 nm (± 2 nm)	16 nm (±2 nm)	16 nm (±2 nm)
Ham's F12 culture medium	16 nm (±2 nm)	24 nm (±3 nm)	N/A	N/A	N/A	N/A	N/A	N/A

Figure 4.1 (A, C, E) shows representative images obtained from TEM of the 14 nm and 20 nm AuNPs suspended in water, RPMI culture medium, and Ham's F12 culture medium; whilst Figure 4.2 (A, C) shows images of the PEG-liganded AuNPs in water and in RPMI culture medium. All AuNPs were primarily spherical in shape, with some ellipsoid nanoparticles present. This polydispersity was probably due to the conditions of synthesis where factors such as salt concentration, pH, and temperature have been shown to affect this (Li *et al.* 2011; Zabetakis *et al.* 2012). In addition, as compared to AuNPs in water, all of the AuNPs retained their shape and size when resuspended in RPMI and Ham's F12 culture medium, with minimal signs of particle agglomeration present. As expected, the citrate stabilised 14 nm AuNPs were of similar size as the PEG-liganded 14 nm AuNPs.

4.1.2 Absorbance spectra

All AuNPs in suspension obtained from Mintek were dark red, as expected and previously reported in literature (Murphy *et al.* 2008), and retained their colour following suspension in medium thereby suggesting that they remained singularly dispersed. Figure 4.1 (B, D, F) shows the absorbance spectra between 400 nm and 800 nm obtained from the 14 nm and 20 nm AuNPs suspended in water, RPMI culture medium, and Ham's F12 culture medium; whilst Figure 4.2 (B, D) shows the absorbance spectra of the PEG-liganded AuNPs in water and in RPMI culture medium. Plasmon absorption is clearly visible in these images and the maximum absorbance peak was automatically identified by the instrument's software. Similar shaped spectra were observed in all images.

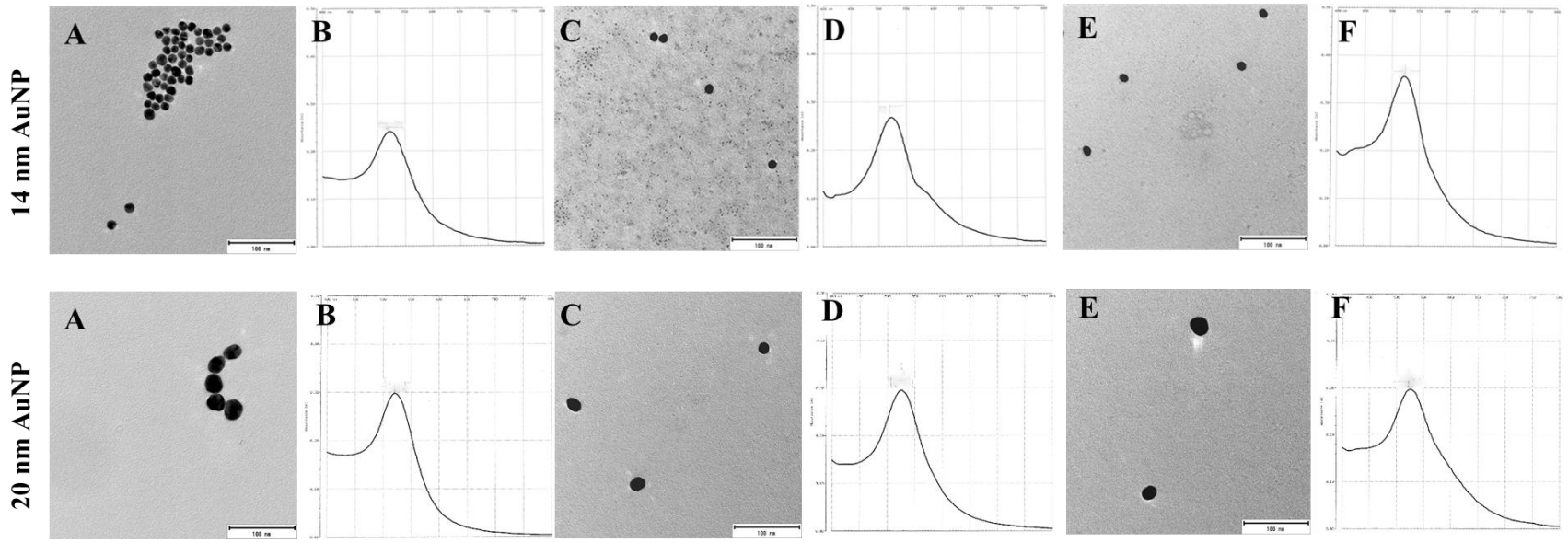

Figure 4.1 Representative TEM images (A, C, E) and absorbance spectra from 400 nm to 800 nm (B, D, F) of 14 nm AuNPs (top), 20 nm AuNP (bottom). AuNPs were suspended in water (A, B), RPMI culture medium (C, D), or Ham's F12 culture medium (E, F). Scale bars in the TEM images = 100 nm.

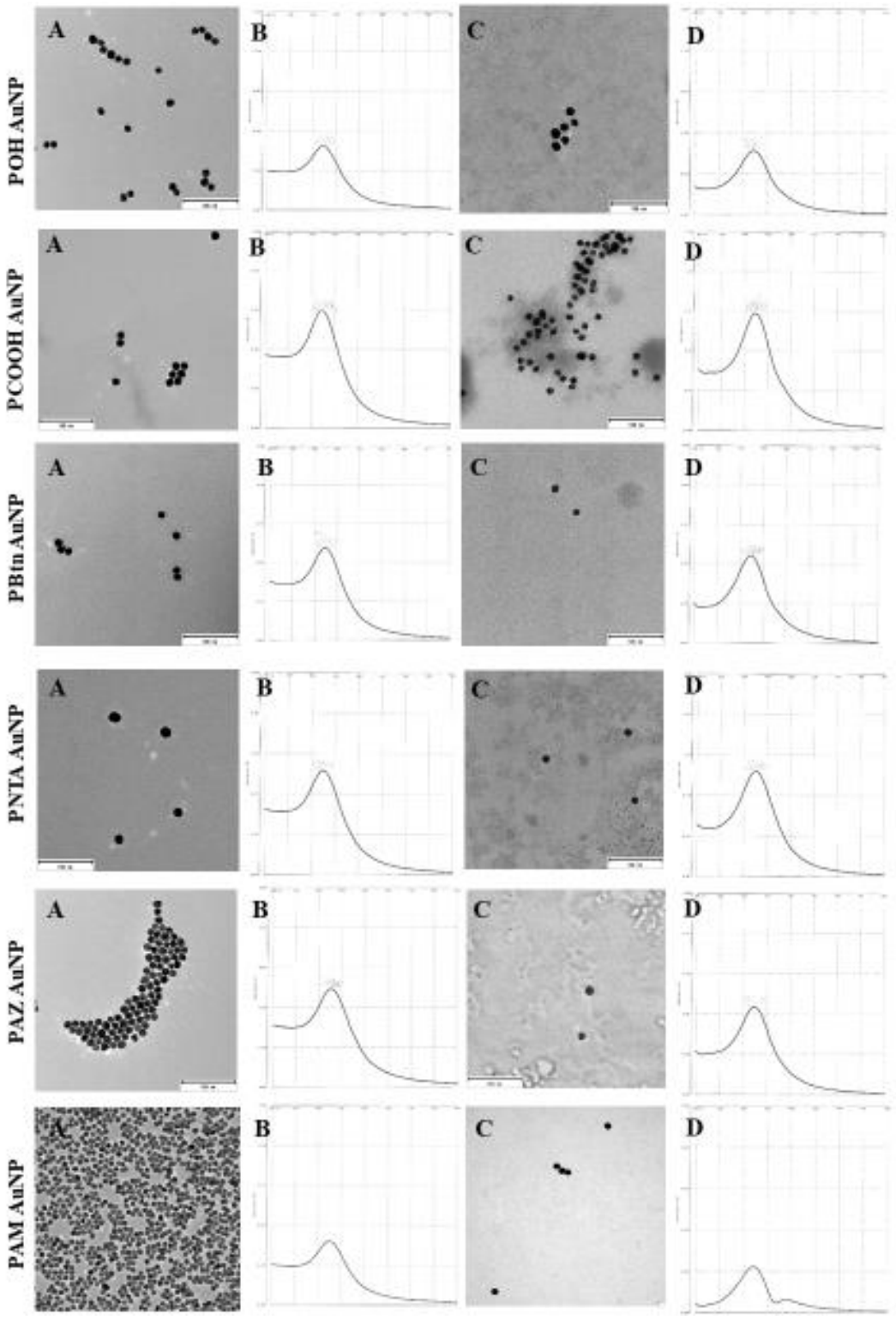

Figure 4.2 Representative TEM images (A, C) and absorbance spectra from 400 nm to 800 nm (B, D) of POH, PCOOH, PBtn, PNTA, PAZ, and PAM AuNPs (top to bottom). AuNPs were suspended in water (A, B) or RPMI culture medium (C, D) prior to analysis. Scale bars in the TEM images = 100 nm.

A summary of the maximum absorbance peaks is shown in Table 4.2 where it can be observed that there were no considerable changes when the AuNPs were suspended in either of the culture medium, as compared to that of water. For all of the AuNPs suspended in both water and culture media, UV-Vis spectra confirmed a predominant peak at approximately 521-526 nm. For the PAM AuNPs, a minor second peak was present when the AuNPs were suspended in RPMI culture medium (Figure 4.2 bottom row D) at 587 nm, suggesting some aggregation however only minimal aggregation was observed in the TEM images. The position of the maximum absorbance peaks are similar to that reported in literature for colloidal AuNPs of similar size (Fraga *et al.* 2013; Jain *et al.* 2006; Link and El-Sayed 1999), and this confirms that no changes in shape or aggregation occurred once suspended in either culture medium.

4.1.3 Zeta Potential

The zeta potential of the AuNPs as provided by Mintek in milli-Q water, and following their suspension in culture medium, is presented in Table 4.2. With the exception of the PAM AuNP, all of the AuNPs were negatively charged in water in the range of -18 to -38 mV, whilst the PAM AuNP was positively charged at +9.3. However, when the AuNPs were suspended in either RPMI or Ham's F12 culture medium, all nanoparticles showed a slightly negative charge in the range of -6 and -12 mV.

4.1.4 Effect of AuNPs on pH of culture medium

The pH at 37°C of the AuNPs suspended in culture medium was measured and compared to that of the culture medium alone in order to determine if there was a biologically relevant change in pH once the AuNPs were added. Results presented in Table 4.2 show no noteworthy changes in pH. In all instances, the pH of the culture media containing AuNPs remained close to that of the media alone and no biologically significant changes were observed.

Table 4.2 Physicochemical properties of the AuNPs

	Absorbance Peak			**Zeta Potential (mV)**			**pH at 37**	
	Water	**RPMI culture medium**	**Ham's F12 culture medium**	**Water (provided on Certificate of Analysis)**	**RPMI culture medium**	**Ham's F12 culture medium**	**RPMI culture medium (pH 7.47)**	**Ham's F12 culture medium (pH 7.60)**
14 nm AuNP	522 nm	523 nm	523 nm	-33.5	-10.2	-11.4	7.34	7.53
20 nm AuNP	521 nm	526 nm	526 nm	-37.9	-12.1	-11.3	7.39	7.62
POH AuNP	522 nm	522 nm	N/A	-36.0	-9.4	N/A	7.50	N/A
PCOOH AuNP	523 nm	524 nm	N/A	-31.7	-9.4	N/A	7.48	N/A
PBtn AuNP	523 nm	523 nm	N/A	-18.9	-8.3	N/A	7.46	N/A
PNTA AuNP	524 nm	525 nm	N/A	-26.4	-6.6	N/A	7.50	N/A
PAZ AuNP	526 nm	523 nm	N/A	-20.8	-7.5	N/A	7.48	N/A
PAM AuNP	524 nm	521 nm	N/A	+9.3	-8.7	N/A	7.58	N/A

4.1.5 Endotoxin assays

The interference of the 14 nm AuNPs on three *in vitro* endotoxin assays, namely the LAL chromogenic assay, the LAL gel-clot method, and the recombinant Factor C (rFC) assay, was investigated.

4.1.5.1 Maximum Valid Dilution (MVD)

The MVD for each assay was calculated using an endotoxin limit of 0.5 EU/ml and the supplied kit sensitivity value. These MVD are presented in Table 4.3 and were used to validate the dilutions used in the interference experiments.

Table 4.3 Maximum valid dilution (MVD) values for each assay

Assay	**Sensitivity (EU/ml)**	**Maximum valid dilution**
Chromogenic assay	0.1 EU/ml	5
Gel-clot assay	0.0313 EU/ml	16
rFC assay	0.005 EU/ml	100

4.1.5.2 LAL Chromogenic Assay

Average absorbance values of particle controls assessed for the LAL Chromogenic assay are shown in Table 4.4. Interestingly, with the exception of the undiluted sample, the absorbance values of the particle controls were lower than those of the blank. These values were subtracted from the samples and PPCs' absorbance readings where relevant.

Table 4.4 Average absorbance at 405 nm of particle controls and blank wells

Dilution Factor (AuNP concentration in nM)	**Average absorbance**	**Standard Deviation**
Blank	0.091	0.002
Undiluted (5 nM AuNP)	0.125	0.016
5x (1 nM AuNP)	0.064	0.003
10x (0.5 nM AuNP)	0.057	0.002
50x (0.1 nM AuNP)	0.051	0.002

Calculation of the endotoxin concentration of the undiluted 5 nM AuNP sample produced values above the range of the standard curve >1 EU/ml, and therefore this concentration was not used in further analyses. The endotoxin concentrations were calculated for the unspiked samples and the PPCs containing 0.5 EU/ml. If there is no interference, the difference between the values of the unspiked samples and the PPC should be the concentration of the endotoxin in the PPC ± 25%, therefore between 0.375 and 0.625 EU/ml. For all dilutions, the difference in the calculated concentrations between the unspiked samples and the PPC were all below the recommended range (Table 4.5), which is indicative of inhibition. Regardless, the MVD value for this assay is five (Table 4.3) and therefore all dilutions greater than five would not have been valid even if the inhibition was overcome.

Table 4.5 Calculated endotoxin concentration (EU/ml)

Dilution Factor (AuNP concentration in nM)	**Calculated concentration (EU/ml) for unspiked samples**	**Calculated concentration (EU/ml) of 0.5 EU/ml PPC**	**Difference**
5x (1 nM AuNP)	0.650	0.925	0.275
10x (0.5 nM AuNP)	0.414	0.576	0.162
50x (0.1 nM AuNP)	0.337	0.653	0.316

4.1.5.3 LAL Gel-clot Assay

The lysate sensitivity was calculated to be 0.03125 EU/ml, which corresponded with the expected sensitivity of the kit. To screen for interference of the AuNPs with the assay, AuNPs at various concentrations were spiked with endotoxin standard and assayed using standard procedures. The geometric mean endpoint at each AuNP concentration was calculated and is shown in Table 4.6. The calculated endpoint at dilution factor of 5 and 10 is 0.0156 EU/ml, i.e. at a spiked endotoxin concentration of 0.0156 EU/ml a positive result was seen suggesting either genuine endotoxin contamination or enhancement of the reaction. At a dilution factor of 50, the endpoint was the same as the lysate sensitivity, suggesting that either there is no contamination or that the enhancement was overcome; however, the MVD for this assay was calculated to be 16 and therefore this dilution is greater than what is acceptable.

Table 4.6 Calculated geometric mean endpoints of endotoxin in AuNP suspension.

Dilution Factor (AuNP concentration in nM)	**Calculated endpoint**
5x (1 nM AuNP)	0.0156 EU/ml
10x (0.5 nM AuNP)	0.0156 EU/ml
50 x (0.1 nM AuNP)	0.312 ml

4.1.5.4 rFC Assay

Wells containing AuNPs at concentrations ranging 0.5 nM to 5 nM showed no fluorescence at 360nm excitation, 440 nm emission, as compared to wells containing water only.

To determine inhibition/enhancement of the assay, PPCs were run alongside unspiked samples and the spike recovery was calculated (Table 4.7). The undiluted AuNP sample had a spike recovery of only 2%, suggesting inhibition of the assay. The spike recovery values obtained from all diluted samples all fall within the recommended range of 50-200% as recommendation by the manufacturer of the kit. The calculated MVD for this assay is 100 and therefore all the dilutions are valid.

Table 4.7 Calculated endotoxin concentrations. Spiked samples at 0.5 EU/ml endotoxin standard added to the AuNP suspension

Dilution Factor (AuNP concentration in nM)	**Calculated concentration (EU/ml) for unspiked sample**	**Calculated concentration (EU/ml) of 0.5 EU/ml PPC**	**Difference between PPC and unspiked sample**	**Spike recovery**
Undiluted (5 nM AuNP)	0.059	0.066	0.008	2%
5x (1 nM AuNP)	0.120	0.565	0.445	89%
10x (0.5 nM AuNP)	0.069	0.558	0.490	98%
50x (0.1 nM AuNP)	0.019	0.479	0.460	92%

4.1.6 Effect of AuNPs on Redox Potential of medium

The results of the relative ORP measurements of the AuNPs in RPMI culture medium are shown in Figure 4.3. Although all of the nanoparticles showed a negative ORP reading, there were no significant differences between the AuNPs and the RPMI culture medium alone.

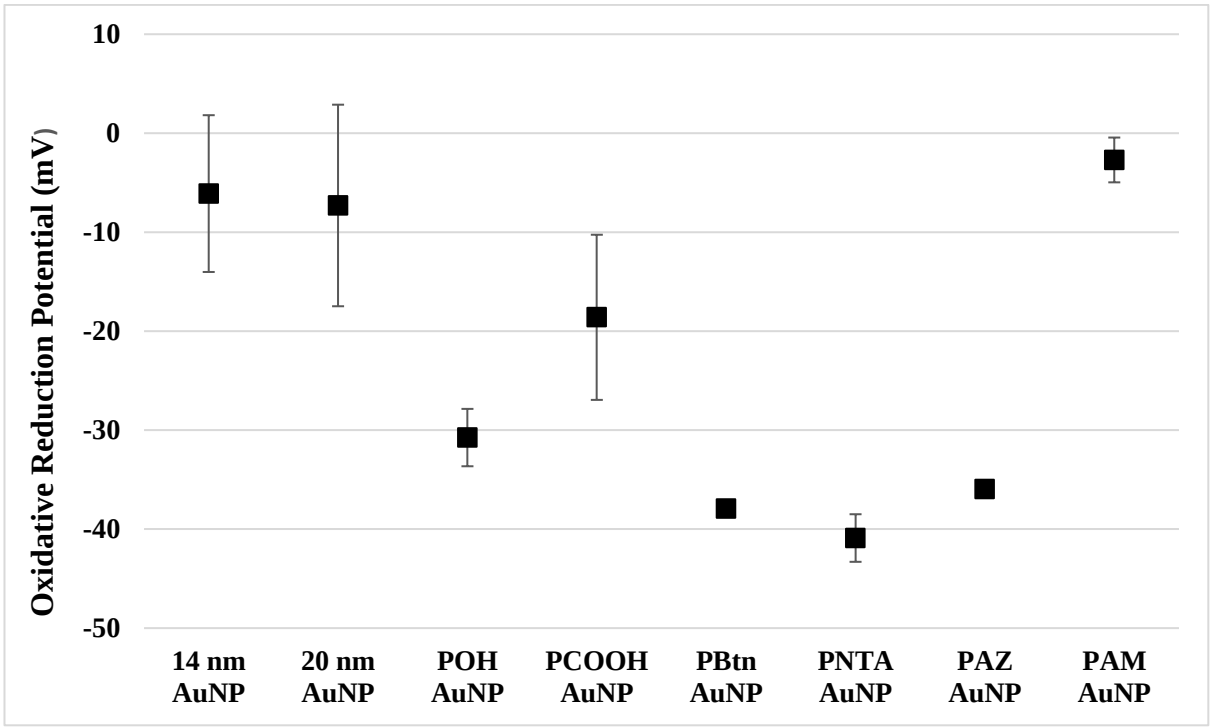

Figure 4.3 Relative changes in ORP measurements. RPMI culture medium alone was used to zero the electrode and values shown are those relative to the culture medium Error bars reflect the standard deviation. n = 2.

4.2 Surface Activity

4.2.1 Measurement of Free Radicals

Figure 4.4 shows a representative ESR spectrum showing the 1:2:2:1 splitting constant of the spin adduct of the hydroxyl radical with DMPO (DMPO-OH). The intensity of the "middle" two peaks of the splitting constant, as indicated by arrows, was measured and this signal intensity correlates to the amount of radicals trapped. These measured intensities of the free radical study are shown in Figure 4.5. The green bar represents a baseline measurement that is the average intensity obtained from 10 mM H_2O_2 and 100 mM DMPO. AuNPs were tested at various concentrations and were mixed with 10 mM H_2O_2 and 100 mM DMPO prior to ESR measurements. All values were corrected for the intensity of 100 mM DMPO alone. With the exception of PCOOH, all experiments showed a dose-dependent decrease in the intensity obtained, as compared to the H_2O_2 with DMPO. Although not dose-dependent, the intensity readings obtained from the experiments with PCOOH showed intensity readings approximately half of the baseline.

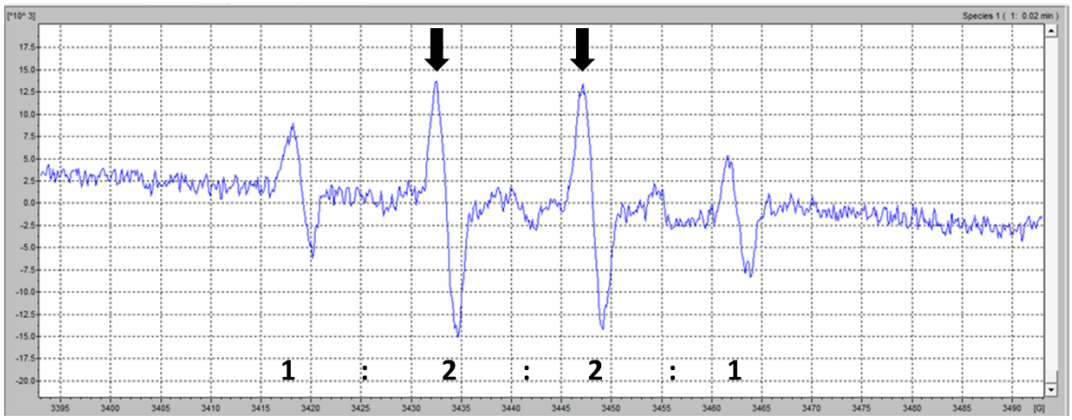

Figure 4.4 Representative ESR spectrum across a varying magnetic field (x-axis) of DMPO-OH, showing the expected 1:2:2:1 hyperfine splitting of the peak intensity (y-axis). Black arrows indicate the peaks that are measured to obtain the intensity used to estimate free radical concentration.

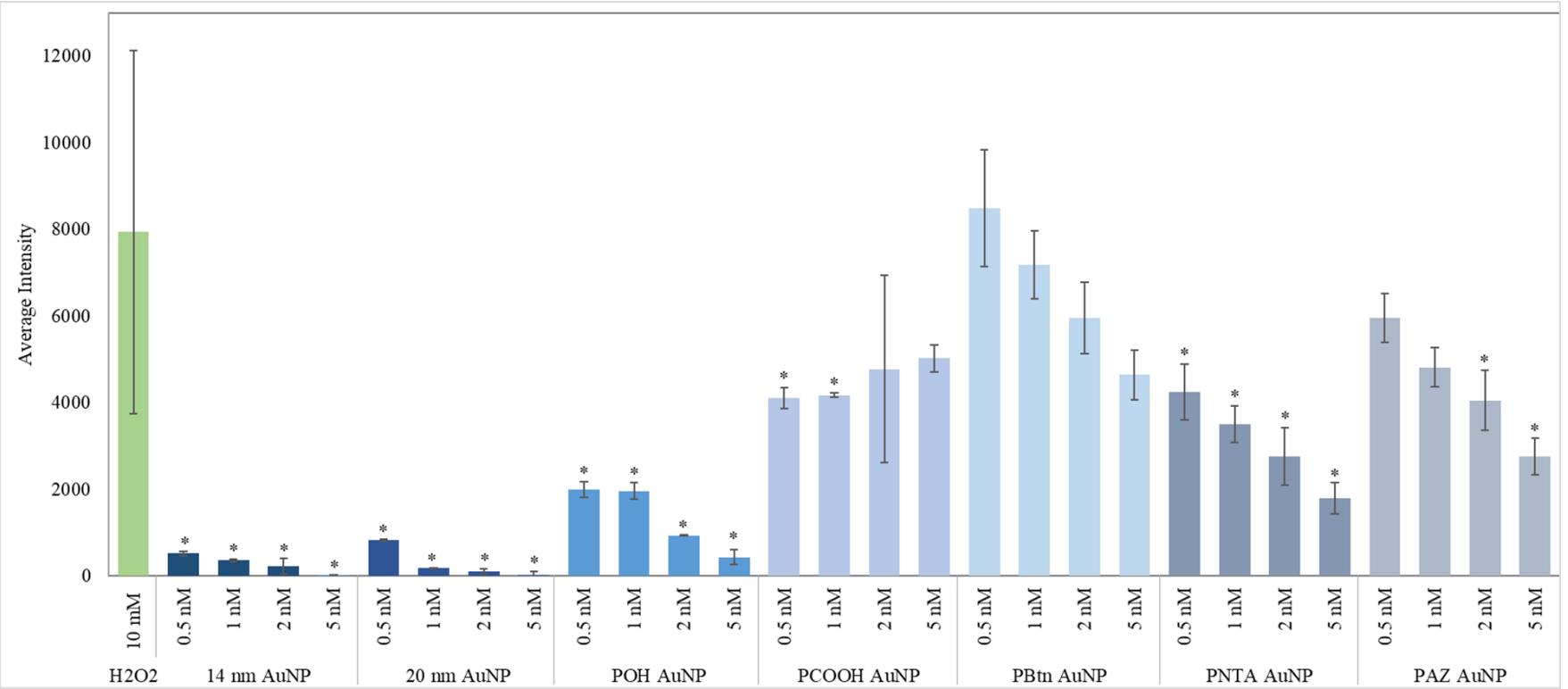

Figure 4.5 Average intensity readings obtained from ESR measurements. n = 2. Error bars represent standard deviation. * $p < 0.01$.

4.2.2 8-Isoprostane

The potential for 14 nm AuNPs to interfere with the 8-Isoprostane EIA Kit was investigated by spiking known 8-isoprostane standards with either 1 nM or 5 nM AuNPs. The calculated 8-Isoprostane concentrations of the 40 pg/ml and the 8 pg/ml prepared samples, either with or without AuNP spikes, are shown in Figure 4.6. For both the 40 pg/ml and 8 pg/ml samples, a decrease in the calculated concentration of 8-isoprostane was observed as the AuNP concentration increased, suggesting interference of the AuNPs with the assay. The Non-Specific Binding (NSB) wells spiked with AuNPs showed no differences in absorbance as compared to the control NSB wells (data not shown).

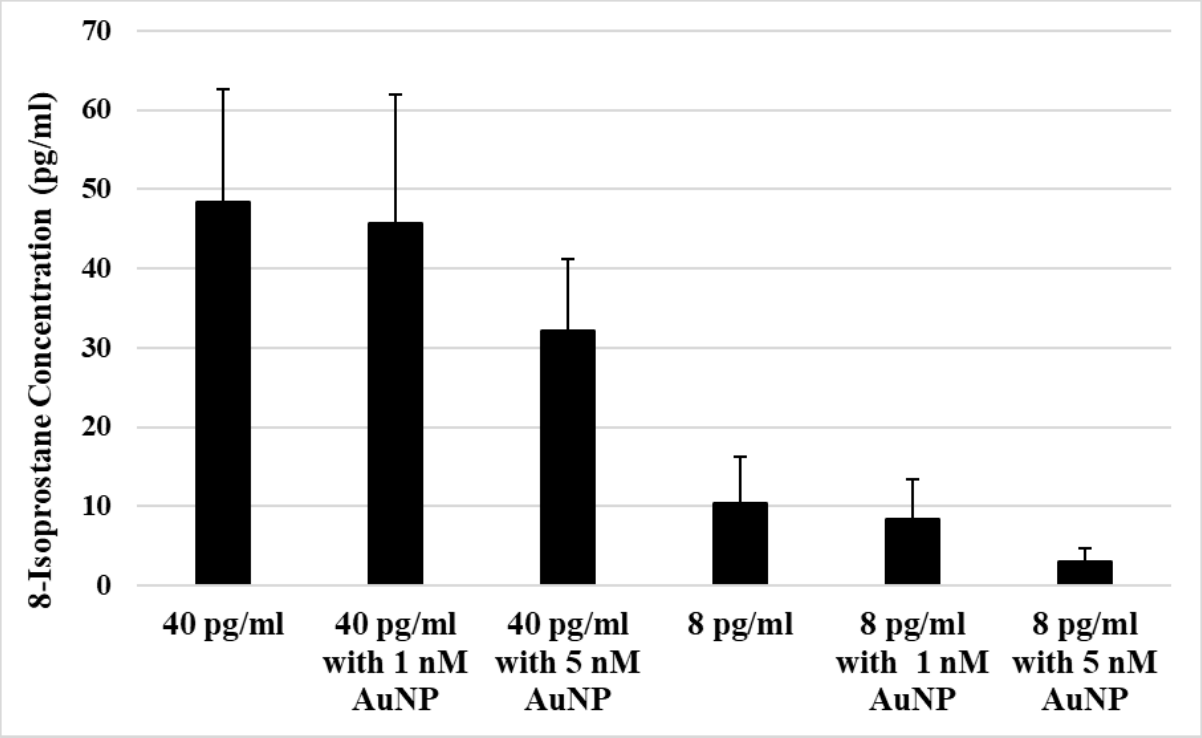

Figure 4.6 Calculated concentrations of known samples (40 pg/ml and 8 pg/ml), either without AuNPs or with 1 nM or 5 nM AuNP spikes.

4.3 *In vitro* toxicity assays

4.3.1 Applicability of assay systems to AuNPs

4.3.1.1 XTT assay

Figure 4.7 (A) shows the toxicity results of the BEAS-2B cells treated with 14 nm AuNPs based on the XTT assay. Hydrogen peroxide was used as a positive control and a clear decrease in absorbance can be observed, indicative of a decrease in viability. Based on the XTT assay, it can be deduced that at 1 nM the AuNPs exhibit only mild toxicity, however at 5 nM there is an increase in viability as compared to the untreated control cells.

To investigate potential interference of the AuNPs with the optical readout of the assay, AuNPs in culture medium were added to unreduced XTT and the absorbance was measured at 450 nm, the results of which are shown in Figure 4.7 (B). As it can be seen, an AuNP concentration dependent increase in the absorbance was observed in the absence of cells but in the presence of unreduced XTT. Subsequently, the absorbance values of particle-containing medium controls, as seen in Figure 4.7 (B), were subtracted from the XTT viability data, shown in Figure 4.7 (A). From this amended data (Figure 4.7 (C)), a conclusion can be made that dose-dependent toxicity is produced relative to the untreated cells.

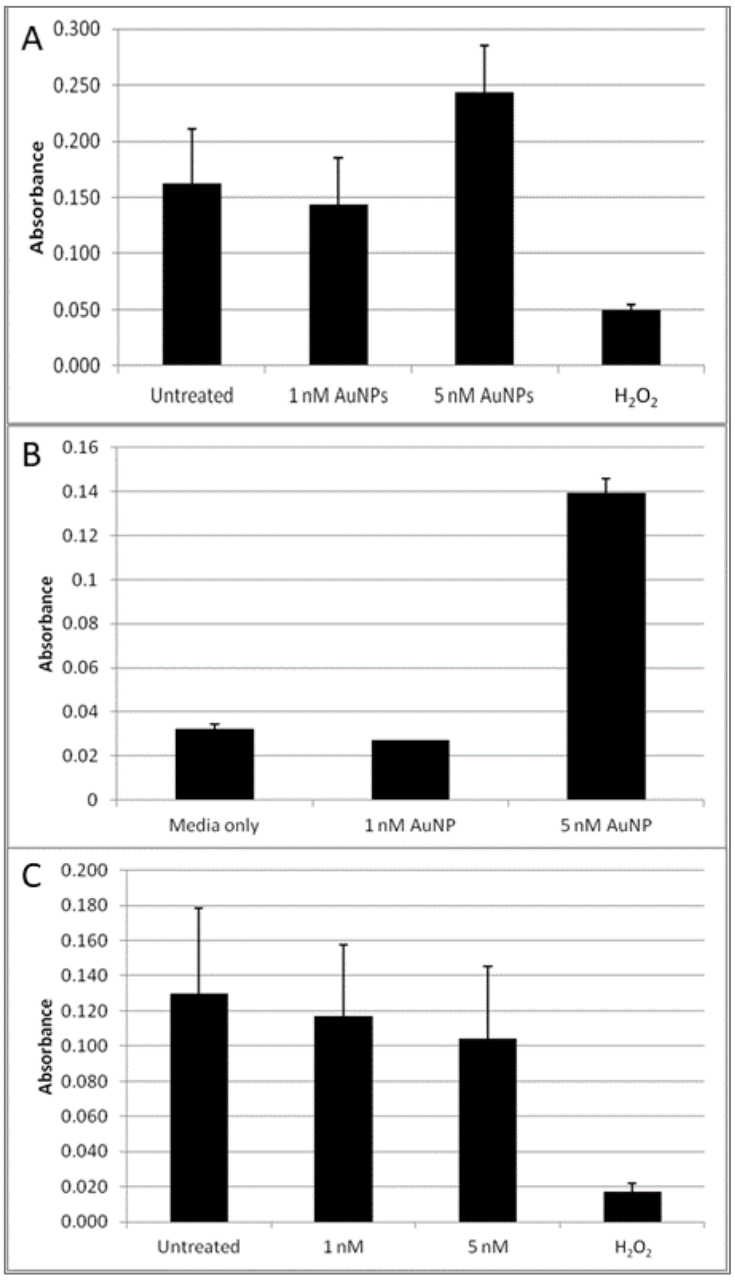

Figure 4.7 Toxicity and interference studies of 14 nm AuNPs using the XTT assay. (A) BEAS-2B cells were treated with either 1 nM or 5 nM of 14 nm AuNPs for 1 hour prior to toxicity testing using the *In Vitro* Toxicology Assay Kit (XTT assay). Absorbance measured at 450 nm and a reference wavelength of 600 nm. (B) The absorbance of 1 nM and 5 nM AuNPs in culture medium and with unreduced XTT at 450 nm. (C) Absorbance values obtained when data from (B) was subtracted from (A).

4.3.1.2 LDH assay

The fluorescence of the product of the CytoTox-ONE™ assay is measured at 560 nm excitation, 590 nm emission; however, at these settings, no meaningful fluorescence was observed when the particles were measured alone and therefore the possibility of optical interference was disregarded when calculating the cytotoxicity based on LDH release. Figure 4.8 shows the cytotoxicity of the 14 nm AuNPs as determined by this assay. The fluorescence of the wells where there is maximum LDH release due to complete cell lysis was determined and then, in accordance to the manufacturer's instructions, cytotoxicity is expressed as a percentage of this maximum LDH release. From this assay data, the AuNPs are considered non-toxic to the cells under the same conditions as the XTT experiment shown above.

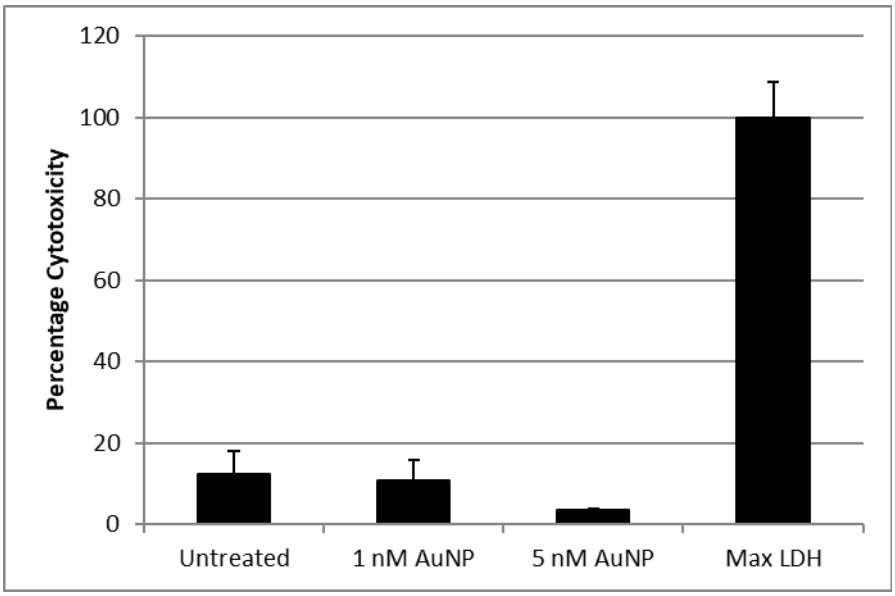

Figure 4.8 Cytotoxicity of 14 nm AuNPs to BEAS-2B cells using the LDH assay. Cells were exposed to either 1 nM or 5 nM AuNPs for 1 hour prior to determination of cytotoxicity.

4.3.1.3 ATP assay

The basis of product detection of the CellTiter-Glo® Luminescent Cell Viability Assay is luminescence; however, no meaningful luminescence was observed when the particles were measured alone and therefore the potential for optical interference was disregarded when calculating the viability based on the ATP assay. Figure 4.9 (A) shows the toxicity of 14 nm AuNPs to BEAS-2B cells based on this kit, which measures the amount of ATP present. For this assay, cells are lysed to release intracellular ATP, followed by a luciferase reaction to produce a stable luminescent signal proportional to the ATP present. In this assay system, the manufacturer's guidance manual states that cell washing and the removal of culture medium is not required. From the results presented in this figure, it can be concluded that AuNPs were toxic in a concentration dependent manner under the same conditions as the XTT and LDH assays shown above.

However, an experiment was conducted to investigate the interference of the AuNPs on the reaction that occurs in the ATP assay, namely the conversion of luciferin substrate to luminescent oxyluciferin in the presence of ATP. The results are shown in Figure 4.9 (B) where it can be seen that with an increase in AuNP concentration, a decrease in luminescent signal is observed, suggesting that the AuNPs are interfering with the conversion of luciferin to oxyluciferin at high concentrations. If a comparison of results is made between Figure 4.9 (A) and Figure 4.9 (B), it is possible that the observed decrease in viability at 5 nM AuNPs in Figure 4.9 (A) could be caused by interference of the AuNP with the assay reaction. Therefore, although the AuNPs do not produce a luminescent signal themselves, these NPs do interfere with the conversion of the substrate to a luminescent product.

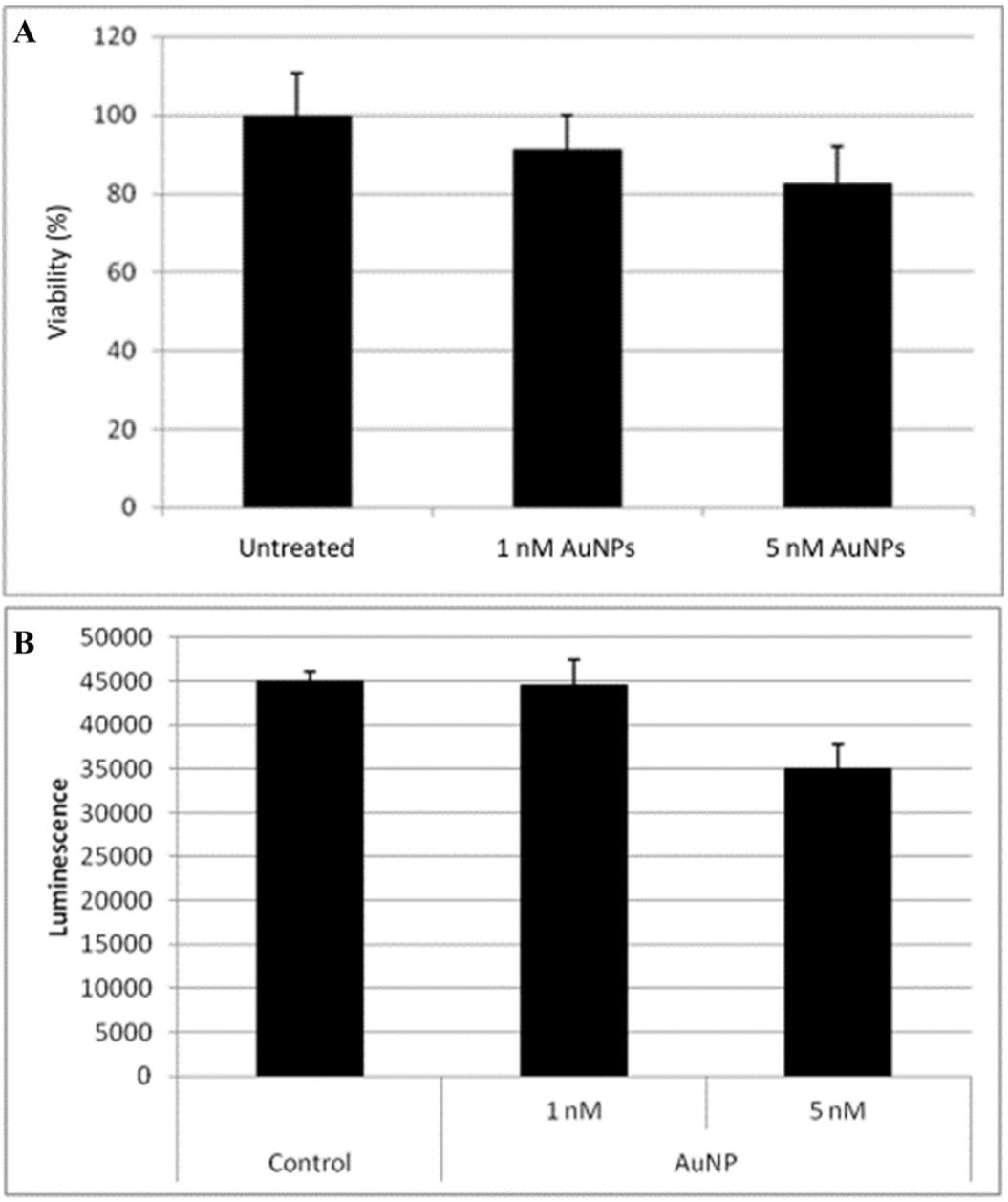

Figure 4.9 Toxicity and interference studies of 14 nm AuNPs using the ATP assay. (A) Viability of BEAS-2B cells treated with either 1 nM or 5 nM of 14 nm AuNPs for 1 hour as calculated using the ATP assay. Luminescent signal was measured and viability is expressed as a percentage of the untreated control cells. (B) Luciferin substrate from the CellTiter Glo assay was incubated with ATP and 14 nm AuNPs to produce the luminescent product oxyluciferin prior to measurement of the luminescent signal.

4.3.1.4 Colony Forming Efficiency (CFE) assay

A full characterisation of the AuNPs used in the study can be found in the final report (Ponti *et al.* 2014). Figure 4.10 shows the toxicity of the 14nm AuNPs to the MDCK cell line where the percentage toxicity has been calculated relative to the untreated control. In all experiments, as part of the acceptance criteria, the positive control resulted in 100% toxicity and no colonies were observed. Dose-dependent toxicity was observed although this was not statistically significant.

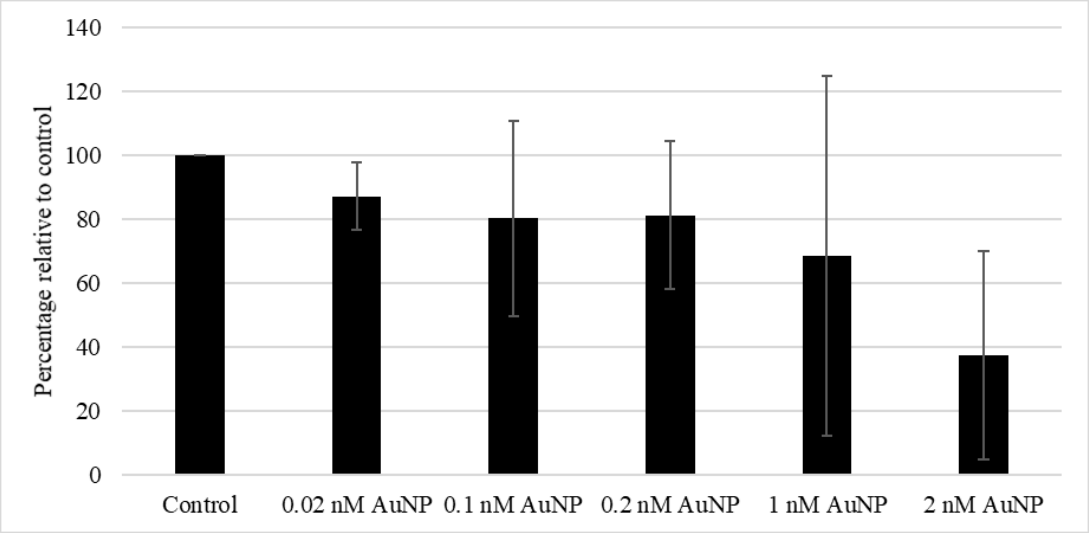

Figure 4.10 Percentage relative toxicity of 14 nm AuNPs to MDCK cells, as determined by the CFE assay

4.3.1.5 Applicability of Impedance Technology

Impedance technology such as the xCELLigence RTCA system assesses the cell index in real time which acts as a measure of cell viability. This system was established in our laboratory and its applicability for use in nanotoxicity studies was assessed by using the 14 nm and 20 nm AuNPs in BEAS-2B cells and CHO cells.

Growth curves of the two cell lines seeded at different concentrations were run to determine ideal seeding concentrations for experimental work. Each seeding concentration of each cell line had its own unique growth curve, as can be seen in Figure 4.11. These growth curves guided the selection of a seeding concentration for further experiments, based on the desire to treat the cells in the early stages of the log growth phase. The seeding concentration for further experiments was selected at 1 x 10^4 cells/well and 3 x 10^3 cells/well for the BEAS-2B cells and the CHO cells respectively. After seeding, both cell lines were allowed to proliferate under standard culturing conditions prior to treatments.

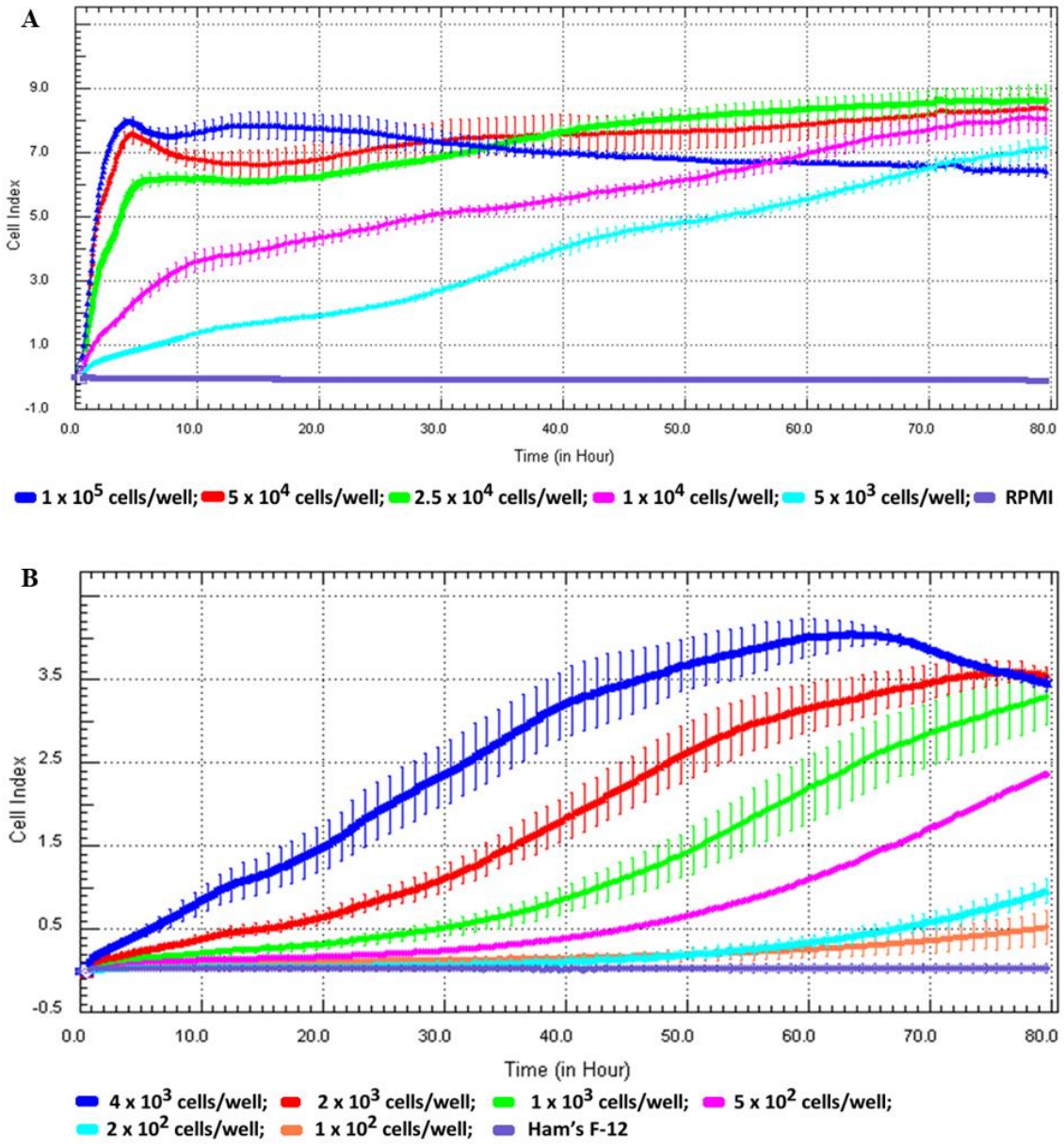

Figure 4.11 Proliferation curves of (A) BEAS-2B cells, and (B) CHO cells, seeded at a range of concentrations.

Figure 4.12 shows the cell index of BEAS-2B cells, which were either untreated or treated with 500 µM hydrogen peroxide as a positive control for cell death, where it caused a decrease in the cell index. A final concentration of 5 nM 20 nm AuNPs in RPMI culture medium were added to wells containing medium without cells at approximately 24 hours, resulting in negligible changes in the cell index, shown in red. A similar trend was observed with 14 nm AuNPs (Results not shown).

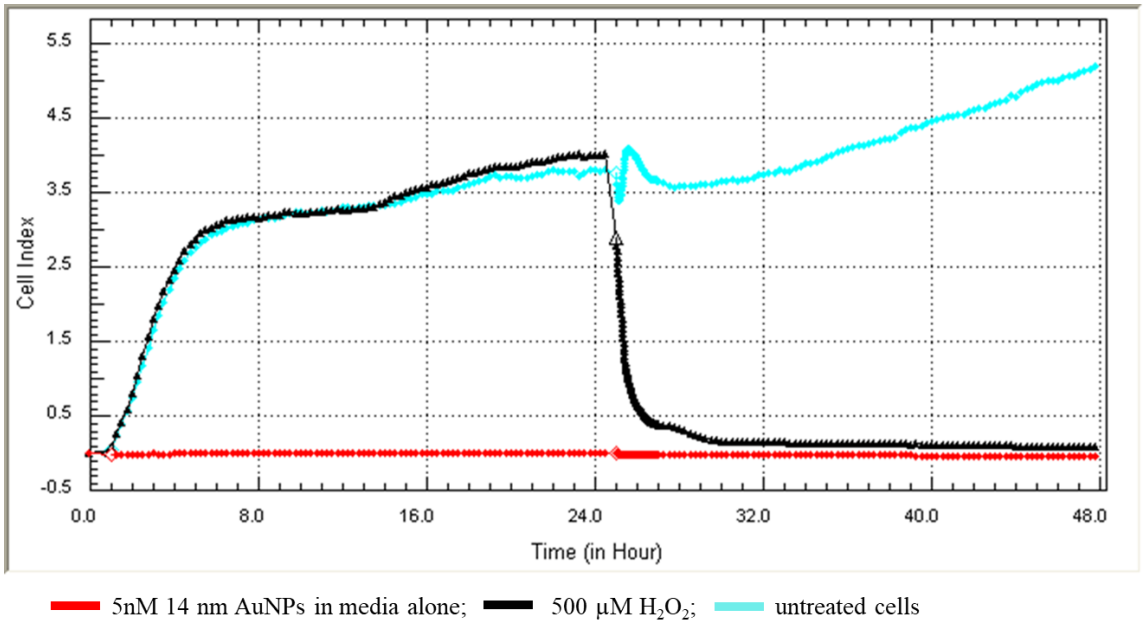

Figure 4.12 Cell index of BEAS-2B cells showing toxicity of 500 µM hydrogen peroxide and effect of 5 nM 14 nm AuNPs in medium on cell index.

Figure 4.13 illustrates the normalised cell index over time of the BEAS-2B (Figure 4.13 A and B), and the CHO cells (Figure 4.13 C and D) when treated with the 14 nm and 20 nm AuNPs. In all cases, cells were treated 24 hours after seeding and the cell index was normalised at the point of treatment. Both cell lines had its own unique growth curve and treatment was carried out whilst the cells were in the early stages of log growth phase. The slope of the curves, a term describing the changing rate of the CI within a given time period, was calculated between the point of treatment and point of confluence. For BEAS-2B cells, confluence was reached approximately 3 and a half days after seeding, whilst CHO cells reached confluence approximately 2 and a half days after seeding. Any significant differences between the untreated and treated slopes are indicated in figure legend.

In this figure, it can be seen that, by the time confluence is reached in the untreated BEAS-2B control cells, the cells treated with 14 nm AuNPs showed significant differences from the untreated controls (Figure 4.13 A). However, the BEAS-2B cells treated with both AuNPs showed a similar growth trend as the untreated control cells and no dose-dependent response was observed (Figure 4.13 A and B). It should also be noted that, within the first hour of treatment of the BEAS-2B cells with 14 nm AuNPs, no differences in CI, and accordingly no toxicity, was observed between the treated and untreated cells which is in contrast to the results obtained from the XTT and ATP assays shown in the previous section. When considering the toxicity at the point of confluence of the CHO cells, both the 14 nm and 20 nm AuNPs showed significant differences and an apparent dose-response (Figure 4.13 C and D), and the 20 nm AuNPs showed greater toxicity based on the greatest decrease of CI.

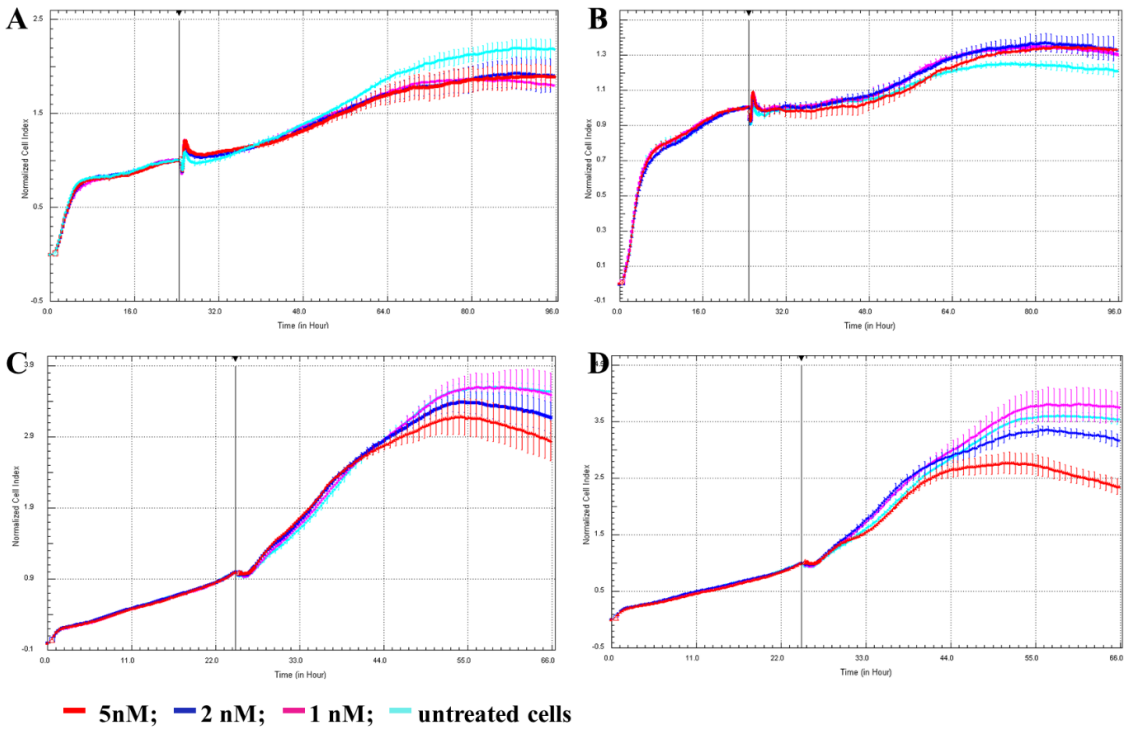

Figure 4.13 Normalised cell index of cells treated with AuNPs.
BEAS-2B cells (A and B) and CHO cells (C and D) were treated with 14 nm AuNPs (left panel) and 20 nm AuNPs (right panel). BEAS-2B and CHO cells were seeded and allowed to recover for 24 hours prior to treatment for 72 hours or 42 hours respectively. The slope of the curves was calculated and t-test conducted to determine differences between treated and untreated control cells. In (A) all treatments were statistically different from untreated control ($p < 0.05$) whilst no significant differences were observed in (B). In (C), 2 nM ($p < 0.05$) and 5 nM ($p < 0.01$) were statistically different from untreated control; whilst in (D) both 2 nM and 5nM treatments were statistically different from the untreated control at $p < 0.01$; $n \geq 3$.

4.3.2 Cytotoxicity of AuNPs in BEAS-2B cells

The xCELLigence RTCA system was used to assess cytotoxicity of the AuNPs in the BEAS-2B cell line over 24 hours of treatment, the results of which are shown in Figure 4.14 where the normalised cell index is plotted over time. The planned uptake experiments require short incubation periods, specifically 2 hours; however, it can be seen that none of the AuNPs are toxic to the cells even after 24 hours as the curves for the treated cells follow that of the untreated cells.

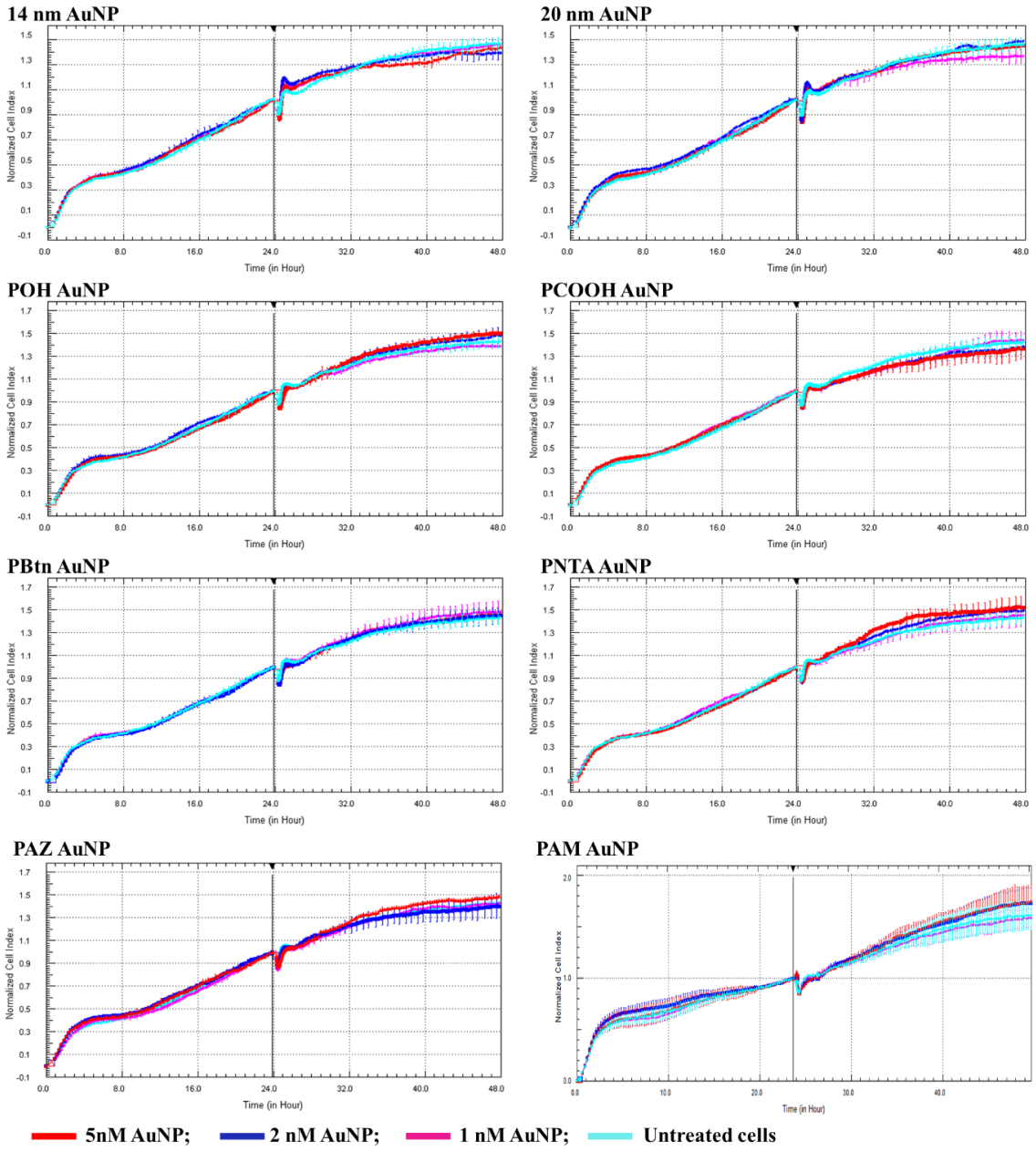

Figure 4.14 Cytotoxicity, as represented by normalised cell index, of BEAS-2B cells treated with AuNPs for 24 hours. Cells were allowed to proliferate for 24 hours prior to treatment and the cell index was normalised at the point of treatment.

4.3.3 Cytokinesis-block micronucleus (CBMN) assay for assessment of genotoxicity

The CBMN assay was used for the assessment of genotoxicity of the 14 nm, 20 nm, and PCOOH AuNPs in BEAS-2B cells. The Replication Index (RI) values from each type of the AuNP treated samples are shown in Table 4.8. The RI is defined as "the proportion of cell division cycles completed in a treated culture, relative to the untreated control" (OECD 2016b). As can be seen in the table, all samples have an RI value around 100%, indicating that these samples had no cytostatic effect as compared to the untreated control.

Table 4.8 Calculated Replication Index (RI) of the treated samples in the CBMN assay

Sample	Concentration	RI
14 nm AuNP	1 nM	101%
	2 nM	106%
	5 nM	96%
20 nm AuNP	1 nM	96%
	2 nM	115%
	5 nM	114%
PCOOH	1 nM	121%
	2 nM	106%
	5 nM	103%

Figure 4.15 shows representative images of binucleated (A-C) and multinucleated (D) BEAS-2B cells, and indicates a typical MN (Figure 4.15 B) and NPB (Figure 4.15C) obtained during scoring.

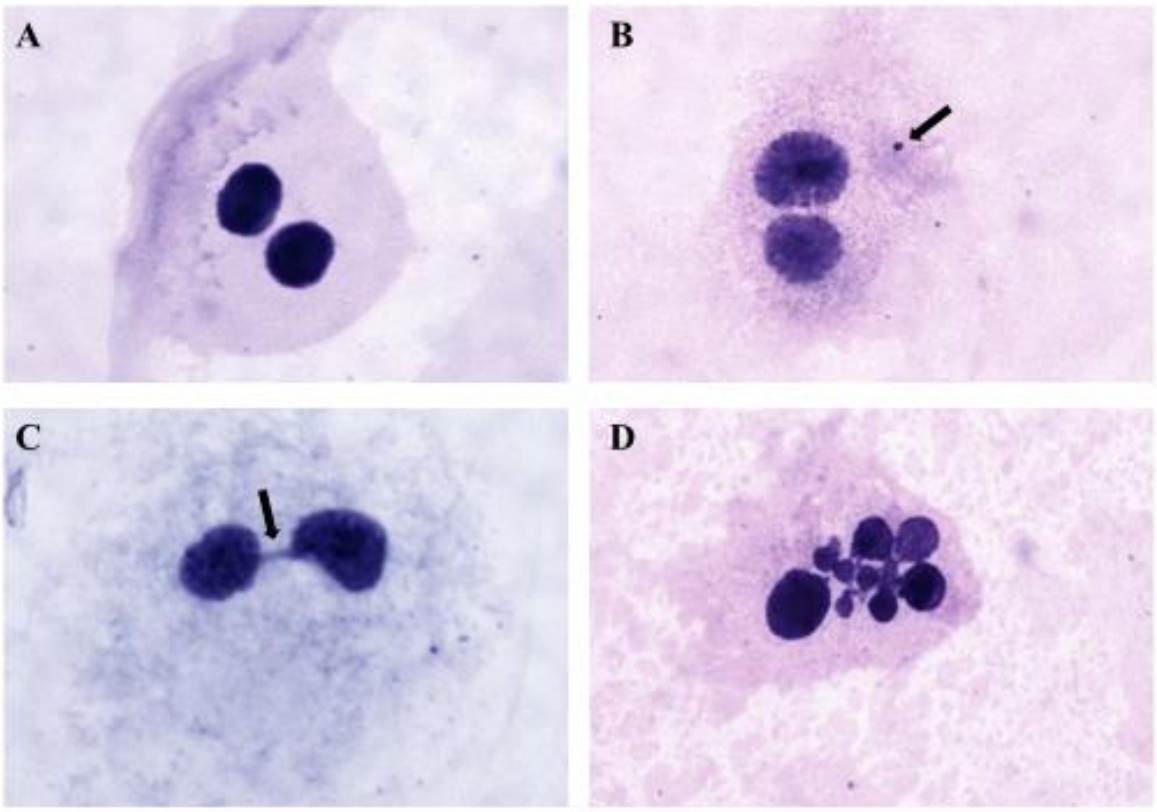

Figure 4.15 Representative images obtained from the CBMN assay.

(A) Binucleated cell with no damage; (B) Binucleated cell showing a micronuclei (MN) indicated by arrow; (C) Binucleated cell showing nucleoplasmic bridge (NPB) indicated by arrow; and (D) multinucleated cell.

The frequencies of MN and NPB per 1 000 binucleated cells are shown in Figure 4.32. Values obtained from the treated samples were all similar to the untreated control and no dose-dependent increase was observed.

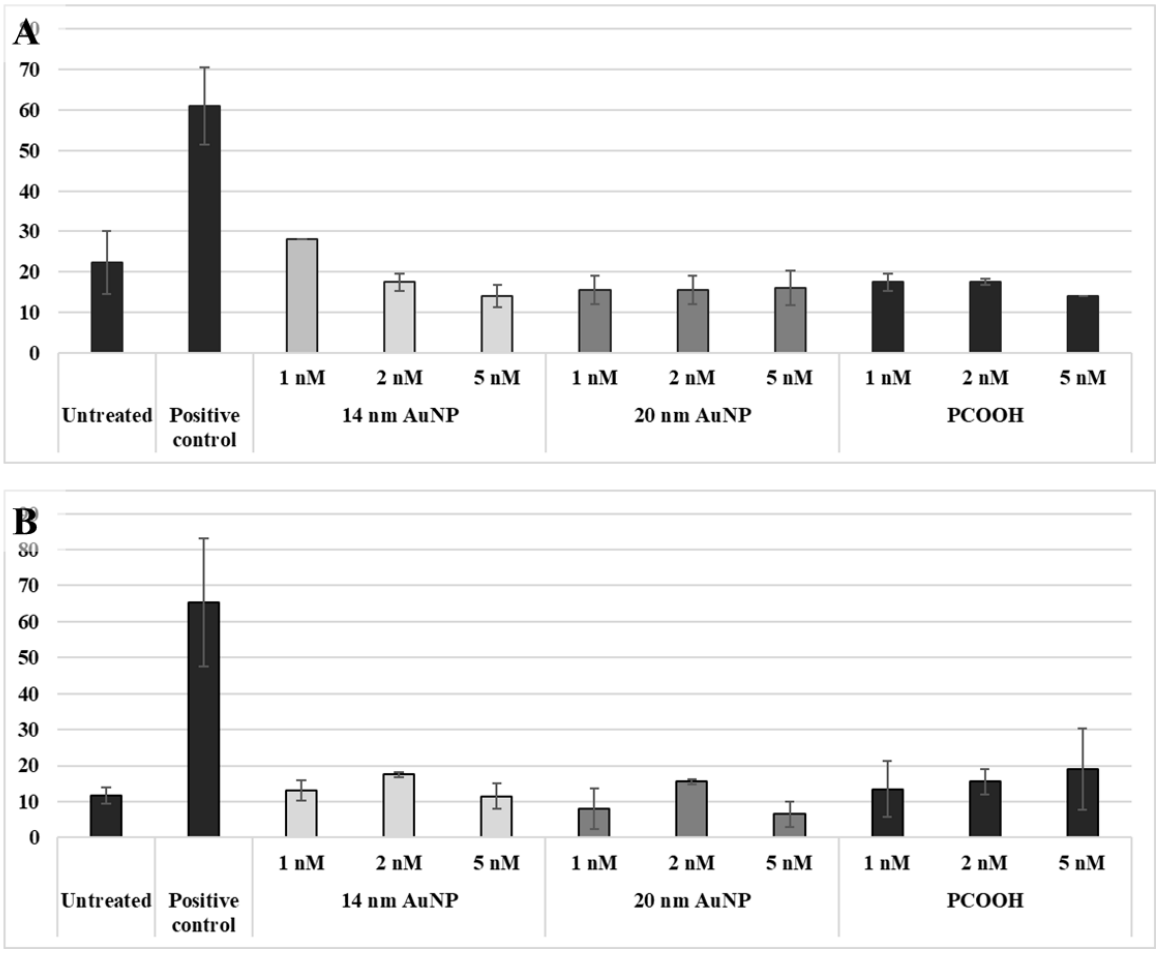

Figure 4.16 Frequencies of (A) micronuclei, and (B) nucleoplasmic bridges per 1000 binucleated cells. No statistically significant differences were observed.

4.4. Uptake of AuNPs

4.4.1 Applicability of the CytoViva HSI system for label-free assessment of uptake

To investigate the applicability of the CytoViva to assess the uptake of AuNPs, 14 nm and 20 nm AuNPs were investigated in BEAS-2B and CHO cells.

4.4.1.1 Focal planes

The CytoViva Hyperspectral Imaging (HSI) System provided dark-field images of the cells following their incubation with AuNPs and fixation. To observe the internalisation of the particles, it was possible to focus the microscope on various focal planes throughout the fixed cells. Figure 4.17 shows a single BEAS-2B cell that has been incubated with 1 nM of 14 nm AuNPs for an hour. The image illustrates 4 focal planes within the cell. In (A) the particles are out of focus, but as the focus of the microscope moves through (B) to (D), one is able to observe various particles within the outline of the cell which come into and then go out of focus, thereby confirming that the AuNPs have been internalised. This approach has been used to confirm internalisation of TiO_2 NPs in fibroblasts (Allouni *et al.* 2012), and silver NPs in nematodes (Meyer *et al.* 2010).

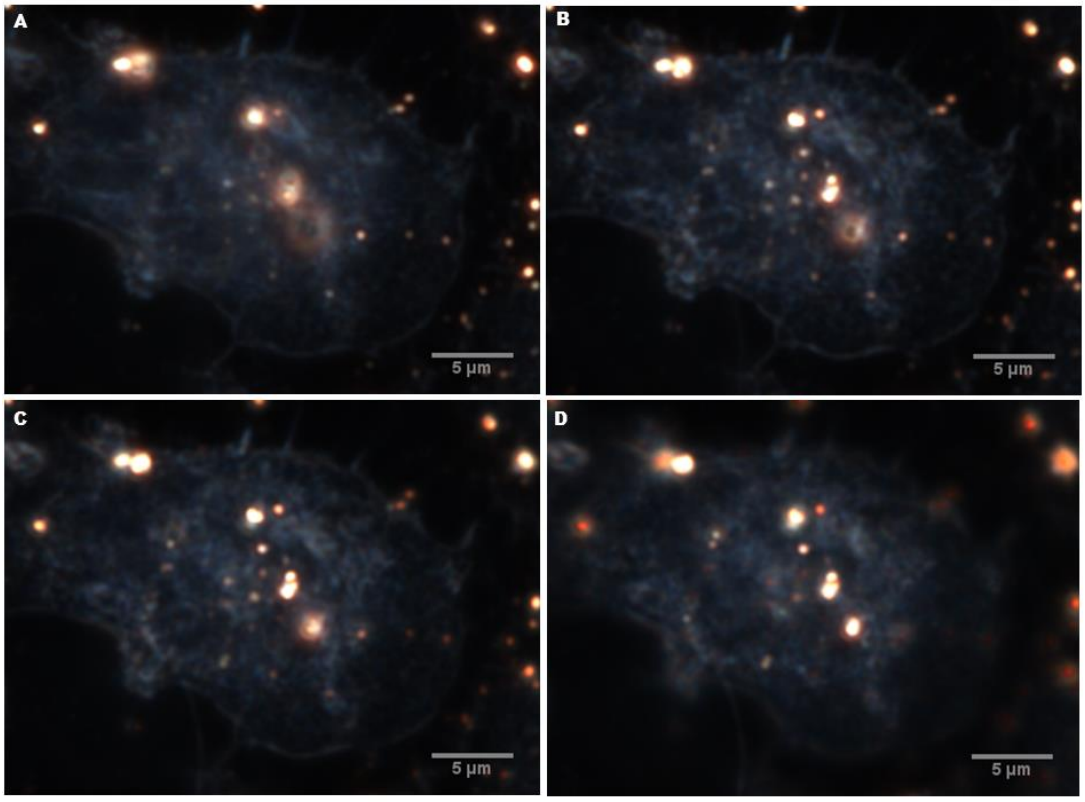

Figure 4.17 Dark-field image at 100x magnification of BEAS-2B cells incubated with 14 nm AuNPs for 1 hr to demonstrate the observation of internatised AuNPs through various focal planes within the cell. Scale bars = 5 µm.

4.4.1.2 Dark-field images of two cell lines

Whilst establishing the applicability of the CytoViva HSI system to observe uptake of the AuNPs, preliminary experiments were conducted using the 14 nm and 20 nm AuNPs in two cell lines after 1, 4, and 6 hours' incubation. Figure 4.18 and Figure 4.19 show representative images of the BEAS-2B and CHO cells respectively, where uptake of the AuNPs was confirmed in both cell lines. In BEAS-2B cells, the 14 nm (Figure 4.18 A) and 20 nm (Figure 4.18 B) AuNPs showed high levels of uptake, even after an hour of incubation. In Figure 4.19, minimal AuNP uptake was observed in the CHO cells after an hour. However, an increase and high accumulation of the nanoparticles was observed for the 14 nm (Figure 4.19 A) and 20 nm (Figure 4.19 B) AuNPs after 4 and 6 hours with the 20 nm AuNPs cellular uptake being higher than that of the 14 nm AuNPs. In both cell lines, the particles seemed to accumulate and form agglomerates within the cells.

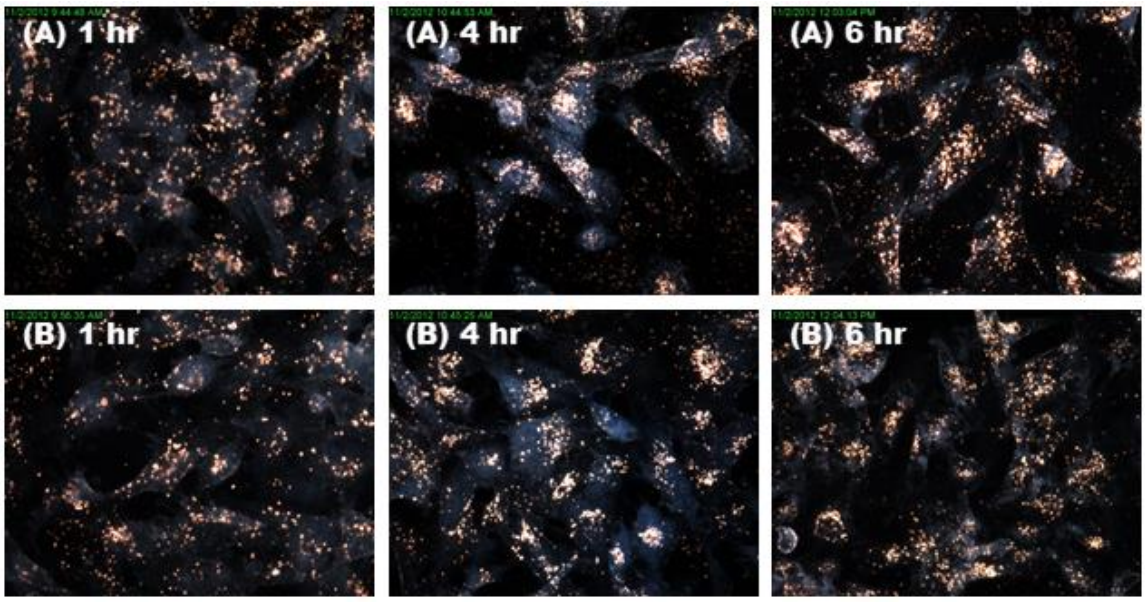

Figure 4.18 Dark-field images of BEAS-2B cells incubated with AuNPs. Dark-field images were captured at 60x magnification of BEAS-2B cells incubated with either (A) 14 nm or (B) 20 nm AuNPs for 1 hr, 4 hrs, or 6 hrs.

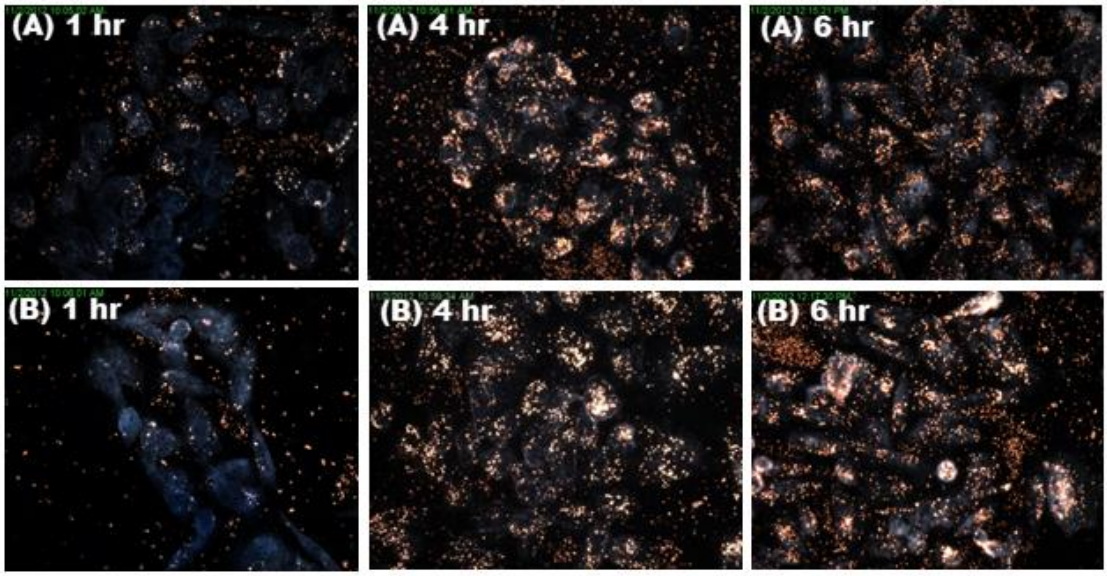

Figure 4.19 Dark-field images of CHO cells incubated with AuNPs. Dark-field images were captured at 60x magnification of CHO cells incubated with either (A) 14 nm or (B) 20 nm AuNPs for 1 hr, 4 hrs, or 6 hrs.

4.4.1.3 Spectral profiles of singularly dispersed vs agglomerated AuNPs

Figure 4.20 represents the spectral profiles of 14 nm and 20 nm AuNPs. Nanoparticle solution was spread on a slide and allowed to dry prior to HSI. Ten randomly selected spectra were obtained from nanoparticles that appeared to be either singularly dispersed (A and C) or had formed larger agglomerates (B and D) on the slide. Each coloured line represents the spectrum from a single pixel, and these collections of representative spectra form a known spectral library of the nanoparticles. In these figures, it can be seen that individually dispersed AuNPs of the two sizes tend to have homogenous curves within the sample, as represented in Figure 4.20 A and C for 14 nm and 20 nm nanoparticles, respectively. The AuNPs at both sizes tend to have a predominant single peak at approximately 670 nm. Figure 4.20 B and D illustrate a range of spectra for agglomerated 14 nm and 20 nm AuNPs, respectively. The non-uniformity of these spectra may probably be due to the different sizes of the agglomerates in the sample. In addition, the spectral profiles of the agglomerated AuNPs tend to have broader peaks than their singularly dispersed counterparts as well as the appearance of a second peak at approximately 800 nm.

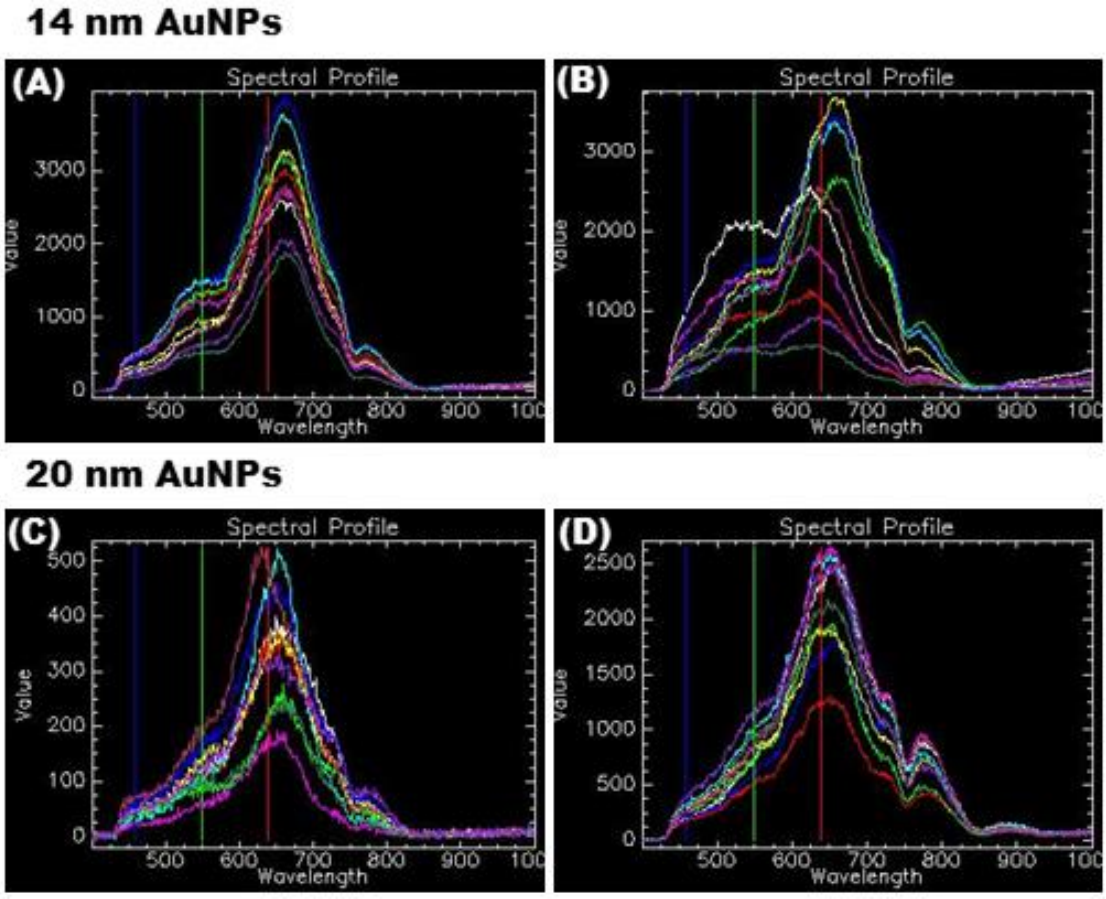

Figure 4.20 Spectral profiles of 14 nm and 20 nm AuNPs.

Ten spectral profiles of randomly selected AuNPs that appeared visually to be either (A and C) in single suspension, or (B and D) agglomerated nanoparticles. Each coloured line represents the spectrum from a single pixel.

4.4.1.4 Principal Component Analysis (PCA)

Image processing techniques such as principal component analysis are widely used for data dimensionality reduction and feature extraction (Chang *et al.* 1998; Suganthy and Ramamoorthy 2012). Therefore PCA was run on the spectra of singularly dispersed and of agglomerated 14 nm and 20 nm AuNPs in order to identify the principal components (PCs) that are responsible for the spectral variation between the different sized nanoparticles.

The PCA score plot of Factor 1 vs Factor 2 is shown in Figure 4.21. The first two factors identified by PCA account for over 90% of the variance observed. It can be seen in this figure that the points representing singularly dispersed AuNPs are more closely orientated, whilst the points for the agglomerated AuNPs are widely dispersed and no distinct clusters can be identified. This suggests that there is not sufficient difference between the spectra of the different AuNPs for PCA to discriminate between them. Subsequently, the HSI spectra may be used to confirm the presence of gold nanoparticles but may not be used to discriminate between particle sizes.

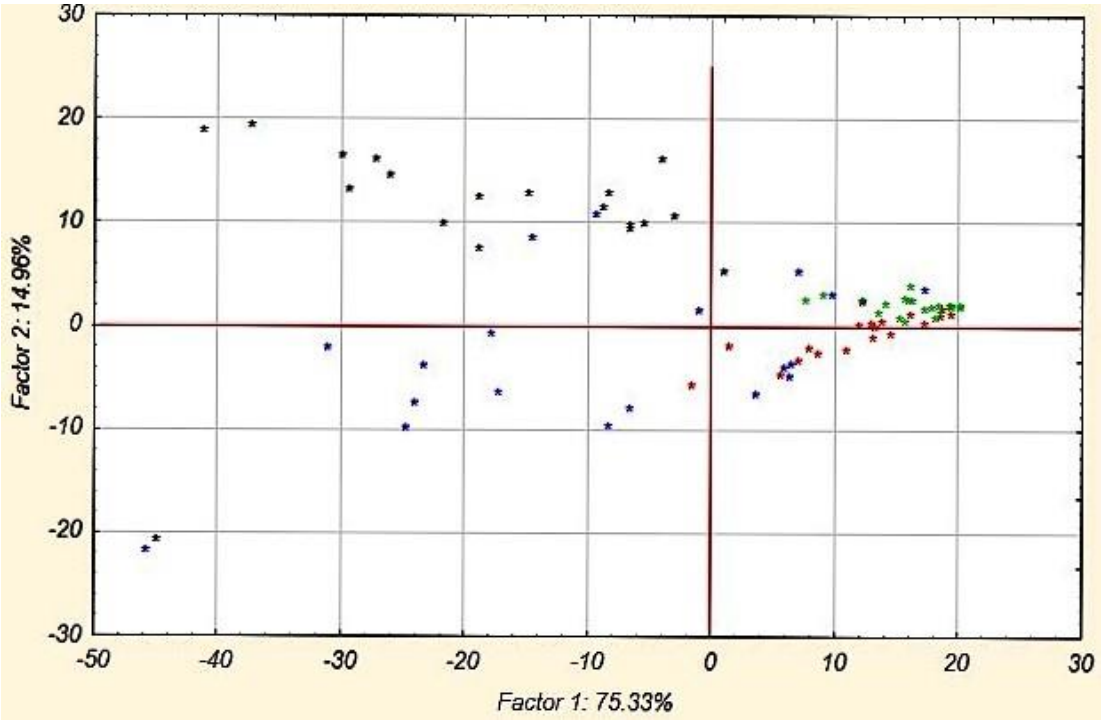

Figure 4.21 PCA analysis of 14 nm and 20 nm AuNP spectra.

PCA score plot of Factor 1 vs Factor 2 for the spectra obtained for 14 nm singularly dispersed AuNPs (red), 14 nm agglomerated AuNPs (blue), 20 nm singularly dispersed AuNPs (green), and 20 nm agglomerated AuNPs (black).

4.4.1.5 Representative images of SAM

Spectral Angle Mapper (SAM) is a process for the identification of a known material in an image acquired using hyperspectral imaging. The process is performed by comparing the known spectra for a material to unknown spectra and identifying pixels in the unknown image that map the known spectra, irrespective of the light intensity.

Using this process on hyperspectral scans of the cells incubated with the AuNPs, a representative output was obtained (Figure 4.22). In this figure the HSI scan of BEAS-2B cells incubated with 1 nM 14 nm AuNPs for 4 hours represents an "unknown" spectral image (Figure 4.22 A). The known spectral library of the singularly dispersed 14 nm AuNPs was mapped against this image (Figure 4.22 B), and the spectral library of agglomerated 14 nm AuNPs was also mapped (Figure 4.22 C).

Both the agglomerated and singularly dispersed spectral libraries mapped onto the images of the cells, thereby verifying the presence of gold nanoparticles in the cells. However, it can be seen that the agglomerated AuNPs matched more pixels within the cells than the singularly dispersed AuNPs indicating that there is a better match with the agglomerated spectral library than the singularly dispersed spectral library.

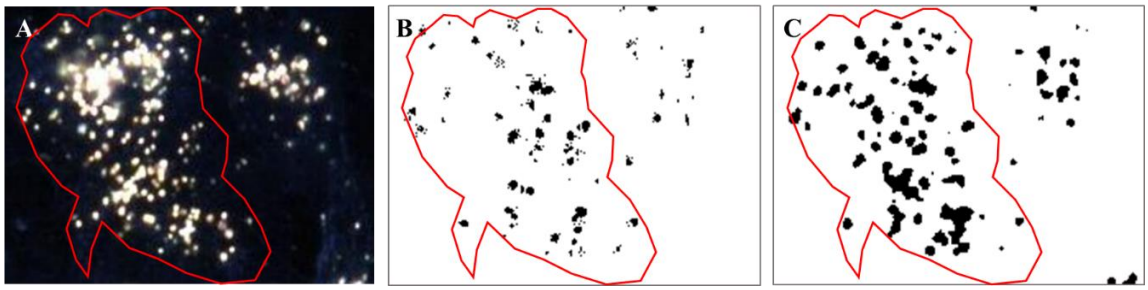

Figure 4.22 Representative images of the SAM analyses.
(A) HSI scan of BEAS-2B cells treated with 1 nM 14 nm AuNPs for 4 hours; (B) SAM image indicating pixels of (A) that matched the spectral library of 14 nm singularly dispersed nanoparticles; (C) SAM image indicating pixels of (A) that matched the spectral library of the 14 nm agglomerated nanoparticles. The red line indicates the approximate outline of the cell.

Spectral profiles of AuNPs were collected from scans of cells treated with either 14 nm AuNPs (Figure 4.23) or 20 nm AuNPs (Figure 4.24). These were acquired from both BEAS-2B cells (Figure 4.23 A and 4.24 A) and CHO cells (Figure 4.23 B and 4.24 B). By visual inspection, it can be seen that the spectra appear more similar to those of the agglomerated spectra than to the singularly dispersed spectra (Figure 4.20).

Therefore, the presence of agglomerated rather than singularly dispersed gold nanoparticles within the cells could be assumed. This assumption was based on the observations made when using SAM, and through visual observations made from the spectral profiles of AuNPs in the absence of cells (Figure 4.20) and those from inside the cells (Figure 4.23 and Figure 4.24).

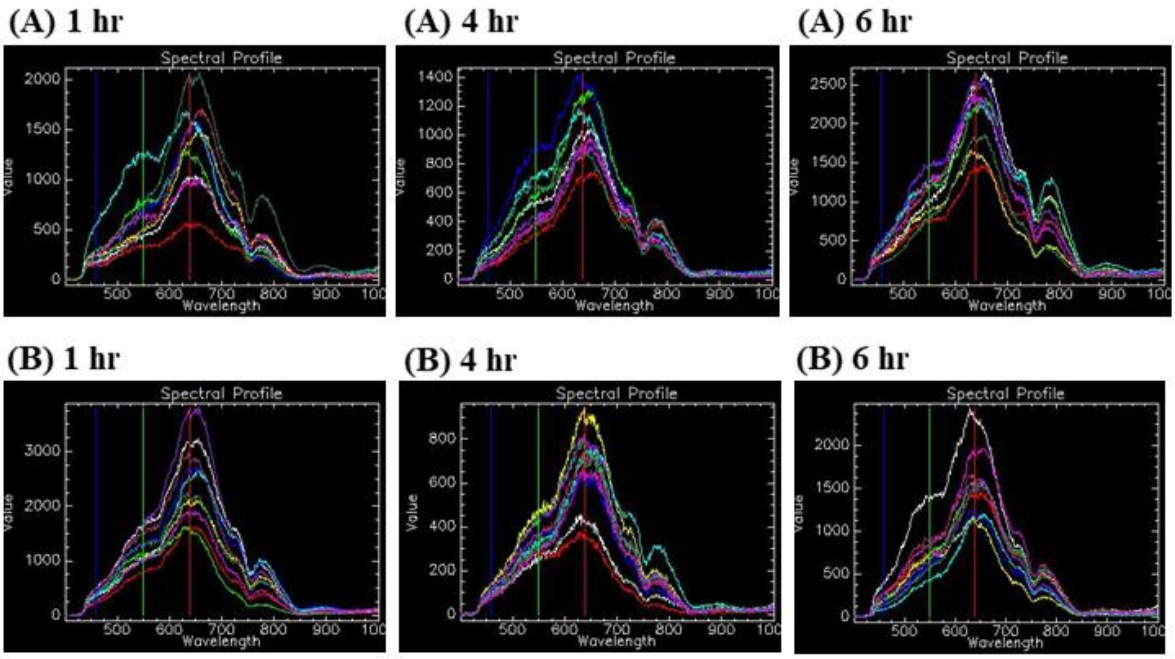

Figure 4.23 Spectral profiles of 14 nm AuNPs following cellular uptake.
Spectral profiles of 14 nm AuNPs were collected following uptake in (A) BEAS-2B, and (B) CHO cells after 1 hr, 4hrs, or 6 hrs. Each image represents the spectral profiles of 10 randomly selected nanoparticles, and each coloured line represents the spectrum from a single pixel.

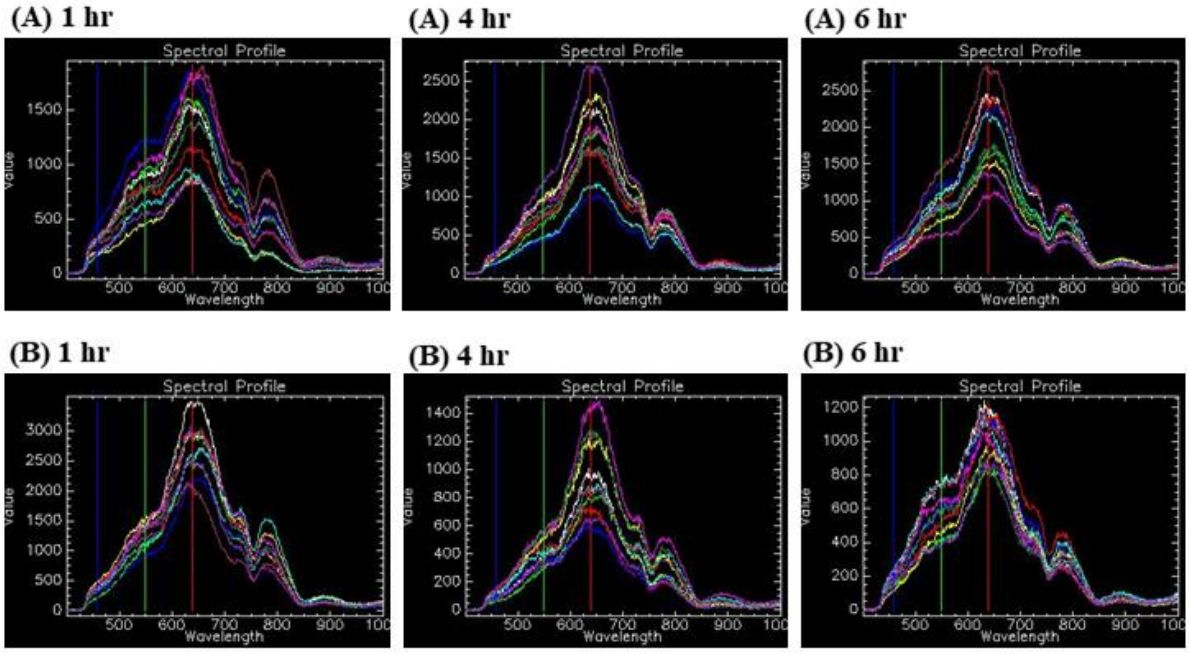

Figure 4.24 Spectral profiles of 20 nm AuNPs following cellular uptake.
Spectral profiles of 20 nm AuNPs were collected following uptake in (A) BEAS-2B, (B) CHO cells after 1 hr, 4hrs, or 6 hrs. Each image represents the spectral profiles of 10 randomly selected nanoparticles, and each coloured line represents the spectrum from a single pixel.

4.4.2 Uptake of AuNPs into BEAS-2B cells

4.4.2.1 Assessment of uptake of AuNPs after 2 hours at 37°C and 4°C

For the studies on the mechanism and intracellular localisation of the AuNPs following uptake, an incubation time of 2 hours was chosen. To confirm that this incubation time was sufficient for uptake to occur, BEAS-2B cells were treated for 2 hours with AuNPs under standard culturing conditions. Representative dark-field images are shown in Figure 4.25. In this figure, uptake of the 14 nm and 20 nm citrate-stabilised and PCOOH AuNPs are clearly observed as bright gold particles evident within the cells. The POH, PBtn, PNTA, PAZ, and PAM AuNPs did not appear to enter the cells, as no gold particles can be seen.

To investigate the energy dependence of nanoparticle uptake, cells were incubated with AuNPs at 4°C in order to inhibit active processes by this lowered temperature (dos Santos *et al.* 2011). Compared to the uptake observed in Figure 4.25, Figure 4.26 shows no uptake of the citrate-stabilised or PCOOH AuNPs that were shown to enter the cells at 37°C. The POH, PBtn, PNTA, PAZ, and PAM AuNPs did not enter the cells at 4°C, which was expected since no uptake was observed at 37°C.

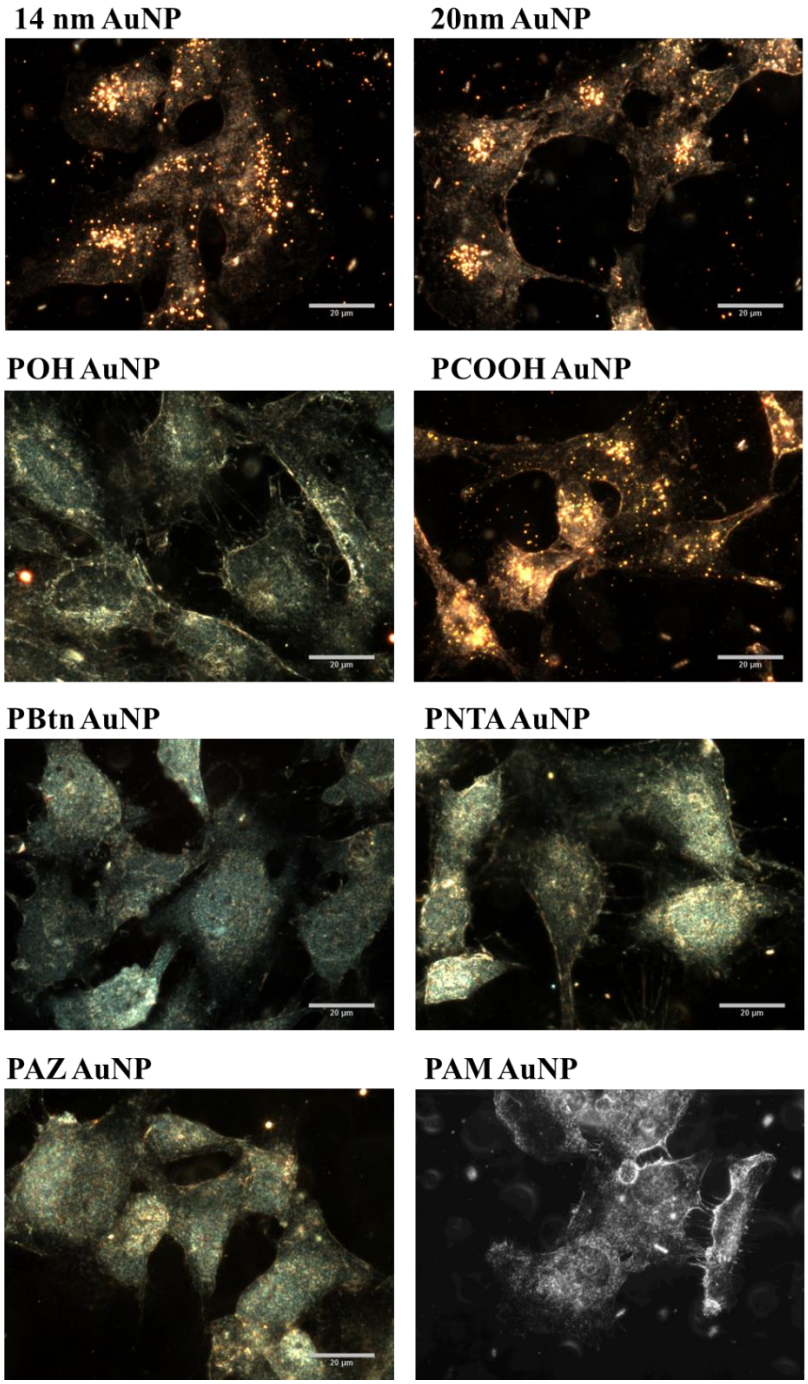

Figure 4.25 Dark field images of BEAS-2B cells incubated with AuNPs for 2 hours at 37°C. Cells were treated at 1 nM AuNP. Dark-field images were captured at 60x magnification. Scale bars = 20 µm.

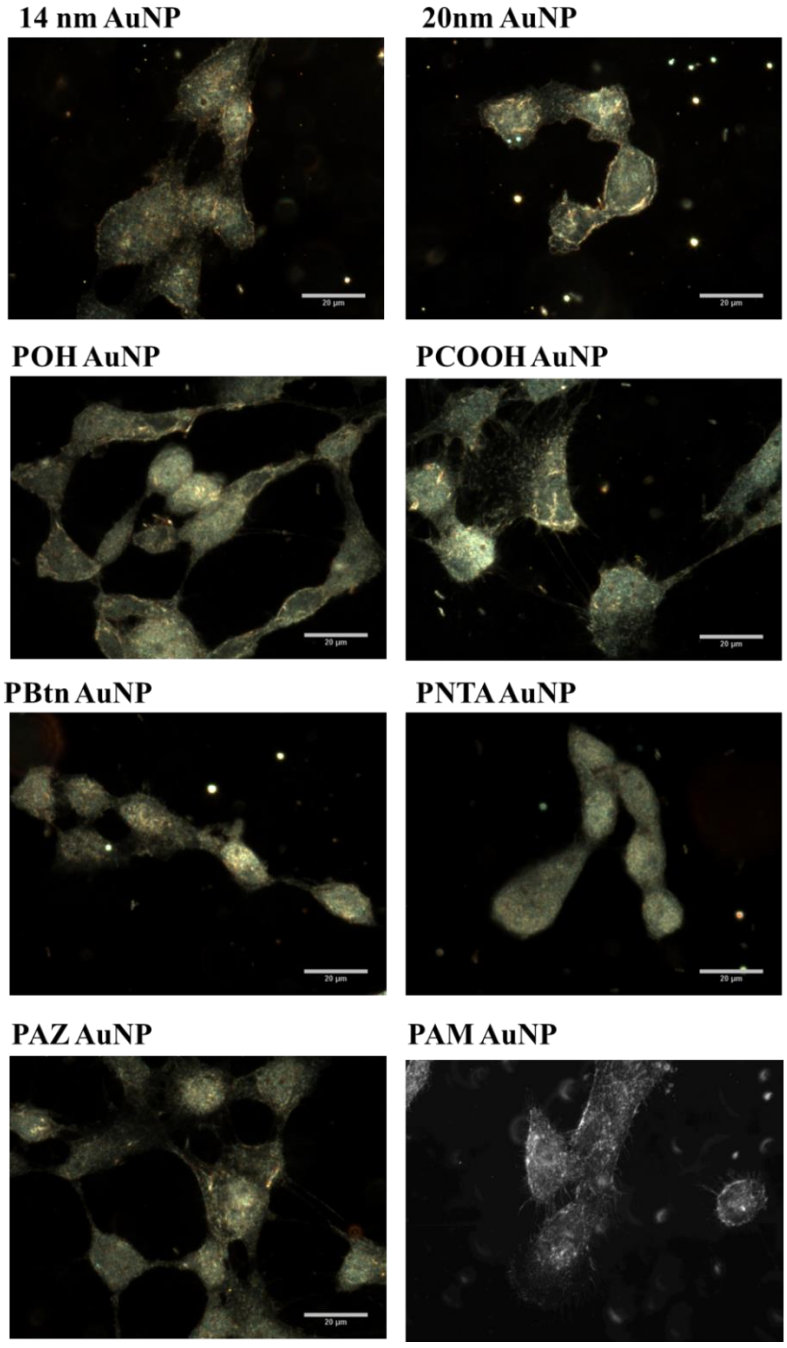

Figure 4.26 Dark field images of BEAS-2B cells incubated with AuNPs for 2 hours at 4°C. Cells were pre-incubated at 4°C for 30 mins prior to addition of AuNPs at 1 nM AuNP. Dark-field images were captured at 60x magnification. Scale bars = 20 µm

4.4.2.2 Assessment of uptake of AuNPs after 24 hours at 37°C

Since no uptake of the POH, PBtn, PNTA, PAZ, or PAM AuNPs was observed after 2 hours, a further experiment was conducted on these AuNPs to investigate whether an extended incubation period of 24 hours would allow for uptake to occur. As can be observed in Figure 4.27, even after 24 hours, no cellular uptake of these AuNPs was evident.

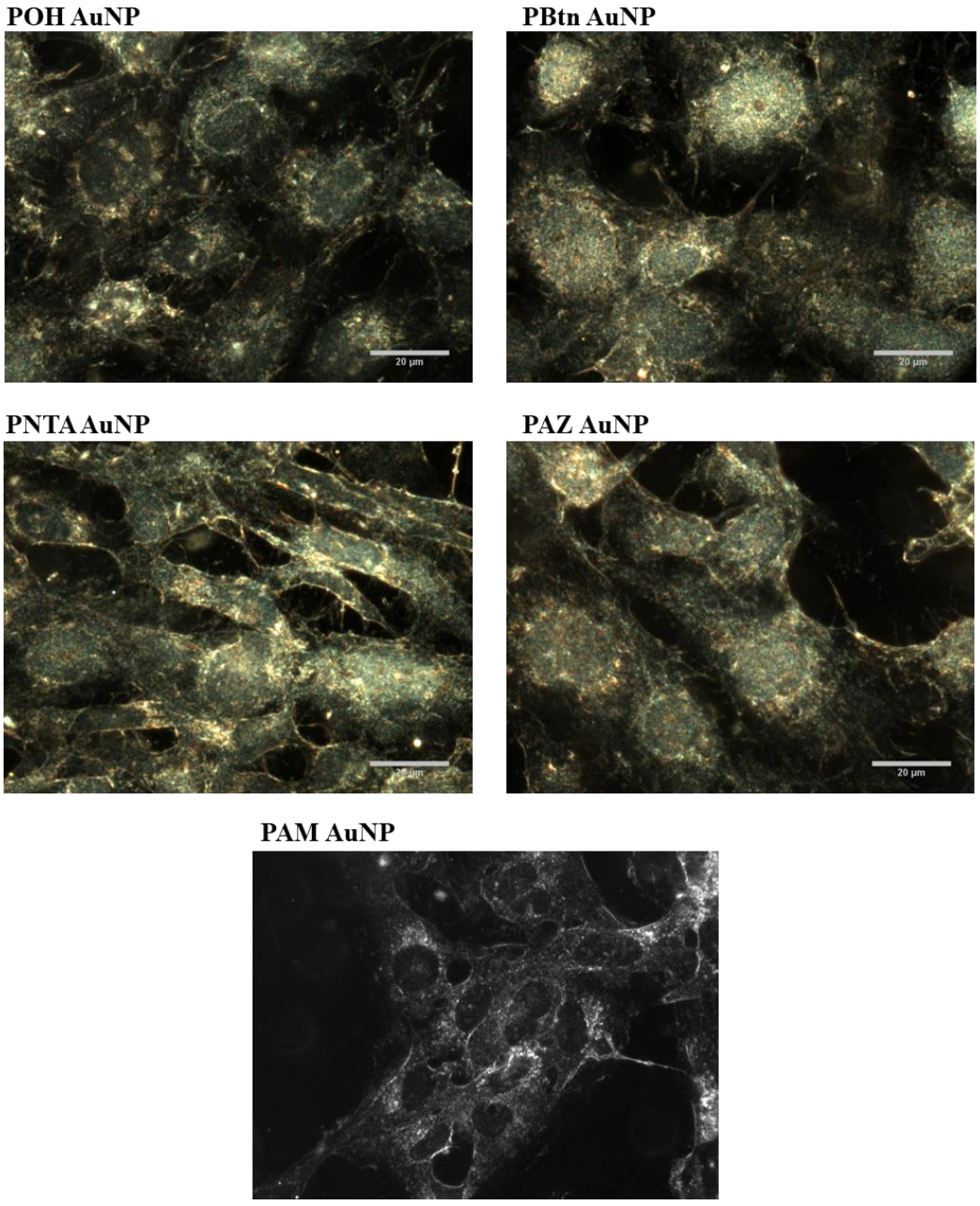

Figure 4.27 Dark field images of BEAS-2B cells incubated with AuNPs for 24 hours at 37°C. Cells were treated at 1 nM AuNP. Dark-field images were captured at 60x magnification. Scale bars = 20 µm.

4.4.3 Mechanism of uptake of AuNPs in BEAS-2B cells

4.4.3.1 Cytotoxicity of Inhibitors

Prior to uptake studies, it is essential to assess the cellular toxicity of the inhibitors to ensure that the treatment concentrations used are not toxic to the cells in question. Indeed, cytotoxicity was observed when BEAS-2B cells were treated with a range of concentrations of genistein (Figure 4.28) and chlorpromazine (Figure 4.29). The cells were treated for 24 hours and both inhibitors showed dose- and time-dependent toxicity. The time period of interest was the first three hours following treatment Figure 4.28 B and Figure 4.29 B as this was the period during which the mechanism of uptake experiments were conducted. From this data, a concentration was chosen for subsequent experiments that showed minimal toxicity at 3 hours incubation and corresponded with effective inhibition as reported in literature, namely 200 µM genistein and 14 µM chlorpromazine.

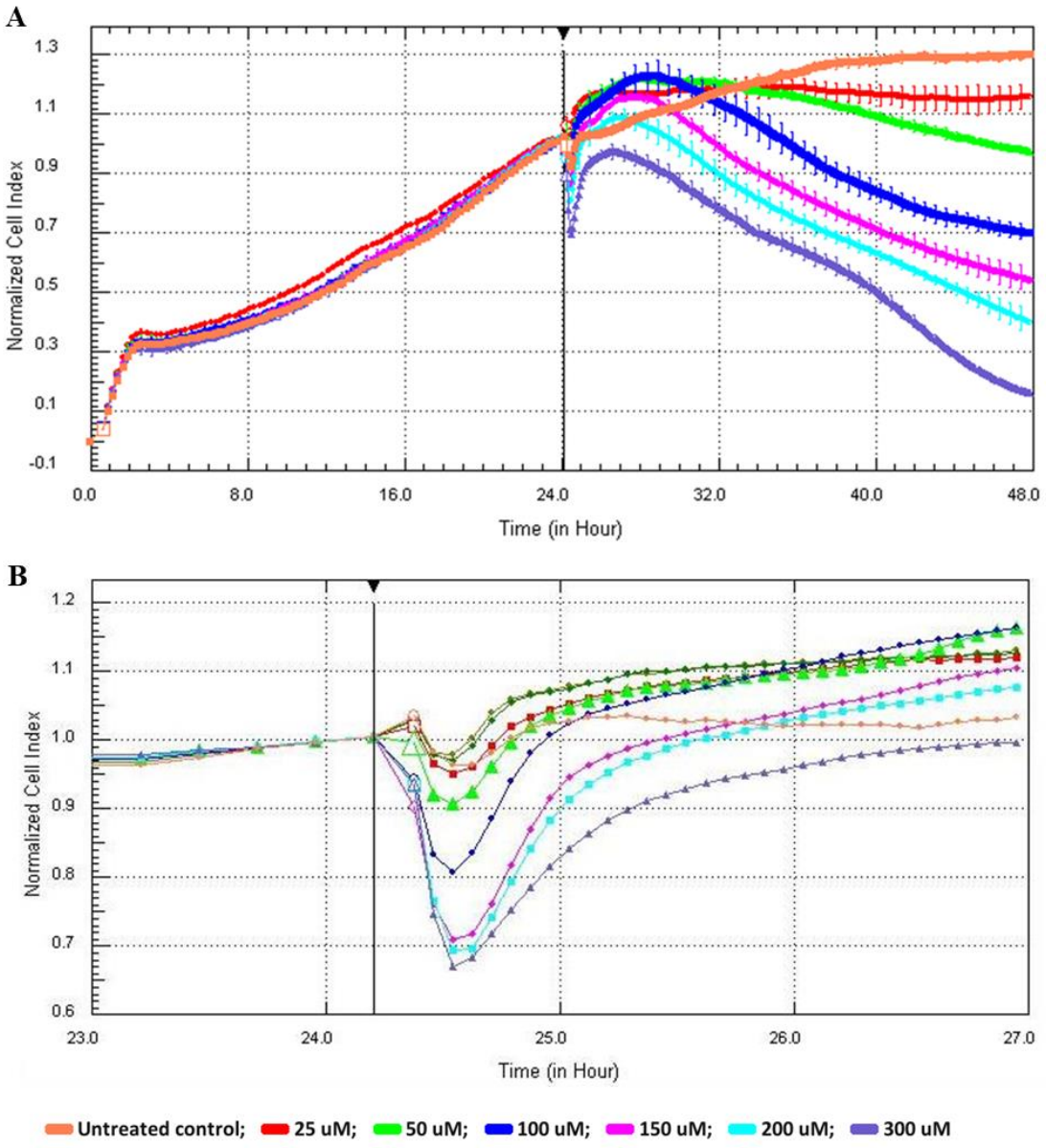

Figure 4.28 Cytotoxicity of genistein to BEAS-2B cells, represented by normalised cell index. BEAS-2B cells were treated with a range of concentrations from 25 µM to 300 µM. (A) CI values shown prior to treatment and for 24 hours after addition of inhibitor; (B) CI shown for approximately 2 and a half hours after treatment. Each concentration was run in triplicate; each figure is a representative image of one of two independent experiments.

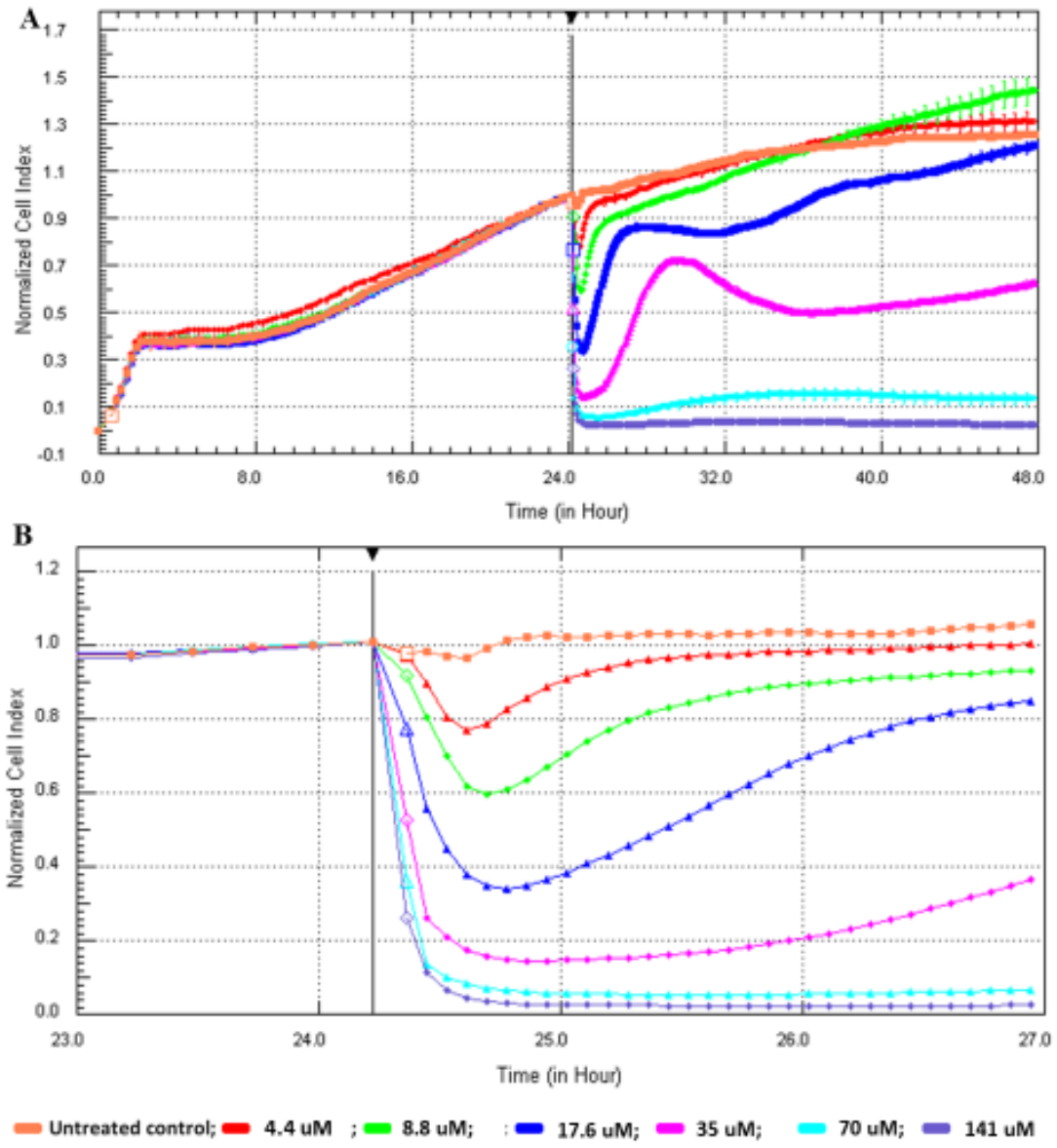

Figure 4.29 Cytotoxicity of chlorpromazine, represented by normalised cell index. BEAS-2B cells were treated with a range of concentrations from 4.4 µM to 141 µM. (A) CI values shown prior to treatment and for 24 hours after addition of inhibitor; (B) CI shown for approximately 2 and a half hours after treatment. Each concentration was run in triplicate; each figure is a representative image of one of two independent experiments.

4.4.3.2 Effects of inhibitors on uptake of AuNPs

The effect of the inhibitors was determined by semi-quantitative analysis using hyperspectral scanning, followed by SAM, and image analysis using ImageJ to determine the percentage area of the cells that mapped to the AuNPs tested. Box and whisker plots showing the distribution of data is shown in Figure 4.30. With all AuNPs, genistein values were considerably lower than that of the untreated controls, whilst chlorpromazine showed minimal effect suggesting that genistein was able to inhibit the uptake of the AuNPs.

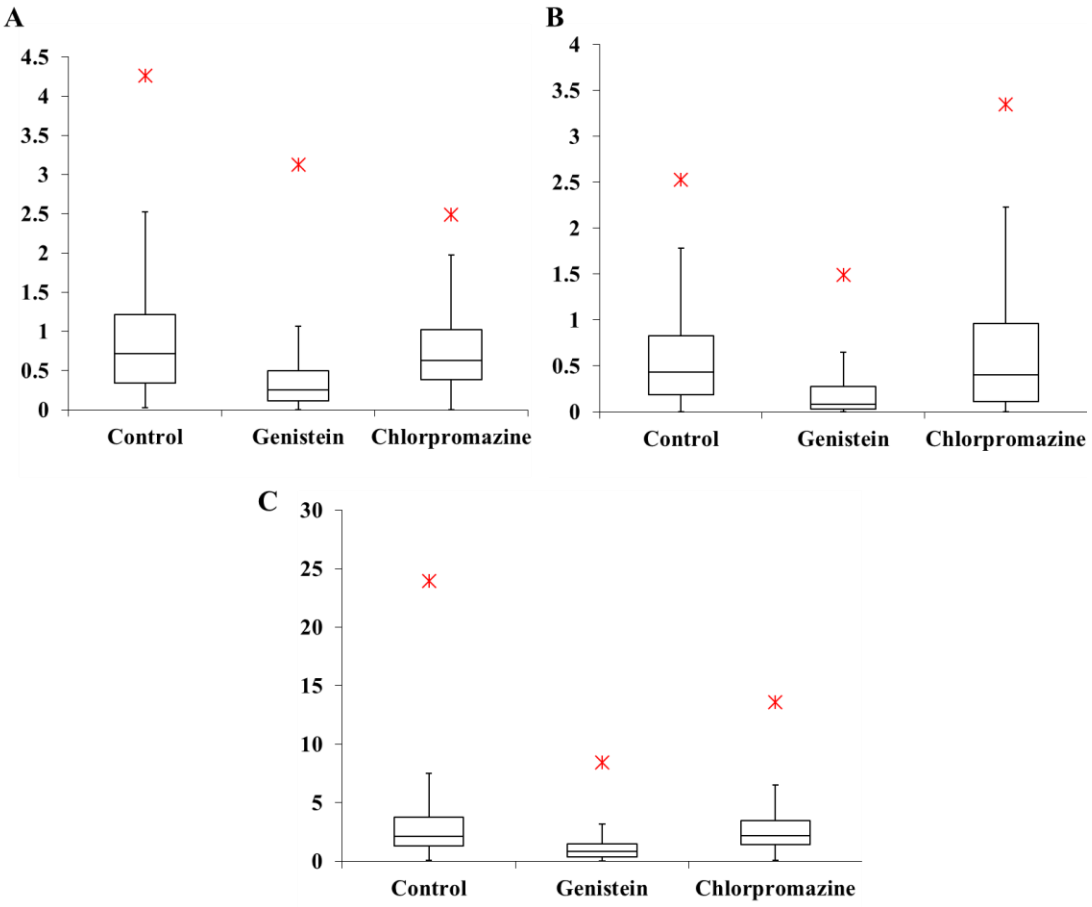

Figure 4.30 Box and whisker chart showing the distribution of data from the inhibition of uptake experiments of (A) 14 nm AuNPs, (B) 20 nm AuNPs, and (C) PCOOH AuNPs. The box represents the interquartile range (IQR), whilst the whiskers represent 1.5 x IQR. For simplicity, only the maximum outlier is shown as ✳. Data obtained from 2 replicates of 2 independent experiments, minimum 180 cells analysed.

4.4.4 Localisation of AuNPs using TEM

TEM was used to observe the intracellular localisation of the AuNPs within the BEAS-2B cells after 2 hours incubation. Representative images of cells treated with 14 nm AuNPs, 20 nm AuNPs, and PCOOH AuNPs can be seen in Figure 4.30, Figure 4.31, and Figure 4.32 respectively. AuNPs were observed in the majority of cells analysed and the AuNPs were mostly found inside vesicles although free lying particles were also observed in the cytoplasm. The particles were found either singularly or in small clusters.

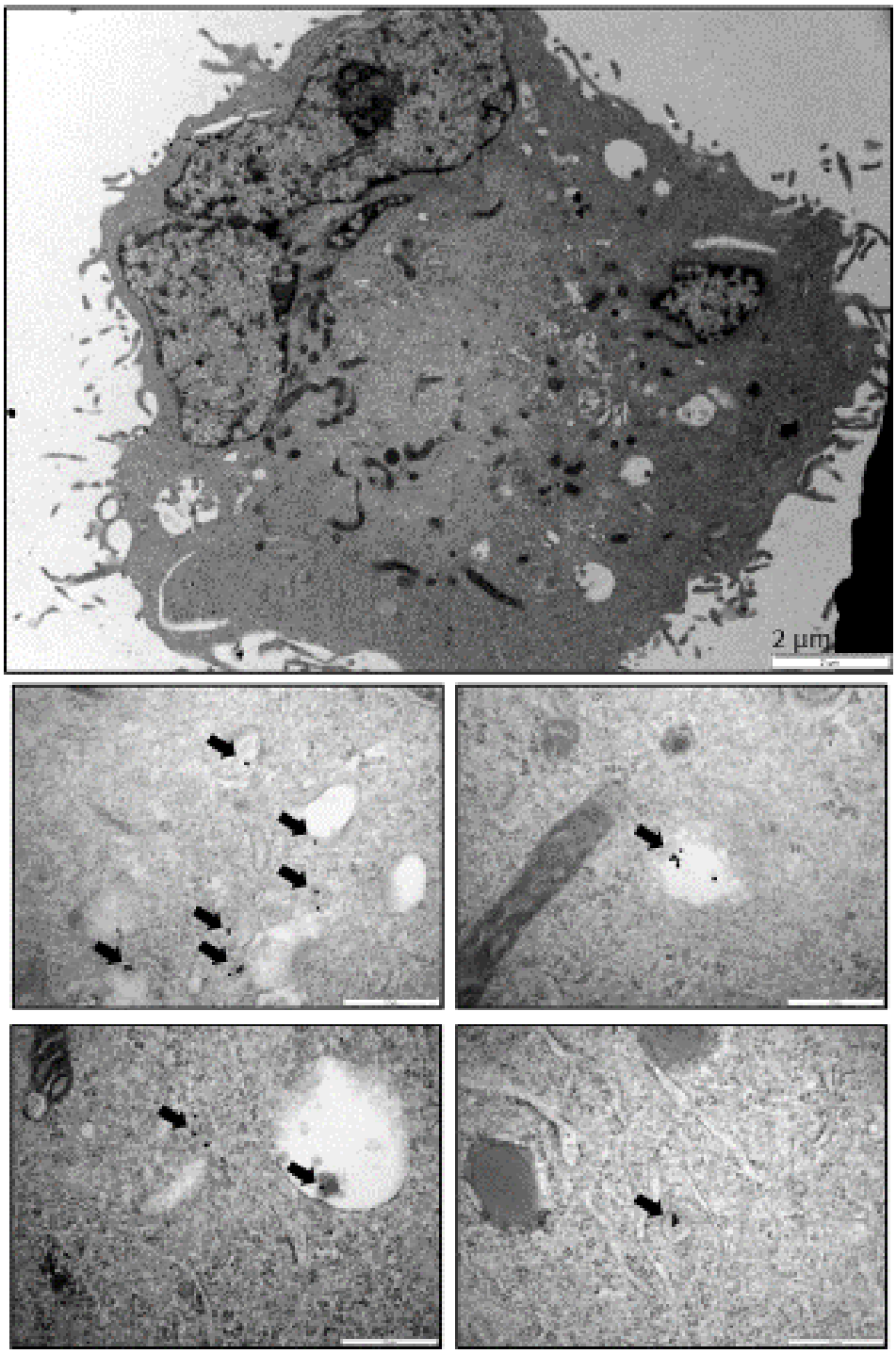

Figure 4.31 Representative TEM images of BEAS-2B cells treated with 14 nm AuNPs for 2 hours. Top image shows a single cell, whilst magnification of regions within the cell are shown in the remaining images (Scale bar = 0.5 µm) and arrows indicate nanoparticles either singularly dispersed or in small clusters.

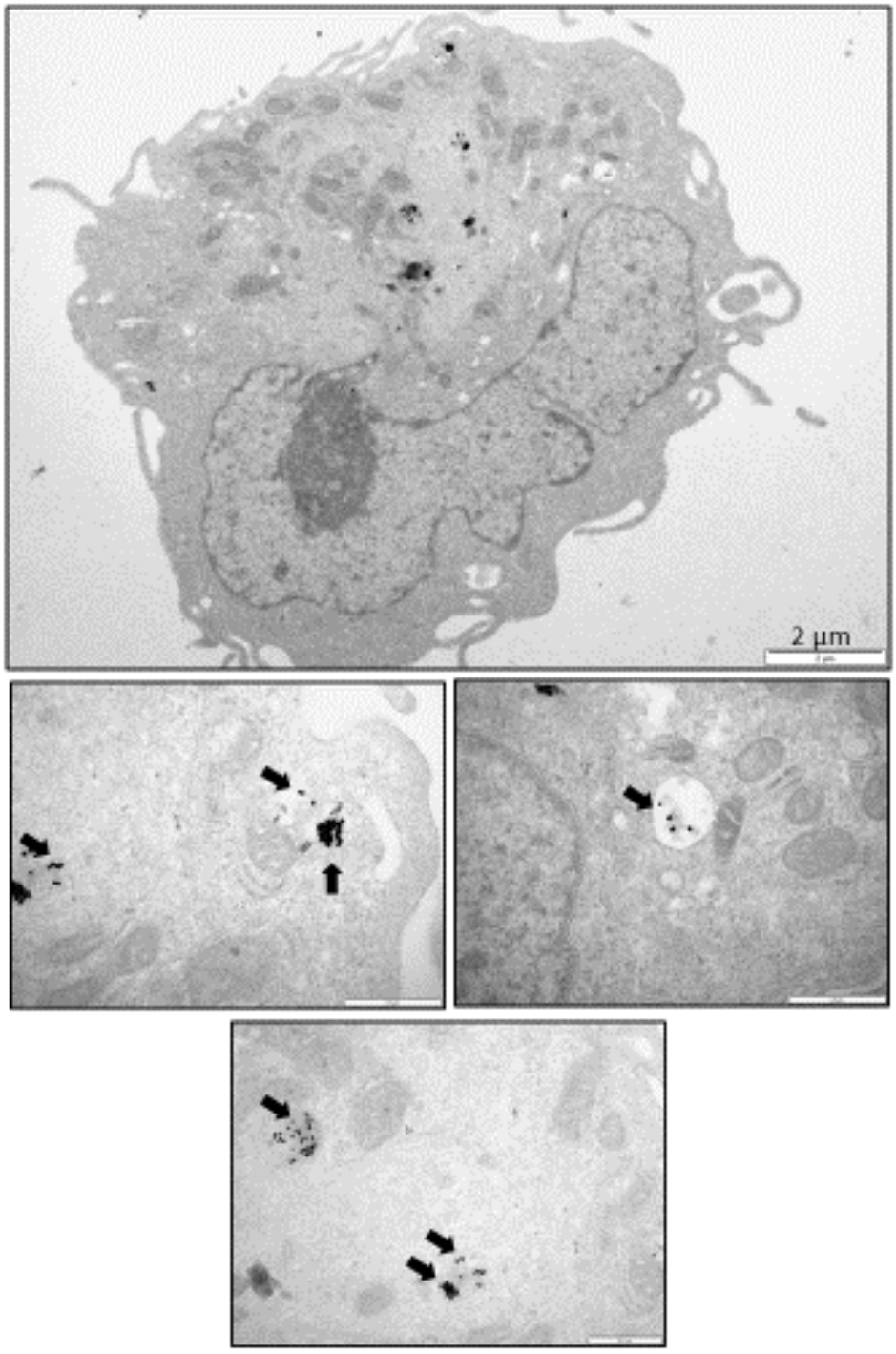

Figure 4.32 Representative TEM images of BEAS-2B cells treated with 20 nm AuNPs for 2 hours. Top image shows a single cell, whilst magnification of regions within the cell are shown in the remaining images (Scale bar = 0.5 µm) and arrows indicate nanoparticles either singularly dispersed or in small clusters.

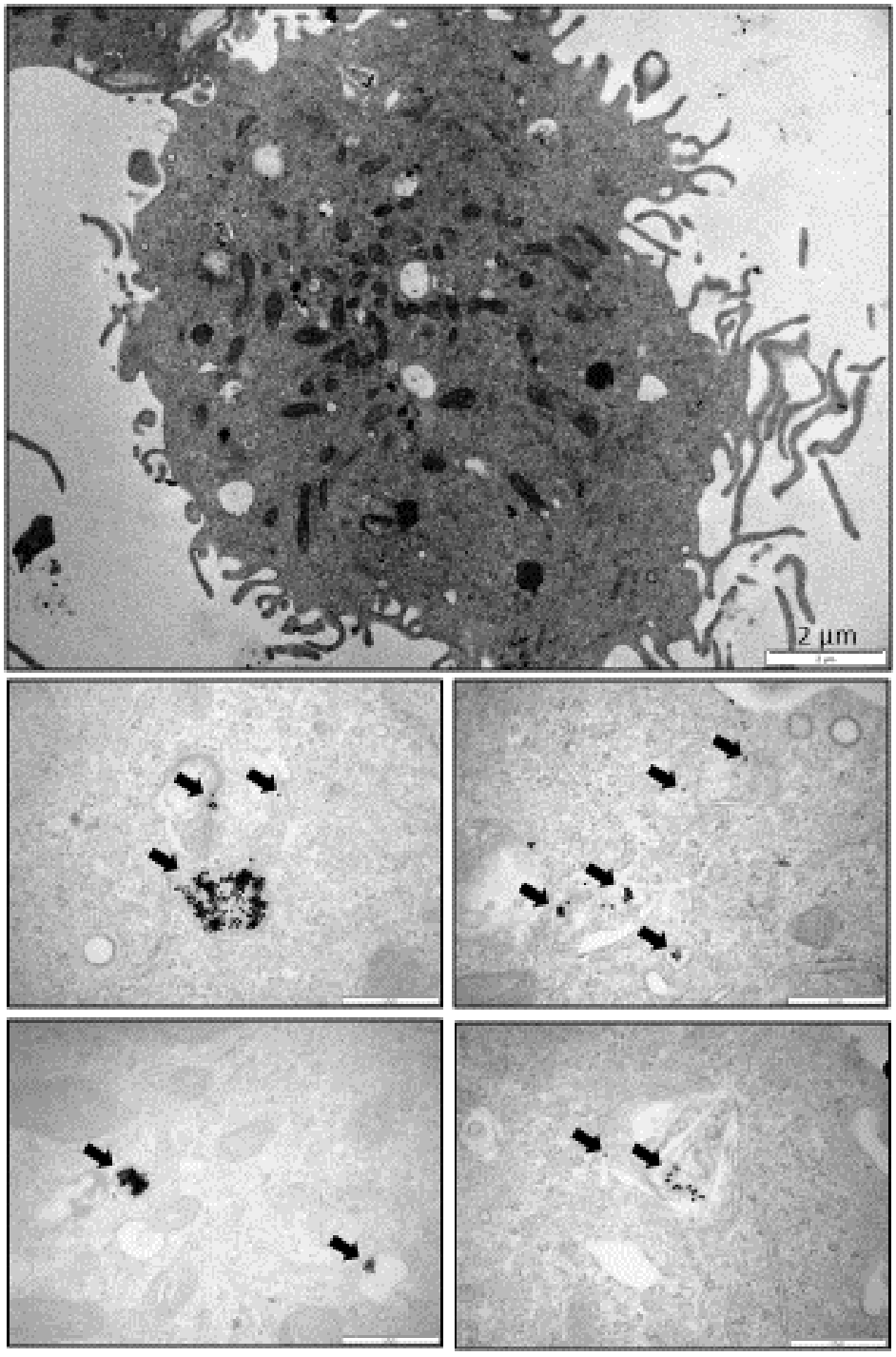

Figure 4.33 Representative TEM images of BEAS-2B cells treated with PCOOH AuNPs for 2 hours. Top image shows a single cell, whilst magnification of regions within the cell are shown in the remaining images (Scale bar = 0.5 µm) and arrows indicate nanoparticles either singularly dispersed or in small clusters.

Chapter 5 – Discussion

Hazard identification is an important aspect of the risk assessment of nanomaterials. In this study, the nanoparticles of choice were gold nanoparticles and therefore a number of *in vitro* studies, which are currently used for the hazard identification of chemicals, were assessed for their applicability to gold nanoparticles. Subsequently, appropriate tests were implemented to determine the toxicity, intracellular uptake and localization, as well as the mechanisms involved in the uptake of the gold nanoparticles. Moreover, the present study investigated the effect of size and different functional groups on the toxicity, genotoxicity, and uptake of these nanoparticles. In addition, this study detailed the physicochemical properties and surface activity as an essential part in the assessment of the toxicity and intracellular uptake of the investigated gold nanoparticles. Finally, recommendations are made for the appropriate *in vitro* assay systems for the hazard identification of gold nanoparticles.

5.1 Physicochemical Properties

In the hazard identification component of the risk assessment of nanoparticles, it is essential to characterise their physicochemical properties prior to any tests conducted. For example, size, shape, surface ligands and functional groups, and surface charge need to be determined. Subsequently, these physicochemical parameters of the tested gold nanoparticles were investigated and presented in Section 4.1.

In addition to these physicochemical parameters, it was also essential to confirm their sterility prior to any tests being conducted. Subsequently, the identification of a preferable endotoxin-detection assay for gold nanoparticle suspensions was investigated. However, possible interference of the sample with the assay must always be considered and controlled when these tests are performed. Indeed, possible interference of the AuNPs with all three of the assays was observed in this study. Previous studies have shown conflicting results with regard to the ability of the AuNPs to interfere with the traditional LAL chromogenic assay. Dobrovolskaia et al.,

2010 observed inhibition of the assay whilst Li et al., 2015 did not, even though both authors have used the same kit, the QCL-1000 kit from Lonza,. This kit was also used in the present study, where interference could be observed through the use of PPCs and dilution of the samples within the acceptable MVD could not overcome the observed inhibition. In addition, particle-only controls in water and stop reagent (25% acetic acid) were included to investigate the influence with the optical readout at 405 nm. Should the nanoparticles be optically active and show an increased absorbance, this possibly could be controlled by subtraction of the particle control values to mitigate the increased absorbance. However, with the exception of the undiluted AuNP sample, the absorbance values of the particle controls were lower than those of the blank (Table 4.4), suggesting that the presence of AuNPs interferes with the optical readout of the assay. This could possibly be caused by the addition of the acetic acid, since a drastic change in pH has been shown to disrupt the negative charge on citrate stabilised AuNPs which leads to aggregation of the NP suspension (Wager *et al.* 2014). According to the manufacturer's instructions, either acetic acid or sodium dodecyl sulfate (SDS) solution can be used as a stop reagent. In the previous study where no interference was observed the authors used SDS as the stop reagent (Li *et al.* 2015); whilst the authors who did observe interference did not specify which stop reagent was used (Dobrovolskaia *et al.* 2010). It is therefore possible that the nature of stop reagent used may influence the aggregation state of the AuNPs, which may, in turn, influence the optical reading of the LAL chromogenic assay.

The gel-clot assay was included in this study since this format does not involve any form of optical readout. Nevertheless, this study found possible interference, in the form of enhancement, since the PPCs at 5 and 10 times dilution of AuNPs were positive at an endpoint of 0.0156 EU/ml, whilst the sensitivity of the test is 0.03125 EU/ml (Table 4.6). Due to the qualitative nature of the gel-clot assay, interference testing can only give an indication of inhibition, whilst enhancement of the assay cannot be distinguished from actual endotoxin contamination. It is generally accepted

that enhancement of an endotoxin assay is less dangerous than inhibition since it may result in a product that has acceptable endotoxin levels failing an endotoxin test; however, in the case of inhibition, the possibility exists that a product with unacceptable levels may be incorrectly deemed safe (Dawson 2005). Therefore enhancement is less of a concern than inhibition; however a previous study has also shown AuNPs to interfere with the gel-clot assay (Dobrovolskaia *et al.* 2010) although these authors observed inhibition of the assay. Since both studies observed interference, albeit different types, this assay would not be recommended.

A drawback of all LAL-based assays is the lack of specificity due to the reactivity of the assay components to fungal contamination, thereby making the rFC assay an attractive option (Ding and Ho 2001). In the current study, inhibition was observed in the rFC assay when the undiluted AuNP sample was used for the PPC; however, this inhibition could be overcome through dilution (Table 4.7). An earlier study has also observed significant inhibition of this assay by AuNPs at 5 nM (Li *et al.* 2015), which corresponds to the observations in the undiluted sample of the current study. Based on the spike recovery observed in their study, levels of inhibition did decrease as the sample was diluted; however, the authors still did not recommend the use of the rFC assay in AuNP concentrations greater than 1 nM, and rather recommended a modified version of the LAL chromogenic assay as being most suitable for nanoparticle samples. However, these authors did not take into account the MVD of the assay, and therefore further dilution of their sample may have been possible. In the present study, an AuNP concentration of 1 nM corresponded to the dilution factor of 5, at which point the inhibition was overcome. The endotoxin limit chosen in this study is that for medical devices, namely 0.5 EU/ml,(FDA 2012) which, taking into account the high sensitivity of this assay (0.005 EU/ml), allows for a MVD of 100 for the rFC assay. Therefore, the lack of inhibition observed at a dilution factor of 5 is well within the MVD and is a valid dilution. For medical devices that come into contact with cerebrospinal fluid the endotoxin limit is 0.06 EU/ml,(FDA 2012) which would allow for a MVD of 12 for this assay; and therefore, at a dilution factor of 5, the assay

would even be valid for this type of device which has stricter limits. The ability of the rFC assay to overcome the observed inhibition within the MVD, as well as the fact that this assay cannot be activated by contaminating β-glucans, makes it a preferable option for the testing of endotoxin contamination in AuNPs.

In summary, the physicochemical properties of the nanoparticles were successfully characterised. For the detection of endotoxin, the interference in the rFC assay could be overcome through dilution of the AuNP sample; whilst interference in the form of inhibition of the chromogenic assay could not be overcome, and possible interference in the form of enhancement was observed with the gel clot assay. Therefore, the rFC assay was recommended as a highly sensitive and specific assay for the testing of endotoxin contamination in AuNP samples.

5.2 Surface Activity

The ability of the AuNPs to generate free radicals was measured using the spin trap DMPO and H_2O_2. Interestingly, the AuNPs were able to reduce the intensity of the ESR signal below the baseline reading (Figure 4.5), suggesting that the AuNPs were possibly able to scavenge free radicals. A study has found that the apparent scavenging of radicals, assessed by ESR, may rather be caused by a quenching effect on the DMPO-OH radical (Li *et al.* 2004). Another study on the interactions of gold nanoparticles with free radicals, suggested that a reduction of ESR signal may be caused by the adsorption of the gold nanoparticles to the free radicals TEMPO, TEMPAMINE, and TEMPONE (Zhang *et al.* 2003). To further investigate the scavenging activity of AuNPs in this study, probes such as 4-aminotempo or 4-iodoacetamidotempo could be used and analysed by ESR (Ionita *et al.* 2008).

The 8-Isoprostane EIA Kit was then investigated for the potential for the AuNPs to cause lipid peroxidation in the BEAS-2B cells. It was found that the 14 nm AuNPs interfered with the detection of 8-isoprostane, resulting in an underestimation of the concentration (Figure 4.6). This was not due to optical interference as there were

multiple wash steps to remove AuNPs, and the Non Specific Binding (NSB) wells spiked with AuNPs showed no differences in absorbance readings as compared to the control non-specific binding wells. The interference was possibly due to interactions with the assay components that could not be overcome through experimental controls. It is possible that other methodologies to detect lipid peroxidation as an indicator of oxidative stress-induced toxicity could be implemented, however, since no cytotoxicity was observed in BEAS-2B cells using the xCELLigence RTCA system, this was not explored further.

5.3 Applicability of conventional toxicity assays and the use of label free methodologies in the hazard identification of gold nanoparticles

The applicability of different *in vitro* tests for the hazard assessment of gold nanoparticles was investigated where the main concern was their interference with the optical measurements implemented in these assay systems. Such optical interference in a few conventional *in vitro* toxicity assays, reliant on optical detection, by AuNPs was extensively investigated in our laboratory, with the aim of identifying preferable assays to be used for the *in vitro* assessment of the cellular effects of AuNPs. As a result, two label-free methods were investigated.

Initial cytotoxicity studies performed using the XTT, LDH, and ATP assays, all of which rely on optical detection, showed conflicting results on the toxicity of 14 nm AuNPs (Figure 4.7, Figure 4.8, Figure 4.9), which suggested the possibility of interference of the AuNPs with one or more of these techniques. Although the data observed using the XTT assay on the toxicity of AuNPs agree with those presented earlier by other investigators using MTT (Freese *et al.* 2012b), the lack of toxicity of these nanoparticles using LDH in the present study was in contrast with those presented by these same authors. Cytotoxicity of AuNPs, as determined by the LDH assay, has also been observed in other studies (Choi *et al.* 2012; Mateo *et al.* 2014). This could however have been because the assay protocols used by these authors were absorbance based, where the absorbance of the final product was measured at

490 nm; whereas in the present study, the detection of the release of LDH was fluorescence-based. Commercially available toxicity assays, including the ones in this study, frequently rely on the optical properties of a reaction product as in indicator of toxicity or viability. Traditionally, the accepted norm for the application of *in vitro* cytotoxicity assay systems is the inclusion of medium controls in the experimental setup with no attention to the optical properties of the particles themselves or the particles' interactions with the assay reagents.

In the present study, interference was observed with the ATP bioluminescence assay system; however, this was not due to the optical properties of the AuNPs, but rather interference with the production of the measured end-product suggesting that the AuNPs were capable of interfering with the assay substrate and the subsequent products. Kroll et al. (2009), discusses different *in vitro* methodologies used for nanoparticle toxicity assessment and summarized nanoparticle characteristics such as high adsorption capacity, surface charge, and catalytic activity as potential causes of the interference of nanoparticles with toxicity assays. Kroll *et al.*, 2012 suggested an approach to prevent interference of nanoparticles with *in vitro* toxicity assays that involves altering assay protocols or lowering particle concentrations. However, the authors did observe that interference was assay- and particle-specific, and recommended that each *in vitro* methodology be evaluated for each individual nanoparticle. These recommendations may however address the interference of extracellular particles present in the culture medium but could not exclude interference by the particles that have already internalized the cells.

One of the methodologies that has been considered, which does not rely on any optical measurements, is the CFE assay. The OECD WPMN interlaboratory comparison study on the CFE assay has therefore aimed to assess the applicability of this assay for the testing of the cytotoxicity of nanomaterials. As part of the work presented in this thesis (Figure 4.10), the CFE assay results obtained from the round robin collaboration with 11 other participating laboratories, has shown good intra-

and interlaboratory reproducibility (Ponti *et al.* 2014). This assay could therefore reliably be used for the hazard identification of gold nanoparticles as well as of other nanoparticles as it has the advantage over conventional toxicity assays for not relying on optical detection of an endpoint, or conversion of a substrate, and therefore avoids test interference by nanoparticles. Although this assay was shown to be applicable and therefore recommended for the testing of the *in vitro* toxicity of nanomaterials, it is quite laborious and has a low throughput.

An additional disadvantage of conventional cytotoxicity assays is that they generally measure toxicity/viability after a predetermined incubation period, thereby potentially missing information. This challenge, together with the demonstration of optical interference with many conventional assays, has necessitated the use of alternate system that does not rely on optical detection or conversion of substrates to products, and can be monitored in real time. The use of cell impedance technology, such as the xCELLigence RTCA system, to ascertain the cytotoxicity of nanoparticles can overcome both these challenges thereby removing the necessity to perform traditional, time-consuming assays at numerous time points. The xCELLigence RTCA system ascertains cell viability through the measurement of impedance changes caused by the attachment or detachment of cells to the electrode-covered surface of the wells of special E-Plates used with the system. This impedance is represented as a Cell Index (CI) that reflects the state of the ionic environment at the electrode/solution interface, which, in turn, is influenced by the presence of cells cultured in wells on top of these electrodes. CI values have therefore been used to monitor cell viability where cell adhesion was considered as the cell viability end-point (Baumann *et al.* 1999; Ke *et al.* 2011).

In the present study, the applicability and value of this label-free cell-impedance technology to assess AuNP toxicity was initially performed with 14 nm and 20 nm citrate stabilized AuNPs on both CHO cells and BEAS-2B cells (Figure 4.13), and this work was published (Vetten *et al.* 2013). The system easily and conveniently

provided information on the growth curves of these two cell lines, indicating ideal cell seeding concentrations and growth patterns to guide recovery and incubation periods. During this preliminary work, the citrate stabilized AuNPs showed minimal toxicity to the BEAS-2B cells; whilst CHO cells were more sensitive and the 20 nm AuNPs were more toxic than the 14 nm AuNPs. In the present study this technology was shown to eliminate the possibility of the AuNPs interfering with assessment of viability as the particle-only controls showed no influence on CI; and therefore assists in avoiding dealing with contradictory results sometimes observed when comparing results from traditional assays.

Cell-based label-free technologies such as the xCELLigence RTCA system have been implemented as part of the preclinical drug development process (Atienza *et al.* 2006; Atienzar *et al.* 2013; Fang 2006; Kustermann *et al.* 2013) and also for the evaluation of the cytotoxicity of a variety of dissolved chemicals (Ceriotti *et al.* 2007; Xing *et al.* 2005). This technology has also been used to assess the cytotoxicity of a variety of nanoparticles including silica (Pisani *et al.* 2015; Yang *et al.* 2010), cobalt ferrite (Mariani *et al.* 2012), silver (Sambale *et al.* 2015), gold (Chueh *et al.* 2014; Tarantola *et al.* 2011) , quantum dots and gold nanorods (Tarantola *et al.* 2009), metal oxides ZnO, CuO, and TiO_2 (Seiffert *et al.* 2012), fullerenes, carbon nanotubes and Fe_3O_4 (Dönmez Güngüneş *et al.* 2017), and other inorganic nanoparticles (Otero-Gonzalez *et al.* 2012).

It is important to note that our results, generated with the RTCA technology, on the toxicity of 14 nm AuNPs to BEAS-2B cells after 1 hour's incubation did not correlate well with those generated with the conventionally used XTT- or ATP-based toxicity assays. However, positive correlation between cell impedance and conventional assays for the toxicity of chemicals has been reported in the literature. For example, a correlation was found in the toxicity of drugs when assessed by either neutral red uptake assay or the RTCA (Kustermann *et al.* 2013), or in the cytotoxicity of sodium arsenite, cadmium chloride and *cis*-platinum assessed by MTT and RTCA (Ceriotti *et*

al. 2007), or in the immunocytotoxicity of baboon sera on pig cells with the MTT and RTCA (Quereda *et al.* 2010) or cell toxicity assay using the Sulforhodamine B for staining proteins and measuring absorbance at a wavelength of 565 nm in correlation to RTCA (Limame *et al.* 2012). Surprisingly, such correlation was also observed between impedance-based technology and the MTS assay for the assessment of CTAB-capped gold nanoparticles of difference shapes (Tarantola *et al.* 2009; Tarantola *et al.* 2011). However, in the present study interference was observed with the final products obtained from these assay systems and subsequently no such correlation could be observed between our data generated by these conventional assay systems and that of the RTCA. The current study has shown that the impedance technology provides a more accurate indication of whether something is toxic or non-toxic, and, together with its ease of use, is therefore recommended as a preferable assay for *in vitro* cytotoxicity testing for the hazard assessment of nanoparticles.

5.4 Effect of AuNPs on cytotoxicity and genotoxicity of BEAS-2B cells

As the preferable cytotoxicity assay, the RTCA system was then used to observe the toxicity of the 14 nm and 20 nm AuNPs, and the 14 nm PEG-liganded AuNPs (POH AuNP, PCOOH AuNP, PBtn AuNP, PNTA AuNP, PAZ AuNP, and PAM AuNP) in the BEAS-2B cell line for up to 24 hours (Figure 4.14). No toxicity was observed for any of the AuNPs, regardless of their size, surface coating or initial surface charge. When compared to previous studies of AuNPs of similar size range (10 nm - 24 nm) and surface coatings (citrate and PEG-liganded), the results concur with some studies but not with others. Citrate stabilized AuNPs in this size range were found to be non-toxic or only minimally toxic to K562, HeLa, A549, BEAS-2B, NHBE, HepG2, and HEK 293 cells (Chen *et al.* 2009; Connor *et al.* 2005; Khan *et al.* 2007; Schlinkert *et al.* 2015; Tlotleng *et al.* 2016). However, they have been found to result in a decrease in proliferation to CF-31 cells (Pernodet *et al.* 2006), and cytotoxicity to A549, A431, and NCI-H1975 (Choi *et al.* 2012). Hydroxyl-PEG AuNPs were found to be toxic to HegG2 and HeLa cells (Li *et al.* 2018), whilst the PCOOH-liganded AuNPs used in

the current study were shown to be non-toxic to HEK 293 cells but highly toxic in a dose-dependent manner to HepG2 cells (Tlotleng *et al.* 2016).

Since most of these studies made use of conventional *in vitro* toxicity assays, the possibility of interference influencing these results cannot be excluded; nonetheless, this data suggests a cell-type dependent response to AuNPs. The initial studies conducted in the present study to validate the xCELLigence system supports this suggestion, since differences in toxicity over an extended incubation period were observed between BEAS-2B cells and CHO cells. This is further supported by the results mentioned above in the Tlotleng et al. (2016) study that was conducted in our laboratory where the PCOOH-AuNPs were those investigated in the present work. Alternative study on 10 nm citrate stabilized AuNPs also observed the absence of toxicity to BEAS-2B cells after 24 hours (Schlinkert *et al.* 2015) suggesting that the BEAS-2B cell line may be fairly resistant to AuNP-induced cytotoxicity.

Even in the absence of cytotoxicity, genotoxity may occur and is an important aspect of toxicity testing. The micronucleus assay was chosen to assess chromosome damage in the present study, as this assay provides a measure of both chromosome loss and chromosome breakage, and was shown to be free of interference from gold nanoparticles (George *et al.* 2017). The CBMN assay was implemented as this procedure makes use of Cyt-B which blocks the polymerisation of actin during cytokinesis, and enables the accumulation of binucleated cells (Fenech 2000), thereby ensuring that only cells that have undergone mitosis in the presence of the test compound are scored (Doak *et al.* 2009). Since Cyt-B is known to inhibit endocytosis, BEAS-2B cells were first incubated for 2 hours with the AuNPs to allow for uptake to occur prior to the addition of Cyt-B. Even with confirmation of uptake of the AuNPs after two hours, the AuNPs tested negative for genotoxicity in BEAS-2B cells (Figure 4.16), which concurs with the results in CHO cells conducted on these AuNPs (George *et al.* 2017).

5.5 The use of the CytoViva as a label-free methodology to assess uptake

In any cytotoxicity assay conducted on nanoparticles, it is also essential to confirm their cellular internalization for correct interpretation of results obtained with cytotoxicity assay systems. Initially, 14 nm and 20 nm citrate stabilized AuNPs were used in both BEAS-2B cells and CHO cells to establish the methodologies in our laboratory, and to demonstrate the usefulness of the CytoViva hyperspectral imaging (HSI) system to assess label-free intracellular uptake. This work was published with the cytotoxicity interference work and preliminary xCELLigence work described above (Vetten *et al.* 2013). The CytoViva HSI system has also been implemented for other nanomaterials including for the determination of the potential distribution of multi-walled carbon nanotubes (MWCNT) in different regions and target cells in the lung (Mercer *et al.* 2011), for the assessment of a panel of metal nanoparticle catalysts for their antifungal activities against *Candida albicans* (Weinkauf and Brehm-Stecher 2009), and for the assessment of internalization of silver nanoparticles and subsequent cellular changes in U937 cells in relation to toxicity (Lim *et al.* 2012).

By adjusting the focal planes through the cells, the dark field CytoViva images confirmed uptake of the AuNPs (Figure 4.17), and dark-field images provided visual confirmation at various time points of the uptake (Figure 4.18 and Figure 4.19). Cell type dependent uptake was observed and the AuNPs appeared to agglomerate within the cells. Hyperspectral scans of the AuNPs showed differences in the spectral profiles of singularly dispersed and agglomerated 14 nm and 20 nm AuNPs (Figure 4.20). Principal Component Analysis (PCA) was performed on the spectra; however, there were not sufficient differences to discriminate between the profiles with this analysis (Figure 4.21). Spectral angle mapping (SAM) was used to identify AuNPs within scans of the cells using the spectral library for agglomerated AuNPs (Figure 4.22).

5.6 Uptake of AuNPs into BEAS-2B cells

In addition to uptake studies performed for hazard identification studies of nanoparticles, it is also essential to investigate as to the mechanisms involved in their cellular uptake in relation to their surface coating and functional groups present on their surfaces. Cellular uptake of the AuNPs into BEAS-2B cells was therefore determined at 1 nM concentration where uptake was observed only with citrate-stabilised and PCOOH AuNPs but not with POH, PBTN, PNTA, or PAZ AuNPs at both 2 hours and 24 hours incubations (Figure 4.25 and Figure 4.27). A similar lack of uptake was also observed in the literature for methoxy-PEG coated gold nanorods into SKBR3 cells (Rayavarapu *et al.* 2010) and also a much lower levels of uptake for methyl ether-PEGylated AuNPs compared to that of citrate-stabilised AuNPs (Cruje and Chithrani 2015).

In the present study, since all the AuNP samples were of similar shape and size, with almost neutral surface charge when suspended in culture media, the differences in uptake between the AuNPs carrying different functional groups may have been due to other effects such as ligand orientation and ligand density. The arrangement of ligands as either ordered striations or random distribution has been shown to influence uptake of nanoparticles, presumably through cell membrane interactions (Verma *et al.* 2008). In addition, ligand density has been shown to have a significant effect on binding of targeted nanoparticles to cells (Elias *et al.* 2013) and also the density as well as the degree of polymerisation of PEG on nanoparticles were shown to influence the ligand-receptor binding of the NPs to cells, thereby influencing their endocytosis (Li *et al.* 2014). PEG density has also been shown to be a key factor for phagocytosis in THP-1 cells (Bazile *et al.* 1995), whilst PEG ligand organisation was shown to influence uptake via passive diffusion across the cell membrane of HCT-116 cells (Lund *et al.* 2011). Therefore, it would seem necessary to assess the ligand density and structure on the nanoparticles used in the current study, in order to determine the impact of these factors on endocytosis. Analyses such as these can be performed through theoretical computational modelling such as Density Functional

Theory (DFT) (Mdluli *et al.* 2011; Xu *et al.* 2015), or experimentally imaged using Scanning Tunnelling Microscopy (STM) (Jackson *et al.* 2004). Although not often addressed in literature, the chirality of the nanoparticles could also potentially influence the interaction of nanoparticles with cell membranes, and these interactions could be investigated using molecular dynamics (MD) simulations (Skandani and Al-Haik 2013).

As the CytoViva hyperspectral scanning and SAM can identify AuNPs, the possibility of using this analysis to quantify the amount of uptake was explored as well as to investigate the mechanisms involved in the intracellular uptake. Since endocytosis is an energy- and temperature-dependent active process, it can be inhibited by incubation at low temperatures (Munn 2001). Subsequently, the nominal uptake of both the citrate-stabilised and PCOOH AuNPs at 4°C could confirm that indeed their cellular uptake was active receptor–mediated endocytosis as was previously described for nanoparticles (Alkilany and Murphy 2010).

Subsequently, this study has investigated clathrin- and caveolin-mediated endocytosis as potential mechanisms of endocytosis of the citrate-stabilised and PCOOH AuNPs, as these pathways have both previously been shown to be relevant to the uptake of AuNPs (Chithrani and Chan 2007; Nativo *et al.* 2008; Ng *et al.* 2015; Xian *et al.* 2012). Clathrin-mediated endocytosis involves the formation of clathrin-coated invaginations of the cell membrane that engulfs macromolecules, and are pinched off through the GTPase activity of dynamin, forming clathrin-coated vesicles. These vesicles go on to form early endosomes, then late endosomes, and most likely will finally fuse with lysosomes, that is to say they follow the endolysosomal pathway (Bareford and Swaan 2007; Kou *et al.* 2013; Stern *et al.* 2012). Through this pathway, the internalised macromolecules are then degraded in the acidic, enzyme-rich environment of the lysosomes (Bareford and Swaan 2007). In contrast, caveolin-mediated endocytosis involves caveolin enriched flask-shaped invaginations that also make use of dynamin to cut off the vesicles from the cell membrane. These

vesicles fuse with endosomes to form caveosomes, thereby are able to avoid the endolysosomal pathway and subsequent lysosomal degradation, and instead move to the endoplasmic reticulum (ER) (Bareford and Swaan 2007; Kou *et al.* 2013; Stern *et al.* 2012). Caveolae are also possibly involved in the transcytosis of proteins and lipids across cells (Cheng and Nichols 2016). Therefore, by investigating the mechanism of uptake will also determine the intracellular fate of the nanoparticles.

Our study made use of chlorpromazine and genistein, chemical inhibitors of clathrin- and caveolin-mediated endocytosis, respectively. Inhibition of these pathways are due to the ability of chlorpromazine to cause clathrin to accumulate in late endosomes (Boylan *et al.* 2012) whereas the action of genistein as a tyrosine kinase inhibitor, to block internalisation (Pelkmans 2005). Both of these inhibitors have successfully been used in BEAS-2B cells to inhibit clathrin-mediated (Boylan *et al.* 2012; Cox *et al.* 2015; Haniu *et al.* 2013; Maruyama *et al.* 2015; Ortega *et al.* 2014) and caveolin-mediated (Kim *et al.* 2012) endocytosis.

In the present study, genistein was shown to inhibit uptake of both the citrate-stabilised and the PCOOH AuNPs by approximately 50%, suggesting a caveolin-mediated endocytosis pathway (Figure 4.30). Similar to the current study, caveolin-mediated endocytosis was also shown to be the relevant mechanism of uptake of a much smaller size 4.5 nm Au-cysteine-Cy5 nanoparticles (Xian *et al.* 2012). In contrast, some previous studies investigating AuNPs of similar size to those in the present study have shown clathrin-mediated uptake (Chithrani and Chan 2007; Ng *et al.* 2015) where in the first of these studies, the surface of the AuNPs were coated with the protein transferrin (Chithrani and Chan 2007), the uptake of which is well-established as a clathrin-mediated mechanism (Le Roy and Wrana 2005; McMahon and Boucrot 2011). In the second study, the AuNPs were coated with FBS with the aim of facilitating uptake by endocytosis (Ng *et al.* 2015). Taken together, these previous studies and the data from the current study reiterate the importance of the surface functionalisation of AuNPs on the mechanism of endocytosis.

To investigate further the intracellular localisation of the 14 nm, 20 nm, and PCOOH AuNPs within the BEAS-2B cells, studies were conducted using TEM. AuNPs were found inside vesicles and in the cytosol, whilst none were observed in nuclei or associated with any other organelles (Figure 4.31, Figure 4.32, Figure 4.33). The accumulation of AuNPs within vesicles following uptake is in agreement with a previous study of 5 nm and 15 nm citrate stabilised AuNPs in Balb/3T3 cells (Coradeghini *et al.* 2013), and of 14 nm α-lipoyl-ω-methoxy PEG AuNPs in RAW264.7 cells (Liu *et al.* 2012), although neither of these studies observed individual particles in the cytosol. However, one study of 16 nm citrate stabilised AuNPs in HeLa cells observed AuNPs within vesicles and dispersed in the cytosol (Nativo *et al.* 2008).

As mentioned earlier, the mechanism of uptake will determine the intracellular fate of the NPs. In previous studies using BEAS-2B cells, cysteine poly-L-lysine DNA nanoparticles were taken up by caveolin-mediated endocytosis and were shown to avoid the endolysosomal pathway (Kim *et al.* 2012). The same group showed that poly-l-histidine poly-l-lysine DNA nanoparticles were taken up by BEAS-2B cells by clathrin-mediated endocytosis and entered the degradative endolysosomal pathway (Boylan *et al.* 2012). Together, these studies show that both endocytosis pathways are pertinent in BEAS-2B cells and subsequently the surface ligands and the functional groups may determine their intracellular fate.

Recently, literature has shown that the endocytosis mechanism, subsequent pathway and intracellular fate of nanoparticle uptake appear to affect toxicity. Sabella and colleagues (2014) showed that toxicity of AuNPs was influenced by the mechanisms of uptake, where AuNPs were non-toxic when found in the cytosol following energy independent uptake; whereas AuNPs that were taken up by active endocytosis, and trapped in lysosomes, were toxic. The authors proposed that the observed toxicity was due to intracellular release of ions, triggered by the degradative acidic conditions

within lysosomal cellular compartments; and named this mechanism the "lysosomal-enhanced Trojan horse effect" (LETH mechanism) (Sabella *et al.* 2014). In the same year, the clathrin-mediated endocytosis of cobalt oxide (Co_3O_4) in BEAS-2B cells showed their accumulation in lysosomes and linked toxicity of the nanoparticles to intracellular solubilisation of cobalt, in a similar Trojan-horse type mechanism (Ortega *et al.* 2014). This general mechanism for intracellular toxicity was shown to be applicable for other metal-containing nanoparticles, but not for NPs that were unable to release toxic ions (Sabella *et al.* 2014); therefore these authors suggested that intracellular release of ions may cause ion-specific toxicity or lysosomal damage. Recently, an integrated theory on nanoparticle toxicity was published where lysosomal membrane permeabilisation (LMP) was suggested as the key factor in determining particle bioactivity and adverse effects (Bunderson-Schelvan *et al.* 2016). Together these studies suggest that following caveolin-mediated uptake in BEAS-2B cells, nanoparticles may be able to bypass endolysosomal degradation, and the subsequent release of ions, and therefore may explain the observed lack of toxicity seen in the present study.

In the present study, the surface coating of AuNPs was shown to impact the uptake of these particles with no observed cytotoxicity in a bronchial epithelial cell line. Hyperspectral imaging and spectral angle mapping was used to provide a label-free methodology for semi-quantitative analysis of uptake. Through this methodology, caveolin-mediated endocytosis was identified as the mechanism of uptake of the citrate-stabilised and PCOOH AuNPs. Together with the observed lack of toxicity, these results support the hypothesis that the mechanism of endocytosis pathway will dictate intracellular localisation and subsequent toxicity.

Chapter 6 – Conclusions and Recommendations

The risk assessment of nanomaterials is essential both now and in the coming years to ensure the safe development and use of nanomaterials. This study focused on the important component of risk assessment, namely hazard identification. The latter requires the implementation of a number of *in vitro* and *in vivo* tests that need to be conducted for chemicals. To satisfy these requirements, number of test systems were explored and tested for their applicability in the hazard identification of gold nanoparticles *in vitro*. Once the applicability of these tests were confirmed, they were implemented in the assessment of the toxicity, surface activity, genotoxicity, sterility, and intracellular uptake of gold nanoparticles. With these test systems, it was possible to investigate the effects of size, surface functionalization and surface charge on their toxicity, intracellular uptake and localisation, as well as mechanisms involved in cellular uptake.

From the results obtained, the following conclusions can therefore be made concerning the hazard identification of gold nanomaterials:

1. This study reiterates that physicochemical characterization of nanomaterials is an essential aspect of hazard identification as the characteristics of the nanoparticles play an important role in the cellular interactions and the subsequent adverse effects. An understanding of the physicochemical properties will aid in the identification of critical properties that influence toxicity of nanomaterials. Some of the important physicochemical properties that can influence the toxicity include size, shape, and surface chemistry including surface charge of nanomaterials.

2. The physicochemical properties of nanomaterials, in particular their optical and catalytic properties, can interfere with *in vitro* toxicity testing assay systems i.e. XTT, ATP, and 8-isoprostane assays. On the other hand, there was no such interference with the LDH assay.

3. The CFE and the cell impedance xCELLigence RTCA assay systems were identified as two systems were free of interference by nanoparticles, with the observation that the former was labour intensive and low throughput and the latter was easy to operate and was of high throughput in nature. Using the RTCA assay system, it was possible to show the effect to the physicochemical properties including size and surface ligands and their functional groups on the surface of the gold nanoparticles tested on their toxicity.

4. Following testing for interference of gold nanoparticles with endotoxin assays used to confirm the sterility of the nanomaterials used, the rFC assay was determined to be most suitable.

5. With the aim of proposing additional assay systems where there will not be interference by nanoparticles, the CytoViva HSI system was investigated to assess cellular uptake of nanoparticles. It could be shown that indeed, there was no interference by gold nanoparticles in this assay system. Moreover, the mechanisms involved in this uptake could be elucidated and also this uptake could be correlated to the physicochemical properties of nanoparticles including the presence of surface ligands and the functional groups they carried.

Accordingly, the following recommendations can be made:

1. It is always necessary to investigate the interference of nanomaterials with the test systems implemented for their hazard assessment. Ideally, tests to be used are label-free methodologies where the measurement of the effects observed do not rely on optical measurements.

2. Prior to the commencement of hazard assessment of nanomaterials, it is of utmost importance to determine their physicochemical properties as well as their sterility. Such assessments will allow a more reliable correlation of these physicochemical properties to their cellular effects including toxicity and uptake.

3. With reliable *in vitro* tests in the hazard assessment component of nanomaterials, it will be possible to conduct not only the risk assessment of these nanomaterials, but also will provide sufficient data generated from reliable toxicity tests for the prediction of the risk of newly synthesised nanomaterials. This in turn, will eliminate the necessity of conducting similar risk assessments for every nanomaterial synthesised or used in the different consumer products already available in the market or to be registered in different countries.

Chapter 7 – Future Work

Conducting *in vitro* toxicity tests are one of the requirements in the hazard assessment of nanomaterials. It is however also essential that mechanisms of their toxicity are also elucidated to enable intervention and more importantly allow the synthesis of safer nanomaterials by changing their physicochemical properties. To this end, the following recommendations for future work may be proposed:

1. The present study did not investigate possible co-localisation of gold nanoparticles with lysosomes. As per newly proposed role for the lysosomal membrane permeabilisation in the toxicity of nanomaterials and the role it plays in the ensuing inflammation and cell death, it will be very much desirable to investigate this aspect further.

2. Future studies should also include other test systems such as *in vitro* air liquid interface (ALI), which mimics inhalation exposures and therefore it will be possible to assess toxicity via inhalation route.

3. Considering the results indicating the importance of ligands and the functional groups in toxicity and intracellular uptake and localisation, additional studies should be conducted to assess the orientation and density of these ligands to be able to predict their interaction with cells.

4. In addition, the applicability of different modelling in the hazard identification of nanomaterials should be investigated further. These may include the *In vitro* Sedimentation, Diffusion and Dosimetry (ISDD) model to assess the delivered dose of nanomaterials during *in vitro* cell cultures especially when establishing a dose-response relationship for the investigated nanomaterials. Moreover, the applicability of the Quantitative Structure-Activity

Relationship (QSAR) used for chemicals, should be investigated for nanomaterials in their hazard assessment.

Appendices

Appendix A: Ethics Clearance

M130574

R14/49 Ms Melissa A Vetten

HUMAN RESEARCH ETHICS COMMITTEE (MEDICAL)

CLEARANCE CERTIFICATE NO. M130574

NAME: (Principal Investigator)	Ms Melissa A Vetten
DEPARTMENT:	Molecular Medicine & Haematology National Institute for Occupational Health
PROJECT TITLE:	In Vitro Assessment of the Toxcitiy of Gold Nanoparticles
DATE CONSIDERED:	Ad hoc
DECISION:	Approved unconditionally
CONDITIONS:	
SUPERVISOR:	Prof MaryGulumain
APPROVED BY:	Professor PE Cleaton-Jones, Chairperson, HREC (Medical)

DATE OF APPROVAL: 21/06/2013

This clearance certificate is valid for 5 years from date of approval. Extension may be applied for.

DECLARATION OF INVESTIGATORS

To be completed in duplicate and **ONE COPY** returned to the Secretary in Room 10004, 10th floor, Senate House, University.

I/we fully understand the conditions under which I am/we are authorized to carry out the above-mentioned research and I/we undertake to ensure compliance with these conditions. Should any departure be contemplated, from the research protocol as approved, I/we undertake to resubmit the application to the Committee. **I agree to submit a yearly progress report.**

Principal Investigator Signature Date

PLEASE QUOTE THE PROTOCOL NUMBER IN ALL ENQUIRIES

Appendix B: Copyright permission for *Particle and Fibre Toxicology* publication

BioMed Central The Open Access Publisher | PARTICLE AND FIBRE TOXICOLOGY

this article | search | submit a manuscript | register

Part Fibre Toxicol. 2013; 10: 50. PMCID: PMC3853235
Published online 2013 Oct 9. doi: 10.1186/1743-8977-10-50 PMID: 24103467

Label-free *in vitro* toxicity and uptake assessment of citrate stabilised gold nanoparticles in three cell lines

Melissa A Vetten,[1,2] Nonhlanhla Tlotleng,[1,2] Delia Tanner Rascher,[3] Amanda Skepu,[3] Frankline K Keter,[3] Kailen Boodhia,[1] Leigh-Anne Koekemoer,[1] Charlene Andraos,[1,2] Robert Tshikhudo,[3] and Mary Gulumian[✉1,2]

[1]Toxicology Section, National Institute for Occupational Health (NIOH), P O Box 4788, Johannesburg 2000, South Africa

[2]Haematology and Molecular Medicine, School of Pathology, University of the Witwatersrand, Johannesburg 2000, South Africa

[3]Nanotechnology Innovation Centre (NIC), Advanced Materials Division, Mintek, Private Bag X 3015, Randburg 2125, South Africa

[✉]Corresponding author.

Melissa A Vetten: melissa.vetten@nioh.nhls.ac.za; Nonhlanhla Tlotleng: nonhlanhla.tlotleng@nioh.nhls.ac.za; Delia Tanner Rascher: deliatanner@gmail.com; Amanda Skepu: amandas@mintek.co.za; Frankline K Keter: franklinek@mintek.co.za; Kailen Boodhia: kailen.boodhia@nioh.nhls.ac.za; Leigh-Anne Koekemoer: leighanne.koekemoer@nioh.nhls.ac.za; Charlene Andraos: charlene.andraos@nioh.nhls.ac.za; Robert Tshikhudo: robertt@mintek.co.za; Mary Gulumian: mary.gulumian@nioh.nhls.ac.za

Received 2013 Jan 25; Accepted 2013 Sep 28.

Copyright © 2013 Vetten et al.; licensee BioMed Central Ltd.

This is an open access article distributed under the terms of the Creative Commons Attribution License (http://creativecommons.org/licenses/by/2.0), which permits unrestricted use, distribution, and reproduction in any medium, provided the original work is properly cited.

Abstract

Background

Reliable *in vitro* toxicity testing is needed prior to the commencement of *in vivo* testing necessary for hazard identification and risk assessment of nanoparticles. In this study, the cytotoxicity and uptake of 14 nm and 20 nm citrate stabilised gold nanoparticles (AuNPs) in the bronchial epithelial cell line BEAS-2B, the Chinese hamster ovary cell line CHO, and the human embryonic kidney cell line HEK 293 were investigated.

Methods

Cytotoxicity of the AuNPs was assessed via traditional XTT-, LDH-, and ATP-based assays, followed by cell impedance studies. Dark-field imaging and hyperspectral imaging were used to confirm the uptake of AuNPs into the cells.

Results

Creative Commons

creative commons
LEGAL CODE

Attribution 2.0

CREATIVE COMMONS CORPORATION IS NOT A LAW FIRM AND DOES NOT PROVIDE LEGAL SERVICES. DISTRIBUTION OF THIS LICENSE DOES NOT CREATE AN ATTORNEY-CLIENT RELATIONSHIP. CREATIVE COMMONS PROVIDES THIS INFORMATION ON AN "AS-IS" BASIS. CREATIVE COMMONS MAKES NO WARRANTIES REGARDING THE INFORMATION PROVIDED, AND DISCLAIMS LIABILITY FOR DAMAGES RESULTING FROM ITS USE.

License

THE WORK (AS DEFINED BELOW) IS PROVIDED UNDER THE TERMS OF THIS CREATIVE COMMONS PUBLIC LICENSE ("CCPL" OR "LICENSE"). THE WORK IS PROTECTED BY COPYRIGHT AND/OR OTHER APPLICABLE LAW. ANY USE OF THE WORK OTHER THAN AS AUTHORIZED UNDER THIS LICENSE OR COPYRIGHT LAW IS PROHIBITED.

BY EXERCISING ANY RIGHTS TO THE WORK PROVIDED HERE, YOU ACCEPT AND AGREE TO BE BOUND BY THE TERMS OF THIS LICENSE. THE LICENSOR GRANTS YOU THE RIGHTS CONTAINED HERE IN CONSIDERATION OF YOUR ACCEPTANCE OF SUCH TERMS AND CONDITIONS.

1. Definitions

a. **"Collective Work"** means a work, such as a periodical issue, anthology or encyclopedia, in which the Work in its entirety in unmodified form, along with a number of other contributions, constituting separate and independent works in themselves, are assembled into a collective whole. A work that constitutes a Collective Work will not be considered a Derivative Work (as defined below) for the purposes of this License.

b. **"Derivative Work"** means a work based upon the Work or upon the Work and other pre-existing works, such as a translation, musical arrangement, dramatization, fictionalization, motion picture version, sound recording, art reproduction, abridgment, condensation, or any other form in which the Work may be recast, transformed, or adapted, except that a work that constitutes a Collective Work will not be considered a Derivative Work for the purpose of this License. For the avoidance of doubt, where the Work is a musical composition or sound recording, the synchronization of the Work in timed-relation with a moving image ("synching") will be considered a Derivative Work for the purpose of this License.

c. **"Licensor"** means the individual or entity that offers the Work under the terms of this License.

d. **"Original Author"** means the individual or entity who created the Work.

e. **"Work"** means the copyrightable work of authorship offered under the terms of this License.

f. **"You"** means an individual or entity exercising rights under this License who has not previously violated the terms of this License with respect to the Work, or who has received express permission from the Licensor to exercise rights under this License despite a previous violation.

2. Fair Use Rights. Nothing in this license is intended to reduce, limit, or restrict any rights arising from fair use, first sale or other limitations on the exclusive rights of the copyright owner under copyright law or other applicable laws.

3. License Grant. Subject to the terms and conditions of this License, Licensor hereby grants You a worldwide, royalty-free, non-exclusive, perpetual (for the duration of the applicable copyright) license to exercise the rights in the Work as stated below:

a. to reproduce the Work, to incorporate the Work into one or more Collective Works, and to reproduce the Work as incorporated in the Collective Works;

b. to create and reproduce Derivative Works;

c. to distribute copies or phonorecords of, display publicly, perform publicly, and perform publicly by means of a digital audio transmission the Work including as incorporated in Collective Works;

d. to distribute copies or phonorecords of, display publicly, perform publicly, and perform publicly by means of a digital audio transmission Derivative Works.

e. For the avoidance of doubt, where the work is a musical composition:

i. **Performance Royalties Under Blanket Licenses**. Licensor waives the exclusive right to collect, whether individually or via a performance rights society (e.g. ASCAP, BMI, SESAC), royalties for the public performance or public digital performance (e.g. webcast) of the Work.

ii. **Mechanical Rights and Statutory Royalties**. Licensor waives the exclusive right to collect, whether individually or via a music rights agency or designated agent (e.g. Harry Fox Agency), royalties for any phonorecord You create from the Work ("cover version") and distribute, subject to the compulsory license created by 17 USC Section 115 of the US Copyright Act (or the equivalent in other jurisdictions).

f. **Webcasting Rights and Statutory Royalties**. For the avoidance of doubt, where the Work is a sound recording, Licensor waives the exclusive right to collect, whether individually or via a performance-rights society (e.g. SoundExchange), royalties for the public digital performance (e.g. webcast) of the Work, subject to the compulsory license created by 17 USC Section 114 of the US Copyright Act (or the equivalent in other jurisdictions).

The above rights may be exercised in all media and formats whether now known or hereafter devised. The above rights include the right to make such modifications as are technically necessary to exercise the rights in other media and formats. All rights not expressly granted by Licensor are hereby reserved.

4. Restrictions. The license granted in Section 3 above is expressly made subject to and limited by the following restrictions:

a. You may distribute, publicly display, publicly perform, or publicly digitally perform the Work only under the terms of this License, and You must include a copy of, or the Uniform Resource Identifier for, this License with every copy or phonorecord of the Work You distribute, publicly display, publicly perform, or publicly digitally perform. You may not offer or impose any terms on the Work that alter or restrict the terms of this License or the recipients' exercise of the rights granted hereunder. You may not sublicense the Work. You must keep intact all notices that refer to this License and to the disclaimer of warranties. You may not distribute, publicly display, publicly perform, or publicly digitally perform the Work with any technological measures that control access or use of the Work in a manner inconsistent with the terms of this License Agreement. The above applies to the Work as incorporated in a Collective Work, but this does not require the Collective Work apart from the Work itself to be made subject to the terms of this License. If You create a Collective Work, upon notice from any Licensor You must, to the extent practicable, remove from the Collective Work any reference to such Licensor or the Original Author, as requested. If You create a Derivative Work, upon notice from any Licensor You must, to the extent practicable, remove from the Derivative Work any reference to such Licensor or the Original Author, as requested.

b. If you distribute, publicly display, publicly perform, or publicly digitally perform the Work or any Derivative Works or Collective Works, You must keep intact all

copyright notices for the Work and give the Original Author credit reasonable to the medium or means You are utilizing by conveying the name (or pseudonym if applicable) of the Original Author if supplied; the title of the Work if supplied; to the extent reasonably practicable, the Uniform Resource Identifier, if any, that Licensor specifies to be associated with the Work, unless such URI does not refer to the copyright notice or licensing information for the Work; and in the case of a Derivative Work, a credit identifying the use of the Work in the Derivative Work (e.g., "French translation of the Work by Original Author," or "Screenplay based on original Work by Original Author"). Such credit may be implemented in any reasonable manner; provided, however, that in the case of a Derivative Work or Collective Work, at a minimum such credit will appear where any other comparable authorship credit appears and in a manner at least as prominent as such other comparable authorship credit.

5. Representations, Warranties and Disclaimer

UNLESS OTHERWISE MUTUALLY AGREED TO BY THE PARTIES IN WRITING, LICENSOR OFFERS THE WORK AS-IS AND MAKES NO REPRESENTATIONS OR WARRANTIES OF ANY KIND CONCERNING THE WORK, EXPRESS, IMPLIED, STATUTORY OR OTHERWISE, INCLUDING, WITHOUT LIMITATION, WARRANTIES OF TITLE, MERCHANTIBILITY, FITNESS FOR A PARTICULAR PURPOSE, NONINFRINGEMENT, OR THE ABSENCE OF LATENT OR OTHER DEFECTS, ACCURACY, OR THE PRESENCE OF ABSENCE OF ERRORS, WHETHER OR NOT DISCOVERABLE. SOME JURISDICTIONS DO NOT ALLOW THE EXCLUSION OF IMPLIED WARRANTIES, SO SUCH EXCLUSION MAY NOT APPLY TO YOU.

6. Limitation on Liability. EXCEPT TO THE EXTENT REQUIRED BY APPLICABLE LAW, IN NO EVENT WILL LICENSOR BE LIABLE TO YOU ON ANY LEGAL THEORY FOR ANY SPECIAL, INCIDENTAL, CONSEQUENTIAL, PUNITIVE OR EXEMPLARY DAMAGES ARISING OUT OF THIS LICENSE OR THE USE OF THE WORK, EVEN IF LICENSOR HAS BEEN ADVISED OF THE POSSIBILITY OF SUCH DAMAGES.

7. Termination

a. This License and the rights granted hereunder will terminate automatically upon any breach by You of the terms of this License. Individuals or entities who have received Derivative Works or Collective Works from You under this License, however, will not have their licenses terminated provided such individuals or entities remain in full compliance with those licenses. Sections 1, 2, 5, 6, 7, and 8 will survive any termination of this License.

b. Subject to the above terms and conditions, the license granted here is perpetual (for the duration of the applicable copyright in the Work). Notwithstanding the above, Licensor reserves the right to release the Work under different license terms or to stop distributing the Work at any time; provided, however that any such election will not serve to withdraw this License (or any other license that has been, or is required to be, granted under the terms of this License), and this License will continue in full force and effect unless terminated as stated above.

8. Miscellaneous

a. Each time You distribute or publicly digitally perform the Work or a Collective Work, the Licensor offers to the recipient a license to the Work on the same terms and conditions as the license granted to You under this License.

b. Each time You distribute or publicly digitally perform a Derivative Work, Licensor offers to the recipient a license to the original Work on the same terms and conditions as the license granted to You under this License.

c. If any provision of this License is invalid or unenforceable under applicable law, it shall not affect the validity or enforceability of the remainder of the terms of this License, and without further action by the parties to this agreement, such provision shall be reformed to the minimum extent necessary to make such provision valid and enforceable.

d. No term or provision of this License shall be deemed waived and no breach consented to unless such waiver or consent shall be in writing and signed by the party to be charged with such waiver or consent.

e. This License constitutes the entire agreement between the parties with respect to the Work licensed here. There are no understandings, agreements or representations with respect to the Work not specified here. Licensor shall not be bound by any additional provisions that may appear in any communication from You. This License may not be modified without the mutual written agreement of the Licensor and You.

Creative Commons is not a party to this License, and makes no warranty whatsoever in connection with the Work. Creative Commons will not be liable to You or any party on any legal theory for any damages whatsoever, including without limitation any general, special, incidental or consequential damages arising in connection to this license. Notwithstanding the foregoing two (2) sentences, if Creative Commons has expressly identified itself as the Licensor hereunder, it shall have all rights and obligations of Licensor.

Except for the limited purpose of indicating to the public that the Work is licensed under the CCPL, neither party will use the trademark "Creative Commons" or any related trademark or logo of Creative Commons without the prior written consent of Creative Commons. Any permitted use will be in compliance with Creative Commons' then-current trademark usage guidelines, as may be published on its website or otherwise made available upon request from time to time.

Creative Commons may be contacted at https://creativecommons.org/.

« Back to Commons Deed

Appendix C: Copyright permission for *Nanomedicine: Nanotechnology, Biology, and Medicine* publication

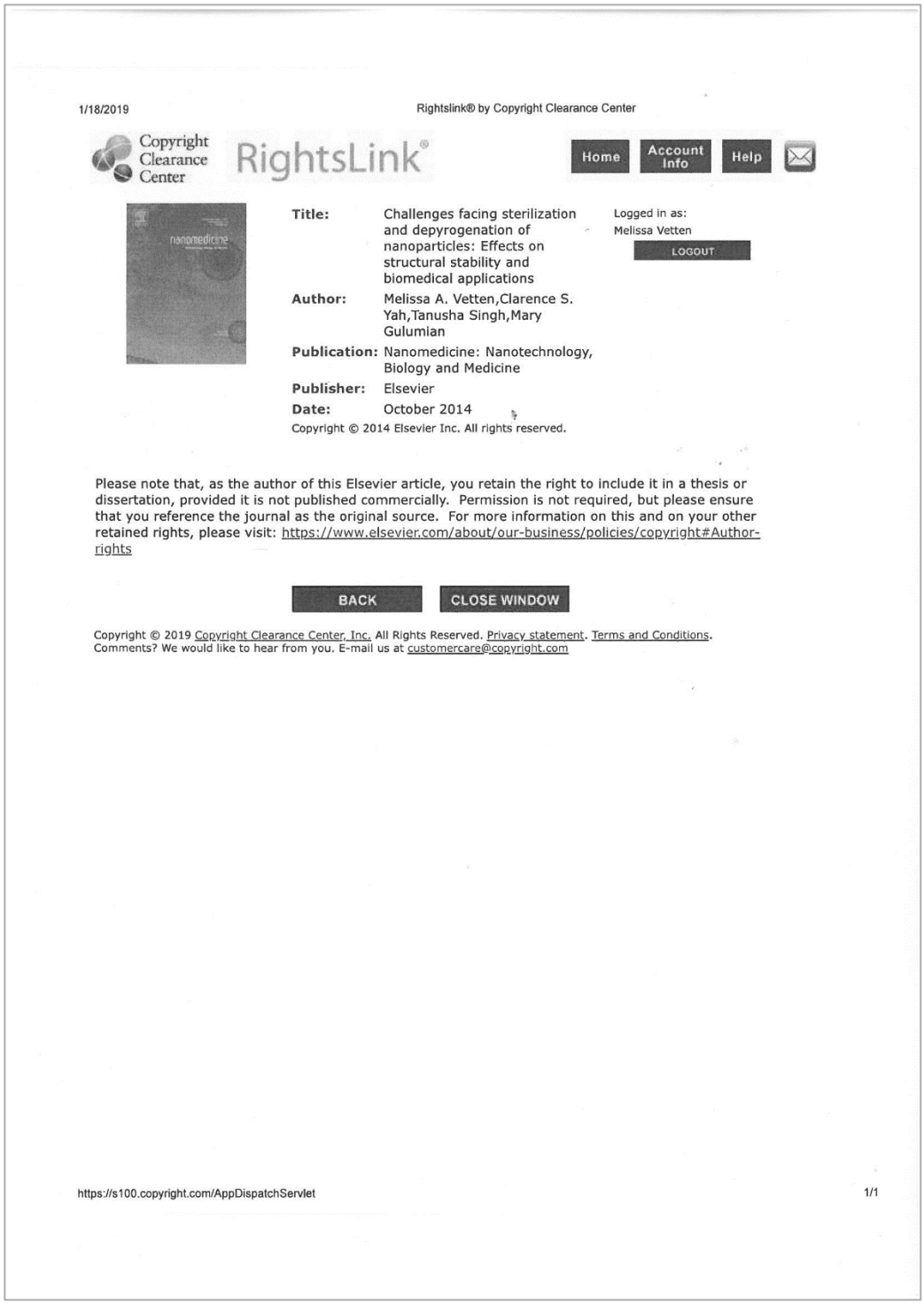

1/18/2019 Rightslink® by Copyright Clearance Center

Copyright Clearance Center RightsLink®

Home | Account Info | Help

Title:	Challenges facing sterilization and depyrogenation of nanoparticles: Effects on structural stability and biomedical applications
Author:	Melissa A. Vetten,Clarence S. Yah,Tanusha Singh,Mary Gulumian
Publication:	Nanomedicine: Nanotechnology, Biology and Medicine
Publisher:	Elsevier
Date:	October 2014

Logged in as: Melissa Vetten

LOGOUT

Copyright © 2014 Elsevier Inc. All rights reserved.

Please note that, as the author of this Elsevier article, you retain the right to include it in a thesis or dissertation, provided it is not published commercially. Permission is not required, but please ensure that you reference the journal as the original source. For more information on this and on your other retained rights, please visit: https://www.elsevier.com/about/our-business/policies/copyright#Author-rights

BACK CLOSE WINDOW

Copyright © 2019 Copyright Clearance Center, Inc. All Rights Reserved. Privacy statement. Terms and Conditions.
Comments? We would like to hear from you. E-mail us at customercare@copyright.com

https://s100.copyright.com/AppDispatchServlet 1/1

Appendix D: Copyright permission for *Toxicology and Applied Pharmacology* publication

Copyright Clearance Center RightsLink®

Home | Account Info | Help



Title: Differences in uptake of 14 nm PEG-liganded gold nanoparticles into BEAS-2B cells is dependent on their functional groups

Author: Melissa Vetten,Mary Gulumian

Publication: Toxicology and Applied Pharmacology

Publisher: Elsevier

Date: 15 January 2019

© 2018 Elsevier Inc. All rights reserved.

Logged in as:
Melissa Vetten
LOGOUT

Please note that, as the author of this Elsevier article, you retain the right to include it in a thesis or dissertation, provided it is not published commercially. Permission is not required, but please ensure that you reference the journal as the original source. For more information on this and on your other retained rights, please visit: https://www.elsevier.com/about/our-business/policies/copyright#Author-rights

BACK CLOSE WINDOW

Copyright © 2019 Copyright Clearance Center, Inc. All Rights Reserved. Privacy statement. Terms and Conditions.
Comments? We would like to hear from you. E-mail us at customercare@copyright.com

Appendix E: Copyright permission for *Current Nanoscience* publication

Bentham Science Publishers Ltd. LICENSE
TERMS AND CONDITIONS

Feb 18, 2019

This is a License Agreement between Ms. Melissa Vetten ("You") and Bentham Science Publishers Ltd. ("Bentham Science Publishers Ltd.") provided by Copyright Clearance Center ("CCC"). The license consists of your order details, the terms and conditions provided by Bentham Science Publishers Ltd., and the payment terms and conditions.

All payments must be made in full to CCC. For payment instructions, please see information listed at the bottom of this form.

License Number	4531890195514
License date	Feb 12, 2019
Licensed content publisher	Bentham Science Publishers Ltd.
Licensed content title	Current nanoscience
Licensed content date	Jan 1, 2005
Type of Use	Thesis/Dissertation
Requestor type	Author of requested content
Format	Print, Electronic
Portion	chapter/article
The requesting person/organization is:	Melissa Vetten
Title or numeric reference of the portion(s)	Interference of gold nanoparticles with in vitro endotoxin detection assays
Title of the article or chapter the portion is from	Interference of gold nanoparticles with in vitro endotoxin detection assays
Editor of portion(s)	N/A
Author of portion(s)	Yes
Volume of serial or monograph.	N/A
Page range of the portion	
Publication date of portion	Vol. 15
Rights for	Main product
Duration of use	Life of current and all future editions
Creation of copies for the disabled	no
With minor editing privileges	yes
For distribution to	Worldwide
In the following language(s)	Original language of publication
With incidental promotional use	no
The lifetime unit quantity of new product	Up to 499
Title	In vitro assessment of the toxicity of gold nanoparticles
Institution name	University of the Witwatersrand
Expected presentation date	Mar 2019
Billing Type	Invoice
Billing Address	Ms. Melissa Vetten NIOH 25 Hospital street Constitutional Hill Johannesburg, South Africa 2000 Attn: Ms. Melissa Vetten
Total (may include CCC user fee)	0.00 USD
Terms and Conditions	

TERMS AND CONDITIONS
The following terms are individual to this publisher:

None

Other Terms and Conditions:
STANDARD TERMS AND CONDITIONS

1. Description of Service; Defined Terms. This Republication License enables the User to obtain licenses for republication of one or more copyrighted works as described in detail on the relevant Order Confirmation (the "Work(s)"). Copyright Clearance Center, Inc. ("CCC") grants licenses through the Service on behalf of the rightsholder identified on the Order

Confirmation (the "Rightsholder"). "Republication", as used herein, generally means the inclusion of a Work, in whole or in part, in a new work or works, also as described on the Order Confirmation. "User", as used herein, means the person or entity making such republication.

2. The terms set forth in the relevant Order Confirmation, and any terms set by the Rightsholder with respect to a particular Work, govern the terms of use of Works in connection with the Service. By using the Service, the person transacting for a republication license on behalf of the User represents and warrants that he/she/it (a) has been duly authorized by the User to accept, and hereby does accept, all such terms and conditions on behalf of User, and (b) shall inform User of all such terms and conditions. In the event such person is a "freelancer" or other third party independent of User and CCC, such party shall be deemed jointly a "User" for purposes of these terms and conditions. In any event, User shall be deemed to have accepted and agreed to all such terms and conditions if User republishes the Work in any fashion.

3. Scope of License; Limitations and Obligations.

3.1 All Works and all rights therein, including copyright rights, remain the sole and exclusive property of the Rightsholder. The license created by the exchange of an Order Confirmation (and/or any invoice) and payment by User of the full amount set forth on that document includes only those rights expressly set forth in the Order Confirmation and in these terms and conditions, and conveys no other rights in the Work(s) to User. All rights not expressly granted are hereby reserved.

3.2 General Payment Terms: You may pay by credit card or through an account with us payable at the end of the month. If you and we agree that you may establish a standing account with CCC, then the following terms apply: Remit Payment to: Copyright Clearance Center, 29118 Network Place, Chicago, IL 60673-1291. Payments Due: Invoices are payable upon their delivery to you (or upon our notice to you that they are available to you for downloading). After 30 days, outstanding amounts will be subject to a service charge of 1-1/2% per month or, if less, the maximum rate allowed by applicable law. Unless otherwise specifically set forth in the Order Confirmation or in a separate written agreement signed by CCC, invoices are due and payable on "net 30" terms. While User may exercise the rights licensed immediately upon issuance of the Order Confirmation, the license is automatically revoked and is null and void, as if it had never been issued, if complete payment for the license is not received on a timely basis either from User directly or through a payment agent, such as a credit card company.

3.3 Unless otherwise provided in the Order Confirmation, any grant of rights to User (i) is "one-time" (including the editions and product family specified in the license), (ii) is non-exclusive and non-transferable and (iii) is subject to any and all limitations and restrictions (such as, but not limited to, limitations on duration of use or circulation) included in the Order Confirmation or invoice and/or in these terms and conditions. Upon completion of the licensed use, User shall either secure a new permission for further use of the Work(s) or immediately cease any new use of the Work(s) and shall render inaccessible (such as by deleting or by removing or severing links or other locators) any further copies of the Work (except for copies printed on paper in accordance with this license and still in User's stock at the end of such period).

3.4 In the event that the material for which a republication license is sought includes third party materials (such as photographs, illustrations, graphs, inserts and similar materials) which are identified in such material as having been used by permission, User is responsible for identifying, and seeking separate licenses (under this Service or otherwise) for, any of such third party materials; without a separate license, such third party materials may not be used.

3.5 Use of proper copyright notice for a Work is required as a condition of any license granted under the Service. Unless otherwise provided in the Order Confirmation, a proper copyright notice will read substantially as follows: "Republished with permission of [Rightsholder's name], from [Work's title, author, volume, edition number and year of copyright]; permission conveyed through Copyright Clearance Center, Inc. " Such notice must be provided in a reasonably legible font size and must be placed either immediately adjacent to the Work as used (for example, as part of a by-line or footnote but not as a separate electronic link) or in the place where substantially all other credits or notices for the new work containing the republished Work are located. Failure to include the required notice results in loss to the Rightsholder and CCC, and the User shall be liable to pay liquidated damages for each such failure equal to twice the use fee specified in the Order Confirmation, in addition to the use fee itself and any other fees and charges specified.

3.6 User may only make alterations to the Work if and as expressly set forth in the Order Confirmation. No Work may be used in any way that is defamatory, violates the rights of third parties (including such third parties' rights of copyright, privacy, publicity, or other tangible or intangible property), or is otherwise illegal, sexually explicit or obscene. In addition, User may not conjoin a Work with any other material that may result in damage to the reputation of the Rightsholder. User agrees to inform CCC if it becomes aware of any infringement of any rights in a Work and to cooperate with any reasonable request of CCC or the Rightsholder in connection therewith.

4. Indemnity. User hereby indemnifies and agrees to defend the Rightsholder and CCC, and their respective employees and directors, against all claims, liability, damages, costs and expenses, including legal fees and expenses, arising out of any use of a Work beyond the scope of the rights granted herein, or any use of a Work which has been altered in any unauthorized way by User, including claims of defamation or infringement of rights of copyright, publicity, privacy or other tangible or intangible property.

5. Limitation of Liability. UNDER NO CIRCUMSTANCES WILL CCC OR THE RIGHTSHOLDER BE LIABLE FOR ANY DIRECT, INDIRECT, CONSEQUENTIAL OR INCIDENTAL DAMAGES (INCLUDING WITHOUT LIMITATION DAMAGES FOR LOSS OF BUSINESS PROFITS OR INFORMATION, OR FOR BUSINESS INTERRUPTION) ARISING OUT OF THE USE OR INABILITY TO USE A WORK, EVEN IF ONE OF THEM HAS BEEN ADVISED OF THE POSSIBILITY OF SUCH DAMAGES. In any event, the total liability of the Rightsholder and CCC (including their respective employees and directors) shall not exceed the total amount actually paid by User for this license. User assumes full liability for the actions and omissions of its principals, employees, agents, affiliates, successors and assigns.

6. Limited Warranties. THE WORK(S) AND RIGHT(S) ARE PROVIDED "AS IS". CCC HAS THE RIGHT TO GRANT TO USER THE RIGHTS GRANTED IN THE ORDER CONFIRMATION DOCUMENT. CCC AND THE RIGHTSHOLDER DISCLAIM ALL OTHER WARRANTIES RELATING TO THE WORK(S) AND RIGHT(S), EITHER EXPRESS OR IMPLIED, INCLUDING WITHOUT LIMITATION IMPLIED WARRANTIES OF MERCHANTABILITY OR FITNESS FOR A PARTICULAR PURPOSE. ADDITIONAL RIGHTS MAY BE REQUIRED TO USE ILLUSTRATIONS, GRAPHS, PHOTOGRAPHS, ABSTRACTS, INSERTS OR OTHER PORTIONS OF THE WORK (AS OPPOSED TO THE ENTIRE WORK) IN A MANNER CONTEMPLATED BY USER; USER UNDERSTANDS AND AGREES THAT NEITHER CCC NOR THE RIGHTSHOLDER MAY HAVE SUCH ADDITIONAL RIGHTS TO GRANT.

7. Effect of Breach. Any failure by User to pay any amount when due, or any use by User of a Work beyond the scope of the license set forth in the Order Confirmation and/or these terms and conditions, shall be a material breach of the license created by the Order Confirmation and these terms and conditions. Any breach not cured within 30 days of written notice thereof shall result in immediate termination of such license without further notice. Any unauthorized (but licensable) use of a Work that is terminated immediately upon notice thereof may be liquidated by payment of the Rightsholder's ordinary license price therefor; any unauthorized (and unlicensable) use that is not terminated immediately for any reason (including, for example, because materials containing the Work cannot reasonably be recalled) will be subject to all remedies available at law or in equity, but in no event to a payment of less than three times the Rightsholder's ordinary license price for the most closely analogous licensable use plus Rightsholder's and/or CCC's costs and expenses incurred in collecting such payment.

8. **Miscellaneous.**

8.1 User acknowledges that CCC may, from time to time, make changes or additions to the Service or to these terms and conditions, and CCC reserves the right to send notice to the User by electronic mail or otherwise for the purposes of notifying User of such changes or additions; provided that any such changes or additions shall not apply to permissions already secured and paid for.

8.2 Use of User-related information collected through the Service is governed by CCC's privacy policy, available online here:
http://www.copyright.com/content/cc3/en/tools/footer/privacypolicy.html.

8.3 The licensing transaction described in the Order Confirmation is personal to User. Therefore, User may not assign or transfer to any other person (whether a natural person or an organization of any kind) the license created by the Order Confirmation and these terms and conditions or any rights granted hereunder; provided, however, that User may assign such license in its entirety on written notice to CCC in the event of a transfer of all or substantially all of User's rights in the new material which includes the Work(s) licensed under this Service.

8.4 No amendment or waiver of any terms is binding unless set forth in writing and signed by the parties. The Rightsholder and CCC hereby object to any terms contained in any writing prepared by the User or its principals, employees, agents or affiliates and purporting to govern or otherwise relate to the licensing transaction described in the Order Confirmation, which terms are in any way inconsistent with any terms set forth in the Order Confirmation and/or in these terms and conditions or CCC's standard operating procedures, whether such writing is prepared prior to, simultaneously with or subsequent to the Order Confirmation, and whether such writing appears on a copy of the Order Confirmation or in a separate instrument.

8.5 The licensing transaction described in the Order Confirmation document shall be governed by and construed under the law of the State of New York, USA, without regard to the principles thereof of conflicts of law. Any case, controversy, suit, action, or proceeding arising out of, in connection with, or related to such licensing transaction shall be brought, at CCC's sole discretion, in any federal or state court located in the County of New York, State

of New York, USA, or in any federal or state court whose geographical jurisdiction covers the location of the Rightsholder set forth in the Order Confirmation. The parties expressly submit to the personal jurisdiction and venue of each such federal or state court.If you have any comments or questions about the Service or Copyright Clearance Center, please contact us at 978-750-8400 or send an e-mail to info@copyright.com.
v 1.1

Questions? customercare@copyright.com or +1-855-239-3415 (toll free in the US) or +1-978-646-2777.

Appendix F: Permission to use the image shown in Figure 2.3

Melissa Vetten

From: Info Account <info@aceabio.com>
Sent: 22/05/2017 19:14
To: Melissa Vetten; Barbara Moore (Barbara@anatech.co.za)
Cc: Info Account
Subject: RE: ACEA Contact Form

Follow Up Flag: Follow up
Flag Status: Flagged

Categories: URGENT

Dear Melissa,

Thanks for informing us the usage of the xCELLigence instrument and technology. Yes, you have permission to use it, as long as you reference the source. Thanks.

ACEA Customer Support
info@aceabio.com

-----Original Message-----
From: ACEA Biosciences Inc [mailto:info@aceabio.com]
Sent: Sunday, May 21, 2017 11:03 PM
To: Info Account
Subject: ACEA Contact Form

From: [your-name] <melissa.vetten@nioh.nhls.ac.za>
Company: National Institute for Occupational Health
Phone:

Message Body:
Good morning

I am contacting you to seek permission to use the image on https://www.aceabio.com/products/rtca-sp/ that explains cellular impedance in my PhD thesis. I will reference your website.

Please confirm if this is acceptable.

Kind Regards,
Melissa Vetten

--
This e-mail was sent from a contact form on ACEA Biosciences Inc.

1

References

Abate, W., Sattar, A.A., Liu, J., *et al.* (2017) 'Evaluation of recombinant factor C assay for the detection of divergent lipopolysaccharide structural species and comparison with Limulus amebocyte lysate-based assays and a human monocyte activity assay', *Journal of medical microbiology*, 66(7), 888-897.

Acharya, S. and Hill, R.A. (2014) 'High efficacy gold-KDEL peptide-siRNA nanoconstruct-mediated transfection in C2C12 myoblasts and myotubes', *Nanomedicine: Nanotechnology, Biology and Medicine*, 10(2), 329-337, available: http://dx.doi.org/http://dx.doi.org/10.1016/j.nano.2013.07.015.

Aguilar, Z.P., Aguilar, Y., Xu, H., *et al.* (2010) 'Nanomaterials in medicine', *ECS Transactions*, 33(8), 69-74.

Ajayan, P.M. and Zhou, O.Z. (2001) 'Applications of carbon nanotubes' in *Carbon nanotubes* Springer, 391-425.

Albanese, A., Tang, P.S. and Chan, W.C. (2012) 'The effect of nanoparticle size, shape, and surface chemistry on biological systems', *Annu Rev Biomed Eng*, 14, 1-16, available: http://dx.doi.org/10.1146/annurev-bioeng-071811-150124.

Alkilany, A.M., Nagaria, P.K., Hexel, C.R., *et al.* (2009) 'Cellular Uptake and Cytotoxicity of Gold Nanorods: Molecular Origin of Cytotoxicity and Surface Effects', *Small*, 5(6), 701-708, available: http://dx.doi.org/10.1002/smll.200801546.

Alkilany, A.M. and Murphy, C.J. (2010) 'Toxicity and cellular uptake of gold nanoparticles: what we have learned so far?', *J Nanopart Res*, 12(7), 2313-2333, available: http://dx.doi.org/10.1007/s11051-010-9911-8.

Allouni, Z.E., Hol, P.J., Cauqui, M.A., *et al.* (2012) 'Role of physicochemical characteristics in the uptake of TiO2 nanoparticles by fibroblasts', *Toxicol In Vitro*, 26(3), 469-479, available: http://dx.doi.org/S0887-2333(12)00037-9 [pii] 10.1016/j.tiv.2012.01.019.

Almutary, A. and Sanderson, B.J.S. (2017) 'Up to Date *In-vitro* Artefacts in the Detection of Nanoparticles Toxicity: Short Review', *Journal of Ecology and Toxicology*, 1(1), 2.

Alwis, K.U. and Milton, D.K. (2006) 'Recombinant factor C assay for measuring endotoxin in house dust: Comparison with LAL, and (1 → 3)-β-D-glucans', *American Journal of Industrial Medicine*, 49(4), 296-300, available: http://dx.doi.org/10.1002/ajim.20264.

Ansari, S.A. and Husain, Q. (2011) 'Immobilization of Kluyveromyces lactis β galactosidase on concanavalin A layered aluminium oxide nanoparticles—its future aspects in biosensor applications', *Journal of Molecular Catalysis B: Enzymatic*, 70(3-4), 119-126.

Armentano, I., Dottori, M., Fortunati, E., *et al.* (2010) 'Biodegradable polymer matrix nanocomposites for tissue engineering: a review', *Polymer degradation and stability*, 95(11), 2126-2146.

Arnida, Malugin, A. and Ghandehari, H. (2010) 'Cellular uptake and toxicity of gold nanoparticles in prostate cancer cells: a comparative study of rods and spheres', *Journal of Applied Toxicology*, 30(3), 212-217, available: http://dx.doi.org/10.1002/jat.1486.

Arvizo, R.R., Saha, S., Wang, E., *et al.* (2013) 'Inhibition of tumor growth and metastasis by a self-therapeutic nanoparticle', *Proc Natl Acad Sci U S A*, 110(17), 6700-6705, available: http://dx.doi.org/1214547110 [pii] 10.1073/pnas.1214547110.

Atienza, J.M., Yu, N., Kirstein, S.L., *et al.* (2006) 'Dynamic and label-free cell-based assays using the real-time cell electronic sensing system', *Assay Drug Dev Technol*, 4(5), 597-607, available: http://dx.doi.org/10.1089/adt.2006.4.597.

Atienzar, F.A., Tilmant, K., Gerets, H.H., *et al.* (2011) 'The use of real-time cell analyzer technology in drug discovery: defining optimal cell culture conditions and assay reproducibility with different adherent cellular models', *J Biomol Screen*, 16(6), 575-587, available: http://dx.doi.org/1087057111402825 [pii] 10.1177/1087057111402825.

Atienzar, F.A., Gerets, H., Tilmant, K., *et al.* (2013) 'Evaluation of impedance-based label-free technology as a tool for pharmacology and toxicology investigations', *Biosensors (Basel)*, 3(1), 132-156, available: http://dx.doi.org/10.3390/bios3010132 biosensors-03-00132 [pii].

Bakand, S., Hayes, A. and Dechsakulthorn, F. (2012) 'Nanoparticles: a review of particle toxicology following inhalation exposure', *Inhal Toxicol*, 24(2), 125-135, available: http://dx.doi.org/10.3109/08958378.2010.642021.

Bareford, L.M. and Swaan, P.W. (2007) 'ENDOCYTIC MECHANISMS FOR TARGETED DRUG DELIVERY', *Advanced drug delivery reviews*, 59(8), 748-758, available: http://dx.doi.org/10.1016/j.addr.2007.06.008.

Baruah, S., Khan, M.N. and Dutta, J. (2016) 'Perspectives and applications of nanotechnology in water treatment', *Environmental Chemistry Letters*, 14(1), 1-14.

Baughman, R.H., Zakhidov, A.A. and De Heer, W.A. (2002) 'Carbon nanotubes--the route toward applications', *Science*, 297(5582), 787-792.

Baumann, W.H., Lehmann, M., Schwinde, A., *et al.* (1999) 'Microelectronic sensor system for microphysiological application on living cells', *Sensors and Actuators B: Chemical*, 55(1), 77-89.

Bazile, D., Prud'homme, C., Bassoullet, M.T., *et al.* (1995) 'Stealth Me. PEG-PLA nanoparticles avoid uptake by the mononuclear phagocytes system', *Journal of pharmaceutical sciences*, 84(4), 493-498.

Berridge, M.V., Herst, P.M. and Tan, A.S. (2005) 'Tetrazolium dyes as tools in cell biology: new insights into their cellular reduction', *Biotechnol Annu Rev*, 11, 127-152, available: http://dx.doi.org/10.1016/S1387-2656(05)11004-7.

Bhattacharya, K., Davoren, M., Boertz, J., *et al.* (2009) 'Titanium dioxide nanoparticles induce oxidative stress and DNA-adduct formation but not DNA-breakage in human lung cells', *Part Fibre Toxicol*, 6, 17.

Böttner, S., Jorgensen, M.R. and Schmidt, O.G. (2016) 'Rolled-up nanotechnology: 3D photonic materials by design', *Scripta Materialia*.

Boylan, N.J., Kim, A.J., Suk, J.S., *et al.* (2012) 'Enhancement of airway gene transfer by DNA nanoparticles using a pH-responsive block copolymer of polyethylene glycol and poly-L-lysine', *Biomaterials*, 33(7), 2361-2371, available: http://dx.doi.org/S0142-9612(11)01434-7 [pii] 10.1016/j.biomaterials.2011.11.080.

Boysen, E. (2018) *Nanocomposites, their Uses and Applications*, available: http://www.understandingnano.com/nanocomposites-applications.html [accessed 11 December 2018].

Bunderson-Schelvan, M., Hamilton, R.F., Trout, K.L., *et al.* (2016) 'Approaching a Unified Theory for Particle-Induced Inflammation' in *Biological Effects of Fibrous and Particulate Substances* Springer, 51-76.

Burch, J.B., Svendsen, E., Siegel, P.D., *et al.* (2009) 'Endotoxin exposure and inflammation markers among agricultural workers in Colorado and Nebraska', *Journal of Toxicology and Environmental Health, Part A*, 73(1), 5-22.

Burello, E. and Worth, A.P. (2011) 'A theoretical framework for predicting the oxidative stress potential of oxide nanoparticles', *Nanotoxicology*, 5(2), 228-235.

Burkhard Dick, H., Augustin, A., Pakula, T., *et al.* (2003) 'Endotoxins in ophthalmic viscosurgical devices', *European journal of ophthalmology*, 13(2), 176-184.

Carvalho, T.C., Peters, J.I. and Williams, R.O. (2011) 'Influence of particle size on regional lung deposition--what evidence is there?', *Int J Pharm*, 406(1-2), 1-10, available: http://dx.doi.org/10.1016/j.ijpharm.2010.12.040.

Castranova, V., Huffman, L.J., Judy, D.J., *et al.* (1998) 'Enhancement of nitric oxide production by pulmonary cells following silica exposure', *Environmental Health Perspectives*, 106(Suppl 5), 1165-1169.

Ceriotti, L., Ponti, J., Broggi, F., *et al.* (2007) 'Real-time assessment of cytotoxicity by impedance measurement on a 96-well plate', *Sensors and Actuators B: Chemical*, 123(21 May 2), 769-778.

Chanda, N., Shukla, R., Katti, K.V., *et al.* (2009) 'Gastrin Releasing Protein Receptor Specific Gold Nanorods: Breast and Prostate Tumor Avid Nanovectors for Molecular Imaging', *Nano Letters*, 9(5), 1798-1805, available: http://dx.doi.org/10.1021/nl8037147.

Chang, C.-I., Zhao, X.-L., Althouse, M.L.G., *et al.* (1998) 'Least Squares Subspace Projection Approach to Mixed Pixel Classification for Hyperspectral Images', *IEEE Transactions on Geoscience and Remote Sensing*, 36(3), 898-912.

Chen, Y.S., Hung, Y.C., Liau, I., *et al.* (2009) 'Assessment of the In Vivo Toxicity of Gold Nanoparticles', *Nanoscale Res Lett*, 4(8), 858-864, available: http://dx.doi.org/10.1007/s11671-009-9334-6.

Cheng, J.P.X. and Nichols, B.J. (2016) 'Caveolae: One Function or Many?', *Trends in Cell Biology*, 26(3), 177-189, available: http://dx.doi.org/http://dx.doi.org/10.1016/j.tcb.2015.10.010.

Chithrani, B.D., Ghazani, A.A. and Chan, W.C. (2006) 'Determining the size and shape dependence of gold nanoparticle uptake into mammalian cells', *Nano Lett*, 6(4), 662-668.

Chithrani, B.D. and Chan, W.C. (2007) 'Elucidating the mechanism of cellular uptake and removal of protein-coated gold nanoparticles of different sizes and shapes', *Nano Lett*, 7(6), 1542-1550, available: http://dx.doi.org/10.1021/nl070363y [doi].

Chithrani, B.D., Stewart, J., Allen, C., *et al.* (2009) 'Intracellular uptake, transport, and processing of nanostructures in cancer cells', *Nanomedicine: Nanotechnology, Biology and Medicine*, 5(2), 118-127, available: http://dx.doi.org/http://dx.doi.org/10.1016/j.nano.2009.01.008.

Choi, S.Y., Jeong, S., Jang, S.H., *et al.* (2012) 'In vitro toxicity of serum protein-adsorbed citrate-reduced gold nanoparticles in human lung adenocarcinoma cells', *Toxicol In Vitro*, 26(2), 229-237, available: http://dx.doi.org/S0887-2333(11)00316-X [pii] 10.1016/j.tiv.2011.11.016.

Chueh, P.J., Liang, R.Y., Lee, Y.H., *et al.* (2014) 'Differential cytotoxic effects of gold nanoparticles in different mammalian cell lines', *J Hazard Mater*, 264, 303-312, available: http://dx.doi.org/S0304-3894(13)00882-0 [pii] 10.1016/j.jhazmat.2013.11.031.

Conner, S.D. and Schmid, S.L. (2003) 'Regulated portals of entry into the cell', *Nature*, 422(6927), 37-44.

Connor, E.E., Mwamuka, J., Gole, A., *et al.* (2005) 'Gold nanoparticles are taken up by human cells but do not cause acute cytotoxicity', *Small*, 1(3), 325-327, available: http://dx.doi.org/10.1002/smll.200400093.

Coradeghini, R., Gioria, S., García, C.P., *et al.* (2013) 'Size-dependent toxicity and cell interaction mechanisms of gold nanoparticles on mouse fibroblasts', *Toxicology Letters*, 217(3), 205-216, available: http://dx.doi.org/https://doi.org/10.1016/j.toxlet.2012.11.022.

Cox, R.G., Mainou, B.A., Johnson, M., *et al.* (2015) 'Human Metapneumovirus Is Capable of Entering Cells by Fusion with Endosomal Membranes', *PLoS Pathogens*, 11(12), e1005303, available: http://dx.doi.org/10.1371/journal.ppat.1005303.

Cruje, C. and Chithrani, B. (2015) 'Integration of Peptides for Enhanced Uptake of PEGylayed Gold Nanoparticles', *Journal of Nanoscience and Nanotechnology*, 15(3), 2125-2131.

Daniel, M.C. and Astruc, D. (2004) 'Gold nanoparticles: assembly, supramolecular chemistry, quantum-size-related properties, and applications toward biology, catalysis, and nanotechnology', *Chem Rev*, 104(1), 293-346.

Dawson, E. (2005) *Interference with the LAL test and how to address it*, LAL Update, Vol 22, No.3, available: http://www.acciusa.com/pdfs/newsletter/LAL%20Update%20Vol%2022_No3%20rev%20001.pdf [accessed 29 January 2018].

Di Bucchianico, S., Fabbrizi, M.R., Cirillo, S., *et al.* (2014) 'Aneuploidogenic effects and DNA oxidation induced in vitro by differently sized gold nanoparticles', *International journal of nanomedicine*, 9, 2191.

Di Bucchianico, S., Migliore, L., Marsili, P., *et al.* (2015) 'Cyto-and genotoxicity assessment of Gold nanoparticles obtained by laser ablation in A549 lung adenocarcinoma cells', *Journal of Nanoparticle Research*, 17(5), 213.

Ding, J.L. and Ho, B. (2001) 'A new era in pyrogen testing', *Trends in Biotechnology*, 19(8), 277-281, available: http://dx.doi.org/http://dx.doi.org/10.1016/S0167-7799(01)01694-8.

Doak, S.H., Griffiths, S.M., Manshian, B., *et al.* (2009) 'Confounding experimental considerations in nanogenotoxicology', *Mutagenesis*, 24(4), 285-293, available: http://dx.doi.org/gep010 [pii] 10.1093/mutage/gep010.

Dobrovolskaia, M.A., Germolec, D.R. and Weaver, J.L. (2009) 'Evaluation of nanoparticle immunotoxicity', *Nat Nanotechnol*, 4(7), 411-414.

Dobrovolskaia, M.A., Neun, B.W., Clogston, J.D., *et al.* (2010) 'Ambiguities in applying traditional Limulus amebocyte lysate tests to quantify endotoxin in nanoparticle formulations', *Nanomedicine*, 5(4), 555-562.

Dobrovolskaia, M.A. and McNeil, S.E. (2013) 'Chapter 4: Endotoxin and Engineered Nanomaterials' in Dobrovolskaia, M. A. and McNeil, S. E., eds., *Handbook of Immunological Properties of Engineered Nanomaterials*. Singapore: World Scientific Publishing Co. Pte. Ltd

Donaldson, K., Aitken, R., Tran, L., *et al.* (2006) 'Carbon nanotubes: a review of their properties in relation to pulmonary toxicology and workplace safety', *Toxicological Sciences*, 92(1), 5-22.

Dönmez Güngüneş, Ç., Şeker, Ş., Elçin, A.E., *et al.* (2017) 'A comparative study on the in vitro cytotoxic responses of two mammalian cell types to fullerenes, carbon nanotubes and iron oxide nanoparticles', *Drug and Chemical Toxicology*, 40(2), 215-227, available: http://dx.doi.org/10.1080/01480545.2016.1199563.

dos Santos, T., Varela, J., Lynch, I., *et al.* (2011) 'Effects of transport inhibitors on the cellular uptake of carboxylated polystyrene nanoparticles in different cell lines', *PLoS One*, 6(9), e24438, available: http://dx.doi.org/10.1371/journal.pone.0024438 PONE-D-11-02628 [pii].

Downs, T.R., Crosby, M.E., Hu, T., *et al.* (2012) 'Silica nanoparticles administered at the maximum tolerated dose induce genotoxic effects through an inflammatory

reaction while gold nanoparticles do not', *Mutat Res*, 745(1-2), 38-50, available: http://dx.doi.org/S1383-5718(12)00117-9 [pii] 10.1016/j.mrgentox.2012.03.012.

Elias, D.R., Poloukhtine, A., Popik, V., *et al.* (2013) 'Effect of ligand density, receptor density, and nanoparticle size on cell targeting', *Nanomedicine: Nanotechnology, Biology and Medicine*, 9(2), 194-201.

Eom, H.J. and Choi, J. (2009) 'Oxidative stress of silica nanoparticles in human bronchial epithelial cell, Beas-2B', *Toxicol In Vitro*, 23(7), 1326-1332, available: http://dx.doi.org/S0887-2333(09)00185-4 [pii] 10.1016/j.tiv.2009.07.010.

EPA (2007) *Nanotechnology White Paper*, Washington, DC: U.S. Environmental Protection Agency, available: https://www.epa.gov/sites/production/files/2015-01/documents/nanotechnology_whitepaper.pdf [accessed 6 July 2018].

Fang, Y. (2006) 'Label-free cell-based assays with optical biosensors in drug discovery', *Assay Drug Dev Technol*, 4(5), 583-595, available: http://dx.doi.org/10.1089/adt.2006.4.583.

Farber, J.L. (1994) 'Mechanisms of cell injury by activated oxygen species', *Environ Health Perspect*, 102 Suppl 10, 17-24.

FDA (2012) *Guidance for Industry: Pyrogen and Endotoxin Testing - Questions and Answers*, available:

https://www.fda.gov/drugs/guidancecomplianceregulatoryinformation/guidances/ucm314718.htm#_Toc315937931 [accessed. 16 October 2018].

Fenech, M. (2000) 'The in vitro micronucleus technique', *Mutation Research/Fundamental and Molecular Mechanisms of Mutagenesis*, 455(1), 81-95.

Fenech, M., Chang, W.P., Kirsch-Volders, M., *et al.* (2003) 'HUMN project: detailed description of the scoring criteria for the cytokinesis-block micronucleus assay using isolated human lymphocyte cultures', *Mutat Res*, 534(1-2), 65-75.

Fernández-García, M. and Rodriguez, J.A. (2011) 'Metal oxide nanoparticles', *Encyclopedia of inorganic and bioinorganic chemistry*.

Fraga, S., Faria, H., Soares, M.E., *et al.* (2013) 'Influence of the surface coating on the cytotoxicity, genotoxicity and uptake of gold nanoparticles in human HepG2 cells', *J Appl Toxicol*, 33(10), 1111-1119, available: http://dx.doi.org/10.1002/jat.2865.

Fratoddi, I., Venditti, I., Battocchio, C., *et al.* (2011) 'Core shell hybrids based on noble metal nanoparticles and conjugated polymers: synthesis and characterization', *Nanoscale Research Letters*, 6(1), 98.

Freese, C., Gibson, M.I., Klok, H.-A., *et al.* (2012a) 'Size- and Coating-Dependent Uptake of Polymer-Coated Gold Nanoparticles in Primary Human Dermal Microvascular Endothelial Cells', *Biomacromolecules*, 13(5), 1533-1543, available: http://dx.doi.org/10.1021/bm300248u.

Freese, C., Uboldi, C., Gibson, M.I., *et al.* (2012b) 'Uptake and cytotoxicity of citrate-coated gold nanospheres: Comparative studies on human endothelial and epithelial cells', *Part Fibre Toxicol*, 9, 23, available: http://dx.doi.org/1743-8977-9-23 [pii] 10.1186/1743-8977-9-23.

Frens, G. (1973) 'Controlled nucleation for the regulation of the particle size in monodisperse gold suspensions', *Nature (London), Phys. Sci.*, 241, 20-22.

Fulda, S., Gorman, A.M., Hori, O., *et al.* (2010) 'Cellular stress responses: cell survival and cell death', *International Journal of Cell Biology*, 2010, 214074.

Gao, W., Xu, K., Ji, L., *et al.* (2011) 'Effect of gold nanoparticles on glutathione depletion-induced hydrogen peroxide generation and apoptosis in HL7702 cells', *Toxicology Letters*, 205(1), 86-95.

Georgakilas, V., Perman, J.A., Tucek, J., *et al.* (2015) 'Broad family of carbon nanoallotropes: classification, chemistry, and applications of fullerenes, carbon dots, nanotubes, graphene, nanodiamonds, and combined superstructures', *Chemical Reviews*, 115(11), 4744-4822.

George, J.M., Magogotya, M., Vetten, M.A., *et al.* (2017) 'An investigation of the genotoxicity and interference of gold nanoparticles in commonly used in vitro mutagenicity and genotoxicity Assays', *Toxicological Sciences*, 156(1), 149-166.

Ghosh, S.K. and Pal, T. (2007) 'Interparticle coupling effect on the surface plasmon resonance of gold nanoparticles: from theory to applications', *Chem Rev*, 107(11), 4797-4862, available: http://dx.doi.org/10.1021/cr0680282.

Gonciar, A. (2014) 'Detection of intracellular gold nanoparticles', *Biotechnol Mol Biol Nanomed*, 2(1), 21-25.

Goodman, C.M., McCusker, C.D., Yilmaz, T., *et al.* (2004) 'Toxicity of gold nanoparticles functionalized with cationic and anionic side chains', *Bioconjug Chem*, 15(4), 897-900.

Gratton, S.E., Ropp, P.A., Pohlhaus, P.D., *et al.* (2008) 'The effect of particle design on cellular internalization pathways', *Proc Natl Acad Sci U S A*, 105(33), 11613-11618, available: http://dx.doi.org/0801763105 [pii] 10.1073/pnas.0801763105.

Gu, Y.-J., Cheng, J., Lin, C.-C., *et al.* (2009) 'Nuclear penetration of surface functionalized gold nanoparticles', *Toxicology and applied pharmacology*, 237(2), 196-204.

Guo, S. and Wang, E. (2007) 'Synthesis and electrochemical applications of gold nanoparticles', *Analytica Chimica Acta*, 598(2), 181-192.

Gurr, J.R., Wang, A.S., Chen, C.H., *et al.* (2005) 'Ultrafine titanium dioxide particles in the absence of photoactivation can induce oxidative damage to human bronchial epithelial cells', *Toxicology*, 213(1-2), 66-73, available: http://dx.doi.org/S0300-483X(05)00227-1 [pii] 10.1016/j.tox.2005.05.007.

Haniu, H., Saito, N., Matsuda, Y., *et al.* (2013) 'Culture medium type affects endocytosis of multi-walled carbon nanotubes in BEAS-2B cells and subsequent biological response', *Toxicol In Vitro*, 27(6), 1679-1685, available: http://dx.doi.org/S0887-2333(13)00099-4 [pii] 10.1016/j.tiv.2013.04.012.

Hauck, T.S., Ghazani, A.A. and Chan, W.C. (2008) 'Assessing the effect of surface chemistry on gold nanorod uptake, toxicity, and gene expression in mammalian cells', *Small*, 4(1), 153-159.

Hillegass, J.M., Shukla, A., Lathrop, S.A., *et al.* (2010) 'Assessing nanotoxicity in cells in vitro', *Wiley Interdisciplinary Reviews: Nanomedicine and Nanobiotechnology*, 2(3), 219-231.

Huang, C.C., Aronstam, R.S., Chen, D.R., *et al.* (2010) 'Oxidative stress, calcium homeostasis, and altered gene expression in human lung epithelial cells exposed to ZnO nanoparticles', *Toxicol In Vitro*, 24(1), 45-55, available: http://dx.doi.org/S0887-2333(09)00263-X [pii] 10.1016/j.tiv.2009.09.007.

Huang, X. and El-Sayed, M.A. (2010) 'Gold nanoparticles: optical properties and implementations in cancer diagnosis and photothermal therapy', *Journal of Advanced Research*, 1(1), 13-28.

Hussain, S.M., Warheit, D.B., Ng, S.P., *et al.* (2015) 'At the crossroads of nanotoxicology in vitro: past achievements and current challenges', *Toxicological Sciences*, 147(1), 5-16.

Hussein, A.K. (2016) 'Applications of nanotechnology to improve the performance of solar collectors–Recent advances and overview', *Renewable and Sustainable Energy Reviews*, 62, 767-792.

Hutter, E., Boridy, S., Labrecque, S., *et al.* (2010) 'Microglial response to gold nanoparticles', *ACS Nano*, 4(5), 2595-2606, available: http://dx.doi.org/10.1021/nn901869f.

Ionita, P., Spafiu, F. and Ghica, C. (2008) 'Dual behavior of gold nanoparticles, as generators and scavengers for free radicals', *Journal of materials science*, 43(19), 6571-6574.

ISO (2015) *ISO/TS 80004-2 Nanotechnologies - Vocabulary - Part 2: Nano-objects*, Switzerland: ISO.

Iwanaga, S. (2007) 'Biochemical principle of Limulus test for detecting bacterial endotoxins', *Proceedings of the Japan Academy. Series B, Physical and Biological Sciences*, 83(4), 110-119.

Jackson, A.M., Myerson, J.W. and Stellacci, F. (2004) 'Spontaneous assembly of subnanometre-ordered domains in the ligand shell of monolayer-protected nanoparticles', *Nature Materials*, 3(5), 330-336.

Jain, P.K., Lee, K.S., El-Sayed, I.H., *et al.* (2006) 'Calculated absorption and scattering properties of gold nanoparticles of different size, shape, and composition: applications in biological imaging and biomedicine', *J Phys Chem B*, 110(14), 7238-7248, available: http://dx.doi.org/10.1021/jp057170o.

JRC (2016) 'JRC Nanomaterials Repository: List of Representative Nanomaterials'.

Ke, N., Wang, X., Xu, X., *et al.* (2011) 'The xCELLigence system for real-time and label-free monitoring of cell viability', *Methods Mol Biol*, 740, 33-43, available: http://dx.doi.org/10.1007/978-1-61779-108-6_6.

Kędzierska, A., Kochan, P., Pietrzyk, A., *et al.* (2007) 'Current status of fungal cell wall components in the immunodiagnostics of invasive fungal infections in humans: galactomannan, mannan and (1→ 3)-β-D-glucan antigens', *European Journal of Clinical Microbiology & Infectious Diseases*, 26(11), 755-766.

Kehrer, J.P. (2000) 'The Haber–Weiss reaction and mechanisms of toxicity', *Toxicology*, 149(1), 43-50.

Khalili Fard, J., Jafari, S. and Eghbal, M.A. (2015) 'A Review of Molecular Mechanisms Involved in Toxicity of Nanoparticles', *Adv Pharm Bull*, 5(4), 447-454, available: http://dx.doi.org/10.15171/apb.2015.061.

Khan, J.A., Pillai, B., Das, T.K., *et al.* (2007) 'Molecular effects of uptake of gold nanoparticles in HeLa cells', *Chembiochem*, 8(11), 1237-1240.

Kim, A.J., Boylan, N.J., Suk, J.S., *et al.* (2012) 'Non-degradative intracellular trafficking of highly compacted polymeric DNA nanoparticles', *J Control Release*, 158(1), 102-107, available: http://dx.doi.org/S0168-3659(11)01003-0 [pii] 10.1016/j.jconrel.2011.10.031.

Kim, J.H., Kim, J.H., Kim, K.W., *et al.* (2009) 'Intravenously administered gold nanoparticles pass through the blood-retinal barrier depending on the particle size, and induce no retinal toxicity', *Nanotechnology*, 20(50), 505101.

Knaapen, A.M., Borm, P.J., Albrecht, C., *et al.* (2004) 'Inhaled particles and lung cancer. Part A: Mechanisms', *International Journal of Cancer*, 109(6), 799-809.

Kodiha, M., Wang, Y.M., Hutter, E., *et al.* (2015) 'Off to the Organelles - Killing Cancer Cells with Targeted Gold Nanoparticles', *Theranostics*, 5(4), 357-370, available: http://dx.doi.org/10.7150/thno.10657.

Kou, L., Sun, J., Zhai, Y., *et al.* (2013) 'The endocytosis and intracellular fate of nanomedicines: Implication for rational design', *Asian Journal of Pharmaceutical Sciences*, 8(1), 1-10, available: http://dx.doi.org/http://dx.doi.org/10.1016/j.ajps.2013.07.001.

Kroll, A., Pillukat, M.H., Hahn, D., *et al.* (2009) 'Current in vitro methods in nanoparticle risk assessment: limitations and challenges', *Eur J Pharm Biopharm*, 72(2), 370-377.

Kroll, A., Pillukat, M.H., Hahn, D., *et al.* (2012) 'Interference of engineered nanoparticles with in vitro toxicity assays', *Archives of Toxicology*, 86(7), 1123-1136, available: http://dx.doi.org/10.1007/s00204-012-0837-z.

Kucki, M., Cavelius, C. and Kraegeloh, A. (2014) 'Interference of silica nanoparticles with the traditional Limulus amebocyte lysate gel clot assay', *Innate immunity*, 20(3), 327-336.

Kustermann, S., Boess, F., Buness, A., *et al.* (2013) 'A label-free, impedance-based real time assay to identify drug-induced toxicities and differentiate cytostatic from cytotoxic effects', *Toxicology In Vitro*, 27(5), 1589-1595.

Le Roy, C. and Wrana, J.L. (2005) 'Clathrin- and non-clathrin-mediated endocytic regulation of cell signalling', *Nat Rev Mol Cell Biol*, 6(2), 112-126, available: http://dx.doi.org/nrm1571 [pii] 10.1038/nrm1571 [doi].

Lee, R. and Stokes, E. (2009) 'Twenty-first Century Novel: Regulating Nanotechnologies', *Journal of Environmental Law*, 21(3), 469-482.

Leite, P.E., Pereira, M.R., Santos, C.A., *et al.* (2015) 'Gold nanoparticles do not induce myotube cytotoxicity but increase the susceptibility to cell death', *Toxicol In Vitro*, 29(5), 819-827, available: http://dx.doi.org/S0887-2333(15)00027-2 [pii] 10.1016/j.tiv.2015.02.010.

Li, N., Sioutas, C., Cho, A., *et al.* (2003) 'Ultrafine particulate pollutants induce oxidative stress and mitochondrial damage', *Environ Health Perspect*, 111(4), 455-460.

Li, L., Abe, Y., Kanagawa, K., *et al.* (2004) 'Distinguishing the 5,5-dimethyl-1-pyrroline N-oxide (DMPO)-OH radical quenching effect from the hydroxyl

radical scavenging effect in the ESR spin-trapping method', *Analytica Chimica Acta*, 512(1), 121-124, available: http://dx.doi.org/https://doi.org/10.1016/j.aca.2004.02.020.

Li, J.J., Zou, L., Hartono, D., *et al.* (2008) 'Gold Nanoparticles Induce Oxidative Damage in Lung Fibroblasts In Vitro', *Advanced Materials*, 20, 138-142.

Li, J.J., Hartono, D., Ong, C.-N., *et al.* (2010) 'Autophagy and oxidative stress associated with gold nanoparticles', *Biomaterials*, 31(23), 5996-6003, available: http://dx.doi.org/http://dx.doi.org/10.1016/j.biomaterials.2010.04.014.

Li, C., Li, D., Wan, G., *et al.* (2011) 'Facile synthesis of concentrated gold nanoparticles with low size-distribution in water: temperature and pH controls', *Nanoscale Res Lett*, 6(1), 440, available: http://dx.doi.org/1556-276X-6-440 [pii] 10.1186/1556-276X-6-440.

Li, Y., Kröger, M. and Liu, W.K. (2014) 'Endocytosis of PEGylated nanoparticles accompanied by structural and free energy changes of the grafted polyethylene glycol', *Biomaterials*, 35(30), 8467-8478, available: http://dx.doi.org/http://dx.doi.org/10.1016/j.biomaterials.2014.06.032.

Li, Y., Italiani, P., Casals, E., *et al.* (2015) 'Optimising the use of commercial LAL assays for the analysis of endotoxin contamination in metal colloids and metal oxide nanoparticles', *Nanotoxicology*, 9(4), 462-473.

Li, Y. and Boraschi, D. (2016) 'Endotoxin contamination: a key element in the interpretation of nanosafety studies', *Nanomedicine*, 11(3), 269-287.

Li, X., Hu, Z., Ma, J., *et al.* (2018) 'The systematic evaluation of size-dependent toxicity and multi-time biodistribution of gold nanoparticles', *Colloids and Surfaces B: Biointerfaces*, 167, 260-266.

Lim, D.H., Jang, J., Kim, S., *et al.* (2012) 'The effects of sub-lethal concentrations of silver nanoparticles on inflammatory and stress genes in human macrophages using cDNA microarray analysis', *Biomaterials*, 33(18), 4690-4699, available: http://dx.doi.org/S0142-9612(12)00278-5 [pii] 10.1016/j.biomaterials.2012.03.006.

Limame, R., Wouters, A., Pauwels, B., *et al.* (2012) 'Comparative analysis of dynamic cell viability, migration and invasion assessments by novel real-time technology and classic endpoint assays', *PLoS One*, 7(10), e46536, available: http://dx.doi.org/10.1371/journal.pone.0046536 PONE-D-12-11765 [pii].

Link, S. and El-Sayed, M.A. (1999) 'Size and Temperature Dependence of the Plasmon Absorption of Colloidal Gold Nanoparticles', *The Journal of Physical Chemistry B*, 103(21), 4212-4217, available: http://dx.doi.org/10.1021/jp984796o.

Liu, Y., Shipton, M.K., Ryan, J., *et al.* (2007) 'Synthesis, stability, and cellular internalization of gold nanoparticles containing mixed peptide-poly(ethylene

glycol) monolayers', *Anal Chem*, 79(6), 2221-2229, available: http://dx.doi.org/10.1021/ac061578f [doi].

Liu, Z., Li, W., Wang, F., *et al.* (2012) 'Enhancement of lipopolysaccharide-induced nitric oxide and interleukin-6 production by PEGylated gold nanoparticles in RAW264.7 cells', *Nanoscale*, 4(22), 7135-7142, available: http://dx.doi.org/10.1039/c2nr31355c.

Lund, T., Callaghan, M.F., Williams, P., *et al.* (2011) 'The influence of ligand organization on the rate of uptake of gold nanoparticles by colorectal cancer cells', *Biomaterials*, 32(36), 9776-9784.

Madl, A.K., Plummer, L.E., Carosino, C., *et al.* (2014) 'Nanoparticles, lung injury, and the role of oxidant stress', *Annual review of physiology*, 76, 447.

Magalhaes, P.O., Lopes, A.M., Mazzola, P.G., *et al.* (2007) 'Methods of endotoxin removal from biological preparations: a review', *J Pharm Pharm Sci*, 10(3), 388-404.

Manke, A., Wang, L. and Rojanasakul, Y. (2013) 'Mechanisms of nanoparticle-induced oxidative stress and toxicity', *BioMed Research International*, 2013, 942916, available: http://dx.doi.org/10.1155/2013/942916.

Mariani, V., Ponti, J., Giudetti, G., *et al.* (2012) 'Online monitoring of cell metabolism to assess the toxicity of nanoparticles: the case of cobalt ferrite', *Nanotoxicology*, 6(3), 272-287, available: http://dx.doi.org/10.3109/17435390.2011.572302.

Marquis, B.J., Love, S.A., Braun, K.L., *et al.* (2009) 'Analytical methods to assess nanoparticle toxicity', *Analyst*, 134(3), 425-439.

Maruyama, K., Haniu, H., Saito, N., *et al.* (2015) 'Endocytosis of Multiwalled Carbon Nanotubes in Bronchial Epithelial and Mesothelial Cells', *BioMed Research International*, 2015, 793186, available: http://dx.doi.org/10.1155/2015/793186.

Mateo, D., Morales, P., Ávalos, A., *et al.* (2014) 'Oxidative stress contributes to gold nanoparticle-induced cytotoxicity in human tumor cells', *Toxicology Mechanisms & Methods*, 24(3), 161-172, available: http://dx.doi.org/10.3109/15376516.2013.869783.

Matsui, E.C., Hansel, N.N., Aloe, C., *et al.* (2013) 'Indoor pollutant exposures modify the effect of airborne endotoxin on asthma in urban children', *American journal of respiratory and critical care medicine*, 188(10), 1210-1215.

Mccullough, K.Z. and Weidner-Loeven, C. (1992) 'Variability in the LAL test: comparison of three kinetic methods for the testing of pharmaceutical products', *J. Parent. Sci. Technol*, 46(3), 69-72.

McMahon, H.T. and Boucrot, E. (2011) 'Molecular mechanism and physiological functions of clathrin-mediated endocytosis', *Nat Rev Mol Cell Biol*, 12(8), 517-533, available: http://dx.doi.org/http://www.nature.com/nrm/journal/v12/n8/suppinfo/nrm3151_S1.html.

Mdluli, P.S., Sosibo, N.M., Mashazi, P.N., *et al.* (2011) 'Selective adsorption of PVP on the surface of silver nanoparticles: a molecular dynamics study', *Journal of Molecular Structure*, 1004(1), 131-137.

Mercer, R.R., Hubbs, A.F., Scabilloni, J.F., *et al.* (2011) 'Pulmonary fibrotic response to aspiration of multi-walled carbon nanotubes', *Part Fibre Toxicol*, 8, 21, available: http://dx.doi.org/1743-8977-8-21 [pii] 10.1186/1743-8977-8-21.

Meyer, J.N., Lord, C.A., Yang, X.Y., *et al.* (2010) 'Intracellular uptake and associated toxicity of silver nanoparticles in *Caenorhabditis elegans*', *Aquat Toxicol*, 100(2), 140-150, available: http://dx.doi.org/S0166-445X(10)00264-X [pii] 10.1016/j.aquatox.2010.07.016.

Milne, G.L., Yin, H., Hardy, K.D., *et al.* (2011) 'Isoprostane generation and function', *Chemical Reviews*, 111(10), 5973-5996, available: http://dx.doi.org/10.1021/cr200160h.

Mintzer, M.A. and Grinstaff, M.W. (2011) 'Biomedical applications of dendrimers: a tutorial', *Chemical Society Reviews*, 40(1), 173-190.

Mironava, T., Hadjiargyrou, M., Simon, M., *et al.* (2010) 'Gold nanoparticles cellular toxicity and recovery: effect of size, concentration and exposure time', *Nanotoxicology*, 4(1), 120-137, available: http://dx.doi.org/10.3109/17435390903471463.

Mitchell, G.R. and Tojeira, A. (2016) *Controlling the Morphology of Polymers: Multiple Scales of Structure and Processing*, Springer.

Morita, T., Tanaka, S., Nakamura, T., *et al.* (1981) 'A new (1→ 3)-β-D-glucan-mediated coagulation pathway found in limulus amebocytes', *FEBS letters*, 129(2), 318-321.

Mortimer, M., Gogos, A., Bartolome, N., *et al.* (2014) 'Potential of hyperspectral imaging microscopy for semi-quantitative analysis of nanoparticle uptake by protozoa', *Environ Sci Technol*, 48(15), 8760-8767, available: http://dx.doi.org/10.1021/es500898j.

Munn, A.L. (2001) 'Molecular requirements for the internalisation step of endocytosis: insights from yeast', *Biochimica et Biophysica Acta (BBA) - Molecular Basis of Disease*, 1535(3), 236-257, available: http://dx.doi.org/http://dx.doi.org/10.1016/S0925-4439(01)00028-X.

Murphy, C.J., Gole, A.M., Stone, J.W., *et al.* (2008) 'Gold nanoparticles in biology: beyond toxicity to cellular imaging', *Acc Chem Res*, 41(12), 1721-1730.

Murugan, K., Choonara, Y.E., Kumar, P., *et al.* (2015) 'Parameters and characteristics governing cellular internalization and trans-barrier trafficking of nanostructures', *International journal of nanomedicine*, 10, 2191.

Nativo, P., Prior, I.A. and Brust, M. (2008) 'Uptake and intracellular fate of surface-modified gold nanoparticles', *ACS Nano*, 2(8), 1639-1644, available: http://dx.doi.org/10.1021/nn800330a 10.1021/nn800330a [pii].

Nazari, A., Riahi, S., Riahi, S., *et al.* (2010) 'Influence of Al2O3 nanoparticles on the compressive strength and workability of blended concrete', *Journal of American Science*, 6(5), 6-9.

Nel, A., Xia, T., Madler, L., *et al.* (2006) 'Toxic potential of materials at the nanolevel', *Science*, 311(5761), 622-627.

Neun, B.W. and Dobrovolskaia, M.A. (2011) 'Detection and quantitative evaluation of endotoxin contamination in nanoparticle formulations by LAL-based assays' in *Characterization of nanoparticles intended for drug delivery* Springer, 121-130.

Ng, C.T., Tang, F.M.A., Li, J.J.e., *et al.* (2015) 'Clathrin-Mediated Endocytosis of Gold Nanoparticles In Vitro', *The Anatomical Record*, 298(2), 418-427, available: http://dx.doi.org/10.1002/ar.23051.

Ng, C.T., Yip, G.W.C., Chen, E.S., *et al.* (2018) 'Gold nanoparticles induce serum amyloid A 1–Toll-like receptor 2 mediated NF-kB signaling in lung cells in vitro', *Chemico-biological interactions*, 289, 81-89.

Noh, S.M., Kim, W.-K., Kim, S.J., *et al.* (2007) 'Enhanced cellular delivery and transfection efficiency of plasmid DNA using positively charged biocompatible colloidal gold nanoparticles', *Biochimica et Biophysica Acta (BBA) - General Subjects*, 1770(5), 747-752, available: http://dx.doi.org/http://dx.doi.org/10.1016/j.bbagen.2007.01.012.

OECD (2011) *Nanosafety at the OECD: The First Five Years 2006-2010*. France: OECD

OECD (2015) *No. 44, Dossier on Gold Nanoparticles*, France: OECD.

OECD (2016a) *Physical-Chemical Properties of Nanomaterials: Evaluation of Methods Applied in the OECD-WPMN Testing Programme*, France: OECD.

OECD (2016b) 'Test No. 487: *In Vitro* Mammalian Cell Micronucleus Test' in *OECD Guidelines for Testing of Chemicals, Section 4: Health Effects*, France: OECD.

OECD (2018a) *OECD Database on Research into the Safety of Manufactured Nanomaterials*, available: http://www.oecd.org/env/ehs/nanosafety/oecddatabaseonresearchintothesafetyofmanufacturednanomaterials.htm [accessed 12 December 2018].

OECD (2018b) *Testing Programme of Manufactured Nanomaterials - Overview*, available: http://www.oecd.org/chemicalsafety/nanosafety/overview-testing-programme-manufactured-nanomaterials.htm [accessed 15 January 2019].

OECD (2018c) *No. 85, Evaluation of in vitro methods for human hazard assessment applied in the OECD Testing Programme for the Safety of Manufactured Nanomaterials*, France: OECD.

Ong, K.J., MacCormack, T.J., Clark, R.J., *et al.* (2014) 'Widespread nanoparticle-assay interference: implications for nanotoxicity testing', *PLoS One*, 9(3), e90650.

Oostingh, G.J., Casals, E., Italiani, P., *et al.* (2011) 'Problems and challenges in the development and validation of human cell-based assays to determine nanoparticle-induced immunomodulatory effects', *Part Fibre Toxicol*, 8(1), 8, available: http://dx.doi.org/1743-8977-8-8 [pii] 10.1186/1743-8977-8-8.

Ortega, R., Bresson, C., Darolles, C., *et al.* (2014) 'Low-solubility particles and a Trojan-horse type mechanism of toxicity: the case of cobalt oxide on human lung cells', *Part Fibre Toxicol*, 11, 14, available: http://dx.doi.org/1743-8977-11-14 [pii] 10.1186/1743-8977-11-14.

Otero-Gonzalez, L., Sierra-Alvarez, R., Boitano, S., *et al.* (2012) 'Application and validation of an impedance-based real time cell analyzer to measure the toxicity of nanoparticles impacting human bronchial epithelial cells', *Environ Sci Technol*, 46(18), 10271-10278, available: http://dx.doi.org/10.1021/es301599f.

Ownby, D.R., Peterson, E.L., Williams, L.K., *et al.* (2010) 'Variation of dust endotoxin concentrations by location and time within homes of young children', *Pediatric Allergy and Immunology*, 21(3), 533-540.

Paino, I.M., Marangoni, V.S., de Oliveira Rde, C., *et al.* (2012) 'Cyto and genotoxicity of gold nanoparticles in human hepatocellular carcinoma and peripheral blood mononuclear cells', *Toxicol Lett*, 215(2), 119-125, available: http://dx.doi.org/S0378-4274(12)01330-6 [pii] 10.1016/j.toxlet.2012.09.025.

Pan, Y., Neuss, S., Leifert, A., *et al.* (2007) 'Size-dependent cytotoxicity of gold nanoparticles', *Small*, 3(11), 1941-1949.

Panariti, A., Miserocchi, G. and Rivolta, I. (2012) 'The effect of nanoparticle uptake on cellular behavior: disrupting or enabling functions?', *Nanotechnol Sci Appl*, 5, 87-100, available: http://dx.doi.org/10.2147/NSA.S25515 nsa-5-087 [pii].

Parab, H.J., Chen, H.M., Lai, T.-C., *et al.* (2009) 'Biosensing, Cytotoxicity, and Cellular Uptake Studies of Surface-Modified Gold Nanorods', *The Journal of Physical Chemistry C*, 113(18), 7574-7578, available: http://dx.doi.org/10.1021/jp9000169.

Park, E.-J. and Park, K. (2009) 'Increased Gene Expression in Cultured BEAS-2B Cells Treated with Metal Oxide Nanoparticles', *Toxicological Research*, 25(4), 195-201.

Patra, H.K., Banerjee, S., Chaudhuri, U., *et al.* (2007) 'Cell selective response to gold nanoparticles', *Nanomedicine*, 3(2), 111-119, available: http://dx.doi.org/S1549-9634(07)00053-6 [pii] 10.1016/j.nano.2007.03.005.

Pelkmans, L. (2005) 'Secrets of caveolae- and lipid raft-mediated endocytosis revealed by mammalian viruses', *Biochim Biophys Acta*, 1746(3), 295-304, available: http://dx.doi.org/S0167-4889(05)00143-6 [pii] 10.1016/j.bbamcr.2005.06.009.

Pereira, M., Oliveira, L. and Murad, E. (2012) 'Iron oxide catalysts: Fenton and Fentonlike reactions–a review', *Clay Minerals*, 47(3), 285-302.

Pernodet, N., Fang, X., Sun, Y., *et al.* (2006) 'Adverse effects of citrate/gold nanoparticles on human dermal fibroblasts', *Small*, 2(6), 766-773, available: http://dx.doi.org/10.1002/smll.200500492.

Pisani, C., Gaillard, J.-C., Nouvel, V., *et al.* (2015) 'High-throughput, quantitative assessment of the effects of low-dose silica nanoparticles on lung cells: grasping complex toxicity with a great depth of field', *BMC Genomics*, 16(1), 315, available: http://dx.doi.org/10.1186/s12864-015-1521-5.

Ponti, J., Colognato, R., Franchini, F., *et al.* (2009) 'A quantitative in vitro approach to study the intracellular fate of gold nanoparticles: from synthesis to cytotoxicity', *Nanotoxicology*, 3(4), 296-306.

Ponti, J., Kinsner-Ovaskainen, A., Norlen, H., *et al.* (2014) *Interlaboratory comparison study of the Colony Forming Efficiency assay for assessing cytotoxicity of nanomaterials*: Institute for Health and Consumer Protection, Joint Research Centre. Luxembourg: Publications Office of the European Union. available: http://publications.jrc.ec.europa.eu/repository/handle/JRC92910 [accessed. 15 January 2018]

Poole, J.A., Dooley, G.P., Saito, R., *et al.* (2010) 'Muramic acid, endotoxin, 3-hydroxy fatty acids, and ergosterol content explain monocyte and epithelial cell inflammatory responses to agricultural dusts', *Journal of Toxicology and Environmental Health, Part A*, 73(10), 684-700.

Prousek, J. (2007) 'Fenton chemistry in biology and medicine', *Pure and applied chemistry*, 79(12), 2325-2338.

Pushparaj, V.L., Shaijumon, M.M., Kumar, A., *et al.* (2007) 'Flexible energy storage devices based on nanocomposite paper', *Proceedings of the National Academy of Sciences*, 104(34), 13574-13577.

Quereda, J.J., Martinez-Alarcon, L., Mendoca, L., *et al.* (2010) 'Validation of xCELLigence real-time cell analyzer to assess compatibility in xenotransplantation with pig-to-baboon model', *Transplant Proc*, 42(8), 3239-3243, available: http://dx.doi.org/S0041-1345(10)00717-7 [pii] 10.1016/j.transproceed.2010.05.059.

Ray, P.D., Huang, B.-W. and Tsuji, Y. (2012) 'Reactive oxygen species (ROS) homeostasis and redox regulation in cellular signaling', *Cellular signalling*, 24(5), 981-990.

Rayavarapu, R.G., Petersen, W., Hartsuiker, L., *et al.* (2010) 'In vitro toxicity studies of polymer-coated gold nanorods', *Nanotechnology*, 21(14), 145101.

Roveda Júnior, A.C. and Franco, D.W. (2013) 'Nitric oxide releasing-dendrimers: an overview', *Brazilian Journal of Pharmaceutical Sciences*, 49, 1-14.

Ryan, J. (2004) 'Endotoxins and cell culture', *Corning Life Sciences Technical Bulletin*, 1-8.

Sabella, S., Carney, R.P., Brunetti, V., *et al.* (2014) 'A general mechanism for intracellular toxicity of metal-containing nanoparticles', *Nanoscale*, 6(12), 7052-7061, available: http://dx.doi.org/10.1039/c4nr01234h.

Saito, R., Cranmer, B.K., Tessari, J.D., *et al.* (2009) 'Recombinant factor C (rFC) assay and gas chromatography/mass spectrometry (GC/MS) analysis of endotoxin variability in four agricultural dusts', *Annals of occupational hygiene*, 53(7), 713-722.

Sambale, F., Wagner, S., Stahl, F., *et al.* (2015) 'Investigations of the toxic effect of silver nanoparticles on mammalian cell lines', *Journal of Nanomaterials*, 16(1), 6.

Savolainen, K., Alenius, H., Norppa, H., *et al.* (2010) 'Risk assessment of engineered nanomaterials and nanotechnologies--a review', *Toxicology*, 269(2-3), 92-104.

Schins, R.P. (2002) 'Mechanisms of genotoxicity of particles and fibers', *Inhalation toxicology*, 14(1), 57-78.

Schlinkert, P., Casals, E., Boyles, M., *et al.* (2015) 'The oxidative potential of differently charged silver and gold nanoparticles on three human lung epithelial cell types', *J Nanobiotechnology*, 13(1), 1, available: http://dx.doi.org/10.1186/s12951-014-0062-4 s12951-014-0062-4 [pii].

Scott, R.W., Wilson, O.M. and Crooks, R.M. (2005) 'Synthesis, characterization, and applications of dendrimer-encapsulated nanoparticles'. *The Journal of Physical Chemistry B*, 109(2), 692-704.

Seiffert, J.M., Baradez, M.O., Nischwitz, V., *et al.* (2012) 'Dynamic monitoring of metal oxide nanoparticle toxicity by label free impedance sensing', *Chem Res Toxicol*, 25(1), 140-152, available: http://dx.doi.org/10.1021/tx200355m.

Shang, L., Nienhaus, K. and Nienhaus, G.U. (2014) 'Engineered nanoparticles interacting with cells: size matters', *J Nanobiotechnology*, 12, 5, available: http://dx.doi.org/1477-3155-12-5 [pii] 10.1186/1477-3155-12-5.

Shin, S., Song, I. and Um, S. (2015) 'Role of physicochemical properties in nanoparticle toxicity', *Nanomaterials*, 5(3), 1351-1365.

Shukla, R., Bansal, V., Chaudhary, M., *et al.* (2005) 'Biocompatibility of gold nanoparticles and their endocytotic fate inside the cellular compartment: a microscopic overview', *Langmuir*, 21(23), 10644-10654, available: http://dx.doi.org/10.1021/la0513712.

Skandani, A.A. and Al-Haik, M. (2013) 'Reciprocal effects of the chirality and the surface functionalization on the drug delivery permissibility of carbon nanotubes', *Soft matter*, 9(48), 11645-11649.

Slupphaug, G., Kavli, B. and Krokan, H.E. (2003) 'The interacting pathways for prevention and repair of oxidative DNA damage', *Mutation Research/Fundamental and Molecular Mechanisms of Mutagenesis*, 531(1), 231-251, available: http://dx.doi.org/https://doi.org/10.1016/j.mrfmmm.2003.06.002.

Smulders, S., Kaiser, J.-P., Zuin, S., *et al.* (2012) 'Contamination of nanoparticles by endotoxin: evaluation of different test methods', *Part Fibre Toxicol*, 9(1), 41-41.

Sperling, R.A. and Parak, W.J. (2010) 'Surface modification, functionalization and bioconjugation of colloidal inorganic nanoparticles', *Philosophical Transactions of the Royal Society of London A: Mathematical, Physical and Engineering Sciences*, 368(1915), 1333-1383, available: http://dx.doi.org/10.1098/rsta.2009.0273.

Steimer, A., Haltner, E. and Lehr, C.M. (2005) 'Cell culture models of the respiratory tract relevant to pulmonary drug delivery', *J Aerosol Med*, 18(2), 137-182, available: http://dx.doi.org/10.1089/jam.2005.18.137.

Stern, S.T., Adiseshaiah, P.P. and Crist, R.M. (2012) 'Autophagy and lysosomal dysfunction as emerging mechanisms of nanomaterial toxicity', *Part Fibre Toxicol*, 9, 20, available: http://dx.doi.org/1743-8977-9-20 [pii] 10.1186/1743-8977-9-20.

Striggow, B. (2017) *Operating Procedure: Field Measurement of Oxidation-Reduction Potential (ORP)*, Georgia, USA., available: https://www.epa.gov/sites/production/files/2017-07/documents/field_measurement_of_orp113_af.r2.pdf [accessed. 7 January 2019]

Suganthy, M. and Ramamoorthy, P. (2012) 'Principal Component Analysis Based Feature Extraction, Morphological Edge Detection and Localization for Fast Iris Recognition', *Journal of Computer Science*, 8(9), 1428-1433.

Takahashi, H., Niidome, Y., Niidome, T., *et al.* (2006) 'Modification of Gold Nanorods Using Phosphatidylcholine to Reduce Cytotoxicity', *Langmuir*, 22(1), 2-5, available: http://dx.doi.org/10.1021/la0520029.

Tarantola, M., Schneider, D., Sunnick, E., *et al.* (2009) 'Cytotoxicity of metal and semiconductor nanoparticles indicated by cellular micromotility', *ACS Nano*, 3(1), 213-222, available: http://dx.doi.org/10.1021/nn800721j 10.1021/nn800721j [pii].

Tarantola, M., Pietuch, A., Schneider, D., *et al.* (2011) 'Toxicity of gold-nanoparticles: synergistic effects of shape and surface functionalization on micromotility of epithelial cells', *Nanotoxicology*, 5(2), 254-268, available: http://dx.doi.org/10.3109/17435390.2010.528847.

Thorne, P.S., Perry, S.S., Saito, R., *et al.* (2010) 'Evaluation of the Limulus Amebocyte Lysate and Recombinant Factor C Assays for Assessment of Airborne Endotoxin', *Applied and Environmental Microbiology*, 76(15), 4988-4995, available: http://dx.doi.org/10.1128/aem.00527-10.

Tlotleng, N., Vetten, M.A., Keter, F.K., *et al.* (2016) 'Cytotoxicity, intracellular localization and exocytosis of citrate capped and PEG functionalized gold nanoparticles in human hepatocyte and kidney cells', *Cell Biology and Toxicology*, 1-17, available: http://dx.doi.org/10.1007/s10565-016-9336-y.

Tomić, S., Đokić, J., Vasilijić, S., *et al.* (2014) 'Size-dependent effects of gold nanoparticles uptake on maturation and antitumor functions of human dendritic cells in vitro', *PLoS One*, 9(5), e96584, available: http://dx.doi.org/10.1371/journal.pone.0096584.

Trojanowicz, M. (2016) 'Impact of nanotechnology on design of advanced screen-printed electrodes for different analytical applications', *TrAC Trends in Analytical Chemistry*, 84, 22-47.

Trono, J.D., Mizuno, K., Yusa, N., *et al.* (2011) 'Size, concentration and incubation time dependence of gold nanoparticle uptake into pancreas cancer cells and its future application to X-Ray Drug Delivery System', *J Radiat Res*, 52(1), 103-109.

Tsoli, M., Kuhn, H., Brandau, W., *et al.* (2005) 'Cellular uptake and toxicity of Au55 clusters', *Small*, 1(8-9), 841-844.

Turkevich, J., Stevenson, P.C. and Hillier, J. (1951) 'A study of the nucleation and growth processes in the synthesis of colloidal gold', *Discuss. Faraday. Soc.*, 11, 55-75.

Vallhov, H., Qin, J., Johansson, S.M., *et al.* (2006) 'The importance of an endotoxin-free environment during the production of nanoparticles used in medical applications', *Nano Lett*, 6(8), 1682-1686, available: http://dx.doi.org/10.1021/nl060860z.

Verma, A., Uzun, O., Hu, Y., *et al.* (2008) 'Surface Structure-Regulated Cell Membrane Penetration by Monolayer Protected Nanoparticles', *Nature Materials*, 7(7), 588-595.

Vetten, M.A., Tlotleng, N., Tanner Rascher, D., *et al.* (2013) 'Label-free in vitro toxicity and uptake assessment of citrate stabilised gold nanoparticles in three cell lines', *Part Fibre Toxicol*, 10, 50, available: http://dx.doi.org/1743-8977-10-50 [pii] 10.1186/1743-8977-10-50.

Vetten, M.A., Yah, C.S., Singh, T., *et al.* (2014) 'Challenges facing sterilization and depyrogenation of nanoparticles: Effects on structural stability and biomedical applications', *Nanomedicine: Nanotechnology, Biology, and Medicine*, 10, 1391-1399.

Vetten, M. and Gulumian, M. (2019a) 'Differences in uptake of 14 nm PEG-liganded gold nanoparticles into BEAS-2B cells is dependent on their functional groups', *Toxicology and applied pharmacology*, 363, 131-141, available: http://dx.doi.org/https://doi.org/10.1016/j.taap.2018.11.014.

Vetten, M.A. and Gulumian, M. (2019b) 'Interference of Gold Nanoparticles with *In vitro* Endotoxin Detection Assays', *Current Nanoscience*, 15, 1-9, available: http://dx.doi.org/10.2174/1573413715666181212120013.

Villiers, C., Freitas, H., Couderc, R., *et al.* (2010) 'Analysis of the toxicity of gold nano particles on the immune system: effect on dendritic cell functions', *Journal of nanoparticle research : an interdisciplinary forum for nanoscale science and*

technology, 12(1), 55-60, available: http://dx.doi.org/10.1007/s11051-009-9692-0.

von Woedtke, T. and Kramer, A. (2008) 'The limits of sterility assurance', *GMS Krankenhaushygiene Interdisziplinär*, 3(3), Doc19.

Vonarbourg, A., Passirani, C., Saulnier, P., *et al.* (2006) 'Parameters influencing the stealthiness of colloidal drug delivery systems', *Biomaterials*, 27(24), 4356-4373, available: http://dx.doi.org/S0142-9612(06)00294-8 [pii] 10.1016/j.biomaterials.2006.03.039 [doi].

Wager, K., Chui, T. and Adem, S. (2014) 'Effect of pH on the stability of gold nanoparticles and their application for melamine detection in infant formula', *J. Appl. Chem*, 7(8), 5.

Wang, G., Stender, A.S., Sun, W., *et al.* (2010) 'Optical imaging of non-fluorescent nanoparticle probes in live cells', *Analyst*, 135(2), 215-221.

Wang, B., Li, X., Zhang, X., *et al.* (2013) 'Adaptable silicon–carbon nanocables sandwiched between reduced graphene oxide sheets as lithium ion battery anodes', *ACS Nano*, 7(2), 1437-1445.

Wang, M.-S. and Fan, L.-Z. (2013) 'Silicon/carbon nanocomposite pyrolyzed from phenolic resin as anode materials for lithium-ion batteries', *Journal of Power Sources*, 244, 570-574.

Wang, P., Lombi, E., Zhao, F.-J., *et al.* (2016) 'Nanotechnology: A New Opportunity in Plant Sciences', *Trends in plant science*, 21(8), 699-712.

Weinkauf, H. and Brehm-Stecher, B.F. (2009) 'Enhanced dark field microscopy for rapid artifact-free detection of nanoparticle binding to Candida albicans cells and hyphae', *Biotechnol J*, 4(6), 871-879, available: http://dx.doi.org/10.1002/biot.200800358.

Williams, K.L. (2007) 'Chapter 10: Limulus Amebocyte Lysate Discovery, Mechanism, and Applications' in Williams, K. L., ed., *Endotoxins: Pyrogens, LAL Testing and Depyrogenation*, 3rd Edition ed., Boca Raton: CRC Press, Taylor & Francis Group, 191-214.

Xia, T., Kovochich, M., Brant, J., *et al.* (2006) 'Comparison of the abilities of ambient and manufactured nanoparticles to induce cellular toxicity according to an oxidative stress paradigm', *Nano Lett*, 6(8), 1794-1807.

Xia, Q., Li, H., Liu, Y., *et al.* (2017) 'The effect of particle size on the genotoxicity of gold nanoparticles', *Journal of Biomedical Materials Research Part A*, 105(3) 710-719.

Xian, H., Jiazhen, W., Yuping, S., *et al.* (2012) 'Caveolae-mediated endocytosis of biocompatible gold nanoparticles in living Hela cells', *Journal of Physics: Condensed Matter*, 24(16), 164207.

Xing, J.Z., Zhu, L., Jackson, J.A., *et al.* (2005) 'Dynamic monitoring of cytotoxicity on microelectronic sensors', *Chem Res Toxicol*, 18(2), 154-161, available: http://dx.doi.org/10.1021/tx049721s.

Xu, W.W., Gao, Y. and Zeng, X.C. (2015) 'Unraveling structures of protection ligands on gold nanoparticle Au(68)(SH)(32)', *Science Advances*, 1(3), e1400211, available: http://dx.doi.org/10.1126/sciadv.1400211.

Yang, H., Wu, Q., Tang, M., *et al.* (2010) 'In vitro study of silica nanoparticle-induced cytotoxicity based on real-time cell electronic sensing system', *J Nanosci Nanotechnol*, 10(1), 561-568.

Zabetakis, K., Ghann, W.E., Kumar, S., *et al.* (2012) 'Effect of high gold salt concentrations on the size and polydispersity of gold nanoparticles prepared by an extended Turkevich-Frens method', *Gold Bulletin*, 45, 203-211.

Zhang, Z., Berg, A., Levanon, H., *et al.* (2003) 'On the interactions of free radicals with gold nanoparticles', *Journal of the American Chemical Society*, 125(26), 7959-7963.

Zhang, Q., Hitchins, V.M., Schrand, A.M., *et al.* (2011) 'Uptake of gold nanoparticles in murine macrophage cells without cytotoxicity or production of pro-inflammatory mediators', *Nanotoxicology*, 5(3), 284-295, available: http://dx.doi.org/10.3109/17435390.2010.512401.